UNIVERSITY OF ALBERTA

HEAT TRANSFER IN THIN FIBROUS MATERIALS UNDER HIGH HEAT FLUX CONDITIONS

BY

DAVID ANDREW TORVI ©

A thesis submitted to the Faculty of Graduate Studies and Research in partial fulfilment of the requirements for the degree of DOCTOR OF PHILOSOPHY

DEPARTMENT OF MECHANICAL ENGINEERING

EDMONTON, ALBERTA
SPRING, 1997

National Library of Canada

Acquisitions and Bibliographic Services

395 Wellington Street
Ottawa ON K1A 0N4
Canada

Bibliothèque nationale du Canada

Acquisitions et services bibliographiques

395, rue Wellington
Ottawa ON K1A 0N4
Canada

Your file Votre référence

Our file Notre référence

The author has granted a non-exclusive licence allowing the National Library of Canada to reproduce, loan, distribute or sell copies of his/her thesis by any means and in any form or format, making this thesis available to interested persons.

The author retains ownership of the copyright in his/her thesis. Neither the thesis nor substantial extracts from it may be printed or otherwise reproduced with the author's permission.

L'auteur a accordé une licence non exclusive permettant à la Bibliothèque nationale du Canada de reproduire, prêter, distribuer ou vendre des copies de sa thèse de quelque manière et sous quelque forme que ce soit pour mettre des exemplaires de cette thèse à la disposition des personnes intéressées.

L'auteur conserve la propriété du droit d'auteur qui protège sa thèse. Ni la thèse ni des extraits substantiels de celle-ci ne doivent être imprimés ou autrement reproduits sans son autorisation.

0-612-21647-0

Canada

UNIVERSITY OF ALBERTA
LIBRARY RELEASE FORM

NAME OF AUTHOR: DAVID ANDREW TORVI

TITLE OF THESIS: HEAT TRANSFER IN THIN FIBROUS MATERIALS UNDER HIGH HEAT FLUX CONDITIONS

DEGREE: DOCTOR OF PHILOSOPHY

YEAR THIS DEGREE GRANTED: 1997

Permission is hereby granted to the University of Alberta Library to reproduce single copies of this thesis and to lend or sell such copies for private, scholarly or scientific research purposes only.

The author reserves all other publication and other rights in association with the copyright in the thesis, and except as hereinbefore provided neither the thesis nor any substantial portion thereof may be printed or otherwise reproduced in any material form whatever without the author's prior written permission.

Permanent Address:
4724 Chapel Rd., N.W.
Calgary, Alberta
T2L 1A6

DATED: Nov. 29/96

UNIVERSITY OF ALBERTA

FACULTY OF GRADUATE STUDIES AND RESEARCH

The undersigned certify that they have read, and recommend to the Faculty of Graduate Studies and Research for acceptance, a thesis entitled HEAT TRANSFER IN THIN FIBROUS MATERIALS UNDER HIGH HEAT FLUX CONDITIONS by DAVID ANDREW TORVI in partial fulfilment of the requirements for the degree of DOCTOR OF PHILOSOPHY.

JD Dale

Dr. J.D. Dale (Supervisor)

Betty Crown

Dr. E.M. Crown

Dr. T.W. Forest

Dr. W.C. McCaffrey

Roger Barker

Dr. R.L. Barker

Date: Nov. 28, 1996

"...and the fire will test the quality of each man's work."

1 Corinthians 3:13

ABSTRACT

Despite the existence of standardized bench top tests for evaluating fabrics for thermal protective clothing for flash fire and other high heat flux exposures, there are still many questions about the thermal response of these thin fibrous materials under high heat flux conditions. While others have developed analytical and numerical models of these materials, these models are difficult to use and have not been overly successful in predicting fabric temperatures.

The finite element method was used to develop a model of the heat transfer in two common inherently flame resistant fabrics, Nomex® IIIA and Kevlar®/PBI, subjected to the high heat fluxes used in bench top tests, such as the thermal protective performance (TPP) test. The apparent heat capacity method was used to model thermochemical reactions in these materials using information from thermal gravimetric analysis (TGA) and differential scanning calorimeter (DSC) tests. In-depth absorption of radiation, variable thermal properties, and the heat transfer across an air space between the fabric and a test sensor were also included. The absolute temperatures predicted by this relatively simple model are within 4% of those measured by an infrared thermometer. Estimated times to the Stoll second degree burn criterion are within 6% of those from actual tests. Flow visualization was also used to describe the natural convection flow patterns in the air space.

A parametric study conducted using this numerical model indicated that the most important parameters are the boundary conditions used to describe the high heat flux exposure. Effects of varying other parameters, such as fabric thickness and moisture regain were also demonstrated. These results were used to explain differences in the performance of the two fabrics.

Possible modifications to existing bench top test methods were also investigated. From the heat transfer perspective planar tests are shown to be adequate representations of the human body. Fixed duration flame exposure tests provide more information than existing tests. Advantages and disadvantages of using copper disk and skin simulant heat flux sensors were outlined. Different methods used to treat data from these test sensors, and to make skin burn predictions, were also compared.

ACKNOWLEDGEMENTS

The author wishes to acknowledge the following for their help in the preparation of this thesis.

- Dr. J.D. Dale for his supervision of this research.
- Dr. E.M. Crown and Dr. T.W. Forest for their guidance as part of the author's supervisory committee.
- Mark Ackerman, Terry Nord, Bernie Faulkner, Ian Buttar, Allan Muir, Albert Yuen, Crystal Dawley, and Elaine Bitner for their assistance with the design of the experimental apparatus, procedure, and data acquisition system.
- Mike Myo, Ed Savage, and Tannis Grant for conducting some of the experiments described in this thesis.
- The Natural Sciences and Engineering Research Council of Canada, the Province of Alberta, Department of Mechanical Engineering, and E.I. du Pont de Nemours & Company for funding during this research.
- Dominion Industrial Fabrics Company and Hoechst Celanese Corporation for supplying fabrics for this research.
- To the many individuals who have extended friendship and hospitality to our family during our stay in Edmonton (despite my insistence on continuing to cheer for the Calgary Flames and Stampeders).
- My parents, for their inspiration throughout my entire education, and for their example. My brothers and sister, for their sense of humour.
- My wife, Heather, and my son, Joshua, for their unconditional love, support, and patience during this research. Thank you for all of your sacrifices and for allowing me to pursue my dreams. I love you both very much.

TABLE OF CONTENTS

CHAPTER 1 INTRODUCTION 1

1.1 Flash Fires and Other High Heat Flux Exposures 1

1.2 Thermal Protective Clothing 4

1.2.1 Flame Resistance 5

1.3 Skin Burn Predictions 7

1.3.1 Skin Structure and Skin Burns 7

1.3.2 Stoll Second Degree Burn Criterion 9

1.3.3 Henriques Burn Integral 11

1.4 Fabric and Clothing Flammability and Thermal Protection Tests 12

1.4.1 Flammability Tests 14

1.4.2 Bench Top Tests 15

1.4.3 Mannequin Testing 17

1.5 Fabric/Skin Heat and Mass Transfer Models 18

1.5.1 Chen 19

1.5.2 Stoll 20

1.5.3 Government Industry Research Committee on Fabric Flammability 21

1.5.4 Aerotherm 22

1.5.5 Barker 24

1.5.6 Heat and Mass Transfer Models of Other High Temperature Materials 25

1.6 Overview of the Research in this Thesis 26

CHAPTER 2 HEAT TRANSFER MODEL 28

2.1 Effects of the Geometry of the Human Body on Heat Transfer in Fabric Tests 28

2.2 Fabric-Air Gap-Test Sensor System 29

2.3 Thermal Response of Fabric 34

    2.3.1 Thermochemical Reactions 34

    2.3.2 Treatment of In-Depth Absorption of Incident Radiation 38

    2.3.3 Boundary Condition on the Front of the Fabric 47

2.4 Energy Transfer Between Fabric and Test Sensor 50

    2.4.1 Previous Research in the Energy Transfer in Air Gaps in Thermal Protective Clothing 51

    2.4.2 Natural Convection in Enclosures 58

    2.4.3 Treatment of Natural Convection in this Study 62

    2.4.4 Thermal Radiation in the Air Gap 63

    2.4.5 Interaction Between Natural Convection and Radiation Heat Transfer in the Air Gap 65

2.5 Treatment of Test Sensor 67

2.6 Differential Equations for Fabric-Air Gap-Test Sensor System 68

2.7 Solution of Differential Equations Using the Finite Element Model 70

2.8 Finite Element Computer Program 73

2.9 Verification of Model with Closed Form and Other Solutions 75

    2.9.1 Semi-Infinite Solid 75

    2.9.2 Two Layer Semi-Infinite Solid 75

    2.9.3 Lumped Heat Capacity Analysis 78

    2.9.4 Semi-Infinite Solid with Variable Thermal Conductivity 80

2.9.5 Semi-Infinite Solid with In-Depth Absorption of Incident Radiation 83

2.10 Summary 84

CHAPTER 3 NUMERICAL RESULTS 85

3.1 Fabrics Used in this Study 85

3.2 Determination of Relevant Thermal and Thermochemical Properties 86

3.2.1 Preparation of Samples 86

3.2.2 Thickness 86

3.2.3 Density 87

3.2.4 Thermal Conductivity 87

3.2.5 Apparent Heat Capacity and Thermal Decomposition Temperatures 92

3.2.6 Transmissivity and Emissivity 105

3.2.7 Summary of Relevant Fabric Properties 106

3.3 Numerical Results 108

3.4 Parametric Study 108

3.4.1 Thickness 110

3.4.2 Moisture Regain 112

3.4.3 Thermal Conductivity 115

3.4.4 Specific Heat 119

3.4.5 Energies Associated with Thermal Decomposition Reactions 121

3.4.6 Transmissivity 124

3.4.7 Boundary Conditions 125

3.4.8 Air Gap Width 130

3.4.9 Summary of Parametric Study 134

CHAPTER 4 EXPERIMENTAL APPARATUS, PROCEDURE, AND RESULTS 136

4.1 Fabric and Shim Stock Samples 136

4.2 Experimental Apparatus 137

4.2.1 Specimen Holder and Water-Cooled Shutter 139

4.2.2 Heat Flux Sensors 139

4.2.3 Temperature Measuring Devices 144

4.3 Treatment of Test Data 146

4.3.1 Copper Disk Heat Flux Sensors 146

4.3.2 Skin Simulant Heat Flux Sensors 147

4.4 Experimental Procedure 148

4.4.1 Standard Bench Top Tests of Fabric and Shim Stock Specime8s 149

4.4.2 Fixed Duration Bench Top Test 149

4.4.3 Fabric and Shim Stock Temperature Measurements 153

4.5 Experimental Results 153

4.5.1 Effects of Differences in Sample Preparation on Test Resul3s 154

4.5.2 Fabric and Shim Temperatures 156

4.5.3 Interrupted Mass Loss Tests 166

4.5.4 Bench Top Test Results at Different Air Gaps 174

4.5.5 Flow Visualization 177

4.5.6 Existing and Modified Bench Top Test Results 185

4.6 Summary 192

CHAPTER 5 DISCUSSION OF NUMERICAL AND EXPERIMENTAL RESULTS 193

5.1 Comparison of Experimental and Numerical Results 193

5.1.1 Thermal Response of Fabric 193

5.1.2 Bench Top Test Results 200

5.2 Implications of Research to Fabric Design 208

5.3 Implications of Research to Bench Top Test Methods 210

5.3.1 Use of Air Gaps in Bench Top Tests 210

5.3.2 Modified Bench Top Test Methods 210

5.4 Summary 215

CHAPTER 6 CONCLUSIONS AND RECOMMENDATIONS 216

6.1 Conclusions 216

6.2 Recommendations 219

REFERENCES 222

APPENDICES 239

APPENDIX 1: Effects of Cylindrical Geometry on Heat Transfer in Human Skin Under Flash Fire Conditions 240

APPENDIX 2: Comparison of Radiation Heat Transfer Estimates in the Air Gap With and Without Absorption 248

APPENDIX 3: Derivation of Finite Element Matrix Equation 254

APPENDIX 4: Sample Datafile 261

APPENDIX 5: Skin Simulant Temperature Gradients 262

APPENDIX 6: Details of Calculation of Heat Fluxes from Surface Temperatures of Skin Simulant Sensor 268

APPENDIX 7: Data from Individual Fixed Duration Tests 272

CURRICULUM VITAE 277

LIST OF TABLES

2.1 Suggested Critical Air Gap Widths for Protective and other Clothing 53

3.1 Values of Properties for Use in Equation (3.9) for Nomex® IIIA and Kevlar®/PBI Fabrics 103

3.2 Summary of Thermal and Other Properties of Nomex® IIIA and Kevlar®/PBI Fabrics Used in this Study 107

3.3 Range of Values of Thermal and Other Properties Used in the Parametric Study 109

3.5 Required Times to Exceed Stoll Criterion Predicted by Numerical Model for Various Initial Mass Fractions of Moisture 114

3.6 Required Times to Exceed Stoll Criterion Predicted by Numerical Model for Various Constant Values of Thermal Conductivity 117

3.7 Required Times to Exceed Stoll Criterion Predicted by Numerical Model for Various Volume Fractions of Fibres 118

3.8 Required Times to Exceed Stoll Criterion Predicted by Numerical Model for Various Constant Values of Specific Heat 121

3.9 Required Times to Exceed Stoll Criterion Predicted by Numerical Model for Various Values of Energy of Thermal Decomposition Reaction 122

3.10 Required Times to Exceed Stoll Criterion Predicted by Numerical Model for Various Temperature Ranges for Thermal Decomposition Reaction 123

3.11 Required Times to Exceed Stoll Criterion Predicted by Numerical Model for Various Values of Convective Heat Transfer Coefficient 125

3.12 Required Times to Exceed Stoll Criterion Predicted by Numerical Model for Various Values of Flame Temperature and Emissivity 129

4.1 Average Times Required to Exceed Stoll Criterion for Conditioned and Oven-Dried Specimens 155

4.2 Summary of Macro and Microscopic Changes to Nomex® IIIA Fabrics During Bench Top Test Exposures 170

4.3 Summary of Macro and Microscopic Changes to Kevlar®/PBI Fabrics During Bench Top Test Exposures 171

4.4 Comparison of Bench Top Results Using Two Different Test Sensors 185

4.5 Times to Second and Third Degree Burn Predicted for Various Square Wave Heat Fluxes Between 20 and 30 kW/m^2 Incident on Human Skin for 10 s 190

5.1 Predicted Net Heat Flux Incident on Front Surface of Fabric from Meker Burner Flame for Various Front Surface Temperatures 197

5.2 Predicted Times to Second Degree Burn Criteria For Fabrics of Various Thicknesses in Perfect Contact with Copper Disk Test Sensors and Human Skin 214

A1.1 Comparison Between Predicted Times to Second and Third Degree Burn Determined Using the Cylindrical (r_o = 5 cm - arm) and Slab Models 246

A2.1 Effect of Absorption on Predicted Times Required to Exceed Stoll Criterion and Copper Disk Test Sensor Temperature Rises 252

A5.1 Comparison Between Second Degree Burn Predictions Made Using Skin Simulant Sensors with Various Initial Temperature Gradients 266

LIST OF FIGURES

1.1 Comparison Between Heat Fluxes Measured in House Full of Gas (HFOG III) Experiment With Those Estimated for Ideal Flash Fire and Used in Thermal Mannequin Tests 4

1.2 Inherently Flame Resistant Polymers Used in This Work 6

1.3 Stoll Criterion for Time to Second Degree Burn for Various Incident Square Wave Heat Fluxes on Bare Human Skin 10

1.4 Decision Framework for Making Protective Clothing Decisions 13

2.1 Fabric-Air Gap-Test Sensor System 29

2.2 Elemental Volume for Heat Transfer Analysis of Fabric Including Energy Transfers by Conduction, Radiation, and Energy Generated Within the Element 31

2.3a Models for Interaction Between Incident Radiation and the Fibrous Structure - Single Fibre 39

2.3b Models for Interaction Between Incident Radiation and the Fibrous Structure - Collection of Fibres in one Yarn 40

2.3c Models for Interaction Between Incident Radiation and the Fibrous Structure - Collection of Yarns 40

2.4a Three Representations of the Fabric Structure - Single Yarn Model 45

2.4b Three Representations of the Fabric Structure - Two Yarn, Two Layer Model 45

2.4c Three Representations of the Fabric Structure - Two Yarn, Staggered Centres Model 45

2.5 Determining the Cross Sectional Area of a Yarn as a Function of Depth From Its Surface 46

2.6 Absorption of Incident Radiation with Depth using Three Fabric Structure Models 46

2.7 Comparison Between Temperatures of Front and Back of Fabric Predicted Using Various Numbers of Fabric Elements and Time Steps 73

2.8a Flow Diagram for Finite Element Computer Program - Initial and Final Stages 74

2.8b Flow Diagram for Finite Element Computer Program - Temperature Calculations 74

2.9 Comparison Between Surface Temperatures for a Layer in Perfect Contact with a Semi-Infinite Solid Calculated Using the Finite Element Model and the Closed Form Solution of Griffith and Horton 78

2.10 Comparison Between Temperatures Predicted for Steel Shim Stock Piece with Temperature Dependent Specific Heat Using Finite Element Model and Lumped Heat Capacity Model 79

2.11 Comparison Between Temperatures Determined Using Finite Element Model, Closed-Form Solution, and the Integral Method for a Semi-Infinite Slab with Constant Thermal Properties 82

2.12 Comparison Between Temperatures Determined Using Finite Element Model, and the Integral Method for a Semi-Infinite Slab with Variable Thermal Conductivity 82

3.1 Thermal Conductivity of Nomex® Felt, Fabrics, Fibres, and of Air for Temperatures from 300 to 1400 K 92

3.2 Thermogravimetric Curves for Nomex® IIIA and Kevlar®/PBI Specimens 94

3.3 Effect of Increasing Heating Rate on Thermogravimetric Curve 95

3.4 DSC Test Data for Nomex® IIIA 99

3.5 DSC Test Data for Kevlar®/PBI 99

3.6 Specific Heat as a Function of Temperature for Nomex® IIIA 100

3.7 Specific Heat as a Function of Temperature for Kevlar®/PBI 100

3.8 Transmissivity Measurements for Nomex® IIIA and Kevlar®/PBI Fabric Specimens Before and After a 10 s Bench Top Test Exposure 106

3.9 Temperatures of the Front and Back of Nomex® IIIA and Kevlar®/PBI Fabrics Predicted by Numerical Model 108

3.10 Temperatures of Front of Fabric Predicted by Numerical Model for Various Fabric Thicknesses 110

3.11 Temperatures of Back of Fabric Predicted by Numerical Model for Various Fabric Thicknesses 111

3.12 Times Required to Exceed the Stoll Criterion Predicted by Numerical Model for Different Fabric Thicknesses 111

3.13 Temperatures of Front of Fabric Predicted by Numerical Model for Various Initial Mass Fractions of Moisture 112

3.14 Temperatures of Back of Fabric Predicted by Numerical Model for Various Initial Mass Fractions of Moisture 113

3.15 Copper Disk Temperature Rise Predicted by Numerical Model for Various Initial Mass Fractions of Moisture 113

3.16 Temperatures of Front of Fabric Predicted by Numerical Model for Various Constant Values of Thermal Conductivity 116

3.17 Temperatures of Back of Fabric Predicted by Numerical Model for Various Constant Values of Thermal Conductivity 116

3.18 Copper Disk Temperature Rise Predicted by Numerical Model for Various Constant Values of Thermal Conductivity 117

3.19 Temperatures of Front of Fabric Predicted by Numerical Model for Various Constant Values of Specific Heat 119

3.20 Temperatures of Back of Fabric Predicted by Numerical Model for Various Constant Values of Specific Heat 120

3.21 Copper Disk Temperature Rise Predicted by Numerical Model for Various Constant Values of Fabric Specific Heat 120

3.22 Temperatures of Front of Fabric Predicted by Numerical Model for Various Values of Convective Heat Transfer Coefficient 126

3.23 Temperatures of Back of Fabric Predicted by Numerical Model for Various Values of Convective Heat Transfer Coefficient 126

3.24 Copper Disk Temperature Rise Predicted by Numerical Model for Various Values of Convective Heat Transfer Coefficient 127

3.25 Temperatures of Front of Fabric Predicted by Numerical Model for Various Values of Flame Temperature and Emissivity 128

3.26 Temperatures of Back of Fabric Predicted by Numerical Model for Various Values of Flame Temperature and Emissivity 128

3.27 Copper Disk Temperature Rise Predicted by Numerical Model for Various Values of Flame Temperature and Emissivity 129

3.28 Times Required to Exceed Stoll Criterion Predicted by Numerical Model for Air Gap Widths from 0.5 to 20 mm 130

3.29 Relative Magnitudes of Energy Transfer by Conduction/Convection, and Thermal Radiation Across the Air Gap Predicted by Numerical Model for Air Gap Widths of 6, 12, and 20 mm 131

3.30 Rayleigh Number Histories Predicted by Numerical Model for Air Gap Widths of 6, 8, 10, 12, and 20 mm 131

3.31 Maximum Values of Convective Heat Transfer Coefficient Predicted by Numerical Model for Air Gap Widths from 1 to 20 mm 133

3.32 Radiation View Factor as a Function of Air Gap Width 133

4.1 Bench Top Test Apparatus 138

4.2 Close-up View Of Bench Top Test Apparatus Showing Specimen Holder, Water-Cooled Shutter, and Meker Burner 138

4.3 Skin Simulant and Copper Disk Heat Flux Sensors 140

4.4 Mounting of Skin Simulant Sensors in Kaowool Insulating Blocks 143

4.5 Comparison Between Heat Flux Histories Behind a Kevlar®/PBI Specimen Determined Using the 5-point Linear Least Squares Method and All the Data or Only the Data at 0.5 s Increments 148

4.6 Bench Top Test Using a Shutter 150

4.7 Comparison Between Measured Kevlar®/PBI Fabric Temperatures - Conditioned and Oven-Dried 154

4.8 Comparison Between Measured Temperatures of Back of Nomex® IIIA Fabric Specimens - Conditioned and Oven-Dried 155

4.9 Comparison Between Temperatures of Front and Back of Painted Shim Stock Pieces Measured Using 40 AWG Type K Thermocouples 156

4.10 Comparison Between Temperatures of Back of Painted Shim Stock Pieces Measured Using 36 AWG Type K Thermocouple and Infrared Thermometer 157

4.11 Comparison Between Temperatures of Painted Shim Stock Pieces Measured Using Type K Thermocouples in Tests Using Various Air Gap Widths 157

4.12 Comparison Between Temperatures of Nomex® IIIA Fabric Specimens Measured Using Thermocouples in Tests Using Various Air Gap Widths 161

4.13 Comparison Between Temperatures of Kevlar®/PBI Fabric Specimens Measured Using Thermocouples in Tests Using Various Air Gap Widths 161

4.14 Comparison Between the Temperatures of Kevlar®/PBI Fabric Specimens Measured Using Infrared Thermometer and Type K Thermocouple 162

4.15 Comparison Between Temperatures of Back of Nomex® IIIA Fabric Specimens Measured in Tests Using Various Air Gap Widths 163

4.16 Comparison Between Temperatures of Back of Kevlar®/PBI Fabric Specimens Measured Using Type K Thermocouples in Tests Using Various Air Widths 163

4.17 Comparison Between Temperatures of Front and Back of Nomex® IIIA and Kevlar®/PBI Fabric Specimens Measured Using Infrared Thermometer During 20 s Exposure 164

4.18 Comparison Between Temperatures of Back of Nomex® IIIA and Kevlar®/PBI Fabric Specimens Measured Using Type K Thermocouples During 10 s Exposure 165

4.19 Interrupted Mass Loss and TGA Test Results for Nomex® IIIA Fabric Specimens 167

4.20 Interrupted Mass Loss and TGA Test Results for Kevlar®/PBI Fabric Specimens 167

4.21 Nomex® IIIA and Kevlar®/PBI Fabric Specimens from Interrupted Mass Loss Tests 168

4.22 Measured Times Required to Exceed Stoll Criterion for Painted Shim Stock Pieces Tested Using Various Air Gaps 175

4.23 Measured Times Required to Exceed Stoll Criterion for Nomex® IIIA Fabric Specimens Tested Using Various Air Gaps 175

4.24 Measured Times Required to Exceed Stoll Criterion for Kevlar®/PBI Fabric Specimens Tested Using Various Air Gaps 176

4.25 Flow Visualization Arrangement 178

4.26 Flow Patterns Observed in 3/4 in. (19.1 mm) Air Gap 179

4.27 Flow Patterns Observed in 1/2 in. (12.7 mm) Air Gap 181

4.28 Flow Patterns Observed in 3/8 in. (9.5 mm) Air Gap 182

4.29 Flow Patterns Observed in 1/4 in. (6.4 mm) and and 1/8 in. (3.2 mm) Air Gaps 183

4.30 Comparison Between the Heat Fluxes Measured Behind a Kevlar®/PBI Fabric Specimen by Copper Disk and Skin Simulant Heat Flux Sensors for a 10 s Exposure Using a 1/4 in. (6.4 mm) Air Gap 187

4.31 Comparison Between Measured Increases in Copper Disk and Skin Simulant Temperatures Behind a Kevlar®/PBI Fabric Specimen During and After a 10 s Exposure Using a 1/4 in. (6.4 mm) Air Gap 188

5.1 Comparison Between Temperatures of Back of Painted Shim Stock Pieces Predicted Using Numerical Model and Measured Using Infrared Thermometer 194

5.2 Comparison Between Temperatures of Front and Back of Nomex® IIIA Fabric Specimens Predicted Using Numerical Model and Measured Using Infrared Thermometer 195

5.3 Comparison Between Temperatures of Front and Back of Kevlar®/PBI Fabric Specimens Predicted Using Numerical Model and Measured Using Infrared Thermometer 195

5.4 Comparison Between Sensor Temperature and Bench Top Test Results Predicted By Numerical Model and Measured During Actual Bench Top Tests of Painted Shim Stock Pieces with 1/4 in. (6.4 mm) Air Gaps 201

5.5 Comparison Between Sensor Temperatures and Bench Top Test Results Predicted By Numerical Model and Measured During Actual Bench Top Tests of Nomex® IIIA Fabric Specimens with 1/4 in. (6.4 mm) Air Gaps 201

5.6 Comparison Between Sensor Temperatures and Bench Top Test Results Predicted By Numerical Model and Measured During Actual Bench Top Tests of Kevlar®/PBI Fabric Specimens with 1/4 in. (6.4 mm) Air Gaps 202

5.7 Comparison Between Skin Simulant Temperatures Predicted by Numerical Model and Measured During Actual Bench Top Test of Nomex® IIIA Fabric Specimens using 1/4 in. (6.4 mm) Air Gap 203

5.8 Comparison Between Skin Simulant Temperatures Predicted by Numerical Model and Measured During Actual Bench Top Test of Kevlar®/PBI Fabric Specimens using 1/4 in. (6.4 mm) Air Gap 204

5.9 Comparison Between Predicted and Measured Times Required to Exceed Stoll Criterion for Nomex® IIIA Fabric Samples Tested Using Various Air Gaps 205

5.10 Comparison Between Predicted Temperatures of Front of Fabric Samples of Various Thicknesses in Perfect Contact with a Copper Disk Test Sensor and Human Skin 212

5.11 Comparison Between Predicted Temperatures at Various Depths in a 2.0 mm Thick Fabric Sample in Perfect Contact with a Copper Disk Test Sensor and Human Skin 213

5.12 Calculated Heat Fluxes Incident on the Surfaces of Copper Disks and Human Skin in Perfect Contact with Fabrics of Thicknesses of 0.3 and 2.0 mm 215

A1.1 Idealized Models Which Treat Human Skin as a Cylinder of a Slab 240

A2.1 Two Infinite Parallel Plates With a Gas in Between Them 248

A5.1 Temperature Histories at Various Depths in Skin Simulant Sensor Subjected to Heat Flux of about 17 kW/m^2 for 10 s 263

A5.2 Comparison Between Predicted and Measured Surface Temperatures of Skin Simulant During and After a 10 s Exposure to a Heat Flux of About 17 kW/m^2 264

NOMENCLATURE

Notation

A	area (m^2)
A.W.G.	American Wire Gauge
C	circumference (m)
c_p	specific heat ($J/kg \cdot {}^\circ C$)
D	diameter (m)
dt	time step (s)
dx	elemental distance (m)
F	radiation view factor
G	energy generation due to chemical reaction (J/m^3)
g	gravitational acceleration (9.81 m/s^2)
Gr	Grashof number (dimensionless)
H	enthalpy function (J/m^3)
h	convection heat transfer coefficient ($W/m^2 \cdot {}^\circ C$)
i	time step number (dimensionless)
k	thermal conductivity ($W/m \cdot {}^\circ C$)
K_l	loss coefficient ($W/m^2 \cdot {}^\circ C$)
L	thickness (m), latent heat of phase change (J/kg)
l	thickness of one finite element (m)
moist	initial mass fraction of moisture (dimensionless)
Nu	Nusselt number (dimensionless)
n	repeat n times
P	pre-exponential factor (s^{-1})
p	depth from surface (m)
Pr	Prandtl number (dimensionless)
q	heat flux (W/m^2, $cal/cm^2 \cdot s$)
R	ideal gas constant (8.314 $J/kg \cdot mol \cdot {}^\circ C$)
r	radius (m)
Ra	Rayleigh number (dimensionless)

S	location of boundary between phases (m), step function
slope	slope of specific heat with temperature curve (J/kg·K)
T	temperature (°C, K)
t	time (s)
v	volume fraction
x	depth (m)
y	depth (m)
z	depth (m)

Greek symbols

α	thermal diffusivity (m^2/s)
β	coefficient of thermal expansion (K^{-1})
γ	extinction coefficient (m^{-1})
ΔE	activation energy (J/mol, cal/mol)
Δt	time step (s)
δ	air gap width (m)
ε	emissivity (dimensionless)
θ	angular position (rads)
λ	wavelength (μm), root of equation
ν	kinematic viscosity (m^2/s)
ρ	density (kg/m^3), reflectivity
τ	dummy variable of integration (s), time constant of thermocouple (s)
σ	Stefan Boltzmann constant (5.669×10^{-8} $W/m^2 \cdot K^4$)
Ω	Henriques' burn integral value (dimensionless)

Subscripts

a	absorbed, node number
air	air gap
amb	ambient
b	node number, base of insulating block
bh	burner head

c	cross sectional
chem	chemical
cond	conduction
conv	convection
d	node number
e	element
eff	effective
ex	exposure
f	fibre
fab	fabric
felt	felt
fibre	fibre
fl	flame
g	gases
gas	hot gas
h	Hermitian
i	initial, inner
l	after phase change
m	during phase change
o	original, outer
r	reference
rad	radiation
rx	reaction
s	surface of insulating block, prior to phase change, surface
sens	sensor
solid	solid
wtr	water
y	yarn

Superscripts

A	apparent or effective
'	first derivative with respect to x
''	second derivative with respect to x
·	first derivative with respect to time
(j)	time step (j)

CHAPTER 1: INTRODUCTION

A large number of people are injured every year as a result of burns, many of which occur in industrial accidents. For example, it is estimated that there are 7000 clothing-related workplace injuries due to fire in the United States each year, resulting in 200 fatalities [1][1]. In order to minimize or prevent burn injuries from possible accidents, workers wear thermal protective clothing. To properly assess protective clothing alternatives, realistic tests must be performed to determine how much thermal protection clothing can provide.

In the author's previous work [2], a finite element model of bare skin subjected to a flash fire was presented. This work has been extended in order to develop a finite element model of the heat transfer in thin fibrous materials, such as thermal protective fabrics, under the high heat flux conditions used in bench top fabric tests to simulate flash fires. Energy transfers across air spaces between the heated fabric and bench top test sensors are also included in the model. Numerical results from this model are presented in this thesis and compared with experimental results obtained using a bench top test apparatus. This apparatus was also used to evaluate proposed modifications to standard test procedures for protective fabrics.

This introductory chapter describes the flash fire environment, and common fabric tests used to determine the suitability of materials for thermal protective clothing. Research conducted in the area of heat and mass transfer in fabrics subjected to flash fire-like conditions, and other materials subjected to high heat flux conditions is also summarized. An outline of the remainder of this thesis closes the chapter.

1.1 Flash Fires and Other High Heat Flux Exposures

One hazardous situation encountered in the petrochemical industry is the flash fire. Flash fires can result from the release of combustible gas, such as a leak at a well head site, compressor station, or petrochemical plant. They are of short duration, typically less than 5 s, and involve intense heat fluxes. Thermal protective clothing for these high intensity, short duration exposures is designed to protect the worker for several seconds if they happen to be exposed to a flash fire, giving them an opportunity to escape. At the same time, it must also be comfortable to wear under normal working conditions. Therefore it is different from protective clothing which is designed for other applications, where longer exposures to different heat fluxes occur. For example fire fighters' turnout coats are designed to provide protection for long term exposures to moderate heat fluxes and short term exposures to higher heat fluxes which can also occur during the course of their work. However, this clothing would not be appropriate for workers at a well site. Even though the turnout coats would do a good job of protecting the workers if they were caught in a flash fire, the coats would certainly be uncomfortable to wear during the course of their normal duties, especially during summer months.

---

[1] Numbers in square brackets denote references

Protective clothing can be evaluated using tests which simulate possible accidents. The evaluation of the protective qualities can be done by a variety of methods such as predicting the skin burns that a person wearing various fabrics or garments in such accidents would receive. Methods used to make these predictions are described in Section 1.3. In a paper describing the development of one of these tests, Behnke [3] describes some of the visible changes which protective fabrics made of Nomex® undergo after exposures to a 2.0 $cal/cm^2{\cdot}s$ (84 kW/m^2) heat flux for different lengths of time. Fabrics similar to those used in garments from actual industrial accidents were exposed to this heat flux until they resembled the damaged garments. The total energy to the garments was determined from the product of this heat flux and the exposure time necessary to cause the fabric to resemble the damaged garment. If eyewitness accounts of the duration of the exposure were available, an estimate of the heat flux during the accident could be made by dividing the total energy estimate by the time duration estimate. For a variety of accidents, heat fluxes between 1.0 and 3.0 $cal/cm^2{\cdot}s$ (42 to 126 kW/m^2) were estimated, with a flux of about 2.0 $cal/cm^2{\cdot}s$ (84 kW/m^2) being the estimate for a flash fire. Heat fluxes similar to the latter are now used in many tests for flame resistant fabrics and garments, which are described in Section 1.4.

These estimates assume that the changes which were seen in the garments were only dependent on the total energy absorbed, and not on the magnitude of the heat flux itself (e.g. a heat flux of 160 kW/m^2 for 2 s and a heat flux of 40 kW/m^2 for 8 s both represent an energy input of 320 kJ/m^2). This may or may not be the case. Other investigators have reported heat flux measurements for flash fires and other hazards. For example, Holcombe and Hoschke [4] reported estimates of 130-330 kW/m^2 for simulated mine explosions, and 167-226 kW/m^2 for JP-4 fuel fires. Krasny, et al. [5] measured heat fluxes of up to 180 kW/m^2 in seven room fires from just before flashover to flashover and severe postflashover fires.

Recently, the author has participated in an experiment in which a house was partially filled with natural gas, and then the gas/air mixture was ignited (House Full Of Gas (HFOG) III [6]). During this experiment, heat flux sensors used in the University of Alberta thermal mannequin (discussed in Section 1.4.3) were placed in the vicinity of the ignition point in order to measure the heat fluxes from the resulting explosion. As shown in Figure 1.1, the peak heat flux measured during the explosion was about twice the heat flux estimated as that for an ideal flash fire (80 kW/m^2), and about 40% higher than the peak heat flux in a typical thermal mannequin test. Therefore the fluxes used in these existing tests may not be in fact indicative of the accident which is being simulated.

For the work described in this thesis, heat fluxes of the order of 80 kW/m^2 will continue to be used. However, as evident by the above discussion, future work is required to determine more exactly the range of fluxes expected during flash fires and other exposures of interest.

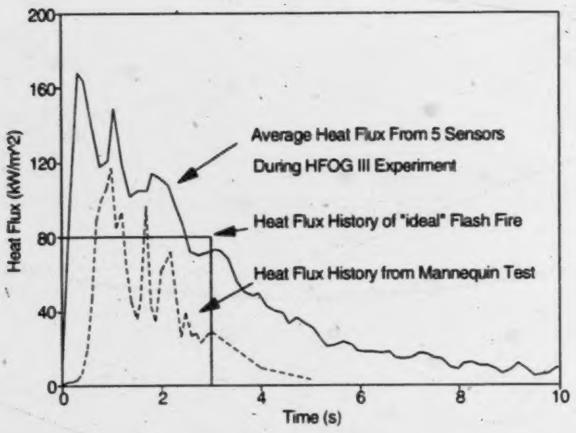

Figure 1.1 Comparison Between Heat Fluxes Measured in House Full of Gas (HFOG III) Experiment with Those Estimated for Ideal Flash Fire and Used in Thermal Mannequin Tests

1.2 Thermal Protective Clothing

Thermal protective clothing is designed to prevent or minimize skin burn damage from flash fires by reducing the heat transfer from the fire to the skin underneath the clothing. This is accomplished by using a garment which is flame resistant and thermal insulating. The garment must also maintain its integrity during the exposure, so that it will not rupture as a worker attempts to escape from a fire.

Some of the desired properties of thermal protective clothing are as follows [7]. The constituent fibres should be flame resistant and non-melting. They should not emit toxic gases at high temperatures. The fibres should be shrink-resistant, and maintain their strength and flexibility even at high temperatures. They should also have a low thermal conductivity so that they transmit as little heat as possible to the underlying skin. Fabrics made of these fibres should shrink very little and not split when exposed to flames, have low air permeability (so as to decrease convective heat transfer through the fabric), and be free of flammable finishes or coatings. The garment itself should have a proper fit and be easy to maintain. Closures and waistbands should be designed so as to reduce possible chimney effects during exposures. Garments must also be comfortable to wear during the normal course of work, which may result in some trade-offs in garment design. An example of this was given earlier when the different protective clothing needs of fire fighters and workers at a well site were compared.

1.2.1 Flame Resistance

Flame resistance is defined as "the property of a material whereby flaming combustion is slowed, terminated, or prevented" [8]. As this ability depends on the specific flame or thermal ignition source, it is a relative, rather than an absolute term, such as "flame proof" (as any fibre or fabric will burn if the exposure is severe enough). As mentioned above, fibres for thermal protective clothing should be flame resistant. Textile materials can be made flame resistant through chemical treatments, or by use of inherently flame resistant fibres. This study is limited to fabrics made of inherently flame resistant fibres.

Inherently flame resistant fibres are those in which the flame resistant properties are built into the polymer or fibre structure. Examples of some inherently flame resistant polymers used in this study are shown in Figure 1.2. These molecules have a "stiff backbone" due to the aromatic groups in the structure, thus there is limited bond rotation [9]. This results in a very stable structure, and therefore very high decomposition and melting temperatures, good thermal resistance and strength retention at high temperatures, and low shrinkage. As the flame resistant properties are inherent in the fibres, they will remain good over the entire working lifetime of the garment. Further details on these fibres can be found in Crown and Kerr [9].

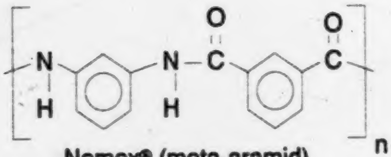

Nomex® (meta-aramid)

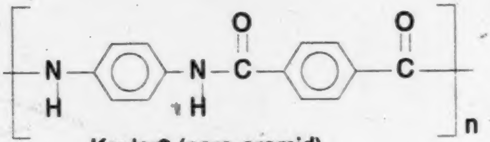

Kevlar® (para-aramid)

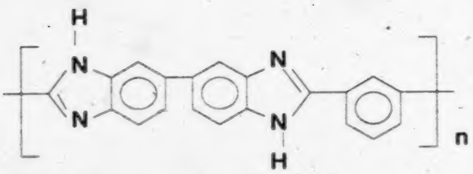

Polybenzimidazole (PBI)

Figure 1.2 Inherently Flame Resistant Polymers Used in This Work

Inherently flame resistant fibres are classified as aramids, novoloids, or polyamide imides. Common aramids are E.I. du Pont de Nemours and Company's Nomex®IIIA (a meta/para-aramid blend) and Kevlar® (a para-aramid), Teijin Fenilon's Conex® (a meta-aramid), and Kermel, SNC's Kermel®. A novoloid which is used is Carborundum Company's Kynol®. A polyamide imide that is in common use is Hoechst Celanese Corporation's polybenzimidazole (PBI). Often these fibres are blended with another fibre to increase their breathability and hence comfort [10].

Samples of three common flame resistant fabrics, Kevlar®/PBI, and Nomex® III and IIIA, were used in this study. Specific details about the fabrics used will be given in Section 3.1.

1.3 Skin Burn Predictions

In the fabric and garment tests which will be described in subsequent sections, individual fabrics or garments are rated on the basis of estimates of the amount of thermal damage which could occur to human skin behind that particular fabric or garment during and/or immediately after a high heat flux exposure. A brief description of human skin and skin burns is given immediately below. Two common methods used to estimate skin burns in fabric or garment tests are then described.

Before proceeding, however, it should be noted that while the term "burn prediction" is used in the literature and this thesis, it must be realized that this is simply a prediction made using a mathematical model of human skin or experimental data from a small number of human or animal experiments. Human skin and its thermal properties vary widely from person to person (due to factors such as the age of the individual), and from body site to body site on an individual. The accidents which occur in industry also vary widely. Therefore, although much effort has been put into making these predictions as realistic as possible, it must be remembered that the predictions are merely a rating system, rather than an indication of how much protection fabrics or garments might actually offer in a real accident. For example, just because the test results of a given fabric indicate it would take 5 s for a second degree burn to occur does not mean that this fabric would necessarily provide 5 s of protection to a worker in the field.

1.3.1 Skin Structure and Skin Burns

Skin is the largest organ of the human body both in terms of surface area (1.6 to 1.9 m^2 for most adults) and weight (about 15% of total body weight). The main regions of the skin are the epidermis, dermis, and subcutaneous tissue. The epidermis is the very thin outer layer of the skin. Typical thicknesses are 0.06 to 0.8 mm, depending on location on the body and individual. It contains no blood vessels or connective tissue, and receives nourishment from the dermis below. The bottom layer of the epidermis is called the basal layer (or stratum corneum), where cells constantly divide to form new cells, which move upwards through the rest of the epidermis. The dermis is much thicker than the epidermis (typically 20 to 30 times). It provides the strength and elasticity for the skin, and contains the glands, hair follicles, lymphatic vessels, nerves, and blood vessels. The subcutaneous tissue consists of connective tissue and specializes in the formation and storage of fat. In some parts of the body, such as the neck or the face, subcutaneous muscle exists under the fat layer. Further details on the skin can be found in [11].

Burns are one of the worst injuries possible to man. Many different local and systemic responses occur in the skin as a result of thermal insult. Burns take a long time to heal and are sometimes difficult to treat clinically. The systemic effects provide further complications which must also be treated. Damage can become a serious social hindrance and a blow to self esteem if it occurs on visible portions of skin.

Different classification systems are used to categorize skin burns. One common method traditionally used (and described below) is to clinically classify burns as first, second, third, or fourth degree burns. As shall be discussed later, burns are temperature and time dependant. Therefore, two different exposures can result in the same degree of burn, but leave the skin with different appearances. Hence, making an exact clinical classification of actual burns is difficult, and in practice may take days. However, the following general comments, summarized from [11], are appropriate.

First degree burns involve damage to the epidermis. There is little damage other than redness in the burned region. There are no systemic effects. Discomfort is temporary, and healing is normally quick with no permanent scarring or discolouration.

Second degree (or partial thickness) burns involve damage to the epidermis and the dermis. Blistering may occur, as well as damage to the structure of the dermis and the circulatory system. There is a loss of fluids, leading to many systemic effects, and a loss of plasma volume, which is a major factor in causing shock in untreated burn patients. Second degree burns may be further classified as superficial or deep, depending on the penetration depth of the injured zone. Superficial second degree burns are those in which a significant fraction of the cells at the base of the dermis are not destroyed. Therefore healing can occur in a normal pattern. Deep second degree burns result in much of the dermal base being lost.

Third degree (full thickness) burns occur when all epidermal elements and the supporting dermal structures are destroyed. This includes the destruction of blood vessels in the burned region. With no blood flow, the cells in this region of full thickness burn eventually die. Large volumes of extravascular fluid are lost due to injury to tissue beneath and surrounding the area of full thickness injury. There is no possibility for spontaneous healing, and skin grafts are required for resurfacing from the margins of the wound.

Fourth degree burns can occur with the incineration of tissue. Muscle, bone, and other structures below the subcutaneous tissue may be injured. Healing is not significantly different from that with third degree burns except for greater complications due to the injuries to underlying tissue.

Besides the aforementioned effects of first, second, third, and fourth degree burns, there are also systemic effects of heat trauma, as a major burn will alter the functions of all organ systems to some extent. Some of these changes are a direct result of the thermal stress and the inflammatory mediators within the body which are released locally into the circulatory system. However most are due to the altered condition of the skin. These systemic changes can include shock resulting from fluid loss, a decrease in cardial output, severe injuries to the respiratory system, an increase in the metabolic rate to compensate for the large heat losses from surface evaporation of water from the injured areas, and other complications such as nutritional defects, and altered immune function.

Two different methods can be used to estimate the times to thermal damage. These two methods, and their advantages and disadvantages are briefly described below.

1.3.2 Stoll Second Degree Burn Criterion

Bench scale tests of protective fabrics (to be discussed in Section 1.4) use data from the work of Stoll and Chianta [12] to make estimates of the time it takes for second degree burn damage to begin to occur for a given exposure. These data are shown in

Figure 1.3. Some of the data were based on observed exposure times required to produce second degree burn in blackened human skin subjected to incident heat fluxes from 0.1 to 0.4 cal/cm^2·s (4.2 to 16.8 kW/m^2) [13]. Other data were theoretically determined for heat fluxes from 0.4 to 1.0 cal/cm^2·s (16.8 to 41.9 kW/m^2).

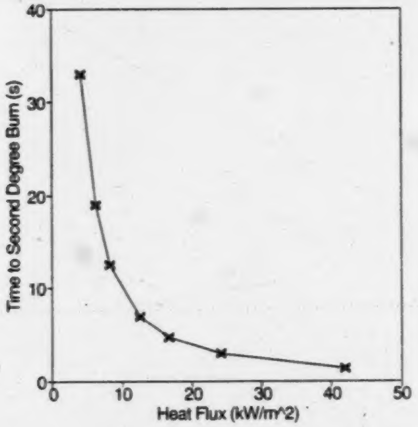

Figure 1.3 Stoll Criterion for Time to Second Degree Burn for Various Incident Square Wave Heat Fluxes on Bare Human Skin

These data are converted to the total amounts of energy which must be absorbed by the skin to cause second degree burns for a given length of exposure. A record of the energy absorbed by a test sensor, such as a copper calorimeter, can hence be compared with this criterion to estimate the time required to produce a second degree burn.

The main advantage to this method of predicting skin burns is its simplicity. Burns can quickly be predicted without the use of sophisticated mathematics. However, Stoll and Chianta state that "in applying these data it is absolutely essential that the heat pulse used be rectangular, for any variation from this shape invalidates the data" [12]. Holcombe and Hoschke [4], among others, have correctly pointed out that the pulse measured behind an exposed fabric is not rectangular. The effect of this on burn predictions will be discussed in Chapters 4 and 5. It should also be noted that this criterion is based on limited data. An average of 2.6 readings were taken at five heat fluxes and no indication was given as to the range of the data at each heat flux level [13].

In addition, as will be shown in Section 4.3.1, the peak heat fluxes under single layers of some thermal protective fabrics may be greater than the upper bound (16.8 kW/m^2) of the heat fluxes used to obtain their experimental data.

1.3.3 Henriques Burn Integral

Henriques [14] found that skin damage could be represented as a chemical rate process, and that a first order Arrhenius rate equation could be used for the rate of tissue damage,

$$\frac{d\Omega}{dt} = P \exp\left(-\frac{\Delta E}{R\,T}\right) \qquad (1.1)$$

Equation (1.1) can be integrated to produce

$$\Omega = \int_0^t P \exp\left(-\frac{\Delta E}{R\,T}\right) dt \qquad (1.2)$$

This integration is performed over the time the basal layer temperature, T, is greater than or equal to 44°C. This temperature was found to be the threshold temperature for thermal damage.

Second degree burns were said to occur when Ω is unity. By fitting experimental data for pig skin burns to Equation (1.2) for $\Omega = 1.0$, the activation energy, ΔE, was found to be 150 000 cal/mol (627 900 J/mol). This activation energy is very close to that of thermal denaturation (destruction through heating) of proteins (such as keratin in the epidermis). Therefore, the investigator postulated that this is the process by which skin tissue is destroyed. The value of the pre-exponential factor, P, was also determined by curve-fitting to be 3.1×10^{98}. However, these values and some of the other calculations in Henriques' paper have been shown to be incorrect [2,15], which will have an effect on burn predictions made using Equation (1.2).

As Equations (1.1) and (1.2) suggest, damage is dependent on temperature and time. For example, at a basal layer temperature of 44°C, a six hour exposure was said to be necessary for irreversible damage to begin, while at 70°C, less than an one second exposure was required. It was also found that first degree burns occurred when $\Omega = 0.53$ in Equation (1.2). Other investigators have also determined constants so that Equation (1.2) can be used to predict third degree burns [16].

Henriques burn integral is used in conjunction with temperature-time data from skin simulants to predict times to second and third degree burn. Details of this procedure will be discussed in Section 4.3.2. This method is valid for any heat flux history, while the Stoll criterion is strictly valid only for rectangular heat fluxes. However, this method is considerably more involved, and requires the use of a computer and specialized software. It should also be noted that Equations (1.1) and (1.2) are also used to make predictions of thermal damage in other exposures, such as laser surgery, with different values for the pre-exponential factor and activation energy. It has been shown that it is very important to ensure that the values of these two parameters are appropriate for the situation being modelled, or incorrect results may be obtained [17].

1.4 Fabric and Clothing Flammability and Thermal Protection Tests

Decisions about the appropriate thermal protective clothing for a particular application can be made using the framework shown in Figure 1.4. Important selection criteria can include [18]:

- protection and safety
- comfort and functional fit
- durability
- functional design details
- appearance
- maintenance
- cost

An example of how protective clothing was chosen for a variety of applications for U.S. Navy fire fighters is given in Stull, et al. [19].

In order to determine the protection offered by candidate materials and garments, flammability tests are first performed on fabric specimens to determine if these materials are in fact flame resistant. Materials that meet flammability criteria can then be tested

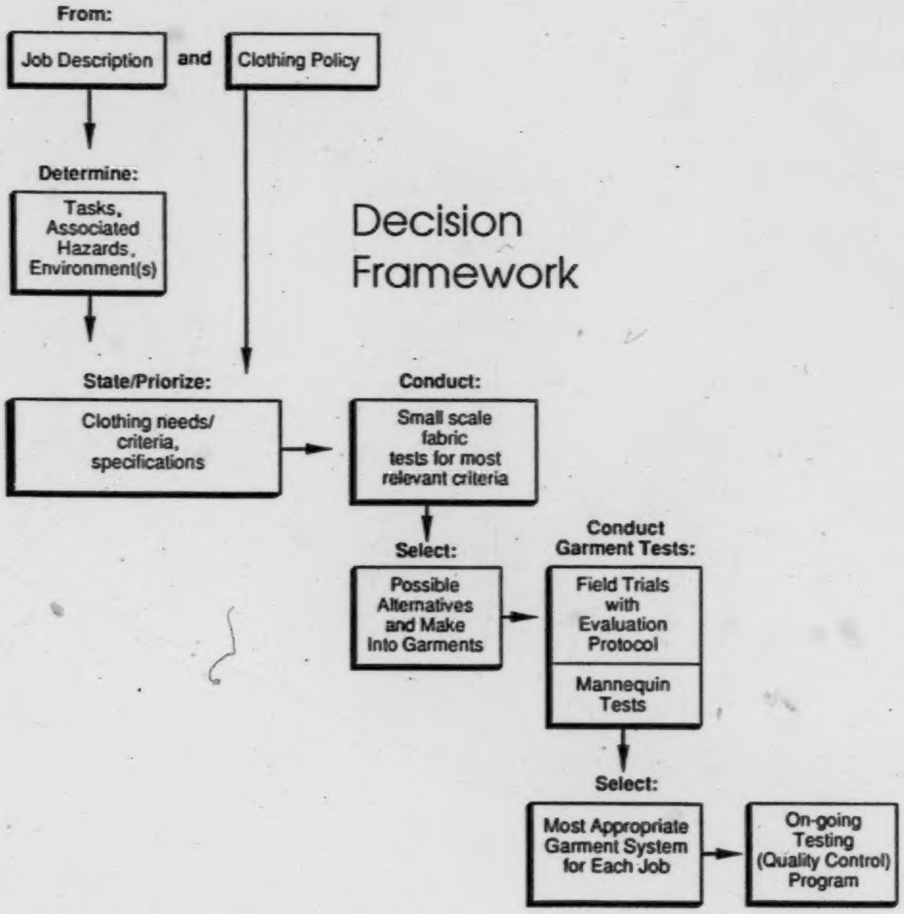
From:
Job Description
and
Clothing Policy
Determine:
Tasks, Associated Hazards, Environment(s)
Decision Framework
State/Priorize:
Clothing needs/ criteria, specifications
Conduct:
Small scale fabric tests for most relevant criteria
Select:
Possible Alternatives and Make Into Garments
Conduct Garment Tests:
Field Trials with Evaluation Protocol
Mannequin Tests
Select:
Most Appropriate Garment System for Each Job
On-going Testing (Quality Control) Program

Figure 1.4 Decision Framework for Making Protection Clothing Decisions. Reprinted from [18] with permission.

using small scale tests which estimate the thermal protection provided by these fabrics under high heat flux conditions. Once possible fabrics have been selected, thermal mannequin tests can be used to estimate the protection which garments made of these materials might offer the worker. These flammability, small scale, and thermal mannequin tests are briefly described below.

1.4.1 Flammability Tests

Flammability tests are used to determine whether a candidate material can be considered flame resistant. These tests measure the ease of ignition, rate of flame spread, ease of extinction, afterglow, heat generated, or the amount and toxicity of combustion products. Some of the most common tests used are briefly described below, and in Crown and Kerr [9], and Conn and Grant [20].

The 45° test method (e.g. CAN/CGSB-4.2 No. 27.5-94 [21], ASTM D 1230 - 94 [22]) uses a 50 mm by 165 mm specimen held in place at 45° to the horizontal. A standard burner flame is applied to the upper surface near the lower end for 1 s. The time for the flame to travel 127 mm is then recorded. As this test fails to ignite many fabrics, it only eliminates dangerously flammable fabrics. However, the test is very reliable in its ability to eliminate these dangerously flammable fabrics.

Various vertical tests (e.g. CAN/CGSB-4.2 No. 27.10-M91 [23], CAN/CGSB-4.2 No. 27.4-94/ISO 6940:1984 [24], Federal Standard for Textile Materials 191A 5903 [25], and ASTM D 3659 [26]) are used. These are more difficult to pass than the 45° test described above. In these tests a specimen is held vertically and a burner flame is impinged on it for a given length of time. The damaged length, afterflame, and afterglow times are measured. Most countries have standards based on these tests for a fabric's resistance to flaming in a fire only. The reliability of each individual test varies considerably.

The Limiting Oxygen Index (LOI) (e.g. ASTM D 2863 [27]) is the lowest concentration of oxygen necessary to support combustion of the sample. The test is conducted by igniting the top of a vertically-oriented sample with a hydrogen flame. By having the fabric burn from top to bottom, the flame itself does not assist in burning the sample, therefore repeatable results are easily obtained. When the fabric ignites, the flows of oxygen and nitrogen are adjusted until the sample is completely consumed at a slow and steady rate. The test is repeated until consistent results are obtained. The LOI is simply the minimum fraction of oxygen in the chamber at which this slow and steady combustion takes place. Atmospheric air is about 21% oxygen, so a LOI less than 21% indicates that the candidate material will burn readily in air, while a LOI greater than 21% indicates that the material will only burn if additional oxygen is available.

As flame resistant clothing was developed for industry, it became necessary to supplement these flammability tests with tests that estimate the protection that these pieces of clothing provide the skin. Tests were developed which include the response of the skin under this clothing to a thermal insult. A review of the development of these and other test methods can be found in [28]. A few of these and other test methods relevant to this study are outlined below.

1.4.2 Bench Top Tests

Behnke [3] devised a test for measuring the performance of fabrics subjected to high heat flux, short duration exposures, such as flash fires and JP-4 fuel fires caused by aircraft carrier deck crashes of planes. This test was based on the work of Stoll, discussed earlier in Section 1.3.2. Various versions of this test are now used to provide a basis of comparing competing fabrics.

In the original Thermal Protective Performance (TPP) test both radiation and convection heat sources were used. Nine quartz tubes powered by a variable voltage supply were used to supply the desired level of radiant energy. A pair of Meker burners supplied the appropriate amount of convective energy. Different tests now use only a burner (or burners), only a radiant source, or both in some combination to provide the same relative contributions of radiation and convection as in the exposure modelled. A water cooled shutter was used to time the exposure. The test fabric itself was mounted over a blackened 40 mm diameter copper disk mounted in an insulating block, which served as a heat flux sensor.

The TPP rating of a fabric is the amount of energy in cal/cm^2 which must be supplied to the fabric until it is estimated that second degree burns of the skin behind the fabric would occur using the Stoll criterion. As a heat flux of 2 cal/cm^2·s (84 kW/m^2) is used, the rating is simply found by multiplying the time to exceed the Stoll criterion by two.

Different versions of this test use different methods of mounting the fabric specimen. ASTM D 4108[2] [29] lists some of the common variations used. The fabric can be unrestrained, or restrained through the use of weights, steel pins, or a restraining plate held in place by clamps. The mounting of the specimen has been shown to have a pronounced effect on test results [30]. The fabric can be separated from the sensor by an 1/4 in. (6.4 mm) air gap, or placed directly in contact with the sensor. Quantifying the energy transfer across this air space was one of the focal points of the research described in this thesis and is described further in the next few chapters. Multiple layers of fabrics can also be tested.

Other similar tests include ISO 9151 [31], which uses a slightly different copper test sensor design from ASTM D 4108, which will be discussed further in Section 4.2.2. In this test fabrics are rated on the basis of the time required for the temperature of the copper disk to rise by 24°C, rather than an estimated time to a second degree burn. The Canadian test [32] includes pins which hold the fabric in place, thus partially testing the fabric's mechanical integrity during the exposure to the flame. A similar test to ASTM D 4108 for a different thermal hazard is NFPA 1971 [33] which uses a combination of a burner and a radiant source to provide the specified heat flux.

These test methods are relatively straight-forward, and can be performed very inexpensively. The analysis of data is fairly simple. Tests which use a convective heat source require no specialized equipment. However, there are some shortcomings to existing bench top test methods. For example, these tests are based on planar geometry, rather than the complex three-dimensional geometry of the body. The mechanical integrity of the fabric is not tested either during or after the exposure in some versions of the TPP test (it is indirectly tested in versions of the test where the fabric is restrained). The nature of the test exposure may be different from that of an actual flash fire. No information on deeper skin burn damage is provided by the tests. In order to address these and other concerns, these existing test methods could be modified in various ways. Several modifications which may address the above and other concerns will be discussed in Chapters 4 and 5.

---

[2] D 4108 was not reapproved in 1995

1.4.3 Mannequin Testing

In order to test protective clothing under more realistic conditions, non-instrumented and instrumented mannequins have been used. By using mannequins, the performance of the entire garment subject to simulated accidents can be evaluated, rather than just the performance of the fabric which makes up the garment. Factors such as the location of closures, finishes, and fit of the garment can then be studied. However, very few of these facilities exist and these tests remain expensive and time consuming.

Rather than using a copper disk test sensor and the Stoll criterion, most modern thermal mannequins use skin simulant heat flux sensors and specialized software to predict the resulting heat transfer in human skin. Skin simulants are materials whose combination of thermal properties is such that the heat transfer in these materials will be similar to the expected heat transfer in human skin. Skin simulants and the analysis of their data will be discussed in more detail in Sections 4.2.2 and 4.3.2. Henriques burn integral is then used to make skin burn predictions. This provides information on deeper third degree burn injuries in addition to the information on second degree burns provided by existing bench top tests.

Thermal mannequins have become progressively more complicated. In the 1940's non-instrumented mannequins were used to observe garment burning behaviour (e.g. the rate and pattern of flame spread), the self-extinguishment process, and the garment area consumed in burning of shirts for forensic purposes [34]. Garments were also tested on wire frame body forms. In 1962, Stoll conducted tests for the United States Navy using leather-covered mannequins equipped with temperature detector paper and melting point indicators [35]. This was the first of many instrumented mannequins. Mannequins which are used to test garments under flash fire conditions include Thermo-Man®, Pyro-man®, and Harry Burns.

Thermo-Man® was first developed by the Aerotherm Division of the Acurex Corporation for the United States Military for testing flight suits in JP-4 fuel fires [36]. It was later purchased by E.I. du Pont de Nemours and Company, who altered its data acquisition system and registered the trade name Thermo-Man®. There are now Thermo-Men at the company's facilities in Wilmington, Delaware and Geneva, Switzerland. A similar mannequin, Pyro-man®, is used for research at North Carolina State University. Propane torches are used to simulate accident scenarios, and a data acquisition system takes information from sensors located over the surface of the mannequin and converts these sets of data into burn predictions for the portion of the body around that sensor. From this information, the percentages of body surface area which receive second and third degree burns can be determined. A Thermo-Leg system has also been developed in conjunction with these mannequins [37]. This system allows the testing of garments under dynamic conditions similar to a worker escaping a flash fire.

"Harry Burns" is a male, size 40 regular, thermally instrumented mannequin, similar to Thermo-Man®, which is used to test flame-resistant clothing in simulated flash fire conditions [38]. Twelve propane diffusion flames are used to simulate flash fire conditions. The information from 110 skin simulant sensors is used to compute the percentages of the body which would experience second and third degree burns using a finite difference computer code.

1.5 Fabric/Skin Heat and Mass Transfer Models

Many investigators have developed analytical or numerical models of the heat and mass transfer in fabrics and underlying skin under different conditions. Many of these models are used in the study of human comfort under normal every-day conditions such as those found in the home or workplace. This particular study is however concerned with heat transfer through inherently flame resistant fabrics under suddenly applied intense heat fluxes. It is expected that models of fabrics under these conditions will be quite different from those for comfort conditions. Therefore, this particular review is limited to models of fabrics under high heat flux exposures such as flash fires or pool fires. A review of some of the work done for comfort and other conditions can be found in Ukponmwan [39]. A review of skin models for high heat flux conditions can be found in the author's previous work [2], and [40].

1.5.1 Chen

Chen [41] developed models of one-dimensional heat transfer through clothing systems consisting of a dry or moist diathermanous fabric, an air gap, and skin exposed to a constant, purely infrared radiant heat source. Predictions made by these models were compared with measured surface temperatures of copper-air skin simulants mounted small distances (e.g. 0.08 - 0.38 mm) behind fabrics irradiated in a solar furnace. The fabric-air gap-skin simulant system was mounted in a vertical orientation. No measurements of fabric temperatures were made as it was thought to be difficult to define the exact location of the "surfaces" of the fabric. Low to medium intensity (less than 4 cal/cm^2·s (168 kW/m^2)) exposures were used, so as to avoid having to model thermochemical effects, such as charring. The predictions made using the dry fabric model were reasonably accurate, assuming that the appropriate thermal physical and optical properties were known.

Chen found that in higher intensity exposures (for the ranges of heat fluxes he used), moisture in the cloth vapourized when heated, and that part of it recondensed on the skin surface. This raised skin temperatures at the beginning of the exposure. In lower intensity exposures, the moisture acted as a heat sink, dissipating part of the incident energy. He modelled the moist fabric using the partial differential equations based on energy and mass balances, and the vapour-liquid equilibrium equation. Moisture transfer by diffusion and bulk flow of vapour were considered, but not diffusion on the fabric surface or through pores in the fibres. The general model included several new nondimensional groups, which accounted for the initial moisture content of the fabric, gas diffusivity, and mass transfer coefficients across the air gap at the front of the fabric. Other groups were used to describe the water vapour pressure curve, fabric moisture content as a function of relative humidity and temperature, and a workable recondensation mechanism.

Chen then assumed that moisture transfer was by diffusion only, and also neglected the sensible heat of the vapour phase in the energy balance. This simplified "engineering" model involved twelve dimensionless groups. A corresponding numerical solution was presented. Skin simulant temperatures were predicted reasonably well using this model for low to medium intensity exposures.

It should be noted that Chen's model did not look at air spaces of the order of those found in bench top tests (e.g. 1/4 in. (6.4 mm)). A single constant overall heat transfer coefficient was used to represent the energy transfers across air spaces in his model. Constant fabric thermal properties were also used in the model, and thermochemical reactions were not included.

1.5.2 Stoll

Stoll's work related to skin burning has already been described in a previous section. Some of her other contributions will now be given. Her early work involved determining skin pain threshold temperatures, and constants for use in Henriques burn integral (Equation (1.2)). Stoll then went on to look at the thermal protection offered by fabrics to skin.

Along with her co-workers Chianta and Munroe [42], she determined the destruction temperature and heat transfer resistance of fabrics using an experimental apparatus for flame contact studies, which eventually led to the development of the previously described TPP test. The insulating effects of air spaces between fabric layers were investigated in order to better explain the performance of multiple layers in fabric tests. This and similar work by others will be described in detail in Section 2.4.1. A simple model of a fabric layer in perfect contact with the skin was developed based on an analytical solution presented by Griffith and Horton [43]. Results from this model were found to be within four percent of experimental results for an assembly of silicon rubber on a skin simulant, after an error in the original derivation of the analytical solution was corrected. However, it was felt that the error would be larger if this analytical model was used in practical situations with their inhomogeneities (e.g. non-homogeneous fabrics, non-constant surface heat fluxes).

Later Stoll and Chianta [44] used Griffith and Horton's critical thickness concept (the thickness of the top layer beyond which the bottom layer does not affect the temperatures in this top layer) to determine the minimum thickness of fabric required to limit the temperature rise in the bottom layer (skin) to a certain value for a given incident flux and exposure time. This critical thickness concept will be further investigated in Chapter 5. They also applied a rectangular pulse of heat and measured the heat passing through the fabric to a skin simulant in order to compare the temperature-time history in the simulant with those for pain and blistering in human skin so as to determine the protective value of individual fabric specimens [12].

1.5.3 Government Industry Research Committee on Fabric Flammability

The Government Industry Research Committee on Fabric Flammability involved four research groups: the Factory Mutual Research Corporation, the Mechanical Engineering Department of the Georgia Institute of Technology, the Gillette Research Institute, and the Massachusetts Institute of Technology (M.I.T.) Department of Chemical Engineering's Fuels Research Laboratory. An overview of the program was written by the Mechanical Engineering Department at M.I.T. [45]. Studies conducted included the following.

- relating the properties of fabrics to their flammability
- determining the probability of ignition of a fabric, given a specific thermal exposure
- examining the ignition and propagation of flames on the fabric, and the resulting heat flux and damage to the skin below. This included examining the effects of fabric weight, orientation, and fabric/body spacing on garments burned on a test mannequin.

This work was primarily concerned with flammable fabrics, some of which were ignited at an edge, rather than energy transfers through flame resistant fabrics. Various methods were used to model the thermal response of these fabrics, with particular emphasis on the prediction of their ignition times. Some information was also given on the magnitudes of the various modes of energy transfer from burning fabrics to skin for various fabric/skin spacings and orientations. The latter information will be discussed in Section 2.4.1.

1.5.4 Aerotherm

In the early 1970's, Howard Morse [46] and his colleagues at the Aerotherm Division of the Acurex Corporation conducted a theoretical and experimental study into the thermal response of clothing covered skin subjected to a JP-4 fuel fire. This research was done in conjunction with the development of the company's thermal mannequin (see Section 1.4.3). Morse and his co-workers were interested in determining the properties or qualities required for good protective clothing, and in evaluating three materials (Nomex®, PBI, and stabilized PBI) for use in air force flight suits.

At the same time, ablation heat shields were being designed for space capsules. One of the charring ablation models used to design these heat shields was modified in order to treat high-performance fabrics. This model of the fabric-skin system included the effects of the following:

- conduction and radiation within and between fabric layers and the skin
- mass losses from fabrics due to pyrolysis
- vapourization of moisture from the fabric and subsequent condensation of water vapour (or other condensible vapours) on the skin
- variations in fabric-fabric and fabric-skin air gaps due to fabric shrinkage
- thermochemical reactions between pyrolysis gases and the environment. Arrhnenius rate equations were used to determine the mass losses and this information was combined with information on the energies associated with the reactions in the energy balances for the fabric. This enabled the model to predict the ignition of fabrics
- variations in fabric properties with temperature
- radiation and convection heat transfer between the system and its surroundings

An one-dimensional finite difference computer code was developed based on the energy balances in the analytical model. Results of a study into the characteristics of JP-4 pool fires were used to determine the appropriate surface boundary conditions for the system. The heat flux from this hazard was found to be approximately 20% convective and 80% radiative.

This model was said to be the first attempt to predict the pyrolysis, ignition, and combustion of fabrics from first principles. It was coupled to a skin burn model based on Henriques burn integral. The model was used, along with laboratory work, to determine the importance of various fabric properties in thermal protective clothing, to study the relative importance of different heat and mass transfer modes, and to test the performance of the three candidate materials.

It was found that the most important fabric characteristics were the dimensional, structural, and thermochemical stabilities. Fabric optical properties were also very important, especially in radiation-dominated exposures such as the pool fire considered here. Thermal properties such as fabric density, specific heat, thermal conductivity, and thickness were of lesser importance. The presence and maintenance of air gaps was very important in providing protection from thermal hazards.

Moisture transfer to, and condensation on, the skin surface is possible, and may represent a significant amount of heat transfer to the skin. However, as the dynamic pressure across a fabric during an exposure and the internal pressures developed by the evaporation of moisture were shown to be similar in magnitude, no conclusions were drawn as to whether most of the moisture will flow towards the skin or the fabric surface during an exposure. It should be noted that these conclusions were for a JP-4 fuel fire and may not be representative of other accidents, such as flash fires.

The relative rankings of the performance of the three candidate materials were the same using either the numerical or experimental results. The researchers felt that there was good agreement between the analytical and experimental results. However, some of the properties that were used in their model were determined by fitting the results of the model to experimental results. For some of the fabrics considered, this still resulted in differences of about 100°C at times.

1.5.5 Barker

Other work of interest in this area has been performed by R.L. Barker and his graduate students at North Carolina State University. Shalev and Barker [47,48] did work to further understand the thermal response of fabrics during bench top tests. They stated that the characteristic nonlinear calorimetric traces in bench top tests can be explained by changes in fabric thermal physical properties throughout the exposure. By running these tests, and stopping them at predetermined increments (0.5 s), changes in fabric thermal and spatial properties during the tests due to pyrolysis, char formation, and shrinkage could be observed.

It was found that basic thermal physical properties changed greatly during TPP exposures. Retention of thermal properties, and not the initial values of these properties was said to determine the heat transfer in these exposures. The polymer to air ratio of the fabric, and the maintenance of its air volume were found to be key to good thermal performance. Air and fibre conduction were found to dominate in this type of exposure; as the fabrics were relatively opaque, direct radiation transmission was not as important. As there was no correlation between bench top test results and air permeability, hot gases did not appear to blow through the fabric, as is often assumed. The ability of a fabric to maintain a profusion of surface fibres was said to be very important in convective exposures, as these were thought to serve as a baffle, which extends the still air boundary layer on the fabric, and increases the effective heat transfer resistance. At these heat flux levels, the specific fibres used had a significant effect on the heat transfer through fabrics. This is unlike lower heat flux levels (such as comfort conditions), where the fabric structure itself is the dominant factor, and the specific fibre type plays a minor role in determining the heat transfer through a fabric. Moisture was said to increase the volumetric heat capacity of a fabric and to also provide an ablative effect, which further increased the thermal protective performance of a fabric. The effects of different thermal properties, including moisture regain, on the thermal response of the fabric and bench top test results will be discussed further in Chapter 3.

The above findings were for a bench top test using a heat source which was 50% convection and 50% radiation. Lee and Barker [49,50] ran bench top tests for single layers of fabrics using combinations of three heat flux levels (0.48 cal/cm^2·s (20 kW/m^2), 1 cal/cm^2·s (42 kW/m^2), and (2 cal/cm^2·s (84 kW/m^2)), and three radiation and convection heat flux compositions (30% radiation and 70% convection, 50% radiation and 50% convection, and 100% radiation and 0% convection). For all fabrics the times required to exceed the Stoll criterion were lowest for the 100% radiation and 0% convection exposure. Except for the 0.48 kW/m^2 exposures, the fabrics insulated best against a 50% radiation and 50% convection exposure. This was said to be partly due to the role of surface fibres, as explained earlier, as well as other factors. In fact competitive comparisons between different fabrics changed depending on the test conditions used. Variations in thermal properties with time for different exposures were presented. Effects of the different test conditions and fabric properties on test results were also discussed. Moisture in fabrics was found to be beneficial to bench top test results in some cases, and detrimental in others [50]. Lee and Barker also measured the temperatures of the front and back sides of the fabric during these exposures using fine gauge thermocouples. Fabric temperature measurements will be further discussed in Chapter 4.

1.5.6 Heat and Mass Transfer Models of Other High Temperature Materials

Like Aerotherm's charring ablator model discussed previously, other models of high temperature materials may be of interest to investigators examining protective clothing for high heat flux exposures. For example NASA has spent considerable effort in designing thermal protective systems for the space shuttle (e.g. [51]). Others have modelled fire exposed composites [52], thin cellulosic materials in microgravity environments [53], and intumescent paint coatings designed to undergo endothermic chemical decomposition and thermochemical expansion in order to provide protection during a fire [54]. A good review of some other models of high temperature materials can be found in [52].

1.6 Overview of the Research in this Thesis

As seen by the above literature review, models of the thermal response of protective fabrics and other materials subjected to high heat flux conditions do exist. However, no model which successfully predicts the thermal response of a flame resistant fabric-air gap-test sensor arrangement during bench top tests has appeared. As will be seen later, these fabrics reach temperatures of many hundreds of degrees Celcius in a matter of seconds. Simple closed-form solutions do not include the variations in thermal properties which would occur over these temperature ranges. Even some of the more complicated models do not include the energies associated with thermochemical reactions which occur at these high temperatures. Other models rely simply on curve-fitting data from tests in order to obtain the energies associated with these reactions. This information is in turn used to predict the temperatures which were used in the original curve-fitting. However, even these models have not been overly successful. In addition, these complex models require the knowledge of the values of many thermal and thermochemical properties over wide ranges of temperatures. Determining this information for fabrics can be difficult and time-consuming. Many of the recent models for high temperatures materials are of interest, but most of these have been developed for longer term exposures of thicker materials rather than very short exposures of very thin fabrics.

Therefore, the goal of this work was to develop an improved model which can be used to predict the thermal response of inherently flame resistant fibrous materials under high heat flux conditions, as well as estimating the energy transfer between the fabric and a bench top test sensor mounted behind it. More specifically, the heat transfer in ASTM D 4108 standard bench top tests of two common inherently flame resistant fabrics, Kevlar®/PBI and Nomex® IIIA, was modelled. These tests used a heat flux of about 80 kW/m^2 and an air gap of 1/4 in. (6.4 mm) between the fabric and a copper calorimeter. This work will help to further the understanding of the thermal response of these materials, and the energy transfers between fabrics and skin or test sensors. The model can also serve as a useful design tool for protective fabrics, allowing the user to determine the effects of varying fabric parameters on the protection a fabric might offer in a flash fire. Besides these direct applications to thermal protective clothing, results of this work should also be useful in the study of other high temperature materials and energy transfers in enclosures.

The model will be described in Chapter 2. Numerical results from the model will be presented in Chapter 3. Included in these results are those from a parametric study (sensitivity study) which illustrate the effects of different fabric thermal properties on the predicted thermal response of the fabric and bench top test results. This information will help to increase the understanding of the roles of different fabric thermal properties on the thermal protection provided by these fabrics. It will also help to indicate where further work is required to better quantify relevant properties over the wide temperature ranges expected in these exposures.

Results from the model will be then be compared with results from actual bench top fabric tests, and videotaped observations, including a flow visualization study inside the air space between the fabric and test sensor. The experimental apparatus developed for this study was also used in a study of alternative small scale test methods for fabrics for flash fire protective clothing. All of this work will be discussed in Chapter 4.

The numerical and experimental results are compared in Chapter 5. Applications of these results to fabric design and test standards will also be discussed. Conclusions of the work described in this thesis, and suggested future work will be given in Chapter 6.

CHAPTER 2: HEAT TRANSFER MODEL

In this chapter the development of a model of the heat transfer in the protective fabric-air gap-test sensor system used in the ASTM D 4108 bench top test will be outlined. The use of one-dimensional planar bench top tests will first be justified. The treatment of the thermal response of the fabric and the energy transfers between the fabric and skin will then be discussed. The application of the finite element method to solve the resulting differential equations will be outlined. Results found using the numerical model will then be compared with those found using several closed form and numerical solutions in order to validate the model.

2.1 Effects of the Geometry of the Human Body on Heat Transfer in Fabric Tests

Existing bench scale fabric tests utilize a planar geometry. Numerical models used to analyze data from thermal mannequin tests assume that the heat transfer inside human skin can be treated as one-dimensional. The human body, on the other hand, exhibits a complex geometry. Therefore, it is important to determine how closely planar fabric tests and one-dimensional heat transfer models represent the heat transfer in the human body. If the planar geometry is not adequate, a more complex test geometry, such as a fabric covered cylinder, may be necessary. More complex heat transfer models of the skin would also be necessary for use with thermal mannequins.

Numerical heat transfer models which treat the skin as either a slab or a cylinder were developed to determine the effect of these geometries on burn predictions under conditions indicative of flash fires. The models assume that the heat flux incident on the skin will be constant over the surfaces of the cylinder and slab, and will be of the same intensity in each case. Details of this work are given in Appendix 1. The differences between the burn predictions made using the two geometries were less than 3% (Table A1.1 in Appendix 1). This indicates that one-dimensional models of the heat transfer in human skin are adequate for mannequin testing. It also indicates that from the heat transfer perspective, the planar geometry used in existing bench top tests is an adequate representation of the more complex geometry of the human body. Therefore, a numerical model of the planar ASTM D 4108 test apparatus will be developed here, rather than that of a more complex test geometry, such as a fabric covered cylinder.

It should be noted that this particular analysis was limited to the heat transfer in human skin under certain assumptions. No attempts were made to determine the effects of the two geometries on aspects of the thermal response of fabrics, such as thermal shrinkage. In addition the value of the heat flux incident on the surface of the skin was assumed to be the same for each geometry. No attempts were made to determine whether the two geometries affect the energy transfers between fabrics and human skin or test sensors differently. If any of these effects are significant, the development of small scale tests such as fabric covered cylinders may be necessary. This and other recommended future work will be discussed in Chapter 6.

2.2 Fabric-Air Gap-Test Sensor System

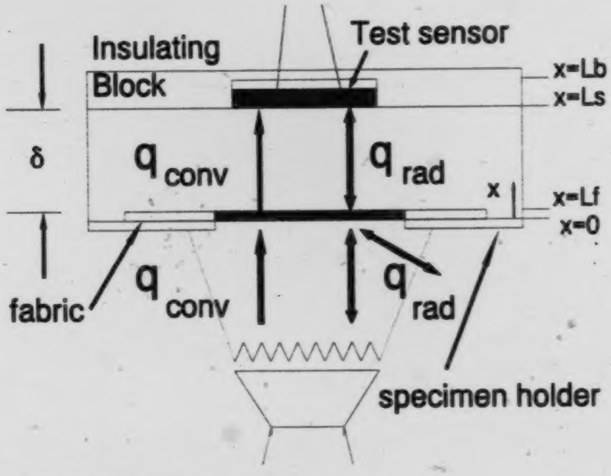

Figure 2.1 Fabric-Air Gap-Test Sensor System

The fabric-air gap-test sensor system used in ASTM D 4108 and other bench top tests and studied here is shown in Figure 2.1. It consists of a flame resistant fabric subjected to a convective and radiative heat flux from a Meker burner below on part of its surface, a test sensor behind the fabric, and an enclosed air space between the fabric and the test sensor. The convective heat fluxes from the hot gases from the burner to the fabric and from the fabric to the test sensor are indicated in the figure by q_{conv}, while the net heat fluxes due to thermal radiation exchanges between the burner head, fabric and ambient, and between the fabric and test sensor are indicated by q_{rad}. The cross section of the apparatus is 150 by 150 mm. The fabric specimen is 100 by 100 mm, while the portion of the fabric specimen which is heated is 50 by 50 mm. The width of the air gap is of the order of 6 mm in standard bench top tests. More details about this particular apparatus will be given in Chapter 4.

A model could also be developed for the case of a fabric-air gap-human skin system. This would be different in that the fabric might be completely heated on its surface rather than only partially heated. The skin would also cover the entire surface behind the fabric, rather than just a portion of it, such as in the bench top test. The bench top test apparatus includes a horizontal enclosure locally heated from below, whereas a fabric-air gap-skin system may form a vertical enclosure heated from the side. While the theory outlined in this chapter is for the test shown in Figure 2.1, it could easily be adapted so as to allow the model to examine fabric-air gap-skin systems in this or other orientations.

It will be seen throughout the next two chapters that representing the precise thermal response of the fabric is very difficult. The goal of this work was to estimate the thermal response of the fabric and the energy transfer between the heated fabric and the bench top test sensor. The temperatures of the fabric will only be measured at certain locations to validate the results of the model. The copper disk test sensor only records an average temperature of the entire copper disk. Hence, even if detailed temperature distributions are determined for the fabric, air gap, and test sensor, it will be difficult to validate these. Therefore, in order to make the problem manageable, heat transfer in the fabric-air gap-test sensor system was assumed to be one-dimensional. The fabric was treated as a slab with thermal properties which represent average values of the thermal properties of the more complex fibrous structure. The fabric was treated as a grey body. Mass transfer was also neglected. These assumptions resulted in a model which is relatively simple, yet, as will be shown in the next few chapters, does a reasonably good job in predicting the thermal response of the fabric and the energy transfer between the fabric and the copper disk. The implications of some of these assumptions will be discussed in Chapter 5.

A volumetric element of the fabric is shown in Figure 2.2.

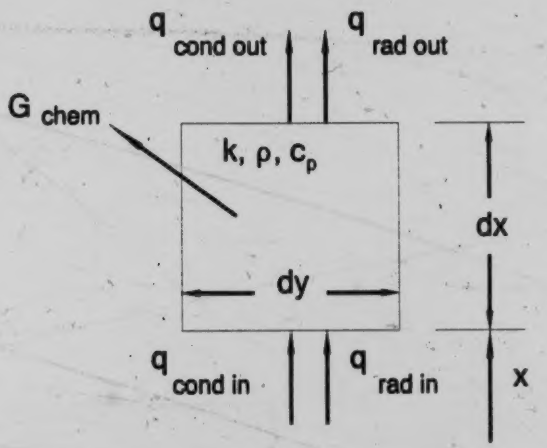

Figure 2.2 Elemental Volume for Heat Transfer Analysis of Fabric Including Energy Transfers by Conduction (cond), Radiation (rad), and Energy Generated Within the Element (G)

In addition to the assumptions discussed above, the heat flux was assumed to be uniform over the heated portion of the fabric. The convective portion of the flux transfers energy to the surface of the fabric, while the radiative portion can penetrate the fabric to a certain depth, depending on the fibrous structure of the fabric. Thermochemical reactions are possible at the temperatures expected in the fabric. The thermal properties of the fabric were taken to be functions of temperature only. Mass transfer was also neglected. Under these assumptions, an energy balance on an infinitesimal element of fabric produces the following differential equation.

$$\rho(T)c_p(T)\frac{\partial T}{\partial t} = \frac{\partial}{\partial x}\left(k(T)\frac{\partial T}{\partial x}\right) - \frac{\partial}{\partial x}\left(q_{rad}\right) + G_{chem} \tag{2.1}$$

where: q_{rad} is the portion of the directly transmitted incident heat flux on the surface of the element due to thermal radiation from the heat source

G_{chem} is the energy generated by thermochemical reactions in the fabric per unit volume, and

ρ, c_p, k, T, and x have their usual meanings.

The boundary conditions are:

at the heated surface (x = 0), for t> 0

$$-k(T)\,\frac{\partial T}{\partial x} = q_{conv} \tag{2.2}$$

where

q_{conv} is the convective portion of the incident heat flux

and at the inner boundary of the fabric (x = L_f), for t > 0

$$-k\,(T)\,\frac{\partial T}{\partial x} = q_{air\ rad} + q_{air\ cond/conv} \tag{2.3}$$

where

$q_{air\ rad}$ is the energy transfer by radiation from the fabric to the skin/test sensor across the air gap, and

$q_{air\ cond/conv}$ is the energy transfer by conduction and convection from the fabric to the test sensor across the air gap

For the test sensor the differential equation is (assuming that the thermal properties do not change much over the limited temperature ranges expected in the sensor)

$$\rho c\,\frac{\partial T}{\partial t} = k\,\frac{\partial^2 T}{\partial x^2} \tag{2.4}$$

The boundary conditions are
at the front surface of the test sensor ($x = L_s$), for $t > 0$

$$-k \frac{\partial T}{\partial x} = q_{air\ rad} + q_{air\ cond/conv} \tag{2.5}$$

and at the base of the air space inside the insulating block immediately behind the test sensor ($x = L_b$) (see Section 2.5), for $t > 0$

$$T = T_{amb} \tag{2.6}$$

where T_{amb} is the ambient temperature, taken as 300 K.

The initial condition is a given temperature distribution, $T_i(x)$ at time zero.

$$T(x, t=0) = T_i(x) \tag{2.7}$$

Here it was assumed that the fabric is initially at a uniform temperature of 40°C, while the copper disk is initially at 30°C. This slight difference in initial temperatures was necessary to avoid singularities in the calculation of the Rayleigh number (discussed in Section 2.4.2) for the air gap between the fabric and copper disk at the first time step. The temperature gradient in the air gap was assumed to be initially linear between these two temperatures.

Details about the treatment of the thermal response of the fabric, the energy transfers across the air gap, and the heat transfer in the test sensor will now be discussed in turn below.

2.3 Thermal Response of Fabric

There are several interesting aspects to the treatment of the thermal response of the fabric, namely the energy generation term due to thermochemical reactions which occur as the fabric is heated, the in-depth absorption of the incident radiation from the heat source, and the boundary condition on the front surface of the fabric. These are discussed in turn below.

2.3.1 Thermochemical Reactions

Heat transfer problems involving thermochemical reactions can be treated using similar methods to those used to treat problems involving phase changes (e.g. freezing and melting). Huang and Usmani [55] give a good review of methods used in finite element models to treat phase change problems. Basically the methods fall into two categories.

> Front-tracking (or two-domain) methods treat the two phases separately and determine the location of the moving boundary between the phases explicitly. Mathematically, these methods solve the appropriate equations in their strong form, that is, their solution satisfies the differential equations at any point in the domain of interest. However, these methods are very difficult to use in cases where phase changes occur over a range of temperatures. In addition, knowledge of the particular location of the boundary between the phases is not always important in some problems such as those under consideration.
>
> Fixed grid (or one-domain) methods, on the other hand, represent the phase change implicitly, treating the two phases as a continuous system. Therefore these methods provide no information about the location of the boundary between the two phases. Mathematically these methods are based on solving the appropriate equations in their weak form (i.e. their solution satisfies the differential equations only at certain discrete points in the domain of interest). These methods can handle phase changes which occur over a range of temperatures, and can handle phase boundaries with complex shapes.

A fixed grid method will be used here. The particular location of the boundary between the two phases - the virgin material and the material which has undergone thermochemical reaction(s) is not of particular interest here. Even if it was of interest to predict this for the idealized homogeneous slab said to represent the fabric, it is uncertain as to how this location could be verified in the actual fibrous material being studied. In addition thermochemical reactions take place over finite temperature ranges rather than at one particular temperature. The particular formulation used in the fixed grid method is called the enthalpy formulation. First let H be the enthalpy function defined by:

$$
\begin{aligned}
H(T) &= \int_{T_r}^{T} \rho c_s(T)\, dT && T < T_m \\
&= \int_{T_r}^{T_m} \rho c_s(T)\, dT + \int_{T_m}^{T} \left(\rho \frac{\partial L}{\partial T} + \rho c_m(T) \right) dT && T_m \le T \le T_l \\
&= \int_{T_r}^{T_m} \rho c_s(T)\, dT + \rho L \\
&\quad + \int_{T_m}^{T_l} \rho c_m(T)\, dT + \int_{T_l}^{T} \rho c_l(T)\, dT && T > T_l
\end{aligned}
\tag{2.8}
$$

where:

T_r	is some reference temperature, less than T_m
T_m	is the temperature at the beginning of the range in which the phase change takes place
T_l	is the temperature at the end of the range in which the phase change takes place
L	is the latent heat for the phase change of interest

and the subscripts s, m, and l refer to the values of the thermal properties in the material before the phase change takes place, while the phase change is taking place, and after the phase change has taken place.

If the two phases were treated separately, the Fourier field equation would need to be solved for each of the two phases simultaneously, with the two equations linked with the equations for continuity of temperature at the boundary between the phases and conservation of energy at the boundary between the phases

$$k_s \frac{\partial T_s}{\partial x} - k_l \frac{\partial T_l}{\partial x} = \rho \, L \, \frac{\partial S}{\partial t} \tag{2.9}$$

where: S is the location of the boundary between the phases at the time of interest

It can be shown that when Equation (2.8) is substituted into the Fourier field equations for the two phases, continuity of temperature at the boundaries, and Equation (2.9), the following differential equation results for $t > 0$, $0 \leq x \leq L$

$$\frac{\partial H}{\partial t} = \frac{\partial}{\partial x} \left(k \frac{\partial T}{\partial x} \right) \tag{2.10}$$

where H is the enthalpy function defined earlier in Equation (2.8). This is known as the basic enthalpy formulation.

Huang and Usmani [55] discuss the advantages and disadvantages of three common methods used to implement the enthalpy formulation. These are

- apparent (or effective) heat capacity method
- enthalpy method
- heat source method

The apparent heat capacity method was chosen for this model. It is very easy to implement in finite element and other numerical routines, as the enthalpy function is not present explicitly in the appropriate differential equations. Therefore these equations will be the same as for a problem without phase changes, allowing existing numerical routines to be utilized [56]. The only modification which is necessary is to add a subroutine to calculate values of the apparent heat capacity as a function of temperature. The main disadvantage of the apparent heat capacity method is that small time steps and element sizes are necessary, so that the temperature ranges over which phase changes occur are not "skipped over" as the solution marches on in time and space. As the fabrics of interest here are thin (generally less than 1 mm), and the times of flame exposure are short (10 s), using small element sizes and time steps will not be problematic. Any increases in computation time will be acceptable in light of the savings in program development time, since existing finite element programs can be used with minimal changes. In addition, as will be discussed in Chapter 3, additional efforts to improve the representation of phase changes may not be justifiable in light of the limited accuracy to which thermal and thermochemical properties are known for this problem, and the effects of these values on the numerical results. For problems in which larger time duration exposures are studied, Yao and Chait [56] have presented a version of the apparent heat capacity method which allows larger time steps and coarser element sizes. In addition, the other two enthalpy formulation methods, especially the heat source method could also be used. One other reference of note is Fanucci [57] who used the apparent heat capacity method to model Kevlar® and graphite/epoxy composites under simulated nuclear weapon or laser exposures. The method was used to successfully model rates of increase of temperatures which were similar to those expected in the fabrics studied here.

The apparent heat capacity method utilizes Equation (2.10) by defining an apparent heat capacity as

$$C^{\wedge}(T) \equiv \frac{\partial H(T)}{\partial T} \tag{2.11}$$

substituting (2.11) into (2.10) produces

$$C^{\wedge}(T)\,\frac{\partial T}{\partial t} = \frac{\partial}{\partial x}\left(k(T)\,\frac{\partial T}{\partial x} \right) \tag{2.12}$$

Equations (2.8) and (2.11) give the definition of the apparent heat capacity

$$\begin{aligned} C^{\wedge}(T) &= \rho c_s(T) \qquad T < T_m \\ &= \rho c_m(T) + \frac{\rho L}{T_l - T_m} \qquad T_m \le T \le T_l \\ &= \rho c_l(T) \qquad T > T_l \end{aligned} \tag{2.13}$$

This apparent heat capacity formulation will be used to simplify Equation (2.1). The particular equations used to represent the apparent heat capacity in order to model the thermochemical reactions for the Nomex® IIIA and Kevlar®/PBI fabric specimens will be discussed in Section 3.2.5. It should also be noted that in this particular problem, mass transfer has been neglected. Therefore, this analysis and the resulting numerical model do not include the effects of energy transfers by water vapour or thermal decomposition products, which can occur at the elevated fabric temperatures expected in bench top tests.

2.3.2 Treatment of In-Depth Absorption of Incident Radiation

While an impinging flame is usually referred to as a convective heat source, a significant amount of energy is also transferred by thermal radiation because of the high temperatures of the flame. Correct treatment of the absorption of this radiation by a fibrous material will be very important in developing a model of the thermal response of a flame resistant fabric.

The literature is full of examples of models of heat transfer by thermal radiation in fibrous materials. For example in insulations for buildings, fibres are generally spaced randomly some distance apart and interactions between the fibres and the incident radiation and other fibres are very important. In textile science, there has been considerable work in the past decade or so in developing thin insulative layers for clothing, such as Thinsulite™, or other nonwoven fabrics for other applications. These materials use very fine fibres spaced in a random manner. Models which include the contributions of radiation to the heat transfer in these materials include those developed by Farnworth [58], Stuart and Holcombe [59], and Woo, et al. [60].

In the particular protective fabrics studied here, bundles of fibres are twisted into yarns, which are then placed in somewhat regular patterns in fabrics, rather than a random orientation. The temperatures of interest here are also considerably different from those for human comfort. It will be shown in Chapter 4 that protective fabrics may reach temperatures of about 1000 K during bench top tests, while the temperatures of fabrics at comfort conditions will be about 300 K. Hence the wavelength distributions of the radiation will be considerably different in this problem from those in problems of human comfort. In addition, the fibre sizes in protective fabrics may be different from the fibre sizes in fabrics for human comfort or in insulating layers.

The model of the interaction between the fabric and the incident radiation was developed in stages. These stages are shown in Figure 2.3. First the interaction between the incident radiation of wavelength λ and the fibre of diameter D_f was considered (Figure 2.3a). Next the interaction between the incident radiation and collection of fibres in a yarn of diameter D_y was considered (Figure 2.3b). Finally the interaction between the radiation and the entire fabric structure was considered (Figure 2.3c). To simplify this analysis the fibres and yarns which make up the fabric structure were assumed to be grey bodies.

A measuring microscope was used to determine the order of magnitude of the size of the fibres, D_f, in the fabrics studied. It was found that the distances across the crosssection of the fibres were roughly of the order of 10 - 17 μm. This agrees with Futschik and Witte [61] who quote fibre diameters of 15 - 17 μm from Nomex® fibre technical literature. While these fibres are not necessarily circular in cross section, they were assumed to be so in order to simplify the analysis.

The flame temperature for the Meker burner was estimated to be of the order of 2000 K, and the total emissivity of the flame was estimated as 0.02 (Section 2.3.3). According to Gaydon [62], the majority of the radiation emitted by the flame is in the infrared region of the spectrum. The emission is mostly due to carbon dioxide and water vapour in the hot gases. The strongest absorption bands are those around 4.8 and 2.8 μm. Weaker bands are around 15, 6.7, and 2.0 μm.

It was first assumed that there are no interactions between a single fibre and its neighbours. Therefore independent scattering theory was used. First it was determined whether the fibre is much smaller, much larger, or of the same order of magnitude of size as the wavelengths of interest, as in the first two cases, certain simplifications can be made to the analysis. According to Hottel and Sarofim [63], if the ratio between the circumference of the particle and the wavelength of the incident radiation is greater than five, then particles of interest are considered to be large relative to the wavelength of radiation, allowing simplifications to the analysis. Taking 15 μm as a typical fibre diameter and using 4.8 μm, the longer of the wavelengths of the two main absorption

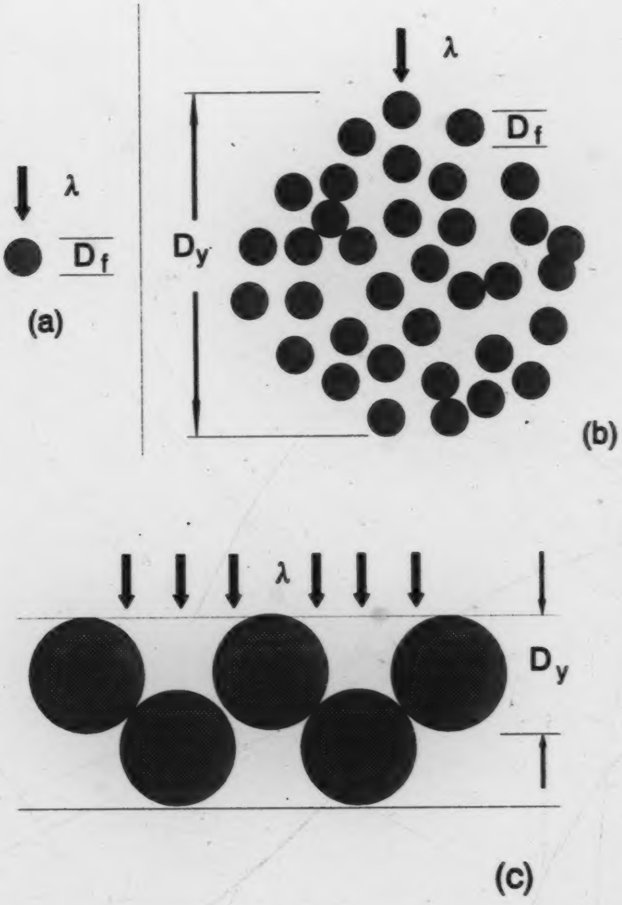

Figure 2.3 Models for the Interaction Between Incident Radiation and the Fibrous Structure a) Single Fibre, b) Collection of Fibres in One Yarn, c) Collection of Yarns (Perpendicular Fibres and Yarns Left Out for the Sake of Clarity)

bands, the ratio of the circumference to wavelength is

$$\frac{\pi\, D_f}{\lambda} = \frac{\pi\; 15}{4.8} \approx 10 \tag{2.14}$$

Therefore the fibres can be treated as being large with respect to the wavelengths of incident radiation. Hottel and Sarofim show that the absorption (K_a) and scattering coefficients (K_s) for this case are

$$K_a = \frac{\varepsilon A_t}{4} \tag{2.15}$$

$$K_s = \frac{\rho A_t}{4} \tag{2.16}$$

where: ε = the emissivity of the fibre

ρ = the reflectivity of the fibre

A_t = the total surface area per unit volume of a fibre

$= 4/D_f$

Using Equations (2.15) and (2.16), it can then be shown that the decay of radiation with depth is

$$\frac{q_{rad}(x)}{q_{rad}(0)} = \exp\left(-\frac{(\varepsilon + \rho)}{D_f}\, x\right) \tag{2.17}$$

This analysis includes only absorption and out-scatter, and does not consider in-scatter or emission. As other authors have estimated the emissivity of fibres to be of the order of 0.95 [60] scattering will be of less importance than absorption and emission. Exchange between the fibres themselves will be considered in the effective thermal conductivity of the fabric (Section 3.2.4). If it is assumed that $\varepsilon + \rho = 1$ then

$$\frac{q_{rad}(x)}{q_{rad}(0)} = \exp\left(-\frac{x}{D_f}\right) \tag{2.18}$$

Therefore, after a distance of one fibre diameter, only 37% of the incident radiation will continue to be transmitted. After a distance of two fibre diameters, only 14% will be continue to be transmitted, while after a distance of three fibre diameters, about 5% of the incident radiation has not been absorbed. Hence most of the incident radiation on one of the fibres of interest will be absorbed or scattered by that fibre.

The above analysis was for a single isolated fibre. In the fabric, fibres are twisted into yarns. In these particular protective fabrics, the fibres are tightly bunched with spaces of no more than about two fibre diameters in between. Most of the fibres are spaced even closer together. Van de Hulst [64] reports an estimate that a mutual distance between particles of at least three times their radius is sufficient in order to consider the scattering by the particles to be independent. In the yarns in the fabrics considered here, many of the spacings between fibres will be closer than this distance. Therefore, it is safe to assume that multiple scattering between the fibres will increase the amount of the incident radiation absorbed or scattered in a given distance over that predicted above using independent scattering theory. In addition, the order of magnitude of the diameters of the yarns was estimated to be 250-400 μm, while the nominal thicknesses of the fabrics in this study will be of the order of 1 mm. Therefore even if it does take up to a few fibre diameters to absorb or scatter the vast majority of the incident radiation, this distance (order of magnitude 3 x 15 = 45 μm) is relatively small compared with the diameter of a yarn, or the thickness of the fabric. Hence, each of the yarns will be treated as opaque, with any incident radiation hitting the surface of a yarn being absorbed in a very small distance from the surface of the yarn.

The protective fabrics considered here are tightly woven, with very few apparent air spaces between the yarns. To determine how tightly woven the fabrics were, the cover of these materials was determined. Cover is defined by Davis [65] as "the proportion of the space in a given area of fabric occupied by warp and filling yarns relative to the empty space". Two methods were used here to determine cover. In the first, a fabric specimen is placed on a microscope lit from below and the image from the microscope is sent to a computer equipped with a EIDETIC CRSIO Remote Sensing Image Analysis System[3]. The image of the fabric can be analyzed by determining how light a portion of this image must be before light is considered to penetrate the fabric at this point. Once a cut-off level has been established, the percentage of the fabric which is cover can be estimated by determining the percentage of the pixels in the image which are darker than this cut-off. The second method estimated the cover by measuring the amount of covered and open spaces in a given area in the fabric specimens using a measuring microscope. Further details about both of these methods can be found in Davis [65]. Both methods gave cover measurements of 93 - 100%. These measurements rely on visible light, which will be at shorter wavelengths than the infrared radiation from the Meker burner flame. This shorter wavelength light will penetrate further than the longer wavelengths of thermal radiation. Therefore, it can be assumed that based on these measurements practically no incident radiation from the flame will be directly transmitted through these particular fabrics.

---

[3] available from EIDETIC Digital Imaging Ltd., Brentwood Bay, B.C.

In order to determine how far incident radiation must travel to be absorbed, three simple models of the fabric structure were examined. These are shown in Figure 2.4. The first (Figure 2.4a) assumes that the fabric is a collection of yarns in contact with one another along the surface of the fabric. The second and third (Figures 2.4b and c) use a staggered arrangement of yarns. If it is assumed that radiation is absorbed once it contacts the yarn, the in-depth absorption of radiation can simply be described by the cross sectional area at any particular depth.

$$\frac{q_{rad}(x)}{q_{rad}(0)} = 1 - \frac{A_c(x)}{A_c(L)} \qquad (2.19)$$

where A_c is the cross sectional area of the yarns normal to the incident radiation. For a cylinder, the cross sectional area at any depth, x, from the tip of its diameter towards its centre on a straight line is proportional to (Figure 2.5)

$$A_c \propto \cos\left(\arc\sin\left(1 - \frac{p}{r}\right)\right) \qquad (2.20)$$

This relation can be utilized along with the position of the yarn(s) at any depth in the three models to predict the fraction of the incident radiation which will be absorbed at any depth. This information is shown in Figure 2.6 for the three models. Also included in Figure 2.6 are three curves which assume that the absorption of radiation in the fabric can be treated using Beer's law with transmissivities of 0.005, 0.01, and 0.05. These values were chosen as being representative of the fabrics of interest here, based on measurements described in Section 3.2.6.

As can be seen by Figure 2.6, the decay of the radiation using the area models is similar to the exponential decay described by Beer's law, other than in the portions of the fabric where there is no decay until the next yarn has yet to be encountered. There was good agreement between the fabric structure models and Beer's law in the upper and lower portions of the fabric. Recall that the simple yarn models do not include interactions between the yarns themselves, which will cause the radiation to decay even more at a given depth inside the fabric structure than predicted by the simple yarn models. Therefore, it was decided to simply model the in-depth absorption of radiation using Beer's Law with an extinction coefficient measured using transmissivity measurements in the infrared region. This will result in a simpler model which will only require the measurement of the transmissivity of the fabric, rather than knowledge of the full fabric structure. The implications of this model will be discussed in light of the numerical and experimental results in Chapters 3 and 5.

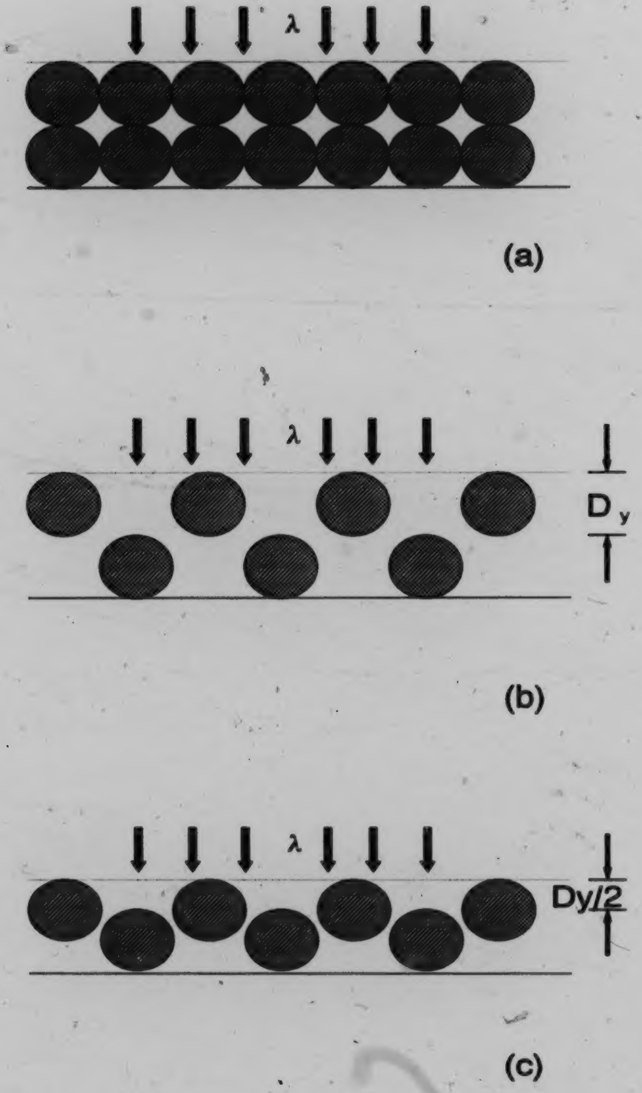

Figure 2.4 Three Representations of the Fabric Structure a) Single Yarn Model, b) Two Yarn, Two Layer Model, c) Two Yarn, Staggered Centres Model (Perpendicular Yarns Not Sketched for the Sake of Clarity)

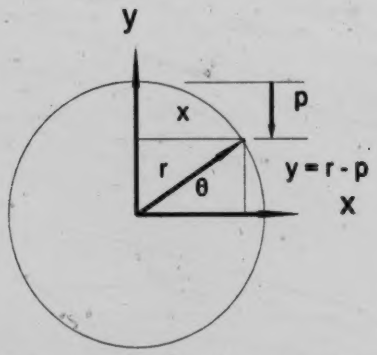

$$A_c \alpha \; r \cos \theta = r \cos (\arcsin ((r-p)/r)$$
$$= r \cos (\arcsin (1 - p/r)$$

Figure 2.5 Determining the Cross Sectional Area of a Yarn as a Function of Depth From Its Surface (p)

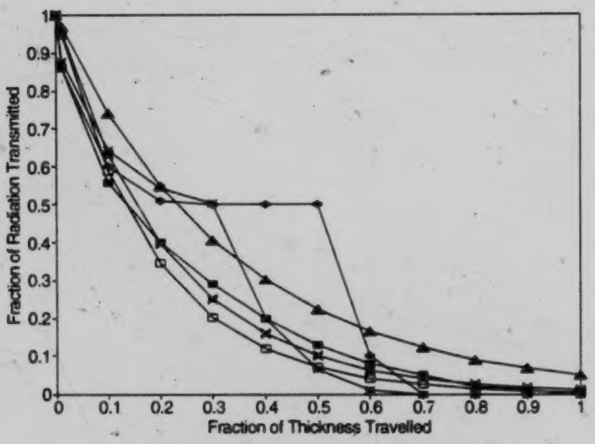

Figure 2.6 Absorption of Incident Radiation with Depth using Fabric Structure Models (■ Figure 2.4a, + Figure 2.4b, * Figure 2.4c) and Beer's Law for Transmissivities of 0.005 (□), 0.01 (X), and 0.05 (▲)

2.3.3 Boundary Condition on the Front of the Fabric

As shown in Figure 2.1 the flame will transfer heat to the fabric by convection and radiation during the exposure. Heat transfer by thermal radiation between the heated portion of the fabric and the burner head itself will occur. The heated portion of the fabric will also transfer heat to the ambient by thermal radiation. This particular model was only concerned with the heating of the fabric and not what happens after the exposure to the flame ends. This was because many of the thermal properties discussed in Chapter 3 were only determined during the heating of a fabric. If information was available, the model could be extended to handle the cooling of the fabric after the exposure ends.

Convection heat transfer will enter the differential equations as the boundary condition on the front of the fabric, given earlier as Equation (2.2). This can now be written as

$$-k(T)\left.\frac{\partial T}{\partial x}\right]_{x=0} = h_{fl}\,(T_g - T_{x=0}) \tag{2.21}$$

where the subscripts fl and g refer to the flame and the hot gases, respectively .

Radiation heat transfer will enter the differential equations through the term q_{rad} in Equation (2.1). This term can be written as

$$\begin{aligned} q_{rad} &= \sigma\varepsilon_g T_g^{\,4} - \sigma\varepsilon_{fab}F_{fab-amb}\,(1-\varepsilon_g)\,(T_{x=0}^{4} - T_{amb}^{4}) \\ &\quad - \frac{\sigma(T_{x=0}^{4} - T_{bh}^{4})}{\left(\dfrac{1-\varepsilon_{fab}}{\varepsilon_{fab}} + \dfrac{1}{F_{fab-bh}(1-\varepsilon_g)} + \dfrac{A_{fab}}{A_{bh}}\dfrac{(1-\varepsilon_{bh})}{\varepsilon_{bh}}\right)} \end{aligned} \tag{2.22}$$

where the subscripts g, fab, amb, and bh refer to the hot gases from the flame, the fabric, the ambient, and the burner head, respectively. The terms on the right hand side of Equation (2.22) represent radiation heat transfer from the hot gases, between the fabric and the ambient, and between the fabric and the burner head, respectively.

The view factors, $F_{fab-amb}$ and F_{fab-bh} for the radiation heat transfer between the fabric and the ambient and burner head, respectively, must now be determined. The heated portion of the fabric is about 50 by 50 mm. The burner head is approximately 40 mm in diameter. The view factor between two plane parallel surfaces, one of differential area and the other of finite area and circular shape is given by Jakob [66] as

$$F_{(d1)2} = \frac{1}{2}\left(1 - \frac{1 + C^2 - B^2}{\sqrt{C^4 + 2C^2(1 - B^2) + (1 + B^2)^2}}\right) \qquad (2.23)$$

where B = the ratio between the radius of the finite circular area and the distance between the two surfaces, and

C = the ratio between the distance from a point in the differential area to the central normal to the circular area, and the distance between the two surfaces (see Figure 31-3 in Jakob [66])

This can be numerically integrated (Gaussian quadratures were used here) to give the value of the view factor for particular values of the sizes of the square and circle, and the spacing between them. Representing the dimensions in the bench top test as a square with 50 mm sides, a 40 mm diameter circle, and a spacing of 50 mm between them, the view factor from the square to the circle is 0.11. Assuming that the fabric only emits radiation to the burner head and the ambient, the view factor from the fabric to the ambient is simply 1 - 0.11 = 0.89.

An estimate of the temperature of the hot gases and their emissivity was also required. Originally it was thought that the temperature of the hot gases could be measured using a thermocouple. However this is very difficult to do. Other methods such as sodium line reversal could also be used. However, it was decided to instead estimate the flame temperature and then determine the effect of varying this parameter during the sensitivity study, discussed in Chapter 3. If the propane is assumed to react with stoichiometric air, then the overall chemical reaction for complete combustion can be written as

$$C_3H_8 + 5\ O_2 + 5(3.76)\ N_2 \rightarrow 3\ CO_2 + 4\ H_2O + 5(3.76)\ N_2 \qquad (2.24)$$

Adiabatic flame temperatures of about 2400 and 2270 K were calculated using STANJAN[4] with and without dissociation, respectively. The adiabatic flame temperature is the maximum possible temperature for this flame. Actual flames will be cooler than this, due to heat transfer from the flame and incomplete combustion. Experimental values of about 2200 K have been reported by Siegel and Howell [67]. Maximum flame temperatures measured in laboratory burners using methane have been shown to be of the order of 2000 to 2100 K by Lewis and von Elbe [68]. It was therefore decided to assume that the flame temperature was 2000 K. This should account for heat transfer from the flame, incomplete combustion, and the extra dilution of the hot gases by the surrounding air. Assuming stoichiometric conditions and a total pressure of 1 atm, and determining the partial pressures of water and carbon dioxide using Equation (2.24), the emissivity of the flame was estimated using the charts given in Hottel and Sarofim [63] and an estimate of the mean beam length of the hot gases using the 50 mm distance between the burner head and the fabric. A value of about 0.02 at a temperature of 2000 K was obtained. Using this emissivity and temperature, the radiation emitted by the flame would be about 18 kW/m^2, which is about 23% of the nominal 80 kW/m^2 heat flux used in bench top tests. This percentage of radiation heat flux to total heat flux agrees with the measurements of Holcombe and Hoschke [4] who reported that approximately 25% of the energy released by a Meker burner was thermal radiation (although it was not specified whether or not they used propane in their Meker burner), and Shalev [48], who found that a Meker burner using propane produced a heat flux which was approximately 70% convective and 30% radiative.

The convective heat transfer coefficient could be determined by looking at convective heat transfer coefficients for impinging jets presented by Martin [69]. However this information is for impinging jets with larger Reynolds numbers than those estimated for the flow of hot gases from the Meker burner. Therefore, it was decided to estimate the convective heat transfer coefficient by subtracting the radiative flux calculated above from the nominal heat flux from the flame. A heat flux of 82 kW/m^2 was used in the experimental work described in Chapter 4. This heat flux is determined by the rate of temperature increase in a 18.0 g bare copper disk test sensor measured during a 10 s flame exposure. Using the thermal properties of this copper disk sensor, a heat flux of 82 kW/m^2 should produce a temperature rise of about 15°C/s. In the case of the copper disk, there will be no direct transmission of radiation. Therefore the q_{rad} term given by Equation (2.22) is included in the surface boundary condition given in Equation (2.21). Substituting the copper disk temperature rise and the flame temperature and emissivity discussed above into Equations (2.21) and (2.22), it was found that a convective heat transfer coefficient of 40 W/m^2·°C gave an average heat flux over the 10 s exposure of 82.5 kW/m^2. In order to determine if this calculated value was of the correct order of magnitude, rough estimates of the flow of propane to the burner, the air/fuel ratio in the burner, the volumetric expansion across the burner, and the air entrainment in the flame were made. Extrapolating the information in Martin [69] for impinging jets to treat the above data, it was estimated that the convective heat transfer coefficient was of the same order of magnitude as calculated above. Therefore, the convective heat transfer coefficient calculated here can be used with some confidence. As with the other parameters, the numerical model will be used to perform a parametric study to determine the effects of varying the convective heat transfer coefficient on the final results. This will be discussed in Chapter 3.

---

[4] available from Stanford University, Palo Alto, CA, U.S.A.

2.4 Energy Transfer Between Fabric and Test Sensors

In the area of thermal protective fabrics, not only is the thermal response of the protective material of interest, but so is the energy transfer between the heated material and the skin or a test sensor. It is this energy transfer which will cause thermal damage to the skin and govern test results. Therefore it is important to understand the various modes of energy transfer which will occur between the fabric and a test sensor or human skin. In this model, the energy transfer between the fabric and the test sensor was described in the boundary conditions given as Equations (2.3) and (2.5).

In this section, previous research into these energy transfers is reviewed, along with research in the general area of energy transfer in enclosures. A model of the energy transfer in the air gap between the heated fabric and a small scale bench top test sensor is then developed.

2.4.1 Previous Research in Energy Transfers in Air Gaps in Thermal Protective Clothing

As mentioned in Section 1.4.2 some existing versions of bench top fabric tests use a 1/4 in. (6.4 mm) air space between the fabric and the test sensor, while other versions place the fabric in contact with the test sensor. Tests using air spaces allow the fabric to heat up independently of the test sensor, thus the fabric will reach higher temperatures and be tested more severely than if it was in contact with a test sensor. As it takes longer for heat to be transferred from the heated fabric across an air space to a test sensor than if the fabric was in contact with the sensor, times to exceed given criteria for bench top tests will be larger for spaced than contact tests. Therefore, differences between the performance of individual fabrics may be more apparent in tests with an air gap. However, it has also been noted that as different fabrics react in different ways thermomechanically during bench top tests, the size of the air space is affected in different ways for different fabrics, which has a major effect on the results of bench top tests using an air gap [4]. As also noted in that paper and discussed in Section 4.5.5, the heat fluxes incident on test sensors in tests which use an air gap are different from the ideal square wave heat flux for which the Stoll criterion is strictly only valid [12]. This may affect the validity of test results. The other alternative, placing the fabric in contact with a test sensor, is said to result in a more severe test of the protection that the fabric offers to the skin. It also avoids some of the problems with thermomechanical effects and data analysis from which the spaced bench top tests may suffer. However, because the times to reach the criteria of interest are much shorter with contact tests, differences between various candidate fabrics may not be as large as with the spaced tests. One investigator who compared the two alternatives with other larger scale tests was Geshury [70] who found that contact tests produced results which correlated better with results from the dynamic Thermo-leg system, while spaced tests produced results which correlated better with those from the static Thermo-man® system.

Assuming that the air gap is in fact used, it is well known that a stagnant air space can be a good insulator. It is also well understood that if an air space is stagnant, its insulating value will increase as the width of the air space increases. However if the air space becomes wide enough, natural convection may occur, which will increase the heat transfer across the air space, and may decrease its value as an insulator. The gap at which convection is initiated is often termed a critical or optimal gap, as the insulation offered by the air space increases with width below this critical value, and decreases with width above this critical value. Several investigators have postulated values of the optimal or critical air gaps between protective fabrics, and other fabric layers or the skin. Some of these values have been determined through analysis or experimentation, while in other cases no reasons are given. A summary of these critical air gap widths is shown in Table 2.1, while a few of these and other pertinent studies are highlighted below.

Table 2.1 Suggested Critical Air Gap Widths for Protective and Other Clothing

Investigator(s)	Critical Air Gap Width (mm)	Orientation	Description	Reasons Given
Rees [71]	8.9	horizontal, heated from below	insulating effect of air space increases with air gap until this spacing, then decreases	measurements on fabric covered hot plate
GIRCFF [45]	varies with orientation	horizontal, 45°, vertical	various modes of heat transfer important at different spacings when determining thermal dose to skin from burning fabrics	measurements of heat flux to skin simulants from burning fabrics and temperatures inside air gap
Stoll and Chianta [42]	4	horizontal, heated from below	optimal air gap between fabric layers, beyond which convection said to begin and fabric perforated by flame	measurements of temperatures in skin simulants behind fabrics and burns to fabric covered rats
Morse, et al. [46]	2.5	not specified	air gaps beyond this width do not provide further protection	analysis of conduction and radiation across air gaps between infinite parallel plates with a temperature difference of 500°C
Cain and Farnworth [72]	10	not specified	beyond this width convection cells can form	none given
Veghte [73]	18	not specified	beyond this width convection cells can occur in air gaps between layers in fire fighters' protective ensembles	none given
Danielsson [74]	2	vertical	convection cells assumed to occur beyond this air gap	none given

Most attempts to model the energy transfer in the air gaps between the fabric and the skin have simply used overall heat transfer coefficients between the two surfaces. One example of this approach was Chen [41] (whose work was discussed in Section 1.5.1) who used a constant overall heat transfer coefficient to model gas conduction and radiation in very small vertical air spaces with widths of 0.4 mm or less. Natural convection was not included, as he estimated that the Grashof number was less than 1, versus the critical value of 2000 for the onset of natural convection in vertical air gaps [75]. However, Chen remarked that the Grashof criteria may not be applicable for fabric covered air spaces as the cloth is porous so the enclosed air may have room to move around. Chen also noted that radiation across the gap would also be significant, and should be considered in more detail. For example, radiation heat transfer was assumed to occur between the back of the fabric and the skin simulant, when in fact the skin simulant can also "see" part of the inside of the fabric due to its porous nature. However this error was estimated not to cause significant errors in his results.

Another example of a model which utilizes an overall heat transfer coefficient for the air gap is the Aerotherm model of the fabric-air gap-skin system discussed in Section 1.5.4 [46]. Here conduction and radiation between infinite parallel plates with given emissivities were considered. Fabric shrinkage, and the effect this had on the size of the air gap was also included. The transfer of energy by products of thermochemical reactions involving the fabric which condense on the surface of the skin was also considered. The value of the overall heat transfer coefficient for the air gap was recalculated at each time step. A model of the heat transfer across air gaps of 0.01, 0.1, and 0.25 in. (0.25, 2.5, and 6.4 mm) between infinite parallel plates by radiation and conduction for a temperature difference of 500°F (278°C) was also used to examine the effect of air space size on the heat transfer between fabrics and skin. It was found that air gaps greater than 0.1 in. (2.5 mm) did not improve protection, as beyond this distance radiation heat transfer is the predominant form of energy transfer for this temperature difference. Below this air gap width, conduction dominates, and hence the protection offered by the air space increases as the width of the air space increases. However, this study simply used infinite parallel plates, rather than examining the heat transfer between finite sized areas, such as in the bench top tests modelled here. In addition, the temperature differences across air gaps in bench top tests will be shown in Chapters 3 and 4 to be much greater than 500°F (278°C). Heat transfer by convection and absorption of radiation by water vapour and gaseous products of thermal decomposition reactions, which may move into the air gap, were not considered in the Aerotherm analysis. Predictions of the temperatures in the skin simulant mounted behind the fabric were not compared with experimental results as no experimental results of the effects of varying the size of the air gap between the fabric and skin were presented.

Other investigators have made statements as to the importance of various modes of energy transfer in air spaces between heated fabrics and skin or test sensors. Geshury [70] noted two stages in the copper disk temperature histories in ASTM D 4108 bench top tests. The first was thought to represent the time period in which the fabric was being heated, while the second began when the fabric had been heated to the point where its rear surface temperature was high enough to emit a significant amount of thermal radiation. Shalev [48] examined the deposits found on bench top test sensors after tests of treated flame resistant cotton fabrics and determined their reevaporation energies using a differential scanning calorimeter (see Section 3.2.5). These energies were found to be insignificant compared with the overall heat transfer. However, others (e.g. Davies, et al. [76]) have found that tars from other flame resistant treated cottons did transfer a significant amount of energy to test sensors in vertical fabric tests.

Others have examined the energy transfers between heated fabrics and skin or test sensors experimentally. Rees [71] measured the percentage thermal insulating value (%T.I.V.) of various fabric/air gap combinations. This %T.I.V. value was simply the percentage by which a fabric reduced the heat loss from a heated copper plate, which was maintained at about the temperature of the human body. Increasing the size of the air gap increased the overall insulative value of the fabric and air gap until an air gap of 0.35 in. (8.9 mm), and then decreased for an air gap of 0.4 in. (10.2 mm). This behaviour was said to occur because convection currents have a greater effect at air gaps above 0.35 in. (8.9 mm), although no calculations were shown to back up this statement.

Stoll and Chianta [42] experimentally determined the relationship between temperature rise at a depth of 0.5 mm below the surface of a skin simulant (total thickness of about 1 cm) and the thickness of an air gap between two 3 oz/sq. yd. (100 g/m^2) fabric layers mounted on top of this simulant and subjected to a flame. Curved plates were used to hold the fabrics so that they had a curvature similar to that found on the human body. It was found that by examining the data during the time period of 1 to 3 s, there appeared to be an air gap thickness which results in the greatest insulative effect. Below this thickness, it was said that conduction is enhanced because of the decreasing thickness of the air gap. Above this thickness, Stoll and Chianta stated that convection currents arise and contribute to the propagation of the flame front through the fabric, which eventually leads to perforation. They also examined the effect of the air space between the two layers on the time to produce a fixed amount of burn damage to the skin of anaesthetized, depilated laboratory rats. In both of these cases, the optimal thickness was found to be about 4 mm. However it must be noted that Stoll and Chianta were examining the air space between two fabrics placed on top of a sensor. Bench top tests of interest here for a single layer fabric contain an air gap between a single fabric layer and a sensor, a different physical situation from what Stoll and Chianta were investigating. As well, from this reference it is unclear whether or not the air spaces were open or closed at the edges of the fabric specimens. In addition, these data were for a single type of fabric, which had a mass per unit area of 3 oz./sq. yd. (100 g/m^2). Many protective fabrics have a nominal mass per unit area of 4.5, 6 oz./sq. yd. (150, 200 g/m^2), or larger. Temperatures in the sensor were considered only during the first three seconds of exposure. Bench top tests which use a 1/4 in. (6.4 mm) air space involve longer exposures than this. It was assumed that an increase in convection was the reason for the decrease in protection offered by the fabric. No analysis was presented to support this theory. For example, convection cells may take longer than 3 s to begin. They also noted that the flames began to penetrate the fabric as the air space increased. This may in fact be the reason for this apparent optimal thickness of air gap between the fabric layers, rather than the onset of natural convection.

Some other examples of experimental work in this area are described by Backer, et. al. [45] in their review of work done by the Government Industry Research

Committee on Fabric Flammability (GIRCFF). Fabric-air gap-skin simulant assemblies with air gaps between 0 and 1 in. (25.4 mm) were exposed to a radiant heat flux of 340 kW/m^2. Temperatures at the back surface of the fabric, the surface of the skin simulant, and various other points in the air space between the fabric and simulant were made. The effects of spacing and orientation on the flame propagation and predicted burn damage from burning fabrics ignited on their edges with a laboratory burner were also studied. Fabrics were placed in horizontal, 45°, and 90° orientations. The spacing at which the thermal dose to the skin reached a maximum was different for each orientation. The transfer of energy to, and hence subsequent injury to the skin from the burning of flammable fabrics was said to be due to radiation from hot gases and the fabric, convection and conduction through the gas phase, condensation of steam and pyrolysis products, and length of exposure to the flame. These modes of energy transfer were used to explain the experimental observations. At fabric-skin spacings where condensation of pyrolysis products did not occur, it was found that radiation and gas conduction each were responsible for about half the total energy transfer across the gap. For smaller spacings where the condensation of pyrolysis products became significant, radiation and condensation of products each contributed 35 to 40% to the total energy transfer, with the remainder being due to gas conduction. It should be noted that this work was primarily concerned with tests involving flammable fabrics, not flame resistant fabrics, placed in a variety of orientations, most of which were different than bench top tests such as ASTM D 4108.

Other experimental work includes Hoschke, et al. [77] who compared estimated pain and burn times for fabrics with different air gaps (0 and 3 mm with the fabric restrained, 3 and 6.4 mm with the fabric unrestrained) and curved copper calorimeters. It was found that increasing the spacing from 3 to 6.4 mm increased pain and burn times by a couple of seconds in aluminized glass and Zirpro™ wool samples. Little differences in results were seen in the flame resistant cotton samples, and it was thought that the energy transfers between the fabric and test sensor were due more to condensation of pyrolysis products on the sensor rather than heat transfer through the material. Benisek and Phillips [78] looked at the effect of changing the air gap from 0 to 8 mm on the estimated times to second degree burn and pain alarm time for fabric specimens made of Zirpro™ wool, an aramid, and flame resistant cotton for an incident heat flux of 3.3 cal/cm^2·s (138 kW/m^2). Their data indicated that the times to second degree burn and pain alarm time continued to increase with increasing air gap up to 8 mm. Therefore, unlike Stoll's work, no optimal spacing was observed.

As seen by the above review, there is no consensus as to the importance of various modes of energy transfer in the air space between the heated fabric and skin or test sensors. Therefore, it was deemed important to examine this part of the problem using information from the general area of natural convection in enclosures. Radiation heat transfer between the heated fabric and the test sensor will also be discussed in a subsequent section.

2.4.2 Natural Convection in Enclosures

Natural convection in enclosures of various orientations has been studied extensively. Examples of areas in which this problem is important include building materials, solar collectors, and electronics. Natural convection in a vertical enclosure heated from one side would be of interest in modelling the heat transfer between fabric and test sensors in some experiments (e.g. a thermal mannequin test), while natural convection in horizontal enclosures is of interest when studying the bench top tests used in the work described in this thesis. Goldstein and Volino [79] include a review of many of the key early papers in natural convection in horizontal enclosures, and Catton [80] has also published a review of work on natural convection in vertical, horizontal, and tilted rectangular enclosures. Due to the orientation of the laboratory test studied here, only natural convection in horizontal enclosures heated from below will be considered here.

Hollands, et al. [81] gave the following correlation for air in a horizontal enclosure heated from below.

$$Nusselt = 1 + 1.44 \left[1 - \frac{1708}{Ra} \right]^{\cdot} + \left[\left(\frac{Ra}{5830} \right)^{1/3} - 1 \right]^{\cdot} \qquad (2.25)$$

where: Nusselt = the Nusselt number (Nu) ($h\delta/k$, here)
Ra = the Rayleigh number $(g\beta\Delta T\delta^3)/(\alpha\nu)$
g = gravitational acceleration (9.81 m/s^2)
α = the thermal diffusivity of the fluid (m^2/s)
β = the thermal expansion coefficient of the fluid temperature (K^{-1})
ΔT = the temperature difference across the enclosure (K)
ν = the kinematic viscosity of the fluid (m^2/s)

The notation $[\ ]^{\cdot}$ in Equation (2.25) indicates that if the argument in the square brackets is negative, the quantity should be taken as zero. The values of the Rayleigh number included in the equation represent the accepted values for the onset of steady natural convection (1708), and the transition to time-unsteady natural convection (5830). This correlation was found to agree with the experimental data of Hollands, et al. and others over a wide range of Rayleigh numbers.

This correlation is strictly valid only for steady state conditions in an enclosure of infinite width heated entirely from below with small differences in temperatures across the enclosure. The situation in the air space between the fabric and the skin or test sensor will be different for several reasons. These will be discussed in turn below.

Transient Conditions: The above work was for steady state conditions in an enclosure. This is the situation in many of the applications in this area (e.g. heat transfer in air gaps in windows and building materials). However, in the case of interest here, the boundary conditions change rapidly with time. Chen [41] points out that this can have a significant effect on the value of the convective heat transfer coefficient. Some investigators have examined transient natural convection in enclosures. Examples include

Mantle-Miller, et al. [82] who studied natural convection in enclosures with a periodically changing bottom plate temperature boundary condition for Rayleigh numbers of the order of 10^8 to 10^9. Goldstein and Volino [79] investigated natural convection in a thick (146 mm) horizontal layer of water subjected to a near-constant heat flux from below, and observed convection currents which occurred only in the bottom of the layer. Thus a critical Rayleigh number based on a conduction layer thickness (the distance which energy has moved into a fluid layer at a given time) rather than the height of the enclosure was used. However, the temperature differences used were much smaller than those across air gaps in bench top fabric tests (less than 5°C rather than 100's of degrees Celcius). As well, air gaps in bench top tests cannot be considered as "thick" layers according to their criteria.

Finite-Sized Enclosures: In the case of interest here, a finite-sized enclosure is used, rather than infinite parallel plates. Catton [80] presents results from his earlier studies of the effect of side walls on the onset of natural convection and the heat transfer during convection. The largest air gap width used in the work described in this thesis was about 20 mm, while the specimen holder is about 150 mm across. Therefore the largest height to width ratio of the air gaps used was about 1 to 7.5. According to Catton's data, the side walls for these height to width ratios will have no effect on the onset of convection or the heat transfer during convection.

Localized Heating: Not only is the enclosure of finite dimensions, but the bottom portion is only partially heated. It is also expected that the heat flux across the heated portion of the fabric will not be constant due to the nature of the flame and the fabric structure. Two other situations which have been studied in which the bottom plate of the horizontal enclosure is locally heated are the cooling of components on circuit boards in the microelectronics area and the study of plumes rising from fires in rooms.

In a study of room fires Torrance, et al. [83] presented pictures from a flow visualization experiment in which a heated disk of radius approximately one-tenth of the height of an enclosure was used. These observations were compared to those from a numerical model of the same situation. Curves of the Nusselt number as a function of the Grashof number, and the heat transfer as a function of the dimensionless time and

Grashof number were presented in a companion paper [84]. Experiments were run for Grashof numbers from 8 x 10^5 to 1 x 10^{10}. These conditions are considerably different from those in the air spaces in these bench top tests, where it will be shown in Chapter 3 that the largest Rayleigh numbers are about 4 x 10^4. In addition, the time scales in room fires are much different from those in short duration fabric tests.

Variable Thermal Properties: In the air gap under consideration there are temperature differences of up to 500°C between the upper and lower boundaries of the enclosure. This is considerably different from almost all of work reported in the literature, where temperature differences between the top and bottom walls are relatively small. It is known that the thermal properties of air change greatly over the large temperature ranges seen in this problem. MacGregor [85] showed that solutions for problems of natural convection in vertical enclosures which include variable thermal properties are different from those which use constant thermal properties.

In solving the Navier Stokes equations for the enclosure, the Boussinesq approximation is normally used. This assumes that the density and the other thermal properties are constant other than in the body force term. Charts prepared by Gray and Giorgini [86] show that for air at ordinary room temperature, the Boussinesq approximation is valid up to a temperature difference across the enclosure of about 29°C.

Investigators who have looked at the effects of variations in thermal properties (especially the density) on the onset of convection and the heat transfer in enclosures include Kuo and Ball (horizontal enclosures) [87], and Sparrow and Gregg (vertical enclosures) [88]. The latter investigators determined that a reference temperature along with constant property relationships could be used to solve problems of free convection on vertical plates. This simplified analysis of the heat transfer agreed with more complicated analyses taking the variable properties into account even for differences between the vertical wall and ambient temperature of up to 1200°F (667°C). However, experimental verification was only provided for enclosures with small temperature differences.

2.4.3 Treatment of Natural Convection in this Study

As can be seen by the above discussion, a detailed description of the natural convection processes occurring in enclosures in bench top tests is daunting. The problem is a transient one in which the boundary conditions and the properties of the fluid in the enclosure change rapidly. Additional energy transfer modes such as mass transfer and radiation can affect the convection heat transfer. The enclosure is locally heated, and the heat flux over the heated section itself is not uniform. In addition, due to the nature of the fibre structure, even if the front of the fabric was evenly heated, the temperatures along the back surface of the fabric would not be uniform at any given time. To completely describe the physics of the enclosure, the temperatures at each point in the space should be known. Ideally these should be compared to measurements in actual enclosures.

Studies which include at least some of these effects have been performed for specific situations (e.g. Pallares, et al. [89]). However, these require large computing resources. In this case an estimate of the heat transfer between the fabric and the skin or test sensor is desired, not the exact temperature distribution in the enclosure. Therefore, in this study it will be assumed that each time step in the model can be treated as quasi-steady state. The simple steady-state correlation of Hollands and Raithby [81] (Equation (2.25)) will then be used for each time step, which has been shown to be quite accurate for steady-state conditions for horizontal enclosures undergoing heating along the entire bottom surface. As discussed earlier, the effects of the side walls will be neglected according to the work of Catton [80]. Localized heating will also be ignored. All of these are expected to result in some differences between predicted and actual convective heat transfer coefficients in the air gap. However, as will be shown in the comparison of the relative magnitudes of the different modes of energy transfer in the air gap, these differences should have less of an effect than differences in parameters which affect the radiation heat transfer (Section 3.4.8). The ability of the model to predict experimental results in bench top tests will be discussed in light of all of these assumptions in Chapter 5. In addition, results of the numerical model using the simple correlation of Hollands and Raithby will be compared with flow visualization observations described in Section 4.5.5 to determine if they also qualitatively predict the behaviour in the air gap during bench top tests.

2.4.4 Thermal Radiation in the Air Gap

Besides natural convection heat transfer, heat transfer by thermal radiation will also be important in the air gap. This is because of the high temperatures expected on the backside of the fabric. A rigorous model of the radiation heat transfer in the air gap would include radiation heat transfer between the fabric, test sensor, specimen holder, insulating block, and side walls. A radiation network could be developed for this analysis [67]. However, it was found that test sensor temperatures obtained by considering only the energy transfers between the heated fabric and test sensor using the finite element model described in this chapter differed only very slightly with those calculated using a more complicated radiation network. Therefore, the model will only include the radiation heat transfer between the heated fabric and test sensor.

First it must be determined whether or not any gases which enter the air gap due to thermal decomposition of the fabric will affect the radiation heat transfer between the fabric and test sensor due to absorption and scattering. The chemical formulae of the fibres were used to determine the amounts of carbon dioxide and water vapour in the air gap assuming complete combustion. The heat transfers by thermal radiation from the fabric to the test sensor with and without including absorption by the gases in the air space and the emission of radiation from these gases to the test sensor were then calculated. These calculations are shown in Appendix 2. It was found that including the absorption and emission of radiation by the gases had a negligible effect on the net heat transfer by thermal radiation between the heated fabric and the test sensor.

To determine whether particles in the air gap would cause significant scattering of the radiation, an attempt was made to determine the sizes and concentrations of the particles in the gases of decomposition reaction products in the air gap. Nomex® IIIA and Kevlar®/PBI fabric specimens were exposed to a Meker burner and a phased Doppler anemometer[5] was used to determine the particle sizes in the gases which came off the back sides of the specimens. This experiment simply indicated that most of the particles in the gas cloud were smaller than 2 μm. Due to the resolution of this device, the exact sizes of the particles could not be determined. A funnel was also used to direct some of the gases into a filter, which turned noticeably darker in colour after a short period of time. The filter was then examined using a measuring microscope where it was found that once again most of the particles were less than 2 μm in size. One other estimate of the size of particles is provided by Drysdale [90] who stated that the mass median diameter in a mist of particles from heated carbon-based materials is of the order of 1 μm.

It was assumed that these particles were 2 μm in diameter, and that the temperature of the fabric is about 1000 K and a grey body. It can be shown using Planck's spectral distribution [67] that 90% of the radiation emitted from the fabric will be at wavelengths of less than 9.4 μm. The ratio of the circumference of these particles to the wavelength of radiation from the fabric is therefore

$$\frac{\pi D_f}{\lambda} = \frac{\pi 2}{9.4} \approx 0.7 \qquad (2.26)$$

According to Hottel and Sarofim [63], if this ratio is less than 0.6, then particles of interest are considered to be small relative to the wavelength of radiation. As this is the highest temperature the fabrics reach, it provides a bound for the wavelength range. Lower temperatures will produce higher wavelengths, which would result in lower ratios between the circumference of the particles and the wavelength. Therefore, depending on how small the particles actually are it may be possible to treat the particles as small relative to the wavelength (which would be considerably simpler to treat than Mie scattering, where the particles are about the same size as the wavelength). However, as no information could be obtained about the exact size distributions and concentrations of the gas, it was decided to ignore scattering in the air gap. If information on the size distributions and concentrations could be obtained, this phenomena could be included in the analysis. Non-optical sizing techniques could be used to determine particle size distributions (e.g. special filters, cascade impactor, electrical techniques). Details of these and other methods can be found in Willeke and Baron [91].

---

[5] available from Dantec Electronics Inc., Mahwah, N.J., U.S.A.

The heat flux due to thermal radiation heat transfer between the heated fabric and test sensor is therefore given by

$$q_{air\ rad} = \frac{\sigma(T_{fab}^{4} - T_{sens}^{4})}{\left(\frac{A_{sens}}{A_{fab}} \left(\frac{1 - \varepsilon_{fab}}{\varepsilon_{fab}} + \frac{1}{F_{fab-sens}} \right) + \frac{1 - \varepsilon_{sens}}{\varepsilon_{sens}} \right)} \tag{2.27}$$

The view factor, $F_{fab-sens}$ can be determined using Equation (2.23) previously used to calculate the view factor between the heated fabric and the burner head, using the dimensions of the heated portion of the fabric (50 by 50 mm), the copper disk (40 mm diameter), and the size of the air space.

Equation (2.27) above is strictly valid only for steady-state heat transfer by thermal radiation. However, as mentioned in Siegel and Howell [67], because of the high speeds at which thermal radiation travels, storage of thermal radiation is generally neglected in the treatment of all but a few problems (e.g. effects of nuclear weapons and astrophysics). Therefore, a quasi-steady-state representation of thermal radiation will be used here, with the heat transfer assumed to be quasi-steady-state at each time step of interest.

2.4.5 Interaction Between Natural Convection and Radiation Heat Transfer in The Air Gap

Now that the equations for the heat transfer by conduction, convection[6], and radiation heat transfer in the air space have been determined, these must be combined to determine the total heat transfer between the heated fabric and the test sensor. The simplest way to treat this interaction is to assume that radiation, conduction, and convection are uncoupled, and hence simply add the heat transfers by each mode. Siegel and Howell [67] mention that this approach gives good results for estimating the heat transfer between parallel plates when the boundaries are black, the medium between the plates is optically thin, and the magnitude of the radiation is much larger than the conduction/convection term. While the boundaries for the enclosure here are not strictly black, they have emissivities of 0.9 or larger. The air space was shown above to be optically thin, and as will be shown later in Section 3.4.8, the heat transfer by radiation is much larger than that by conduction/convection across the air space. Therefore, the conduction/convection and radiation terms were simply added to get the total net heat flux across the air space

---

[6] Conduction will occur for conditions where the Rayleigh number is less than 1708, as discussed in conjunction with Equation (2.25)

$$\begin{aligned} q_{air\ net} &= q_{air\ rad} + q_{air\ conv} \\ &= \frac{\sigma(T_{fab}^4 - T_{sens}^4)}{\left(\frac{A_{sens}}{A_{fab}} \left(\frac{1-\varepsilon_{fab}}{\varepsilon_{fab}} + \frac{1}{F_{fab-sens}} \right) + \frac{1-\varepsilon_{sens}}{\varepsilon_{sens}} \right)} + h_{gap}\,(T_{fab} - T_{sens}) \end{aligned} \tag{2.28}$$

It would be useful to combine the thermal response of the fabric, the energy transfer across the air gap, and the response of the copper disk test sensor into one differential equation. In order to accomplish this, the concept of an effective thermal conductivity was used. This is suggested by Stelzer and Welzel [92] and others. Fourier's law can be written for finite dimensions and constant properties as

$$q = -\frac{k}{\Delta x}\,\Delta T \tag{2.29}$$

Equation (2.28) can be rearranged as

$$q_{air\ net} = \left[\frac{\sigma\ (T_{fab}^2 + T_{sens}^2)\ (T_{fab} + T_{sens})}{\left(\frac{A_{sens}}{A_{fab}} \left(\frac{1 - \varepsilon_{fab}}{\varepsilon_{fab}} + \frac{1}{F_{fab-sens}} \right) + \frac{1 - \varepsilon_{sens}}{\varepsilon_{sens}} \right)} + h_{gap} \right] (T_{fab} - T_{sens}) \tag{2.30}$$

Comparing Equations (2.29) and (2.30) the effective thermal conductivity of the air space is given as

$$k_{eff} = \left[\frac{\sigma(T_{fab}^2 + T_{sens}^2)\ (T_{fab} + T_{sens})}{\left(\frac{A_{sens}}{A_{fab}} \left(\frac{1 - \varepsilon_{fab}}{\varepsilon_{fab}} + \frac{1}{F_{fab-sens}} \right) + \frac{1 - \varepsilon_{sens}}{\varepsilon_{sens}} \right)} + h_{gap} \right] \Delta x_{gap} \tag{2.31}$$

where Δx_{gap} is the total width of the air gap[7]

2.5 Treatment of Test Sensor

The copper disk test sensor shown in Figure 2.1 was modelled as follows. The disk itself is 1.6 mm thick. Thermal properties of pure copper at room temperature taken from standard tables [93] were used. An air space of about 8 mm[8] was placed behind the sensor, just as in the design of the bench top test sensors. This air space was given an effective thermal conductivity to account for conduction heat losses from the back and sides of this disk. In order to determine the appropriate value of this effective conductivity, the disk was heated using the Meker burner for several seconds and then allowed to cool. Using an energy balance on the disk and estimates of the radiative and convective heat losses from the disk, the effective conductivity was determined to be about 25 W/m·°C. As this air space was merely used to account for heat losses from the copper disk, its volumetric heat capacity was assumed to be negligible. The temperature at the base of this air space was assumed to remain constant throughout at the ambient temperature of 300 K during the flame exposure.

---

[7] It should be noted that no matter how many elements are used to represent the air gap, the total width must be used in calculating the effective thermal conductivity, which will then be the same for all elements in the air space

[8] This air space may in fact be large enough for natural convection to occur if the temperature difference is large enough. This was not considered here, but is discussed in [77]

2.6 Differential Equations for Fabric-Air Gap-Test Sensor System

Applying the results from the previous three sections to the equations given in Section 2.1 for the fabric-air gap-test sensor system produces the following differential equation.

$$C^{\wedge}(T)\,\frac{\partial T}{\partial t} = \frac{\partial}{\partial x}\left(k(T)\frac{\partial T}{\partial x}\right) + \gamma\, q_{rad}\exp(-\gamma x) \qquad (2.32)$$

where

$$q_{rad} = \sigma\varepsilon_g T_g^{\,4} - \sigma\varepsilon_{fab}F_{fab\text{-}amb}\,(1-\varepsilon_g)\,(T_{x=0}^4 - T_{amb}^4) - \frac{\sigma(T_{x=0}^4 - T_{bh}^4)}{\left(\dfrac{1-\varepsilon_{fab}}{\varepsilon_{fab}} + \dfrac{1}{F_{fab\text{-}bh}(1-\varepsilon_g)} + \dfrac{A_{fab}}{A_{bh}}\dfrac{(1-\varepsilon_{bh})}{\varepsilon_{bh}}\right)} \qquad (2.33)$$

and γ = the extinction coefficient of the fabric, which can be determined from the transmissivity, τ, and the thickness, L_{fab}, of the fabric using

$$\gamma = -\frac{\ln(\tau)}{L_{fab}} \qquad (2.34)$$

The equation is solved subject to the following initial and boundary conditions:

7

for t = 0

$$T(x) = T_i(x) \qquad (2.35)$$

where $T_i(x)$ is some initial temperature gradient in the fabric-air gap-skin system.

for x = 0, t > 0

$$-k(T)\frac{\partial T}{\partial x} = q_{conv} = h_{fl}\left(T_g - T_{x=0}\right) \tag{2.36}$$

for x = L_b, t > 0

$$T\left(x = L_b\right) = T_{amb} \tag{2.37}$$

As the thermal properties in Equation (2.32) are temperature dependent, and the boundary condition on the front of the fabric and the effective thermal conductivity of the air gap (Equation 2.31) include the fourth power of the temperature, the series of equations to be solved is non-linear. This introduces many complications into the solution of the equations. Stelzer and Welzel [92] discuss methods to reduce the complications introduced by non-linear equations. One of their suggestions was used earlier to treat the energy transfer across the enclosure by using an effective thermal conductivity. Another suggestion is to treat variations in thermal properties with temperature and the values of boundary conditions by taking the values of thermal properties and boundary conditions to be those calculated using the temperatures at the previous time step. Here, the average temperature in each element would be used to determine the values of the appropriate thermal properties for that element, which would then be assumed to be constant for that element for that particular time step. Stelzer and Wenzel suggest that this method is generally appropriate, but not unconditionally stable.

Following this suggestion leads to the following differential equation

$$C^{A}(T)\frac{\partial T}{\partial t} = k(T)\frac{\partial^2 T}{\partial x^2} + \gamma\, q_{rad}\exp(-\gamma x) \tag{2.38}$$

In Section 2.9 the model is verified by comparing its results to those from closed form and other numerical solutions. One of these comparisons was between the finite element model utilizing this method to calculate the thermal properties and boundary conditions and solutions where an iterative technique was used to solve a non-linear equation for appropriate temperatures and values of thermal properties and boundary conditions at each time step. It will be shown that the results using either method are similar for the expected variations in thermal properties and boundary conditions in this problem.

2.7 Solution of Differential Equations Using the Finite Element Method

In this work, the finite element method was chosen to solve the differential equation, as initially it was thought that this model would include complex geometries such as those found on the human body. The finite element method has been used to solve heat transfer problems in many areas of engineering over the past few decades (e.g. [94-96]).. In addition, as many commercial finite element packages contain heat transfer modules, findings from this study may be applied to the analysis of other heat transfer problems using these commercial packages.

Galerkin's weighted residual method was used to formulate a finite element matrix equation to solve the differential equation, subject to the given initial and boundary conditions. This and other weighted residual methods are alternatives to variational methods, which are also commonly used to derive finite element matrix equations. Weighted residual methods, unlike variational methods, do not rely on forming functionals, but instead use the differential equation directly to form a matrix equation. Weighted residual methods can also be used to solve more general problems than the variational methods, which cannot handle first derivatives, dissipation terms, and non-linearities. The derivation of the finite element equation is described in detail in Appendix 3, and is based on [97].

Based on findings from the author's previous work [2], elements based on cubic Hermitian temperature interpolation polynomials were used. These were found to model conduction heat transfer more efficiently than elements utilizing linear or quadratic temperature interpolation polynomials. If the full set of non-linear equations were used in this problem, Hermitian elements might be troublesome, because of the difficulty in integrating the resulting matrices. However, for this case where the properties were assumed to be constant for each element at each time step, tabulated values of the appropriate integrals [98] can be utilized. The Hermitian temperature interpolation polynomials are as follows

$$
\begin{aligned}
T(x) &= \left(2\left(\frac{x^3}{l^3}\right) - 3\left(\frac{x^2}{l^2}\right) + 1 \right) T_a \\
&\quad + \left(\frac{x^3}{l^3} - 2\left(\frac{x^2}{l^2}\right) + \frac{x}{l} \right) l\, k_a \left(\frac{\partial T}{\partial x}\right)_a \\
&\quad + \left(-2\left(\frac{x^3}{l^3}\right) + 3\left(\frac{x^2}{l^2}\right) \right) T_b \\
&\quad + \left(\frac{x^3}{l^3} - \left(\frac{x^2}{l^2}\right) \right) l\, k_b \left(\frac{\partial T}{\partial x}\right)_b \qquad (2.39) \\
&= \lfloor\, f_{h1} \;\; f_{h2} \;\; f_{h3} \;\; f_{h4} \,\rfloor \left\langle \begin{matrix} T_a \\ \left(k_a \dfrac{\partial T}{\partial x}\right)_a \\ T_b \\ \left(k_b \dfrac{\partial T}{\partial x}\right)_b \end{matrix} \right\rangle
\end{aligned}
$$

$$T(x) = \langle f_h \rangle^T \langle T_e \rangle$$

As shown in Appendix 3, the finite element matrix equation for the differential equation is

$$
\begin{aligned}
&\left([B] + \frac{\Delta t}{2} \left([A] - [k] \right) \right) \langle T^{(j+1)} \rangle \\
&\quad = \left([B] + \frac{\Delta t}{2} \left(-[A] + [k] \right) \right) \langle T^{(j)} \rangle \qquad (2.40) \\
&\quad + \frac{\Delta t}{2} \left(\langle BC^{(j)} \rangle + \langle BC^{(j+1)} \rangle \right)
\end{aligned}
$$

or

$$[LHS] <T_e> = <RHS> \qquad (2.41)$$

As the nodes and elements in the model were numbered in order from the surface of the fabric to the back of the air space behind the copper disk, [LHS] is a banded matrix with a bandwidth of four. Therefore a banded matrix solver was used to solve Equation (2.41) at each time step. This decreases the computation time considerably over the time that a Gaussian elimination matrix solver would take to solve Equation (2.41).

It was found that a very small number of Hermitian elements were needed to model the fabric-air gap-test sensor system. The number of elements required for each component in the system were as follows:

• fabric	5 elements
• air gap	1 element
• copper disk	2 elements
• to account for heat losses from copper disk	1 element

No benefit was realized in increasing these numbers of elements. For example, it was found that there was no practical difference between fabric and copper disk temperatures predicted using 5 or 10 elements to model the fabric. Similarly, constant time steps of 0.05 s were found to be adequate, as predictions made using these time steps were practically the same as those made using time steps of 0.02 s. These results are shown in Figure 2.7 below.

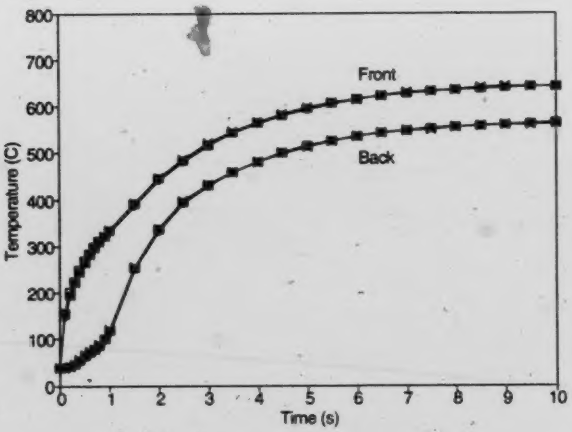

Figure 2.7 Comparison Between Temperatures of Front and Back of Fabric Predicted Using Various Numbers of Fabric Elements and Time Steps (■ - 5 el., $\Delta t = 0.05$ s; X - 10 el., $\Delta t = 0.05$ s; + - 5 el., $\Delta t = 0.02$ s)

2.8 Finite Element Computer Program

A computer program based on the above finite element derivation was written to solve for the nodal temperatures and fluxes. The program was written in Microsoft® QuickBASIC™ 4.5. A flow chart for the program is shown in Figure 2.8.

The program operation is as follows. In the initial stages of the program, shown in Figure 2.8(a), variable declarations are made and parameter values are read (e.g. number of elements, thermal properties, etc.). Vectors of thermal properties for each element, depths from the fabric surface for each node, and initial nodal temperatures and fluxes are formed. A nodal connectivity matrix which relates the node and element numbers, and a vector of elapsed time for each time step are also formed.

The program then marches forward in given time increments. At each time step the incident heat flux and fabric and air gap thermal properties are determined using the temperatures calculated at the previous time step. The [LHS] matrix and the information used to calculate the <RHS> vector are then formed for each element, and then assembled to form the global [LHS] matrix and <RHS> vector using the information in the nodal connectivity matrix. The [LHS] matrix and the <RHS> vector are then constrained by

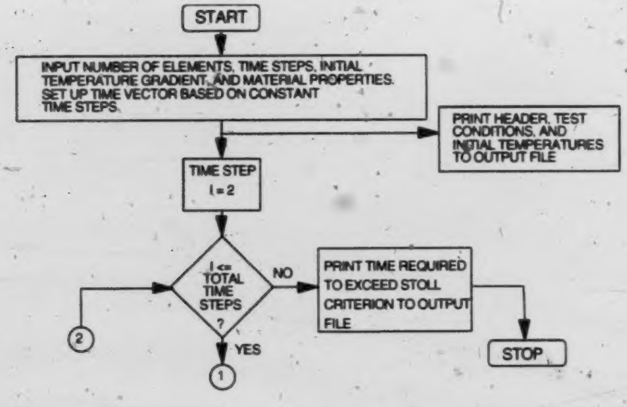
START
INPUT NUMBER OF ELEMENTS, TIME STEPS, INITIAL TEMPERATURE GRADIENT, AND MATERIAL PROPERTIES. SET UP TIME VECTOR BASED ON CONSTANT TIME STEPS.
PRINT HEADER, TEST CONDITIONS, AND INITIAL TEMPERATURES TO OUTPUT FILE
TIME STEP I = 2
I <= TOTAL TIME STEPS ?
NO
YES
PRINT TIME REQUIRED TO EXCEED STOLL CRITERION TO OUTPUT FILE
STOP
2
1

Figure 2.8(a) Flow Diagram of Finite Element Computer Program - Initial and Final Stages

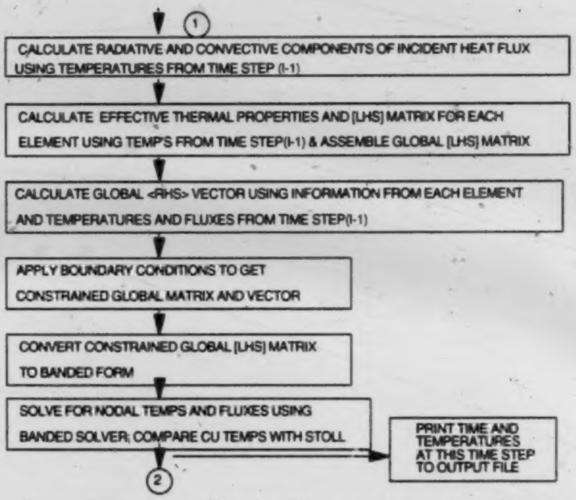
1
CALCULATE RADIATIVE AND CONVECTIVE COMPONENTS OF INCIDENT HEAT FLUX USING TEMPERATURES FROM TIME STEP (I-1)
CALCULATE EFFECTIVE THERMAL PROPERTIES AND [LHS] MATRIX FOR EACH ELEMENT USING TEMP'S FROM TIME STEP(I-1) & ASSEMBLE GLOBAL [LHS] MATRIX
CALCULATE GLOBAL <RHS> VECTOR USING INFORMATION FROM EACH ELEMENT AND TEMPERATURES AND FLUXES FROM TIME STEP(I-1)
APPLY BOUNDARY CONDITIONS TO GET CONSTRAINED GLOBAL MATRIX AND VECTOR
CONVERT CONSTRAINED GLOBAL [LHS] MATRIX TO BANDED FORM
SOLVE FOR NODAL TEMPS AND FLUXES USING BANDED SOLVER; COMPARE CU TEMPS WITH STOLL
PRINT TIME AND TEMPERATURES AT THIS TIME STEP TO OUTPUT FILE
2

Figure 2.8(b) Flow Diagram of Finite Element Computer Program - Temperature Calculations

applying the boundary conditions at the fabric surface and base of the air space behind the copper disk. This constrained [LHS] matrix is then converted into a banded matrix, and the matrix equations are solved for nodal temperatures and fluxes. These steps are shown in Figure 2.8(b).

The program continues to calculate temperatures for the entire flame exposure. The temperature rise in the copper disk at each time step is compared with the Stoll criterion in order to determine the time to reach the criterion. The program prints this time and the temperature history at the surface of the fabric, the middle of the fabric, the back of the fabric, and of the copper disk to a datafile. A sample partial datafile generated by the program is shown in Appendix 4.

2.9 Verification of Model with Closed Form and Other Solutions

In order to validate portions of the computer program separately, temperatures calculated using the model were compared with those determined using closed form and other numerical solutions for several simplified cases.

2.9.1 Semi-Infinite Solid

Temperatures at various depths in human skin subjected to a square wave heat flux were estimated using the current model and the author's previous skin heat transfer model [2]. The results were identical in each case. This indicated that no changes were made by accident to the basic conduction heat transfer model during the course of modifying the original computer program.

2.9.2 Two Layer Semi-Infinite Solid

The closed form solution for a material in perfect contact with a semi-infinite solid was originally presented by Griffith and Horton [43]. Stoll and Chianta [42], while experimentally verifying Griffith and Horton's equation, noted an error, and presented the corrected solution.

The temperature, T_1, of the top layer of thickness L_1 is given by

$$\begin{aligned}
T_1(x,t) - T_1(x,0) = \frac{q}{k_1} \Biggl[\Biggl(2\sqrt{\frac{\alpha_1 t}{\pi}} \exp\left(-\frac{x^2}{4\alpha_1 t}\right) - x\left(1 - erf\left(\frac{x}{2\sqrt{\alpha_1 t}}\right)\right)\Biggr) \\
- \frac{1}{\gamma}\sum_{n=0}^{\infty}\left(-\frac{1}{\gamma}\right)^{n} \Biggl[2\sqrt{\frac{\alpha_1 t}{\pi}} \left(\exp\left(-\frac{(x+2L_1(n+1))^2}{4\alpha_1 t}\right) + \exp\left(-\frac{(x-2L_1(n+1))^2}{4\alpha_1 t}\right)\right) \\
- (x + 2L_1(n+1))\left(1 - erf\left(\frac{x+2L_1(n+1)}{2\sqrt{\alpha_1 t}}\right)\right) \\
+ (x - 2L_1(n+1))\left(1 - erf\left(-\frac{x-2L_1(n+1)}{2\sqrt{\alpha_1 t}}\right)\right)\Biggr]\Biggr]
\end{aligned} \tag{2.42}$$

The temperature, T_2, of the bottom, semi-infinite layer is given by

$$\begin{aligned}
T_2(x,t) - T_2(x,0) = \frac{2q\lambda\sqrt{\alpha_1}}{\gamma}\sum_{n=0}^{\infty}\left(-\frac{1}{\gamma}\right)^{2} \Biggl[2\sqrt{\frac{\alpha_2 t}{\pi}} \exp\left(\frac{-\left(x - L_1\left(1 - \sqrt{\frac{\alpha_2}{\alpha_1}}(2n+1)\right)\right)^2}{4\alpha_2 t}\right) \\
- \left(x - L_1\left(1 - \sqrt{\frac{\alpha_2}{\alpha_1}}(2n+1)\right)\right)\left(1 - erf\left(\frac{x - L_1\left(1 - \sqrt{\frac{\alpha_2}{\alpha_1}}(2n+1)\right)}{\sqrt{2\alpha_2 t}}\right)\right)\Biggr]
\end{aligned} \tag{2.43}$$

where

$$\gamma = \frac{k\rho c_2 + \sqrt{(k\rho c)_1 (k\rho c)_2}}{k\rho c_2 - \sqrt{(k\rho c)_1 (k\rho c)_2}} \tag{2.44}$$

$$\lambda = \left(k_2\sqrt{\alpha_1} - k_1\sqrt{\alpha_2}\right)^{-1} \tag{2.45}$$

and α_1 and α_2 are the thermal diffusivities of the two layers (note that γ and λ are used differently here from in the equations presented earlier in the chapter). The two solutions were used to determine the temperatures at various depths in a thin layer with the same nominal thermal properties as the fabrics used in this study placed in perfect contact with a semi-infinite layer having the same thermal properties as human skin. In the finite element model, five elements were used to model the fabric, while five were used to model the skin. A square wave heat flux of 80 kW/m^2 for 3 s was placed on the surface of the fabric, and temperatures were calculated for 10 s total.

A comparison of the temperatures of the surface of the fabric is shown in Figure 2.9. The temperatures calculated using the finite element model were very close to those calculated using the closed form solutions. Temperatures predicted by the two models at other depths in the system were even closer. The largest differences were seen at the beginning of the exposure and immediately after the end of the exposure to the intense heat flux at 3 s. This indicates that the finite element model can handle the case of multiple layers with different thermal properties. It also serves as a useful check of the original finite element model used to determine the temperatures of human skin.

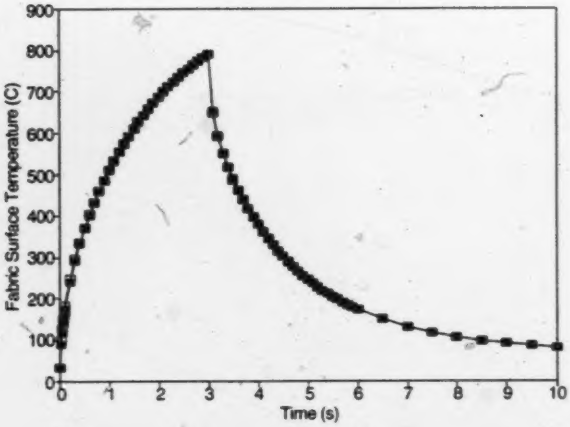

Figure 2.9 Comparison Between Surface Temperatures for a Layer in Perfect Contact with a Semi-Infinite Solid Calculated Using the Finite Element Model (□) and the Closed Form Solution of Griffith and Horton [43] (■)

2.9.3 Lumped Capacity Analysis

In the experiments described in Chapter 4, thin pieces of shim stock were used in bench top tests. These materials were selected to compare the numerical results with experimental results for materials which did not contain moisture, did not thermally degrade, and were opaque. This was done so as to determine whether the model could represent conduction in the materials and the boundary conditions adequately. The temperature of such a piece of steel shim stock during an exposure to a square wave heat flux of 80 kW/m^2 for 10 s was estimated using the computer program and a program based on the non-linear equation that results when the steel shim stock is treated using the lumped capacity method for a unit area(which is appropriate as the Biot number for the shim stock is less than 0.1 [93]).

$$\begin{aligned} \rho c \Delta x \frac{\partial T}{\partial t} &= q_{net} \\ &= q_{inc} - (q_{conv} + q_{air\ conv}) - (q_{rad} + q_{air\ rad}) \end{aligned} \qquad (2.46)$$

where Δx is the thickness of the shim stock, and the incident heat flux, q_{inc}, is its nominal value of 80 kW/m^2 and the losses by convection and radiation from each side are calculated in a similar manner to those in the model of the fabric-air gap-skin system. The equation was solved numerically using the Newton-Raphson false position method at each time step. Two cases were examined.

- constant values of density and specific heat of the metal shim stock. The absolute temperatures predicted using the two programs were very close (less than 1% different) and hence are not plotted.
- constant value of density, and using the variations in the specific heat of steel found in standard tables [93]. The finite element program used the value of specific heat calculated using the temperature at the previous time step, while the lumped capacity model iterated to find the temperature and corresponding value of specific heat at each time step. These results are shown in Figure 2.10.

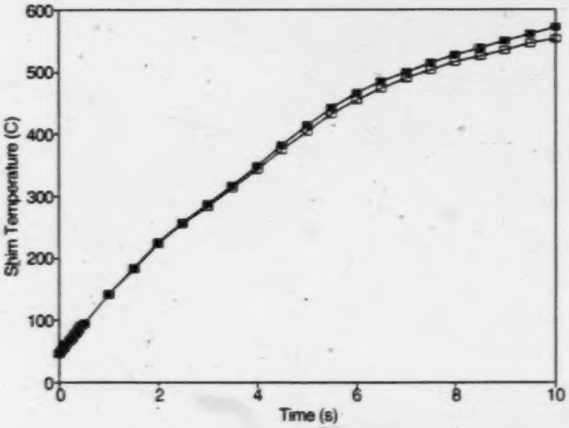

Figure 2.10 Comparison Between Temperatures Predicted for Steel Shim Stock Piece with Temperature Dependent Specific Heat using Finite Element Model (□) and Lumped Heat Capacity Model (■)

Absolute shim stock temperatures predicted by the two models were within 3% of each other when the exposure ended. One of the reasons for the differences was that the temperatures predicted by the finite element model were very dependent on the width of the air space used in the model. As the lumped capacity system treated the shim stock as losing heat to the surroundings by convection and radiation, no thickness of air space needed to be specified. The finite element method treated the heat losses from the shim by introducing effective thermal conductivities to account for the transfer of heat by convection and radiation across finite air spaces, and therefore these losses were dependent on the size of air gap chosen. In addition the relations used in the finite element model to predict convection heat losses are based on convection inside an enclosure rather than convection from a horizontal flat plate to the surroundings.

Based on the above comparisons, it was thought that the finite element model was in fact performing as it should, and that it did do an adequate job of treating the variations in specific heat with temperature by using values calculated using the temperatures at the previous time step. Therefore, treating the fabric and air gap thermal properties in this manner should be acceptable.

2.9.4 Semi-Infinite Solid with Variable Thermal Conductivity

As with the above comparison, a comparison was also made with a simpler case where the thermal conductivity varied with temperature. The integral method (which approximates analytical solutions) was used to solve for the heat transfer in a semi-infinite solid whose thermal conductivity is a function of temperature

$$k(T) = k(T_i)\left(1 - \kappa(T - T_i)\right) \tag{2.47}$$

where κ is a constant. It can be shown that the solution is [99]

$$T(x,t) = T_i + \frac{q\delta}{3k_w}\left(1 - \frac{x}{\delta}\right)^3 \tag{2.48}$$

where δ is the penetration depth, calculated using

$$\delta = \sqrt{\frac{12k_w t}{\rho c}} \tag{2.49}$$

and k_w is the thermal conductivity at the surface, calculated using

$$k_w \, (k_w - k_i)^2 = \frac{4}{3} \frac{(k_i \kappa q)^2}{\rho c} \, t \tag{2.50}$$

and k_i is the thermal conductivity at the initial temperature of the solid, T_i

The semi-infinite solid was given values of density and specific heat representative of the protective fabrics studied here. Two test cases were used. The first assumed a constant value of thermal conductivity of 0.1 W/m·°C, the second used values of $k(T_i) = 0.047$ W/m·°C at 300 K and $\kappa = -0.000415$ W/m^2·°C for Equation (2.47), which were determined by assuming a straight line through the values calculated for the thermal conductivity at 300 K and 700 K using the relationship determined in Section 3.2.4. It was assumed that the fabric was 10 mm thick for the purposes of the finite element model in order to have a semi-infinite solid for the times of interest here. Assuming fabric thicknesses of 5 mm and 25 mm did not have a significant effect on results.

Comparison of the temperatures calculated at the surface of the fabric and at a depth of 1 mm are shown in Figure 2.11 and Figure 2.12. For the case of constant thermal conductivity (Figure 2.11), the results found using the two models were also compared with those from the closed form solution for a semi-infinite slab with the same boundary conditions [100]. It was found that the temperatures calculated using the finite element model and the closed form solution were identical. The temperatures found using the integral method were slightly different from these temperatures (at 10 s , the absolute surface temperatures were 1% different, the absolute temperatures at 1 mm were 3% different). For the variable thermal conductivity case (Figure 2.12), there were some differences between the temperatures calculated using the integral and finite element methods (at 10 s, the absolute surface temperatures were 5% different, the absolute temperatures at 1 mm were 2% different). As both methods are approximations, it is not clear which of the two solutions should be more correct. The integral method takes the variation of thermal conductivity into account implicitly at each time step, while the finite element model relies on values calculated using the temperatures at the previous time step. On the other hand, the finite element model proved to be closer to the closed form solution for the constant property case. Regardless, the finite element model appears to do an adequate job of predicting temperatures in a body over a wide temperature range when the thermal conductivity is temperature dependent.

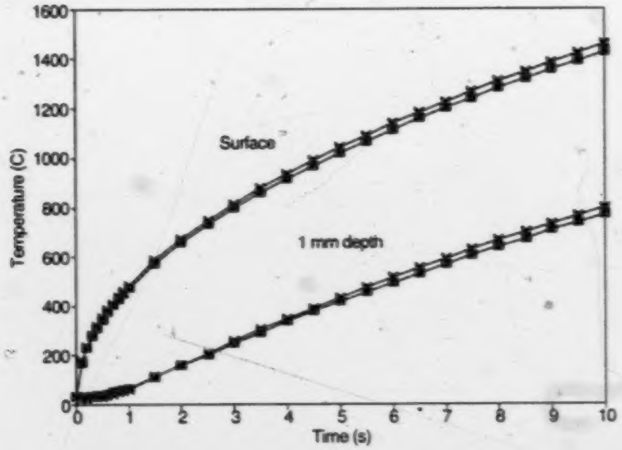

Figure 2.11 Comparison Between Temperatures Determined Using Finite Element Model (□), Closed-Form Solution (+), and the Integral Method (X) for a Semi-Infinite Slab with Constant Thermal Properties

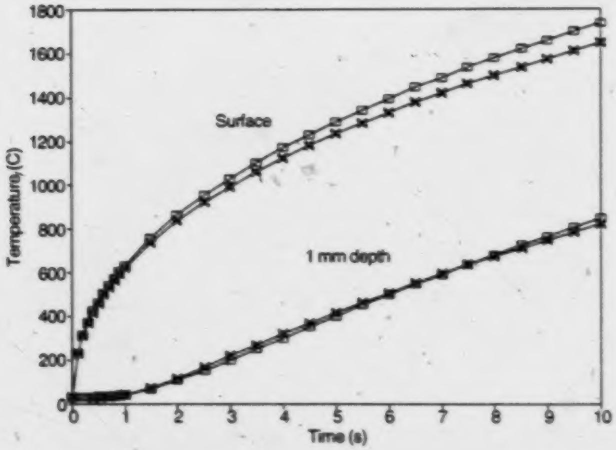

Figure 2.12 Comparison Between Temperatures Determined Using Finite Element Model (□), and the Integral Method (X) for a Semi-Infinite Slab with Variable Thermal Conductivity

2.9.5 Semi-Infinite Solid with In-Depth Absorption of Incident Radiation

The portion of the finite element model which considers the in-depth absorption of radiation using Beer's law was verified by comparing the results of the model with those from the closed form solution for the steady state distribution of temperature in a semi-infinite solid with a known heat flux on its surface, q_{conv} and in-depth absorption of radiation incident on its surface, q_{rad}. The equation used to describe the steady state situation is

$$k \frac{d^2T}{dx^2} + q_{rad}\,\gamma\,\exp(-\gamma x) = 0 \qquad (2.51)$$

The boundary conditions are
at x = 0

$$-k \frac{dT}{dx} = q_{conv} \qquad (2.52)$$

at x = L

$$T = 0 \qquad (2.53)$$

The solution to Equations (2.51) through (2.53) is

$$T(x) = \frac{1}{k}\left[\frac{q_{rad}\,\gamma\left(\exp(-\gamma L) - \exp(-\gamma x)\right)}{\gamma^2} + \left(q_{rad} + q_{conv}\right)\left(L - x\right)\right] \qquad (2.54)$$

Temperatures predicted using the finite element method and the closed form solution were within a small fraction of 1% of one another. The finite element and closed form solution also both predicted that the temperatures in the solid approach those which would be calculated for an opaque solid as the transmissivity of the solid approached zero. Therefore, it can be concluded that the portion of the model which handles the in-depth absorption of radiation is working properly.

2.10 Summary

A model of the heat transfer in fibrous materials subjected to the high heat fluxes of a flash fire has been described. Methods used to treat energies associated with thermal decomposition reactions, absorption of radiation, energy transfers between the fabric and test sensor, and boundary conditions on the front of the fabric were described in detail. The finite element method was used to numerically solve the resulting differential equations. The computer program based on this model was also described. Results from the model compared favourably with results found using closed form and other solutions for several simplified cases. The specific values which will be used for the thermal properties in this model will be determined in the next chapter, along with numerical results obtained using the model.

CHAPTER 3: NUMERICAL RESULTS

In the previous chapter, a numerical model of a bench top test of an inherently flame resistant fabric was developed. In this chapter, results from this numerical model will be presented. First, the techniques used to measure and/or determine the values of the thermal and thermochemical properties to be used in the model will be discussed. Then numerical results for simulated bench top tests of Nomex® IIIA and Kevlar®/PBI fabric specimens will be presented. Lastly results from a parametric study (i.e. sensitivity study) using the numerical model will be presented. This parametric study should help to illustrate the effects of various material properties on the thermal response and bench top test results of protective fabrics.

3.1 Fabrics Used in This Study

Samples of three common flame resistant fabrics, Kevlar®/PBI (60% Kevlar® and 40% PBI), Nomex® III, and Nomex® IIIA, were used in this study. Each had a nominal mass per unit area of 200 g/m^2 (6 oz/yd^2). The Kevlar®/PBI samples were 2/1 twills, while the Nomex® III and Nomex® IIIA samples were plain weaves. The only difference between Nomex® III and Nomex® IIIA is that the Nomex® IIIA contains a static-dissipative fibre to provide extra comfort and protection in workplaces where static electricity may be a problem. It is expected that the two Nomex® fabrics will perform in a similar manner. For example, Nomex® technical literature [101] quotes TPP values of 13.1 and 13.7 cal/cm^2 for 6 oz/yd^2 (200 g/m^2) Nomex® IIIA and III fabrics, respectively. For the numerical modelling and most of the experimental work, the Kevlar®/PBI and Nomex® IIIA samples were used. Nomex® III samples were used only for a portion of the work dealing with investigating alternative bench top test methods, described in Section 4.5.6.

3.2 Determination of Relevant Thermal and Thermochemical Properties

Methods used to determine the thickness, density, thermal conductivity, apparent heat capacity and decomposition temperature ranges, and transmissivity are discussed in turn below.

3.2.1 Preparation of Samples

Before beginning the tests, the fabrics samples were washed twice in medium temperature (50°C) water with moderate mechanical action, using a synthetic detergent. The fabrics were then tumble dried. Unless otherwise specified, fabric specimens 100 by 100 ± 2 mm were cut, and conditioned at 20 ± 2°C, 65 ± 2% relative humidity. Further information on the effects of conditioning fabric samples on bench top test results will be given in Section 4.5.1.

3.2.2 Thickness

Using a particular value of thickness to describe a fabric is somewhat misleading. As the fabric structure varies from location to location on the surfaces of a fabric, so will the thickness. For example, various parts of the fabric structure, such as the individual fibres on the surface of yarns at the fabric surface, have been shown to play key roles in the thermal response of a fabric [48,49]. While thicknesses are generally measured before a bench top test, they have been shown to change during a bench top test exposure [48]. In addition, fabric thicknesses can vary considerably depending on the pressure at which they are measured. Some investigators have therefore treated the thickness by including it in the thermal conductance (the thermal conductivity divided by the thickness) rather than measuring it separately (e.g. [41]).

The thickness of the conditioned fabric specimens was measured using a C&R Model CS-55 thickness tester[9]. Here, measurements were made under 1 kPa pressure using a small (6.5 cm^2) pressure foot. This pressure is in accordance with CAN/CGSB-4.2 No.37-M87 [102], which states that unless otherwise specified, the thickness corresponding to this particular pressure should be taken as the thickness of the fabric. Using this pressure, the average thicknesses were found to be

---

[9] available from Custom Scientific Instruments, Cedar Knolls, N.J., U.S.A.

Nomex® IIIA	0.70 mm
Kevlar®/PBI	0.62 mm

As mentioned above, fabric thicknesses are simply nominal values and will change during an exposure. These particular values of thickness will be used in the model and a parametric study will then be carried out to determine the effect of varying the thickness of the fabric on the thermal response and bench top results of these fabrics.

3.2.3 Density

The fabrics used in these tests have a nominal mass per unit area of 200 g/m^2. These nominal values were confirmed by determining the average masses of several Nomex® and Kevlar®/PBI fabric specimens using a scale and dividing these masses by the nominal surface area of the specimens. For the model, the density of each of the fabrics was taken as the nominal mass per unit area value of 200 g/m^2 divided by the appropriate thicknesses from Section 3.2.2. While the density of the fabrics is expected to change during bench top test exposures, these changes were shown to be relatively small by Shalev [48], and thus the density will be assumed to be constant throughout the exposure. This assumption can be further justified by noting that materials containing Nomex®, Kevlar®, and/or PBI found in a NASA database of properties of thermal protective materials [103] have densities which change very little with temperature from about 20 to 400°C (although no information is provided for higher temperatures at which thermochemical reactions are expected - please see Section 3.2.5).

3.2.4 Thermal Conductivity

A variety of methods can be used to determine the thermal conductivity of a material. For fabrics at comfort conditions or somewhat elevated temperatures a guarded hot plate can be used. Others have also used a thin heater apparatus (an unguarded hot plate) or a heat flow meter. A review of these three methods and their applicability for measurements of the thermal conductivity of thin fabrics is given in [104]. Other methods which can be used include a so-called "pulse" method, similar to that used to determine the thermal absorptivity of the skin simulant sensors used in the work described in this thesis (Section 4.2.2). In a similar manner, Stoll and Chianta [42] and Baker, et al. [105] fitted experimental data to results from analytical models to determine the thermal conductivity of protective fabrics and charring ablators, respectively, under high heat flux conditions. One other novel technique for estimating the values of thermal conductivity of protective fabrics, as described by Shalev [48], is to use data from a differential scanning calorimeter (DSC) (a DSC was used in the study outlined in the following section).

Other than the method which utilizes the DSC, none of these methods are directly applicable here. Guarded or unguarded hot plates, and heat flow meters capable of measuring the thermal conductivities over the wide range of temperatures expected during bench top test exposures were not available for this work . Unless very difficult inverse heat conduction problems are solved, the "pulse" and other methods which determine the thermal conductivity by fitting experimental data must assume that the thermal properties of the material are constant with temperature. These techniques are also dependent on the choice of analytical or numerical model which is used to fit the data. The development of such a model is one of the goals of the present work. In addition, as will be shown in Section 4.5.2, it is very difficult to measure temperatures at specific locations within the fabric. Therefore, it was decided to calculate the thermal conductivity at the temperatures of interest, rather than measuring the values.

The heat transfer in fibrous materials is a combination of conduction and convection in the gases in between fibres, conduction in the solid fibres, and radiation heat transfer between fibres. As the structure of these materials can be thought of as consisting of series and parallel paths for heat transfer, thermal resistant networks are often used to estimate their thermal conductivity, much like the method which is used to estimate heat transfer in composite walls in houses [93]. Futschik and Witte [61] have reviewed models used for fibrous materials and compare the results from these models with measurements made using Nomex® specimens with various fill gases over a pressure range from vacuum conditions to atmospheric, and at temperatures from -180°C to 230°C.

However, these samples were quite different from the fabrics used here. In addition, models which are based on estimating the portions of heat transfer through series and parallel paths in a given fabric structure may not be applicable in this work since, as will be shown in Section 4.5.3, the fabric structure changes in some of these materials when they are heated.

Therefore another approach was taken. Rather than calculating the thermal conductivity as a function of the fabric structure, a simplified model which uses a weighted sum of the contributions from the solid fibres and the air, as well as the contribution of radiation heat transfer between fibres was utilized. This can be represented as

$$k_{eff} = \left(k_{gas} + k_{solid} \right) + k_{rad} \tag{3.1}$$

where the first two terms represent the contributions of gas conduction and convection, and conduction in the solid fibres, and the last term represents the radiation heat transfer between the fibres. Assuming that the relative magnitudes of the contributions of the first two terms to the sum in the brackets are approximately equal to their volume fractions in the fibrous materials

$$k_{eff}(T) = \left(v_{air} k_{air}(T) + (1 - v_{air})\, k_{fibre}(T) \right) + k_{rad}(T) \tag{3.2}$$

where v_{air} is the volume fraction of air in the fibrous material

The NASA database of thermal properties [103] contains an entry for the thermal conductivity of Nomex® felts used as flexible reusable surface insulation for the space shuttle orbiter. Data is given for temperatures from about -155 to 1100°C . The density of this material is given as 86.5 kg/m^3. The density of Nomex® fibres is given by Futschik and Witte [61] as approximately 1443 kg/m^3. The density of PBI fibres is given as 1430 kg/m^3 in PBI technical literature [106]. The density of air at ambient conditions is 1.2 kg/m^3 [93]. Working backwards from the densities of the felt, and those of the fibres and air, it can be shown that the volume fraction of air is about 0.94 for this felt. Now, neglecting the contribution of radiation between the fibres, Equation (3.2) becomes

$$k_{felt}(T) = .94\ k_{air}(T) + 0.06\ k_{fibre}(T) \tag{3.3}$$

As k_{air} is given over a wide range of temperatures in standard tables [93], the values of k_{fib} can be determined at several points over the temperature range of interest using the data from the NASA database. It is also known that the thermal conductivity of Nomex® fibres at room temperature is 0.13 W/m·°C [61]. Taking all of this information into account, an equation which approximates the thermal conductivity of Nomex® fibres over the temperature range of interest was developed.

$$\begin{aligned} k_{fibre}(T) &= 0.13 + 0.0018\ (T\ (K) - 300\ K) \quad T \leq 700\ K \\ &= 1.0 \quad T > 700\ K \end{aligned} \tag{3.4}$$

This equation shows that the thermal conductivity of Nomex® fibres appears to remain approximately constant after about 700 K. As will be seen in the next section, this temperature is close to the temperature range at which thermochemical reactions begin to occur.

The thermal conductivity of the air was also represented by an approximately linear relationships using data from standard tables [93].

$$\begin{aligned} k_{air}(T) &= 0.026 + 0.000068\ (T\ (K) - 300\ K) \quad T \leq 700\ K \\ &= 0.053 + 0.000054\ (T\ (K) - 700\ K) \quad T > 700\ K \end{aligned} \tag{3.5}$$

The volume fractions of air and fibres in the fabrics were then determined. The density of the fabric is 0.2 kg/m^2 divided by the thickness, 0.7 mm. This gives a density of about 286 kg/m^3. Using the densities of air and fibre given above, a volume fraction of about 0.8 for air was calculated. These values are similar to those reported by Shalev [48] for heavier Kevlar®/PBI and Nomex® fabric samples. Substituting these fractions into Equation (3.2) produces

$$k_{eff}(T) = \Big(0.8\ k_{air}(T) + 0.2\ k_{fibre}(T)\Big) + k_{rad}(T) \tag{3.6}$$

Equations (3.4) through (3.6) give a value of the thermal conductivity of the fabrics at 300 K of 0.047 W/m·°C, which is close to the value of 0.042 W/m·°C generally reported in the literature for these fabrics (e.g. [106]). As differences between the thermal conductivities of the Nomex® IIIA and Kevlar®/PBI samples are expected to be very small, these relationships will be used to represent the effective thermal conductivity of both materials. The parametric study discussed later in this chapter should also provide some guidance as to whether any small differences between the thermal conductivities of the two materials will have a significant effect on their temperatures and the protection which they provide.

In Section 2.3.2 the interaction between the incident radiation and the fibrous material was discussed. At that time it was stated that the radiation heat transfer from fibre to fibre would be accounted for in the value of the thermal conductivity of the fabric. A rigorous solution of this would account for the interaction between the individual fibres and would be daunting. However, it will be shown that the portion of the thermal conductivity due to thermal radiation is quite small relative to the total thermal conductivity of the fabric. Therefore, to simplify the analysis, the fibres were assumed to act as a number of infinite plates acting as radiation shields, all of which were placed at the boundaries between adjacent finite elements. Hence the portion of the thermal conductivity due to thermal radiation between the fibres was assumed to simply be equal to

$$k_{rad} = \frac{\sigma \, \varepsilon_{fibre} \, \Delta x \, (T_1^{\,2} + T_2^{\,2}) \, (T_1 + T_2)}{2 - \varepsilon_{fibre}} \tag{3.7}$$

The emissivity of the fibres, ε_{fib}, was taken as 0.95 [60], while in this equation, Δx, was taken as the width of the particular finite element for which the radiation conductivity is being calculated. As mentioned above, this portion of the thermal conductivity is very small. For example for an 100 K temperature difference across one finite element in the fabric, the contribution due to thermal radiation is about 5% of the total thermal conductivity of the fabric.

Therefore the effective thermal conductivity of the fabric was calculated for each element using the temperatures of the nodes of that element at the previous time step and

Equations (3.4) through (3.7). The average temperature of the nodes was used to calculate the first two terms on the right hand side of Equation (3.6), while the two nodal temperatures were used to calculate the radiation term. The estimated values of the thermal conductivity of the fabric are plotted for the temperature range of interest along with the thermal conductivities of the fibres (calculated), air (from standard tables), and Nomex felt (from the NASA database) in Figure 3.1. As with the other properties the effects of variations in the values of thermal conductivity on the temperatures predicted by the model will be discussed later in this chapter.

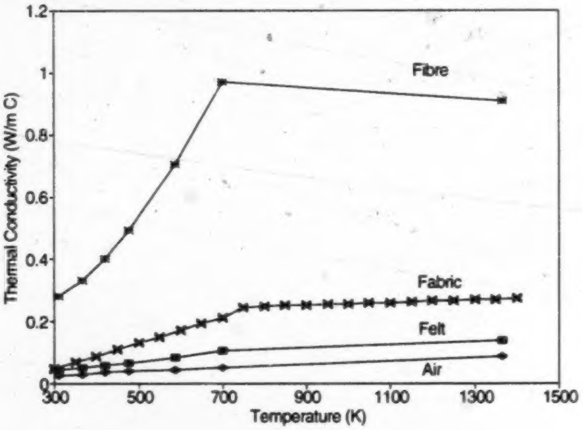

Figure 3.1 Thermal Conductivity of Nomex® Felt (■), Fabrics (X), Fibres (*), and of Air (+) for Temperatures from 300 to 1400 K

3.2.5 Apparent Heat Capacity and Thermal Decomposition Temperatures

As mentioned in Section 2.3.1, the apparent heat capacity method can be used to represent thermochemical reactions implicitly in the differential equations. This method requires a knowledge of the energies associated with chemical reactions, and the temperature range over which these reactions take place. Two standard tests from the area of thermal analysis were used to make estimates of these pieces of information for the fabrics.

Thermal gravimetric analysis (TGA) is a technique where the mass of a sample is measured continuously by a thermobalance while it is heated. The mass loss-temperature data can be used to determine the temperature ranges over which chemical reactions occur as well as determining how much mass is lost in these reactions. A flow of an inert gas such as helium can be used to carry any gaseous products away from the sample in order to determine their composition. TGA tests in this inert environment can be used to provide information on endothermic pyrolysis reactions. A flow of oxygen can be used in place of helium if information about exothermic pyrolysis and oxidation reactions is desired. If TGA tests are run at various heating rates, information about the chemical kinetics of reactions can also be obtained.

Very small (about 10 mg) specimens were cut from Nomex® IIIA and Kevlar®/PBI fabric samples for testing. It should be noted that these specimens were not conditioned, as the tests were performed at a laboratory approximately one hour drive from the conditioning room. This may have some effect on the amount of water evaporated from the fabric when it is heated, but should not affect the information for the reactions which occur at higher temperatures. A BOMEM TG/Plus Analyzer[10] was used. This apparatus includes a Bomem Michelson Fourier Transform Infrared spectrometer, a multi-pass gas cell, and a DuPont 951 Thermal Analyzer. Specimens were heated in stainless steel baskets from about room temperature to 900°C at a rate of 20°C per minute in both helium and oxygen environments. As the apparent heat capacity method was used here, no attempts were made to determine the kinetics of reactions. Information on the kinetics of reactions involving Nomex® and PBI materials produced in the early 1970's is given in Morse, et al. [46]. In addition, as this model did not include mass transfer and the main interest here was the temperature ranges of reactions, no attempts were made to determine the complete composition of the gaseous products of the reactions. Studies have been reported in which the principal components of these compositions were determined for Nomex® [107,46] and PBI [108,46].

Thermogravimetric curves for the two fabrics are shown in Figure 3.2 in both helium and oxygen environments. These curves are similar to those in the literature for

---

[10] available from BOMEM, Inc., Quebec City, Quebec

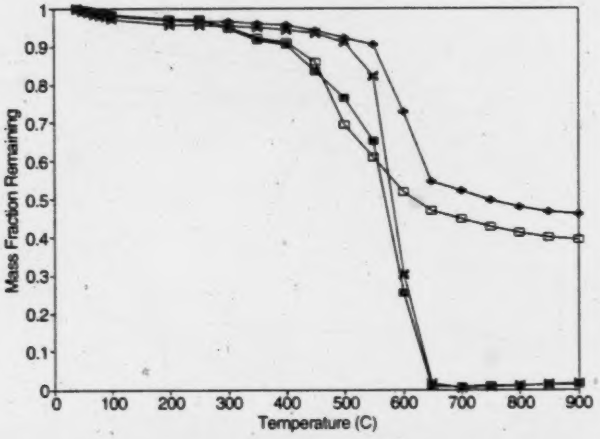

Figure 3.2 Thermogravimetric curves for Nomex® IIIA and Kevlar®/PBI Specimens (Nomex® IIIA in He □, and O2 ■ ; Kevlar®/PBI in He +, and O_2 X)

the two materials (e.g. [109, 106]). From these curves it can be seen that after the water is evaporated out of the sample, the mass of the sample remains fairly constant until the onset of thermal decomposition. The approximate temperature ranges over which the majority of the thermal decomposition occurs for these materials in Helium and Oxygen environments are as follows.

Material	Helium	Oxygen
Nomex® IIIA	430 - 620°C	420 - 640°C
Kevlar®/PBI	575 - 620°C	530 - 660°C

Caution should be exercised when looking at TGA results. While very small specimens are used so as to reduce the differences in temperature across the specimen, in the case of heterogeneous materials such as fabrics these temperatures may not be completely indicative of the whole material. It has also been pointed out that there can be major differences in TGA results conducted by different laboratories, as TGA results are extremely sensitive to the surface-to-volume ratio of the specimens used in the tests [110]. A review of other potential sources of inter-laboratory differences or errors in

TGA tests can be found in Wendlandt and Gallagher [111].

As will be shown in the next two chapters, fabrics in bench top tests are heated at rates of the order of about 10^4°C per minute. Fabric specimens in these particular TGA tests were heated at 20°C per minute. It is well known that the heating rates at which tests are run can affect TGA test results. For example, at higher heating rates certain reactions may not have adequate time to take place. This will tend to increase the temperature at which thermal decomposition takes place and in general to shift the thermogravimetric curve to the right (Figure 3.3). Examples of investigators who have been able to develop equipment to make measurements at higher heating rates and compare these data to those at lower heating rates include Henderson and O'Brien [112] (up to 800°C per minute), Bingham and Hill [113] (3000°C per minute), and Shlensky, et al. [114] (over 600 000°C per minute).

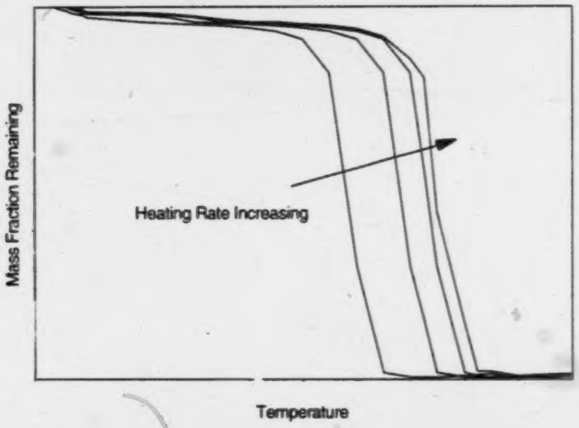

Figure 3.3 Effect of Increasing Heating Rate on Thermogravimetric Curve

Aspects of the latter two examples are of interest to this work. Bingham and Hill [113] found that the temperature at which degradation began in high heating rate tests of several protective fabrics correlated very well with the estimated time to 20% skin damage in fire pit tests. Shlensky, et al. [114] describes various techniques to make measurements under very high heating rates, and discusses the practical problems associated with TGA and other thermal analysis techniques. These authors also discuss the effect of heating rate on thermogravimetric curves for polymers, polymer-based materials, and some natural coals. It was found that these curves do not shift indefinitely as the heating rate increases, but in fact tend to some ultimate thermogravimetric curve which is no longer heating rate dependent (shown schematically in Figure 3.3). This behaviour was also seen in Henderson and O'Brien's [112] data.

Despite the dependence of TGA results on heating rate, in the absence of any other information, the thermal decomposition temperature ranges observed in these TGA tests will be used in the model. The effect of varying these temperature ranges of reactions on the thermal response of fabrics will be discussed in Section 3.4.5. TGA test results will also be compared with measured mass losses during bench top tests in Section 4.5.3.

The differential scanning calorimeter (DSC) is a device in which a sample and some reference material, whose thermal properties are known, are maintained at the same temperature by individual heaters. By comparing the amounts of energy required to maintain the sample and reference material at this temperature, energies of reactions (endothermic or exothermic) and the specific heat of the sample as a function of temperature may be determined. Some of the advantages of using this apparatus for measuring the specific heat include good accuracy, rapid data acquisition, and relatively small sample sizes [115]. A Perkin Elmer DSC-4 with System 7/4 Thermal Analysis Controller[11] was used here. Analysis of the data was performed using a computer equipped with TA-PC Thermal Analysis software[12]. Tests were conducted in a nitrogen environment.

Before testing the fabric specimens, the mass of an aluminum sample pan and top was determined and a DSC test of the empty sample pan and its top from 30 to 500°C at 20°C per minute was conducted. A DSC test of a sapphire reference material using this same heating procedure was then conducted. Data from these two tests were used to help determine the specific heats and energies of reactions of the fabric specimens. Samples of Nomex® IIIA and Kevlar®/PBI fabrics were cut into very small pieces and used to fill aluminum sample pans. Roughly 10 to 14 mg of fabric was used in each pan. A top was then crimped onto each of the sample pans and the mass of each of the filled pans was determined.

---

[11] available from The Perkin-Elmer Corporation, Norwalk, Connecticut, U.S.A.

[12] available from MC^2 Thermal Systems, Antioch, Illinois, U.S.A.

All tests used a heating rate of 20°C per minute. In order to provide highly accurate estimates of the specific heat and energies of reactions over the entire temperature range of this instrument, tests should be run over very small (e.g. 50°C) temperature increments. However, this would prove to be very time consuming, not only for these fabrics, but for any other fabrics which might be modelled in the future. Therefore, the following temperature ranges were used. The specimen was first heated from 30°C up to an intermediate temperature of 200, 300, or 400°C and then cooled. The mass of the specimen and pan were determined after each run. This was repeated a number of times for each specimen. These tests provided information specifically about the evaporation of water from the fabrics and any other thermochemical reactions which might occur at lower temperatures. Finally, the specimen was heated from 30 to 500°C and cooled (once or twice). This was done to provide information about reactions which occur at temperatures around 500°C. The final mass of the fabric sample and pan was then determined.

It should be noted that the maximum temperature possible with this DSC apparatus was 500°C. As shown in the TGA data, thermal decomposition reactions either begin at temperatures greater than 500°C or begin below this temperature but continue past it. Two other methods were used to attempt to overcome this limitation. First DSC tests were run to temperatures up to 525°C at heating rates down to 2°C per minute, as it was thought that using slower heating rates would allow reactions to go to completion at lower temperatures (see Figure 3.3). However, no new information could be obtained using this method. Therefore, differential thermal analysis (DTA) tests using a Perkin-Elmer DTA 1700 Thermal Analyzer with a System 7/4 Controller[13] were run to temperatures of

---

[13] available from The Perkin-Elmer Corporation, Norwalk, Connecticut, U.S.A.

1000°C. This apparatus does not provide information which is as accurate as the DSC and is more difficult to use, but does have a larger temperature range. However, it was determined that establishing an accurate baseline for these materials over a large temperature range was problematic. Therefore, obtaining any information additional to the DSC information would be extremely time-consuming, and hence DTA testing was abandoned.

Examples of the DSC test results are shown in Figures 3.4 and 3.5. These figures show the heat flow to the samples as a function of temperature. From this information, the software determines the specific heat and energies associated with reactions. For example, it was found that the hump shown around 100°C in Figures 3.4 and 3.5 is due to the evaporation of water from the sample, as the energy per unit mass associated with this reaction was about the same as the latent heat of vapourization of water multiplied by the fraction of mass lost in this temperature range. Examples of the specific heat curves are shown in Figures 3.6 and 3.7. The upper experimental curve in each case represents data calculated from a test on a particular sample from 30, to 200 or 300°C, while the lower experimental curve represents data from a later test from 30 to 500°C. This second curve is lower due to the amount of energy which was removed during the heating of the fabric specimen during tests prior to this final test. Another piece of information which will be used in estimating a relationship between specific heat and temperature for each material is the quoted value of the specific heat of these fabrics at room temperature, about 1300 J/kg·°C (e.g. [106]).

The definition of the apparent heat capacity of the fabrics was given earlier as Equation (2.13).

$$\begin{aligned} C^A(T) &= \rho c_s(T) \qquad T < T_m \\ &= \rho c_m(T) + \frac{\rho L}{T_l - T_m} \qquad T_m \le T \le T_l \\ &= \rho c_l(T) \qquad T > T_l \end{aligned} \tag{3.8}$$

As the densities of these two materials are assumed to be constant, any variations in the

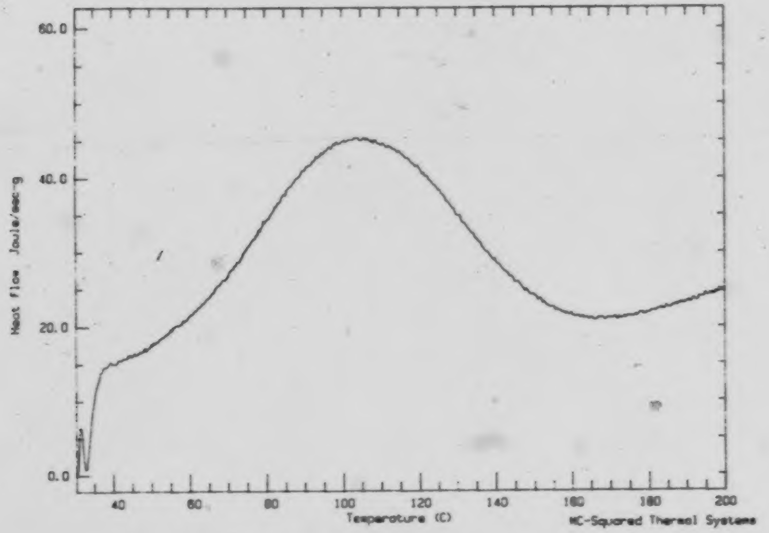

Figure 3.4 DSC Test Data for Nomex® IIIA

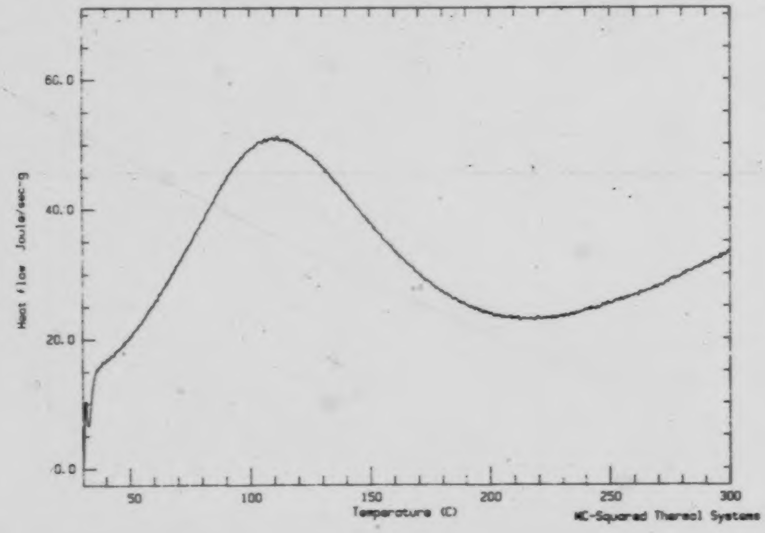

Figure 3.5 DSC Test Data for Kevlar®/PBI

apparent heat capacity with temperature will be due solely to the variations in the specific heat with temperature. Equations for the specific heat as a function of temperature for

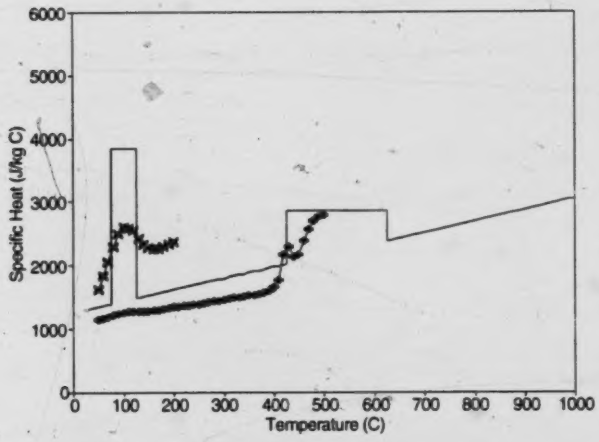

Figure 3.6 Specific Heat as a Function of Temperature for Nomex® IIIA
(X DSC from 30 to 200°C, + DSC from 30 to 500°C, __ Equation (3.9))

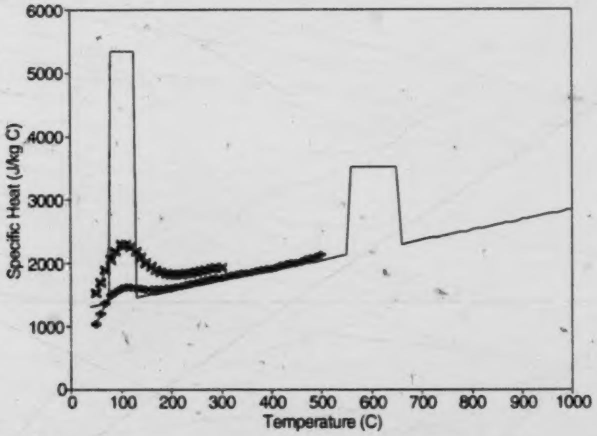

Figure 3.7 Specific Heat as a Function of Temperature for Kevlar®/PBI
(X DSC from 30 to 300°C, + DSC from 30 to 500°C, __ Equation (3.9))

the two fabrics were determined as follows. First the initial value of the specific heat at 300 K was taken as the published value of 1300 J/kg·°C for both fabrics. The slope of the specific heat with temperature curve was then assumed to be equal to the average value of the slopes of all the experimental specific heat-temperature curves for that particular fabric. The initial mass fractions of moisture in Nomex® IIIA and

Kevlar®/PBI fabrics were taken as 5% and 8%, respectively, the moisture regain for each of the fabrics according to PBI technical literature [116]. The energy associated with evaporation of water from the fabric was assumed to take place from 75 to 125°C (remembering that the apparent heat capacity method requires that reactions take place over a range in temperatures rather than a single temperature or very narrow band of temperatures - see Section 2.3.1). The value of the energy associated with the evaporation of moisture from the fabric was taken as the initial mass fraction of moisture in the fabric multiplied by an estimate of the latent heat required to remove the moisture from the fabric, about 2500 kJ/kg[14].

Temperature limits for thermal decomposition reactions were determined using TGA test data from the previous section. The energy associated with the thermal decomposition of Nomex® IIIA cannot be determined precisely using the information from the DSC tests as this reaction had not gone to completion by 500°C. Therefore as a first estimate, it was decided to determine the energy associated with the part of the reaction from 400 to 500°C and double it. The energy associated with the thermal decomposition of Kevlar®/PBI is even more uncertain as the thermal decomposition reactions do not start until temperatures greater than 500°C. Therefore, as a first estimate, it was assumed that the energy associated with the thermal decomposition reactions would be the same as that estimated for the Nomex® IIIA samples. Using all of this information, the equation for the apparent specific heat, $c^{\wedge}(T)$ (i.e. $C^{\wedge}(T) = \rho\, c^{\wedge}(T)$) of the two fabric samples with temperature can be shown to be:

---

[14] this value was estimated from the DSC tests and should account for the latent heat of vapourization of water and the additional energy required to remove moisture from fabrics due to the interaction between the water and the fibrous structure

$$
\begin{aligned}
c^{A}(T) &= 1300 + slope\,(T - 300K) && T < T_{wtr1} \\
&= \frac{\Delta h_{wtr}\,(moist)}{\Delta T_{wtr}} + 1300 + \frac{\Delta T_{wtr}\,slope}{2} && T_{wtr1} \le T \le T_{wtr2} \\
&= 1300 + slope\,(T - 300K) && T_{wtr2} < T < T_{rx1} \qquad (3.9) \\
&= \frac{\Delta h_{rx}}{\Delta T_{rx}} + 1300 + slope\,(T_{rx1} - 300) + \frac{\Delta T_{rx}\,slope}{2} && T_{rx1} \le T \le T_{rx2} \\
&= 1300 + slope\,(T - 300K) && T > T_{rx2}
\end{aligned}
$$

where:		
	Δh_{wtr}	is the latent heat of vapourization of water
	Δh_{rx}	is the energy associated with thermal decomposition
	moist	is the initial mass fraction of moisture in the fabric
	slope	is the slope of the specific heat-temperature curve for each fabric

and the subscripts wtr and rx refer to the vapourization of water and the thermal decomposition reaction and the subscripts 1 and 2 refer to the beginning and end of the temperature range of these reactions. It should be noted that Equation (3.9) is slightly different from Equation (3.8) as Equation (3.9) is for the case of a specific heat which varies with temperature and also incorporates the energies associated with reactions, whereas Equation (3.8) represents the case where the specific heat is constant with temperature other than in the temperature ranges where reactions occur.

Values of the properties in Equation (3.9) for each of the fabrics are shown in Table 3.1 below.

Table 3.1 Values of Properties for Use in Equation (3.9) for Nomex® IIIA and Kevlar®/PBI Fabrics

Constant	Nomex® IIIA	Kevlar®/PBI
Δh_{wtr} (kJ/kg·°C)	2500	2500
moist	0.05	0.08
T_{wtr1} (°C)	75	75
T_{wtr2} (°C)	125	125
slope (J/kg·°C^2)	1.8	1.6
Δh_{rx} (kJ/kg·°C)	130	130
T_{rx1} (°C)	425	550
T_{rx2} (°C)	625	650

The specific heat curves for these two materials determined using Equation (3.9) and the information in Table 3.1 are shown along with the experimental data in Figures 3.6 and 3.7.

It should be noted that the values of the apparent specific heat around 100°C are much larger than would be expected looking at the experimental data. This is because the initial mass fractions of moisture used to calculate the apparent specific heat were the nominal values for conditioned fabrics, while the specimens used in the DSC were not conditioned. The mass losses during these tests indicated that the mass fractions of moisture in the fabrics were in fact less than their nominal values for conditioned fabrics.

It must again be stated that the information used to determine these specific heat equations was from tests of the materials at heating rates of 20°C per minute, while the fabrics are heated at much higher rates in bench top tests. Shlensky, et al. [114] have noted that effective specific heat values should only be used under conditions similar to those in which they were determined. However there are no other methods readily available to determine this information for higher heating rates. In addition, the actual energies of the thermal decomposition reactions remain unknown. Therefore, these specific heat equations must be taken as merely estimates of the actual values. The effects of varying parameters in these equations will be discussed in Section 3.3.5.

In the above discussion, it has been assumed that the thermal decomposition reactions of the fabrics are endothermic as they occur in flame contact tests where there is little oxygen available for exothermic oxidation reactions. Schoppee, et al. [117] have noted that in tests which use a radiant heat source rather than a flame exothermic reactions may be possible due to the significantly higher amount of oxygen available to the fabric. The approximate magnitudes of the energies associated with exothermic reactions involving these materials were determined using a Parr oxygen bomb calorimeter[15]. Average values of 12.7 MJ/kg for Nomex® IIIA specimens and 14.2 MJ/kg for the Kevlar®/PBI specimens were obtained. For comparison Chouinard, et al. [118] report values of about 15.5, 22.0, and 29.0 MJ/kg for the heats of combustion of cotton, polyester, and nylon, respectively, measured using an oxygen bomb calorimeter. If a model of a radiant exposure was attempted this information could be useful in describing the thermochemical reactions. Information on oxidation reactions could also be obtained using TGA and DSC tests. This and other recommended future work is described in Chapter 6.

---

[15] available from Fisher Scientific Limited, Edmonton, AB

3.3.6 Transmissivity and Emissivity

In Section 2.3.2, the in-depth absorption of incident radiation was discussed, along with how Beer's law was chosen to model this phenomena. In order to use Beer's law, the extinction coefficient, γ, for each of the two fabrics of interest must be determined. These can be calculated from the transmissivities of the fabrics using

$$\gamma = -\frac{\ln(\tau)}{L_{fab}} \tag{3.10}$$

A Nicolet Fourier Transform Infrared (FTIR) spectrometer[16] was used to measure the transmissivities of the Nomex® IIIA and Kevlar®/PBI fabric samples. As it was important to also determine if the transmissivities of these fabrics varied significantly during bench top tests, fabric specimens which had been subjected to a heat flux of approximately 80 kW/m^2 for 10 s were tested along with specimens which had not been used in bench top tests. The transmissivity measurements for these specimens are shown in Figure 3.8. Note that the Figures marked "blue" are the Nomex® IIIA specimens, while those marked "gold" are the Kevlar®/PBI specimens. Figure 3.8 also presents results in terms of wave numbers, which are the reciprocal of wavelengths. These tests were performed over the range of wave numbers from about 600 to 4000 cm^{-1}, or wavelengths from about 2.5 to 17 μm. The transmissivities of all the fabrics, both before and after a 10 s exposure, were less than 1% over these wavelengths. This agrees with the cover measurements discussed in Section 2.3.2. For the purposes of the model, a transmissivity of 0.01 was chosen for each of the two fabrics.

An emissivity of 0.9 was chosen for the two fabrics. This agrees with the work of Morse, et al. [46] who measured values between 0.88 and 0.91 for virgin and charred Nomex® and PBI fabrics.

---

[16] Available from Nicolet Instrument Corporation, Madison, WI, U.S.A.

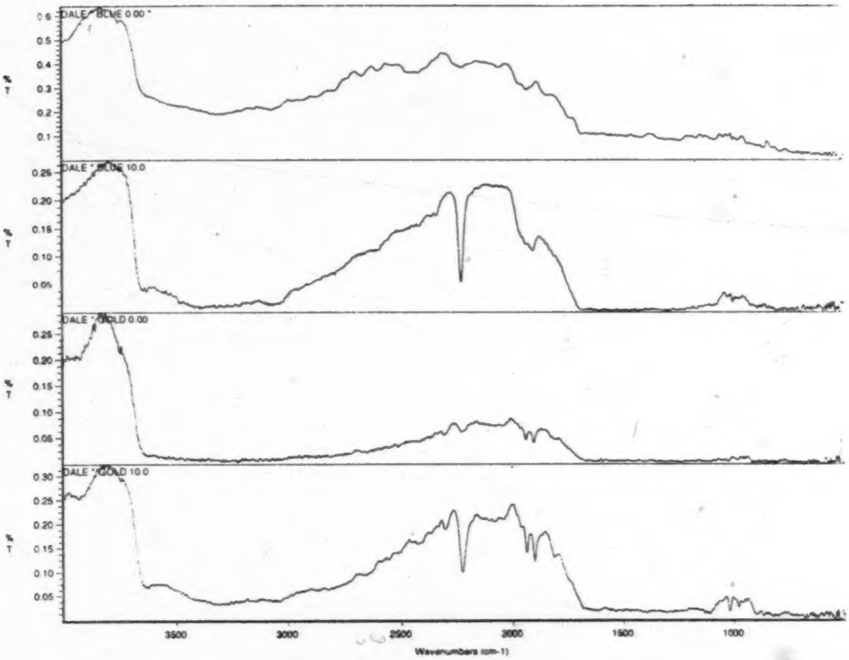

Figure 3.8 Transmissivity Measurements for Nomex® IIIA (Blue) and Kevlar®/PBI (Gold) Fabric Samples Before and After a 10 s Bench Top Test Exposure

3.2.7 Summary of Relevant Fabric Properties

The values of the thermal and other properties of the fabric samples discussed in this section are summarized in Table 3.2 below.

Table 3.2 Summary of Thermal and Other Properties of Nomex® IIIA and Kevlar®/PBI Fabrics Used in this Study

Property	Nomex® IIIA	Kevlar®/PBI
Thickness (mm)	0.7	0.6
Density (kg/m^2)	286	323
Thermal Conductivity (W/m°C)	Equations (3.4) - (3.7) range: 0.047 - 0.255	Equations (3.4) - (3.7) range: 0.047 - 0.255
Apparent Specific Heat (DSC, J/kg·°C)	Equation (3.9), Table 3.2 range: 1300 - 3845	Equation (3.9), Table 3.2 range: 1300 - 5340
Initial Mass Fraction of Moisture	0.05	0.08
Decomposition Reaction Temperature Range (°C) (TGA)	425 - 625	550 - 650
Decomposition Reaction Energy (DSC, endothermic, kJ/kg·°C)	130	130
Enthalpy of Combustion, Oxygen Bomb Calorimeter, exothermic, MJ/kg)	12.7	14.2
Emissivity	0.9	0.9
Transmissivity	0.01	0.01

3.3 Numerical Results

The temperatures of the Nomex® IIIA and Kevlar®/PBI fabric samples were predicted using the numerical model described in Chapter 2 and the thermal properties listed above in Table 3.2. An air gap of 1/4 in. (6.4 mm) was used. The temperatures of the front faces of the two fabrics were practically identical, while the temperatures of the back faces of the two fabrics were only slightly different (Figure 3.9). The times required to exceed the Stoll criterion were as follows:

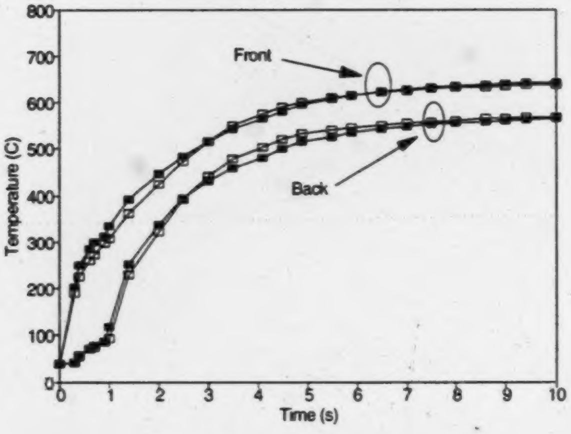

Figure 3.9 Temperatures of the Front and Back of Nomex® IIIA (■) and Kevlar®/PBI (□) Fabrics Predicted by Numerical Model (10 s exposure to nominal 82 kW/m^2 Heat Flux)

Nomex® IIIA	6.55 s
Kevlar®/PBI	6.30 s

In Chapter 4, experiments conducted to verify these results will be described. As will be shown in Chapter 5, these numerical results were similar to the experimental results.

3.4 Parametric Study

As described earlier in this chapter, many of the thermal properties used in the numerical model are difficult to determine, and/or are associated with much uncertainty.

In order to determine the effects of varying these thermal properties on the results from the numerical model, a series of parametric studies was performed. As the thermal properties of the Nomex® IIIA fabric are better known than those for the Kevlar®/PBI fabric, the properties of the Nomex® IIIA fabric were used as the base case for the studies. The range of values for each of the properties used in the parametric studies are given in Table 3.3, while the results of the studies are discussed below.

Table 3.3 Range of Values of Thermal and Other Properties Used in the Parametric Studies

Property	Range of Values used in Parametric Study (typical value for fabrics used in study)
Thickness (mm)	0.3 - 2.0 (0.7)
Moisture Regain (%)	0 - 100 (6)
Thermal Conductivity (W/m·°C)	0.04 - 0.2 (0.04)
Specific Heat (J/kg·°C)	1000 - 3900 (1300)
Decomposition Reaction Temperature Range (°C)	Initial Temperature: 350 - 600 (500) ΔT for Reaction: 100 - 300 (150)
Decomposition Reaction Energy (endothermic, kJ/kg·°C)	30 - 300 (130)
Convective Heat Transfer Coefficient (W/m^2·°C)	25 - 50 (40)
Flame Temperature (°C) (corresponding Emissivity)	1800 - 2200°C (2000°C) (0.018 - 0.22) (0.02)
Air Gap Width (mm)	0.5 - 20 (6)

3.4.1 Thickness

The thickness of the fabric was varied between 0.3 and 2.0 mm. The temperatures predicted for the front and back of a Nomex® IIIA fabric are shown in Figures 3.10 and 3.11, while the times required to exceed the Stoll criterion for different thicknesses are shown in Figure 3.12. It should be noted that for the sake of clarity only temperatures for fabric thicknesses of 0.5, 1.0, 1.5, and 2.0 mm were plotted in Figures 3.10 and 3.11, while the times to exceed the Stoll criterion were plotted for these and other thicknesses in Figure 3.12.

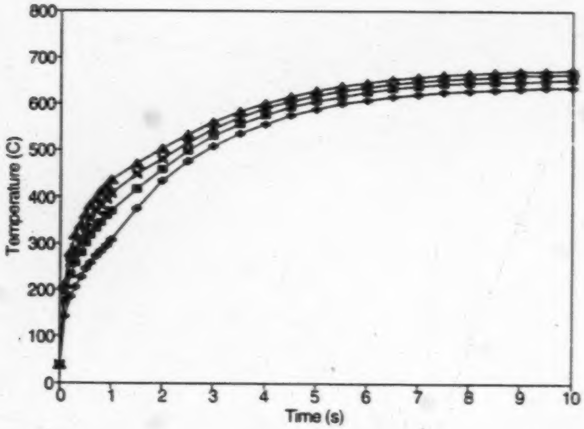

Figure 3.10 Temperatures of Front of Fabric Predicted by Numerical Model for Various Fabric Thicknesses (+ 0.5 mm, ■ 1.0 mm, X 1.5 mm, ▲ 2.0 mm)

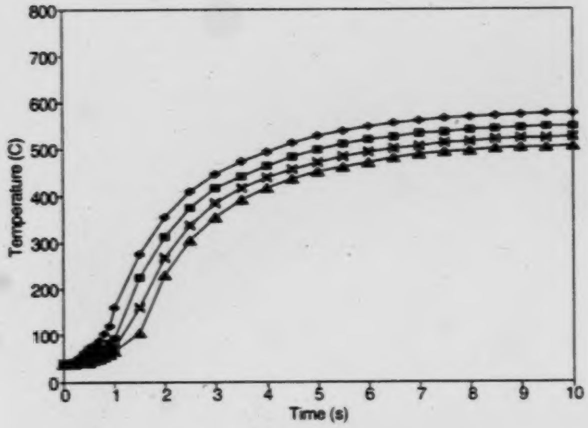

Figure 3.11 Temperatures of Back of Fabric Predicted by Numerical Model for Various Fabric Thicknesses (+ 0.5 mm, ■ 1.0 mm, X 1.5 mm, ▲ 2.0 mm)

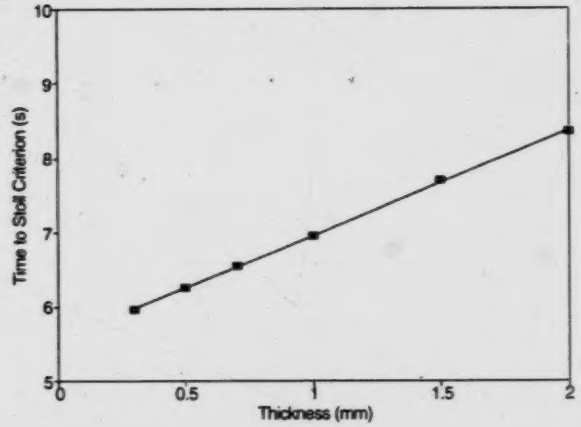

Figure 3.12 Times Required to Exceed the Stoll Criterion Predicted by Numerical Model for Different Fabric Thicknesses

The temperatures of the front of the fabric increased as the thickness increased, while the temperatures of the back of the fabric decreased as the thickness increased. This is expected, as increasing the thickness of the fabric increases the internal resistance to heat transfer within the fabric. This decrease in the temperature of the back of the fabric leads to a decrease in the rate of energy transfer between the fabric and the test sensor across the air space. This in turn results in an increase in the time required to exceed the Stoll criterion. The relationship between the time required to exceed the Stoll criterion and fabric thickness was found to be linear for these fabric thicknesses. This last trend agrees with the experimental work of other investigators (e.g. [119]).

3.4.2 Moisture Regain

The initial amount of moisture in the fabric was varied between 0 and 100%. The temperatures predicted for the front and back of a Nomex® IIIA fabric are shown in Figures 3.13 and 3.14, while the temperatures predicted for the copper disk test sensor are shown in Figure 3.15. The times required to exceed the Stoll criterion for different initial amounts of moisture are given in Table 3.5 below.

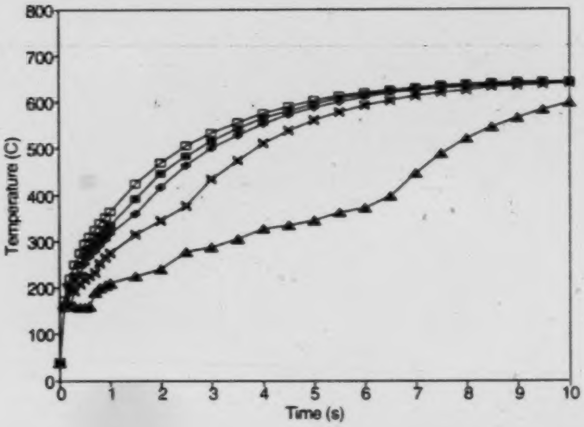

Figure 3.13 Temperatures of Front of Fabric Predicted by Numerical Model for Various Initial Mass Fractions of Moisture (☐ 0.01, ■ 0.05, + 0.10, X 0.25, ▲ 1.00)

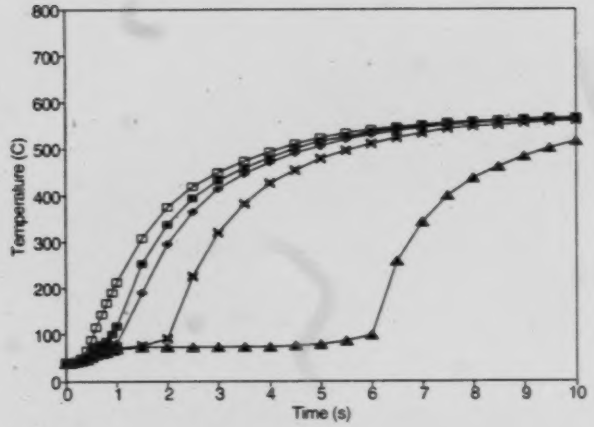

Figure 3.14 Temperatures of Back of Fabric Predicted by Numerical Model for Various Initial Mass Fractions of Moisture (☐ 0.01, ■ 0.05, + 0.10, X 0.25, ▲ 1.00)

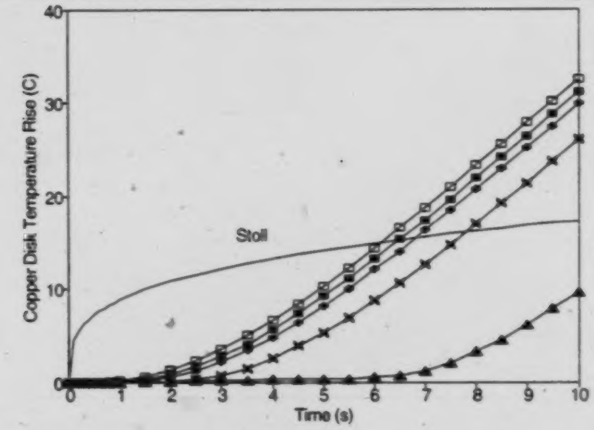

Figure 3.15 Copper Disk Temperature Rise Predicted by Numerical Model for Various Initial Mass Fractions of Moisture (☐ 0.01, ■ 0.05, + 0.10, X 0.25, ▲ 1.00)

Table 3.5 Required Times to Exceed Stoll Criterion Predicted by Numerical Model for Various Initial Mass Fractions of Moisture

Moisture Regain (%)	Time Required to Exceed Stoll Criterion (s)
0	6.15
3	6.35
5	6.55
7	6.65
10	6.85
15	7.15
20	7.50
25	7.80
100	> 10

As the initial amount of moisture in the fabric increased, the predicted rates of increase of the temperatures of the front and back of the fabric, and the copper disk decreased. This was due to the increased amount of energy from the Meker burner which was required to evaporate the water in the fabric. The magnitude of the differences between the temperatures of dry (0%) and conditioned (5 - 7%) fabrics, and the corresponding times required to exceed the Stoll criterion were similar to the differences measured by Lee [120] for 50% convective/50% radiative bench top tests.

It would therefore appear that moisture would enhance the performance of fabrics in bench top tests. However, it must be remembered that only one parameter, the moisture regain, was varied independently, and moisture transfer and the energy transfers associated with it were not included in the numerical model. In Section 1.5.4, work by Morse, et al. [46] was discussed in which it was shown that it is difficult to determine whether water vapour from heated fabrics will travel towards the skin or test sensor or towards the heat source. If some of the moisture from the fabric does in fact travel towards the skin or test sensor, then there may be a point at which increases in the initial moisture content may in fact have a detrimental effect on the protection which a fabric offers. This would be particularly important if studying longer exposures to high heat fluxes. For example, many fire fighters suffer steam burns during the course of their duties. Future work which may help to address this and other concerns will be discussed in Chapter 6.

3.4.3 Thermal Conductivity

The specific heat of the fabric was held constant at 1300 J/kg°C, the nominal value for the fabric at room temperature, while the thermal conductivity was given constant values between 0.04 and 0.2. The temperatures predicted for the front and back of a Nomex® IIIA fabric are shown in Figure 3.16 and 3.17, while the temperatures predicted for the copper disk test sensor are shown in Figure 3.18. The times required to exceed the Stoll criterion for different values of thermal conductivity are given in Table 3.6 below.

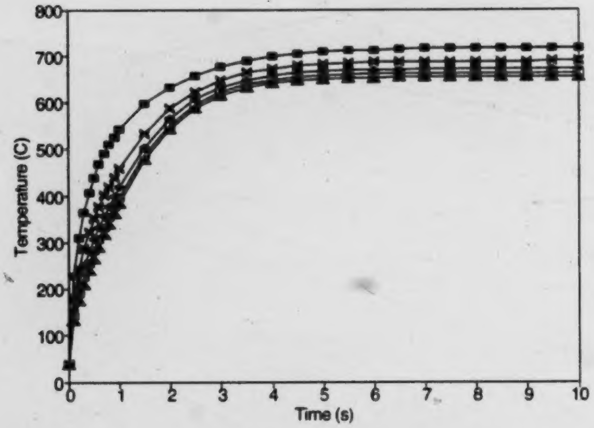

Figure 3.16 Temperatures of Front of Fabric Predicted by Numerical Model for Various Constant Values of Thermal Conductivity (■ 0.04, X 0.08, + 0.12, □ 0.16, ▲ 0.2 W/m·°C)

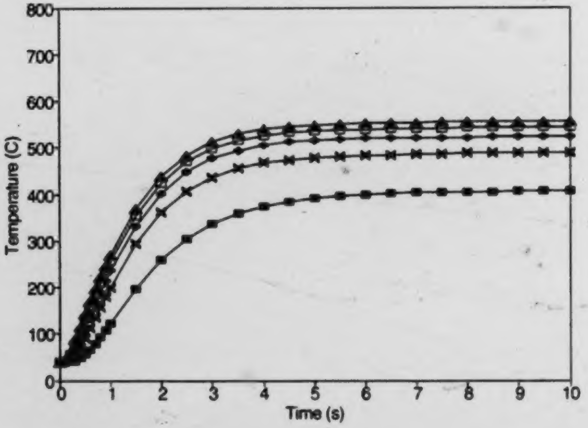

Figure 3.17 Temperatures of Back of Fabric Predicted by Numerical Model for Various Constant Values of Thermal Conductivity (■ 0.04, X 0.08, + 0.12, □ 0.16, ▲ 0.2 W/m·°C)

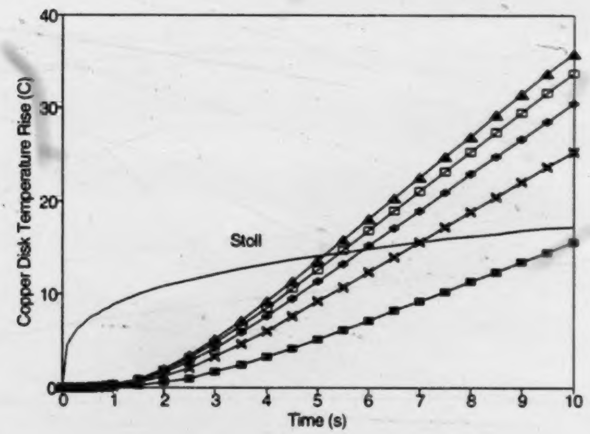

Figure 3.18 Copper Disk Temperature Rise Predicted by Numerical Model for Various Constant Values of Thermal Conductivity (■ 0.04, X 0.08, + 0.12, □ 0.16, ▲ 0.2 W/m·°C)

Table 3.6 Required Times to Exceed Stoll Criterion Predicted by Numerical Model for Various Constant Values of Thermal Conductivity

Thermal Conductivity (W/m·°C)	Time Required to Exceed Stoll Criterion (s)
0.04	> 10
0.08	7.00
0.12	5.95
0.16	5.45
0.20	5.15

The value of thermal conductivity used had some influence on rate of increase of the temperature of the front of the fabric, and an even larger influence on the rate of increase of the temperature of the back of the fabric (Figures 3.16 and 3.17). The differences in the temperatures of the back of the fabric manifested themselves in differences in the copper disk temperatures (Figure 3.18), and hence the times required to exceed the Stoll criterion (Table 3.6). These results are expected for the same reasons discussed above in Section 3.4.1. An increase in the thermal conductivity of the fabric will increase the rate of heat transfer in the fabric, causing the temperature of the back of the fabric to increase faster, and hence increasing the energy transfer between the fabric and the skin or test sensor.

As a practical illustration of how the thermal conductivity could vary from fabric to fabric, the volume fraction of fibre was varied from 5 to 30%. The expressions for thermal conductivity as a function of temperature and volume fractions of fibre and air, discussed earlier in Section 3.2.4 were used. The times required to exceed the Stoll criterion are shown in Table 3.7 below.

Table 3.7 Required Times to Exceed Stoll Criterion Predicted by Numerical Model for Various Volume Fractions of Fibre

Volume Fraction of Fibre (%)	Time Required to Exceed Stoll Criterion (s)
5	7.80
10	7.10
20	6.55
30	6.25

As apparent from the above table, increasing the volume fraction of fibre in the fabric will increase the thermal conductivity of the fabric, and hence decrease the time required to exceed the Stoll criterion. Of course, this statement only takes into account the effect of an increase in volume fraction of fibre on the thermal conductivity of the fabric, and does not account for effects on the mechanical stability of the fabric, other thermal properties of the fabric, etc.

3.4.4 Specific Heat

The thermal conductivity was allowed to vary according to fabric temperature using the equations discussed earlier in Section 3.2.4. The specific heat was given constant values between 1000 and 3900 J/kg·°C. The specific heat was also calculated using Equation (3.9), discussed in Section 3.2.5, and using an empirical relationship given by Schoppee, et al. [121] as being typical for an "average" polymeric material

$$c_p\,(T\,) = 2.22\;T + 629 \tag{3.11}$$

where the temperature, T, is in Kelvin and c_p is given in J/kg·K. The temperatures predicted for the front and back of fabrics with these specific heat values are shown in Figure 3.19 and 3.20, while the temperatures predicted for the copper disk test sensor are shown in Figure 3.21. For the sake of clarity, data predicted using Equation (3.11) were not included in Figures 3.19 through 3.21. However the time required to exceed the Stoll criterion predicted using Equation (3.11), is shown in Table 3.8 below, along with the predictions made using the model and the other specific heat values.

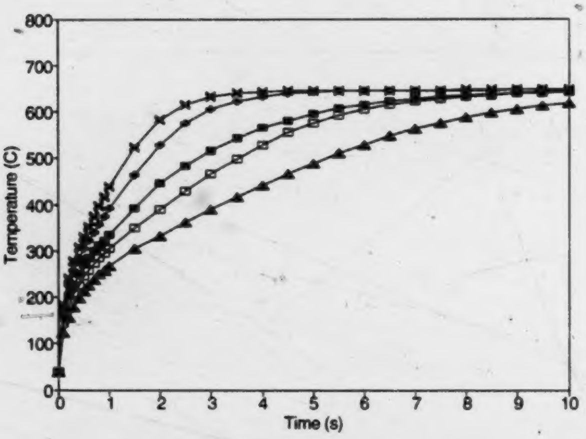

Figure 3.19 Temperatures of Front of Fabric Predicted by Numerical Model for Various Constant Values of Specific Heat (X 1000, + 1300, □ 2600, ▲ 3900 J/kg·°C), and ■ Equation 3.9

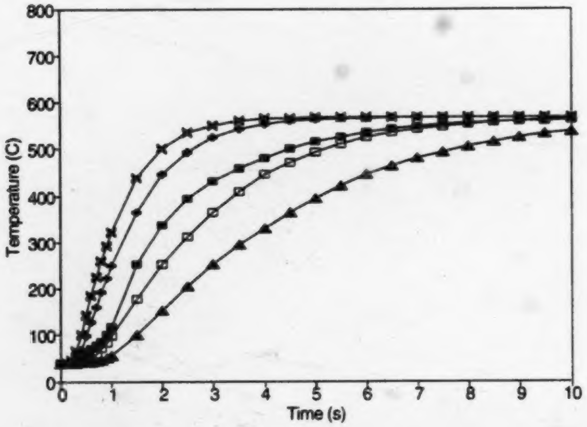

Figure 3.20 Temperatures of Back of Fabric Predicted by Numerical Model for Various Constant Values of Specific Heat (X 1000, + 1300, □ 2600, ▲ 3900 J/kg·°C), and ■ Equation 3.9

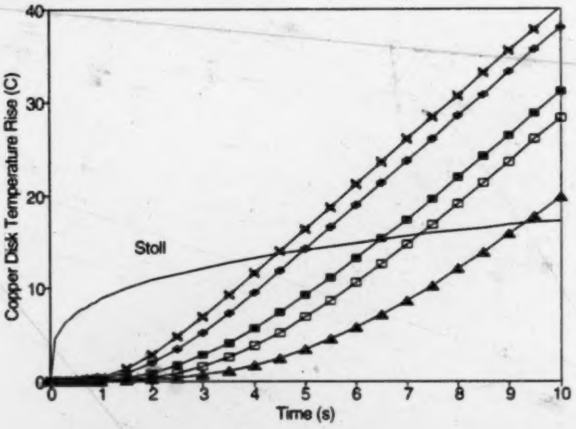

Figure 3.21 Copper Disk Temperature Rise Predicted by Numerical Model for Various Constant Values of Fabric Specific Heat (X 1000, + 1300, □ 2600, ▲ 3900 J/kg·°C), and ■ Equation 3.9

Table 3.8 Required Times to Exceed Stoll Criterion Predicted by Numerical Model for Various Constant Values of Specific Heat

Specific Heat (J/kg·°C)	Time Required to Exceed Stoll Criterion (s)
1000	4.45
1300	5.00
2600	7.25
3900	9.30
Schoppee, et al. (Eqn. (3.11))	6.10
Equation (3.9)	6.55

The value of specific heat used significantly influenced the rate at which the temperature of the front and back of the fabric increased (Figures 3.19 and 3.20), as expected from basic heat transfer theory. Once again, differences in the temperatures of the back of the fabric manifested themselves in differences in the rates of increase of copper disk temperatures (Figure 3.21), and hence the times required to exceed the Stoll criterion (Table 3.8). It should also be noted that Equation (3.9) is for a specific heat based on an apparent heat capacity (see Section 2.3.1), whereas the constant values of specific heat and Schoppee's equation did not include energies associated with the evaporation of moisture and thermal decomposition reactions.

3.4.5 Energies Associated with Thermal Decomposition Reactions

In Section 3.2.5 earlier in this chapter some of the difficulties and uncertainties associated with determining the energies associated with thermal decomposition reactions were discussed. In order to help determine how accurately these energies must be known, the energy associated with this reaction was varied between 30 and 300 kJ/kg. The temperature range over which this energy was to be released was set at 425 to 625°C. To determine the effect of varying the temperature range over which the energy is released at, the energy was set at 130 kJ/kg and the temperature range for the thermal decomposition reaction was varied from 100 to 300°C. The differences in the temperatures of the fabric and the copper disk were minimal, and hence these temperatures are not shown here. The times required to exceed the Stoll criterion are shown in Tables 3.9 and 3.10 below.

Table 3.9 Required Times to Exceed Stoll Criterion Predicted by Numerical Model for Various Values of Energy of Thermal Decomposition Reaction

Reaction Energy (kJ/kg) (endothermic)	Time Required to Exceed Stoll Criterion (s)
30	6.35
60	6.40
80	6.45
100	6.45
130	6.55
150	6.55
200	6.65
300	6.85

Table 3.10 Required Times to Exceed Stoll Criterion Predicted by Numerical Model for Various Temperature Ranges for Thermal Decomposition Reaction

a) Effect of Initial and Final Temperature

Initial Temperature (°C)	Final Temperature (°C)	Time Required to Exceed Stoll Criterion (s)
350	550	6.65
425	625	6.55
500	700	6.40
600	800	6.25

b) Effect of Temperature Range

Initial Temperature (°C)	Final Temperature (°C)	Temperature Range (°C)	Time Required to Exceed Stoll Criterion (s)
425	525	100	6.65
425	575	150	6.60
425	625	200	6.55
425	725	300	6.50

Changes in the energy associated with the thermal decomposition reactions had a minimal effect on the protection offered by the fabrics. This seems counter-intuitive. However, while conditioned fabrics have small amounts of moisture, (e.g. 5% to 8% by mass), the amount of energy required to evaporate this water can be equal to or greater than the amount of energy required for thermal decomposition reactions (e.g. 125 to 200 kJ/kg for evaporation of moisture as compared with 130 kJ/kg for thermal decomposition reactions). This is why the initial amount of moisture in the fabric had a much larger effect on the thermal response and protection offered by the fabrics. Likewise, the temperature range over which the reactions were said to occur had a relatively small effect on the protection offered by the fabrics. Reactions which occur at lower temperatures will "stall" the temperature rise on the back of a fabric, hence reducing the energy transfer to the skin or test sensor, and increasing the time required to exceed the Stoll criterion. It will be shown that this effect is responsible for some of the difference between bench top test results of Nomex® IIIA and Kevlar®/PBI fabric samples in Chapter 5. The temperature range (i.e. ΔT) over which the energy was released had a very minimal effect on the results of the numerical model. These results appear to indicate that further work is not required to refine the estimates of the energies associated with the thermal decomposition reactions for use in this model.

This analysis does not include the effects of decomposition reactions on the mechanical integrity of fabrics, nor is mass transfer of decomposition products considered. Therefore, while the results of the parametric study indicate that it is desirable to have decomposition reactions occur at lower temperatures, caution must be exercised in applying these results. If these reactions severely damage or destroy the mechanical integrity of the fabric, cause it to shrink towards the skin or test sensor, or release large quantities of decomposition reaction products which can condense on the skin or test sensor, decomposition reactions which occur at lower temperatures will certainly decrease the protection which a fabric offers.

3.4.6 Transmissivity

A parametric study of the effect of the transmissivity on fabric temperatures and bench top results was not attempted, as the model of the interaction between the incident radiation and the fibrous structure was based on the assumption that the fabric structure allowed practically none of the incident radiation to pass through the fabric. If other fabrics with a looser fibrous structure are to be modelled, then these may have to be modelled differently from the analysis in Section 2.3.2 which led to the simple Beer's law treatment. A parametric study using such a model could then be conducted.

3.4.7 Boundary Conditions

The effects of the convective heat transfer coefficient for the flow of hot gases from the Meker burner and the flame temperature on the thermal response and bench top test results of the fabric were examined. The convective heat transfer coefficient was varied between 25 and 50 $W/m^2{\cdot}°C$. The temperatures predicted for the front and back of fabrics using these values are shown in Figures 3.22 and 3.23, while the temperatures predicted for the copper disk test sensor are shown in Figure 3.24. The times required to exceed the Stoll criterion for different values of the convective heat transfer coefficient are given in Table 3.11 below.

Table 3.11 Required Times to Exceed Stoll Criterion Predicted by Numerical Model for Various Values of Convective Heat Transfer Coefficient

Convective Heat Transfer Coefficient ($W/m^2{\cdot}°C$)	Time Required to Exceed Stoll Criterion (s)
25	8.30
30	7.55
35	7.00
40	6.55
45	6.15
50	5.75

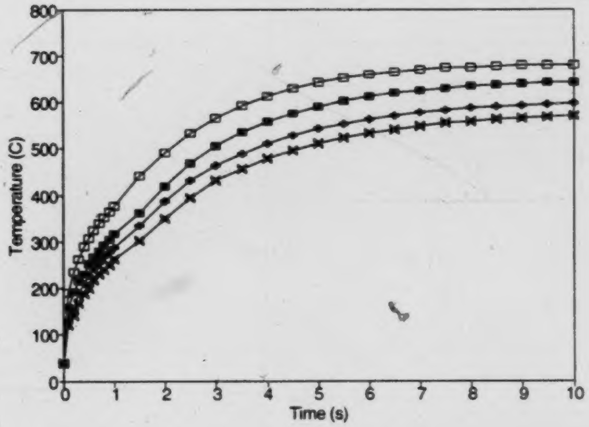

Figure 3.22 Temperatures of Front of Fabric Predicted by Numerical Model for Various Values of Convective Heat Transfer Coefficient (X 25, + 30, ■ 40, □ 50 W/m^2·°C)

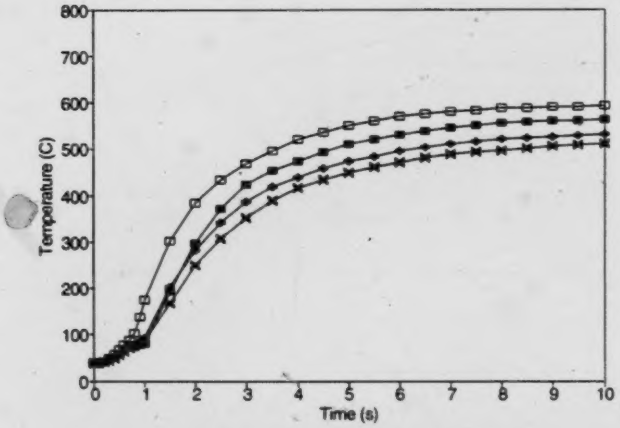

Figure 3.23 Temperatures of Back of Fabric Predicted by Numerical Model for Various Values of Convective Heat Transfer Coefficient (X 25, + 30, ■ 40, □ 50 W/m^2·°C)

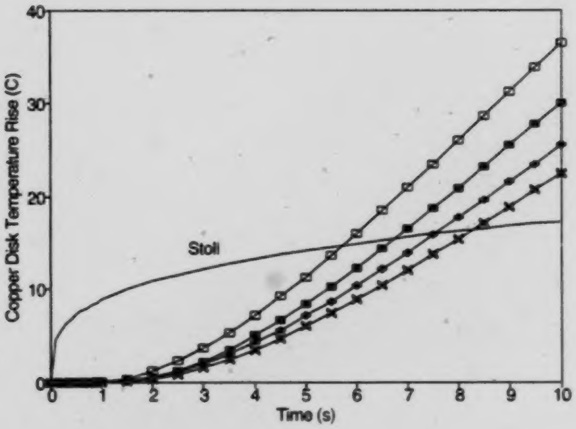

Figure 3.24 Copper Disk Temperature Rise Predicted by Numerical Model for Various Values of Convective Heat Transfer Coefficient (X 25, + 30, ■ 40, □ 50 W/m^2·°C)

The convective heat transfer coefficient on the front face of the fabric had a very large influence on the temperatures of the fabric and the protection that it offers. This parameter, and the flame temperature, are used to define the boundary condition and hence the heat flux incident on the fabric.

The temperature of the flame and its corresponding emissivity was varied between 1800 and 2200°C. The temperatures predicted for the front and back of fabrics using these values are shown in Figures 3.25 and 3.26, while the temperatures predicted for the copper disk test sensor are shown in Figure 3.27. The times required to exceed the Stoll criterion for different values of the flame temperature and emissivity are given in Table 3.12 below.

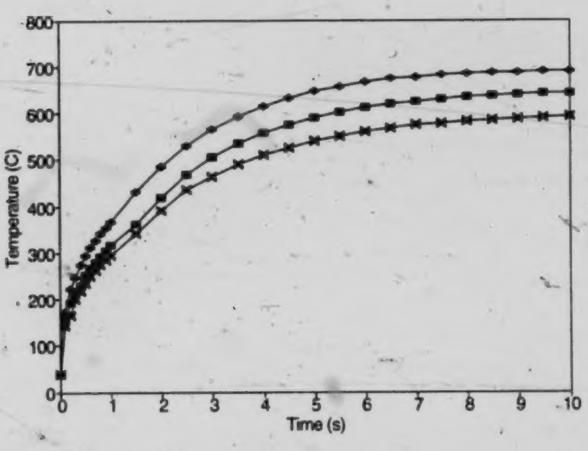

Figure 3.25 Temperatures of Front of Fabric Predicted by Numerical Model for Various Values of Flame Temperature and Emissivity (X 1800°C/0.022, ■ 2000°C/0.02, + 2200°C/0.018)

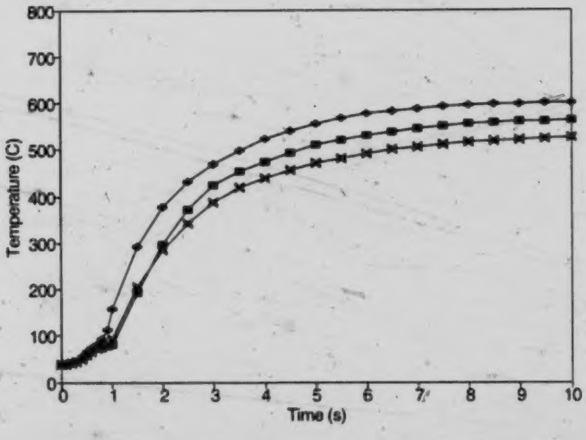

Figure 3.26 Temperatures of Back of Fabric Predicted by Numerical Model for Various Values of Flame Temperature and Emissivity (X 1800°C/0.022, ■ 2000°C/0.02, + 2200°C/0.018)

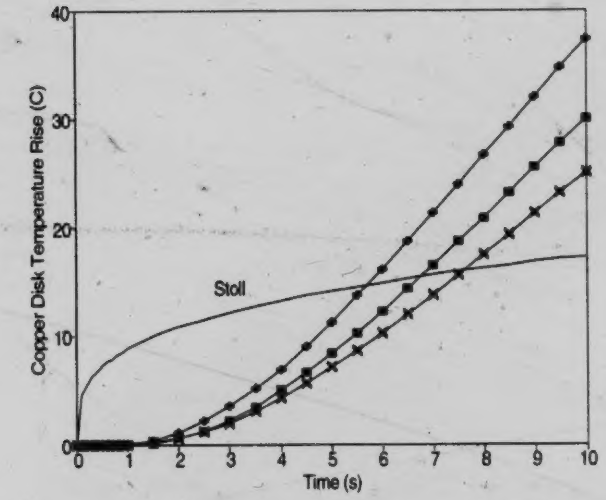

Figure 3.27 Copper Disk Temperature Rise Predicted by Numerical Model for Various Values of Flame Temperature and Emissivity (X 1800°C/0.022, ■ 2000°C/0.02, + 2200°C/0.018)

Table 3.12 Required Times to Exceed Stoll Criterion Predicted by Numerical Model for Various Values of Flame Temperature and Emissivity

Flame Temperature (°C)	Emissivity	Time Required to Exceed Stoll Criterion (s)
1800	0.022	7.60
2000	0.02	6.55
2200	0.18	5.75

As with the convective heat transfer coefficient above, the flame temperature and emissivity had a very large influence on the temperatures and bench top test results of the fabric. In fact, the description of the front boundary condition was the parameter which had the largest effect of all of the parameters examined in this parametric study.

3.4.8 Air Gap Width

As mentioned earlier in Section 2.4, there is some question as to whether there is a critical air gap width between the fabric and test sensor or skin, below which the energy transfer between the fabric and air gap decreases with increasing air gap, and above which the energy transfer increases with increasing air gap. In order to determine whether any critical air gap is predicted using the numerical model, times required to exceed the Stoll criterion were predicted using air gaps between the fabric and test sensor from 0.5 to 20 mm. These results are plotted in Figure 3.28.

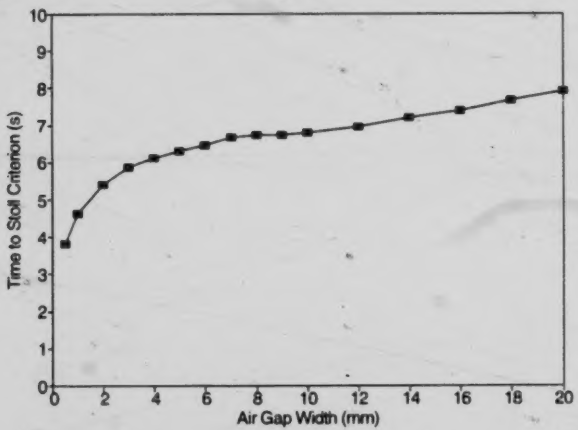

Figure 3.28 Times Required to Exceed Stoll Criterion Predicted by Numerical Model for Air Gap Widths from 0.5 to 20 mm

No critical air gap was indicated, unlike the studies summarized in Table 2.1. There was, however, a point of inflection in the curve at air gaps of about 8 to 9 mm. In order to gain some insight as to the cause of this point of inflection, the two modes of energy transfer in the air gap, conduction/convection, and radiation heat transfer were examined separately. First the relative magnitudes of the two modes were determined at each time step using the numerical model. These data are shown in Figure 3.29 for three particular air gaps, 6, 12, and 20 mm. These data indicate that the heat transfer by convection (actually conduction and convection) is about the same at each air gap, while the heat transfer by thermal radiation is quite different at each air gap.

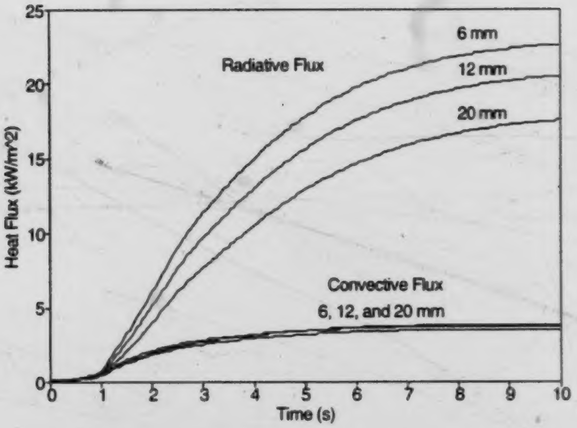

Figure 3.29 Relative Magnitudes of Energy Transfer by Conduction/Convection, and Thermal Radiation Across the Air Gap Predicted by Numerical Model for Air Gap Widths of 6, 12, and 20 mm

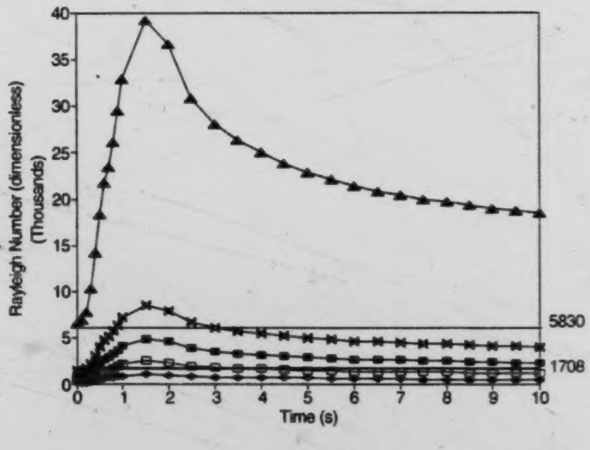

Figure 3.30 Rayleigh Number Histories Predicted by Numerical Model for Air Gap Widths of 6 (+), 8 (□), 10 (■), 12 (X), and 20 mm (▲)

To determine why the magnitude of the conduction and convection heat transfer is about the same at each gap, the Rayleigh number was plotted as a function of time for a number of air gap widths in Figure 3.30. Recalling the discussion in Section 2.4.2

natural convection should begin at a Rayleigh number of about 1700 in an enclosure between two infinite parallel plates heated from below. This criterion is plotted along with the Rayleigh number histories in Figure 3.30, along with the transition to time-unsteady natural convection (Ra = 5830). The estimated Rayleigh numbers indicate that natural convection should occur in air spaces of about 8 mm or larger. The theory also predicts that natural convection should begin fairly quickly after the beginning of the exposure, and be quite vigourous at larger air gap sizes. It should be noted, however, that these results are based on a highly simplified analysis of the heat transfer in the air space. These predictions will be compared with experimental observations in the next two chapters.

The fact that natural convection appears to be more vigourous as the air gap size increases would appear to indicate that the heat transfer by convection should continue to increase with increasing air gap sizes. However, it must be remembered that it is not the extent of natural convection in the air gap which is important, but the energy which is transferred by this process from the heated fabric to the test sensor. Therefore, the maximum value of the convective heat transfer coefficient was compared for different air gap widths (Figure 3.31). At smaller air gap widths before natural convection is initiated, this quantity will actually be the thermal conductance rather than the convective heat transfer coefficient, hence the use of quotation marks in the title on the y-axis). The convective heat transfer coefficient actually decreases with increasing air gap width until an air gap of about 8 mm, then increases very slightly and remains about constant with increasing air gap width. These data demonstrate the importance of the magnitude of the air gap width. Even if strong convection cells are set up in larger air spaces, these will take a finite amount of time to transfer energy from the fabric to the test sensor.

The energy transfer by radiation was also examined. The view factor between the heated portion of the fabric and the copper disk was compared for different air gap widths (Figure 3.32). The view factor decreases as the air gap increases. This explains the fact that the heat transfer by thermal radiation decreases with increasing air gap, as shown in Figure 3.29.

Clearly, these results indicate that while much of the work in the area of the

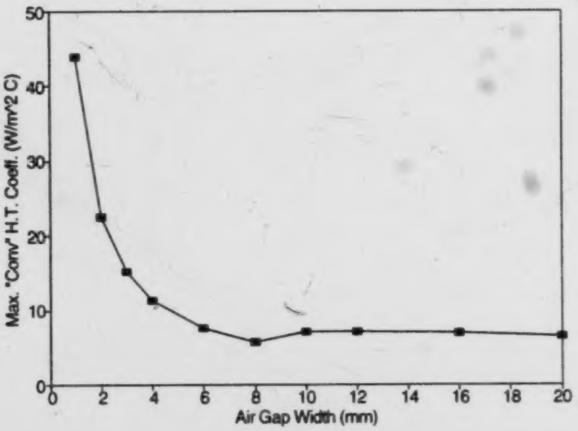

Figure 3.31 Maximum Values of Convective Heat Transfer Coefficient Predicted by Numerical Model for Air Gap Widths from 1 to 20 mm

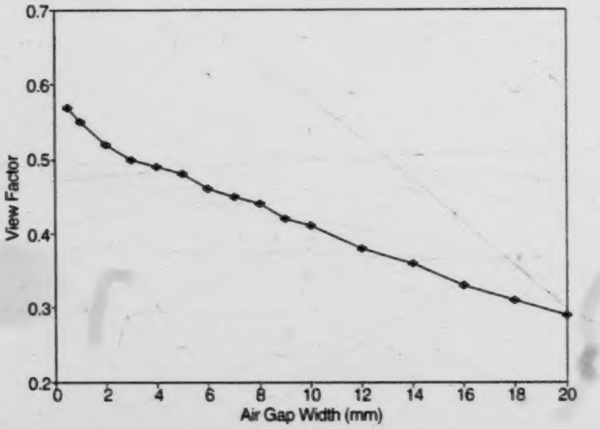

Figure 3.32 Radiation View Factor as a Function of Air Gap Width

energy transfer across the air spaces between protective fabrics and test sensors or underlying skin has been concerned with natural convection in the air spaces, it is the thermal radiation between the fabric and the test sensor which is of primary importance. This mode of energy transfer will be further discussed in Chapter 5 when the results of the numerical model are compared with the experimental results.

3.4.9 Summary of Parametric Study

The parametric study has shown that the thermal properties of interest have various effects on the thermal response and bench top test results of the fabric. Major findings of this study were as follows.

- The time required to exceed the Stoll criterion increases linearly with fabric thickness.
- Changes in the moisture content of the fabric between a completely dried and conditioned state have a relatively small effect on the temperatures of the fabric. The amounts of moisture in conditioned fabrics have a relatively small effect on bench top test results. Larger amounts of moisture can improve the results of bench top tests of fabrics as long as water vapour does not flow towards the skin or a test sensor.
- Increases in the thermal conductivity of the fabric will increase the rate of increase of the temperature of the back of fabric and result in shorter times required to exceed the Stoll criterion.
- Increasing the specific heat of the fabric slows the rate at which the fabric heats up and hence increases the time required to exceed the Stoll criterion.
- The amount of energy released during thermal decomposition reactions had a minimal effect on the thermal response of the fabric and predicted bench top results. The lower the temperature required to initiate the reactions, the better the results of bench top tests. The temperature difference over which the energy is released had a very small effect on the results of the numerical model. Therefore, it may not be very important to exactly define these quantities when modelling fabrics. Due to assumptions in the numerical model regarding thermal decomposition reactions, caution must be exercised in applying these particular results.
- Changes to the flame temperature and emissivity, and the convective heat transfer coefficient of the hot gases from the flame had very large effects on the numerical results.

- The numerical model did not predict an optimal or critical value of the air gap width between the heated fabric and the test sensor. There was a point of inflection in the data at about 8 mm. The energy transfer across the air gap is primarily by radiation, which decreases with increasing air gap width as the view factor between the heated part of the fabric and the test sensor decreases. Natural convection is predicted to occur at air spaces beyond about 8 mm. However, the heat transfer by natural convection will be approximately the same at this and larger air spaces, as the effect of increased natural convection is counterbalanced by the effect of the larger air space which must be traversed.

The limitations of the model and the particular bench top test being studied in this research must be kept in mind when applying the results of this parametric study. For example, only the effect of moisture on the apparent heat capacity was included in this study. No other effects, such as the increase in thermal conductivity with increased moisture regain, or additional mass transfer from water vapour were included in the model. In the next chapter, experiments conducted to validate these results will be discussed. The experimental and numerical results will then be compared in Chapter 5.

CHAPTER 4: EXPERIMENTAL APPARATUS, PROCEDURE, AND RESULTS [17]

In Chapter 3, numerical results from the model described in Chapter 2 were presented. In this chapter experimental work will be described. The main objective of this experimental work was to gather data on the thermal response of the fabrics of interest and their corresponding bench top test results, both of which could be compared with the numerical results. The secondary objective was to use the experimental apparatus to attempt to address some of the limitations of current bench top test techniques by evaluating proposed modifications to standard test procedures.

In this chapter, the bench top test apparatus will first be described. Particular emphasis will be placed on the construction of copper calorimeters used in existing tests, and skin simulant sensors, which have certain advantages over these copper disk sensors. Fabric temperature measurements will be presented, along with bench top test results. As discussed in Chapter 2 and 3, energy transfers in the air space between the fabric and test sensor in these tests are important. The results of bench top tests and flow visualization experiments conducted to quantify and describe these energy transfers will be presented. Modified test procedures and methods of data analysis will also be evaluated.

4.1 Fabric and Shim Stock Samples

As stated in Section 3.1, samples of three common flame resistant fabrics, Kevlar®/PBI, and Nomex® III and IIIA, were used in this study. Each had a nominal mass per unit area of 200 g/m^2 (6 oz/yd^2). The Kevlar®/PBI samples were 2/1 twills, while the Nomex® III and IIIA samples were plain weaves.

Pieces of steel shim stock painted black using TREMCLAD® High-Heat Manifold

---

[17] A version of portions of this chapter has been accepted for publication. Torvi, D.A., Dale, J.D., Ackerman, M.Y., and Crown, E.M., "A Study of New and Existing Bench Top Tests for Evaluating Fabrics for Flash Fire Clothing", Performance of Protective Clothing: 6th Volume, ASTM STP 1273, Jeffrey O. Stull and Arthur D. Schwope, eds., American Society for Testing and Materials, West Conshohocken, PA, 1997

Paint[18] were also used. These were tested in order to provide data to test the numerical model under conditions in which the heated solid would be more homogeneous, not undergo thermal degradation, and would have no internal temperature gradient (as discussed in Section 2.9.3). These shim stock pieces were also used so as to compare the energy transfer across the air gap with a solid bottom boundary to that across an air gap with a porous bottom boundary. The nominal thickness of the shim stock pieces was chosen as 0.003 in. (76 μm) so that the pieces would have approximately the same volumetric heat capacity as the fabric samples, and thus would heat up at about the same rate.

4.2 Experimental Apparatus

The bench top test apparatus used here is shown in Figures 4.1 and 4.2. This apparatus can be used to conduct standard bench top tests such as ASTM D 4108 [29], ISO 9151 [31] and CGSB 155.1 [32]. The test apparatus consists of a Meker burner, a regulator to control the flow of liquid propane gas, a rotameter to measure this flow, a specimen holder assembly, a pneumatic water-cooled shutter, various heat flux sensors, an infrared thermometer, a computer controlled data acquisition system, and a personal computer. Hall effect sensors were mounted on the support for the specimen holder and a piece of metal below the specimen holder in order to sense when the shutter opens and closes, and the burner is moved into place. The magnets for these sensors are attached to the shutter and the arm which holds the burner. One of these magnets can be seen just to the left of the burner in Figure 4.2, while one of the sensors and the wires leading to it can be seen in the lower left hand corner of the same figure. A small container filled with ice was also used to cool some of the heat flux sensors after the tests ended. Details of some of these components are discussed below.

---

[18] available from TREMCO LTD., Toronto, ON

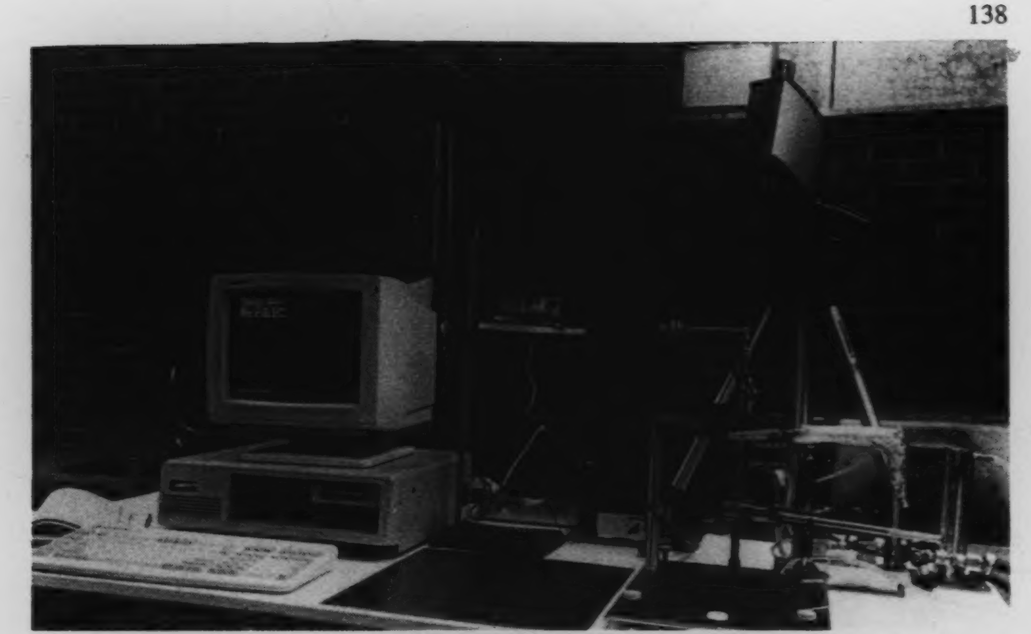

Figure 4.1 Bench Top Test Apparatus

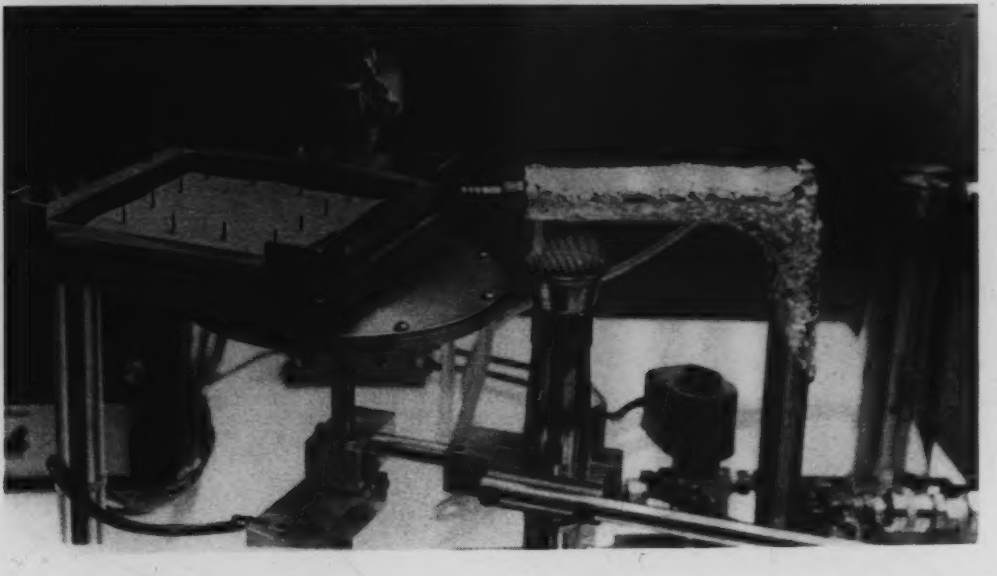

Figure 4.2 Close-up View of Bench Top Test Apparatus Showing Specimen Holder, Water-Cooled Shutter, and Meker Burner

4.2.1 Specimen Holder and Water-Cooled Shutter

A close up of the fabric specimen holder is shown in Figure 4.2. Bench top tests use various methods to hold the fabric specimens in place, which can have a significant effect on test results [30]. This particular specimen holder uses steel pins to hold the fabric, as specified in CGSB 155.1 [32]. This will partially test the fabric's ability to maintain its structural integrity when exposed to the flame. Metal spacers can also be placed on this specimen holder to set a specified air gap between the fabric and the test sensor, such as the air gaps which can occur between a garment and human skin. The specimen holder is mounted so that its upper surface is approximately 50 mm above the top of the Meker burner.

This test rig was also equipped with a shutter so as to precisely control the duration of the exposure of the fabric. This water-cooled, pneumatic shutter can be opened or closed in less than 0.2 s.

4.2.2 Heat Flux Sensors

The heat flux sensors used in the experimental portion of this study are shown in Figure 4.3. In addition to the copper disk heat flux sensors used in standard bench top tests and in the numerical model, skin simulant heat flux sensors similar to those found in the University of Alberta thermal mannequin (Section 1.4.3) were also used.

In ASTM D 4108, and ISO 9151, a copper calorimeter is used as a test sensor. The specifications are very similar in both standards. One difference is that the mass of the disk is specified in ISO 9151 as 18.0 ± 0.05 g whereas no mass is specified in ASTM D 4108. The other difference is the number, type, and mounting procedure of the thermocouple(s) used to read the temperature of the copper disk. In ASTM D 4108, four sets of iron-constantan (Type "J") thermocouples are peened into holes on the back of the disk. In ISO 9151 one copper-constantan (Type "T") thermocouple is soft soldered to the rear surface of the disk. The disk shown in Figure 4.3 is the ASTM D 4108 design. It was found here that differences in bench top test results determined using the two disk designs were less than 5%. This agrees with Hoschke, et al. [77] who found that the heat fluxes measured by both disk designs agreed with those measured by a Medtherm heat

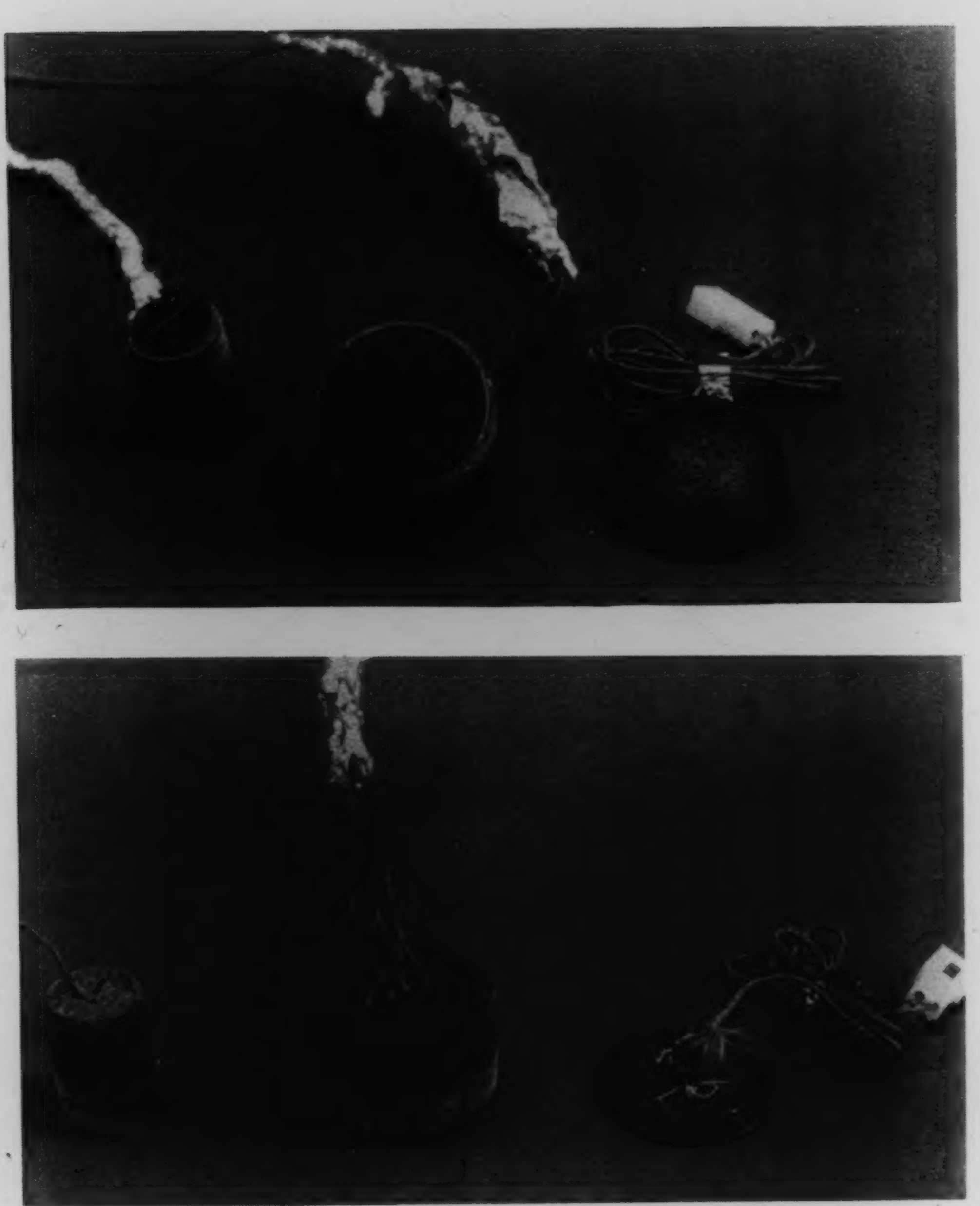

Figure 4.3 Skin Simulant and Copper Disk Heat Flux Sensors (Top Photograph - Front View, Bottom Photograph - Back View)

flux transducer in direct flame exposure tests.

The ISO 9151 disk design was used in this work, as these disks are easier to manufacture than the ASTM D 4108 design. Laying a short length of thermocouple wire on the back on the disk as in the ISO 9151 disk design should also result in smaller errors in temperature measurements than mounting the thermocouples perpendicular to the surface whose temperature is being measured as in the ASTM D 4108 disk design. It was found that it was necessary to silver solder the thermocouple onto the ISO 9151 disk in order to withstand the high temperatures the copper disk reaches (200°C or greater) when exposed directly to the flame when setting the heat flux. The sensor was mounted in a kaowool[19] insulating block. Special mounting pins 1.4 mm in diameter were attached to the back of the disk to hold it in the sensor block rather than using an adhesive as specified in ISO 9151. Although these pins have a much higher thermal conductivity than an adhesive, their cross-sectional area is very small, and an estimate showed that the heat loss through these pins was less than 3% on the input to the disks. A coefficient which accounts for this and other heat losses is discussed in Section 4.3.1.

The copper disk sensors were painted with two very thin layers of the same flat black high temperature manifold paint as used to paint the shim stock pieces (Section 4.1). After a test is completed, the front surface of the test sensor was wiped off in order to remove any residue from products which might condense on the surface of the sensor. If the painted surface became damaged, acetone was used to remove the damaged paint. The disk was then repainted.

Colerceran skin simulant heat flux sensors were also used. Colerceran is an inorganic mixture of calcium, aluminum, silicate with asbestos fibres, and a binder. As will be discussed momentarily, its thermal absorptivity $((k\rho c_p)^{1/2}$ is such that the heat transfer within it will be similar to that in human skin under a suddenly applied heat flux.

Unlike copper calorimeters, skin simulant sensors have an internal temperature gradient during these exposures. The mathematical approach used to determine heat fluxes from test sensor measurements (discussed in the Section 4.3.2) assumes that the temperature inside the skin simulant is initially uniform. However, immediately after a test, these sensors will have an internal temperature gradient. During mannequin tests at the University of Alberta, it may take 30 minutes or more to undress the mannequin, analyze results, wait for sensors to cool, and redress the mannequin. In bench top testing it may take only 5 minutes to remove the specimen, analyze the data, and mount the next specimen. In order to determine if these time frames are adequate for temperatures inside the skin simulants to become uniform, the gradients inside skin simulant sensors were measured and analyzed. Details of this study can be found in Appendix 5. It was found that approximately 20 to 30 minutes were necessary for temperatures to become uniform again. Therefore these internal gradients will not be a problem in mannequin tests. However, for bench top tests it will be important to have a number of skin simulants ready to run consecutive tests, or to allow individual sensors adequate time to cool before beginning the next test.

---

[19] available from Inproheat Industries Ltd., Vancouver, B.C.

Two sizes of skin simulant sensors with diameters of 19 mm and 35 mm were used in these tests. As a result of the above study of sensor temperature gradients, a number of each of these two sizes of sensors were used. The larger diameter was chosen to be close to that of the ASTM D 4108 or ISO 9151 copper disk, while the smaller diameter is similar to the sensors used in the University of Alberta thermal mannequin. The larger sensor had four thermocouples glued on its surface using M-COAT C air-drying silicone rubber[20], at approximately the same locations as specified for the copper disk in ASTM D 4108. A single thermocouple was glued on the surface of the smaller sensor. Test results found using data from the different sizes of sensors were very close, as the actual thermocouple locations were fairly similar in each case.

The skin simulant sensors were placed in kaowool insulating blocks as shown in Figure 4.4. The simulants were manufactured so that they would fit into a small lip just beneath the surface of these blocks, and thus no pins or adhesives were necessary. The surface of each of the skin simulant sensors was painted with the same flat black paint used for the copper disks.

---

[20] available from INTERTECHNOLOGY Inc., Don Mills, ON

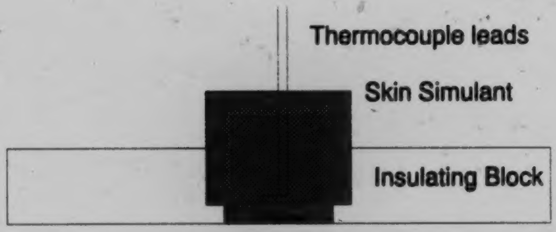

Figure 4.4 Mounting of Skin Simulant Sensors in Kaowool Insulating Blocks

Unlike the relevant thermal properties of the copper disks, which are well known, the skin simulant sensors had to be calibrated individually. To determine their thermal absorptivities, the sensors were each exposed to a known heat flux from a 380 W movie projector lamp powered by a variable voltage power supply. Surface temperature histories of the sensors were then fitted to that predicted by the closed form solution for a semi-infinite solid [100].

$$T\,(x,t)\; - \;T_i = \frac{2\; q_o\,\sqrt{t}}{\sqrt{k\rho c\;\pi}} \tag{4.1}$$

In order to practically carry out the calibration of the sensors, it is necessary to determine the distance the lamp must be placed from each size of heat flux sensor in order to get approximately uniform heat flux distributions across their surfaces. This was done by placing a photocell on a milling table, and traversing a path in the plane parallel to the plane in which the lamp was placed, while recording the output from the photocell with a strip chart recorder. The photocell was placed at distances from about 60 to 190 mm from the lamp in 13 mm increments. From this information, it was found that the lamp must be placed at least 165 mm from a 35 mm diameter sensor, and 90 mm from a 19 mm diameter sensor, in order for the heat flux incident anywhere on the surface of these sensors to be at least 95% of its maximum value for that particular sensor.

Using these distances, the individual sensors were then calibrated. For the particular sensors used it was found that their thermal absorptivities ranged between 1280 and 1487 $J/m^2 \cdot {}^\circ C \cdot s^{1/2}$. These values of thermal absorptivity were used in the numerical routines used to treat the data from the skin simulant sensors, described below in Section 4.3.2.

4.2.3 Temperature Measuring Devices

The transient temperatures of the fabric and shim stock specimens were measured using thermocouples and an infrared thermometer. In order to measure the temperature of the yarns on the front and back surface of the fabric during bench top tests, fine gauge thermocouples were used. While others have used thermocouples to measure fabric temperatures during bench top tests (e.g. [48,120]), there were no details given in these references as to what diameter of wire was used to make these measurements. While larger wires will be more rugged, it is easy to see that these would affect the temperatures of the fabric more than would finer wires. In addition, larger diameter thermocouples would have a slower time response than finer wires. However, finer gauge wires will be more difficult to use.

In order to determine how fine a gauge of thermocouple wire should be used, the diameters of the surface yarns in the fabric were estimated using a microscope. As discussed in Section 2.3.2 the diameters of the yarns are of the order of 250 to 400 μm. As the junction of the thermocouple where the temperature is measured will be at least twice the diameter of the separate thermocouple wires, the thermocouple gauge was chosen so as to be less than one-half of these yarn diameters. Hence wires of 36 and 40 A.W.G. were chosen, as these have diameters of 127 and 80 μm, respectively.

The maximum temperatures of the yarns in these fabrics were expected to be of the order of 1000°C. Therefore, chromel-alumel (Type "K") thermocouple wire was chosen, as this type of thermocouple wire can be used to measure temperatures up to

1350°C for short lengths of time [122].

For thermocouples to be mounted on the front of fabrics, enough insulation was stripped off the thermocouple wires using a soldering iron so that only bare wire would be exposed to the flame. For thermocouples on the back of the fabric it was only necessary to strip enough insulation so that a junction could be made and the thermocouple could be attached to the fabric. Thermocouple junctions were made using a spot welder. When thermocouples were attached to pieces of the steel shim stock a strain gauge welder was used. The thermocouples were sewn onto the front and back surface of fabric specimens using Nomex® thread. In all cases, the thermocouples were mounted parallel to the surface of the fabric or shim stock.

A Barnes Optitherm Model 12-8762 Infrared Thermometer[21] was also used to record the temperatures of the front and back of the fabric during exposures in which the insulating block and test sensor were not placed over top of the fabric specimen. This particular model has a temperature range of 200 to 1700°C, and a centre wavelength of 5.5 μm. The infrared thermometer system consists of a sensing head and a control unit. The sensor head contains adjustable optics so as to focus on objects at different distances. In this case, the sensor head was focused on a circular area with a diameter of about 1 cm on the surface of the fabric or shim stock. As will be discussed later in Section 4.5.2, the instrument records a weighted average of the temperatures inside this viewing area. The emissivity of the object whose temperature is to be measured is selected on this control unit, and the temperature of the object is displayed on its face. Transient measurements were made using an output voltage which is a function of the measured temperature. The infrared thermometer and output voltage was calibrated periodically with a Electro Optical Model WS 143 Blackbody Radiation Source and Model 215B Temperature Controller[22], and its temperature readings were compared with those measured using a Leeds and

---

[21] Available from Barnes Engineering Company, Stamford, Connecticut, U.S.A.

[22] Available from Electro Optical Industries Inc., Santa Barbara, California, U.S.A.

Northrup Model 8632-F Optical Pyrometer[23].

4.3 Treatment of Test Data

A personal computer was used in conjunction with a data acquisition system to record the response of the test sensors, thermocouples, and/or infrared thermometer, and to control the shutter. The outputs from the thermocouples (in the sensors or attached to the fabric) and the infrared thermometer were amplified, then fed into an analogue to digital converter. These operations were done using a Metrabyte DAS-8 board[24]. The data were then fed into a Metrabyte EXP-16 board[25], and read using a computer program that converts the digital output into voltages. These voltages were converted into temperature data using relations found in [122] for thermocouples, or through calibration in the case of the infrared thermometer. Temperatures at each time step were determined from an average of 20 readings of each of the thermocouple and/or infrared thermometer output voltages. The time increments between test data were dependent on the number of channels used for data in a particular test. If only a single test sensor was used, temperatures were recorded about 13 times per second. If three temperature measuring devices were used, temperatures were recorded about five times per second. These temperature data were printed to the screen and a datafile as the test proceeded. Details of how these temperature data were used in bench top tests are given below for each of the test sensors.

4.3.1 Copper Disk Heat Flux Sensors

The test data from the copper disk were analyzed in two different ways. First, the time to exceed the Stoll second degree burn criterion (Section 1.3.2) was determined from the temperature history of the copper disk. As a computer and data acquisition system were used, more sophisticated analysis of the test data was also possible. The instantaneous heat flux at each time step was determined from the temperature data using a lumped capacity analysis [123]

---

[23] Available from Leeds & Northrup Co., Philadelphia, Pennsylvania, U.S.A.

[24] available from Keithley Metrabyte, Cleveland, Ohio, U.S.A.

[25] available from Keithley Metrabyte, Cleveland, Ohio, U.S.A.

$$q(t) = \frac{mc_p}{A}\frac{dT}{dt} + K_l\left(T(t) - T(0)\right) \tag{4.2}$$

where K_l is the loss coefficient (25 W/m^2·°C) discussed previously in Section 2.5.

The use of numerical analysis techniques to determine the instantaneous heat flux at any time step using Equation (4.2) can introduce fluctuations in the calculated heat flux history. One has to be conscious of this and other problems to avoid producing misleading information. For example, the five-point linear least squares method [124] was used here to solve Equation (4.2). If all of the data points were used in the analysis, fluctuations were seen in the heat flux history. Using only data points at larger, equally-spaced time increments eliminated these fluctuations (Figure 4.5). Other techniques are also available to determine heat flux histories from copper disk temperatures ([124],[125]). Other complicatons can arise from timing and resolution errors inherent in the recording of voltages from thermocouples using digital data acquisition systems.

Once the heat flux history was found for the copper disk, this history was used as the input for a finite element model of the heat transfer in human skin [2], along with Henriques burn integral (Section 1.3.3) to determine the estimated times to second and third degree burn.

4.3.2 Skin Simulant Heat Flux Sensors

Under the assumption that the skin simulant was initially at a uniform temperature, Duhamel's theorem can be used to determine the surface heat flux history from the surface temperature history [126].

$$q''(t) = \sqrt{\frac{k\rho c_p}{\pi}}\left[\frac{1}{2}\int_0^t \frac{T_s(t) - T_s(\tau)}{(t-\tau)^{3/2}}\,d\tau + \frac{T_s(t) - T_i}{t^{1/2}}\right] \tag{4.3}$$

Examination of (4.3) shows a singularity in the integral when $\tau = t$. The method of Cook

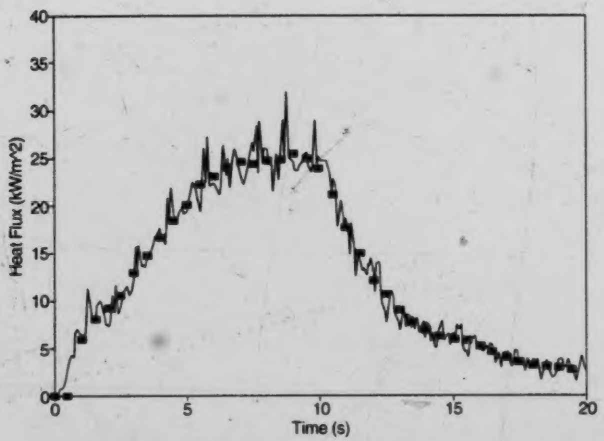

Figure 4.5 Comparison Between Heat Flux Histories Behind Kevlar®/PBI Specimen Determined Using 5-Point Linear Least Squares Method and All the Data (Solid line) or Only the Data at 0.5 s Increments (■)

and Felderman [127] was used to overcome this problem. Specific details are given in Appendix 6.

Once the heat flux incident on the sensor has been determined for each time step, the heat flux history can be placed into the same finite element skin heat transfer model and burn prediction routine used in conjunction with the heat fluxes measured by the copper disk test sensors.

4.4 Experimental Procedure

4.4.1 Standard Bench Top Tests of Fabric and Shim Stock Specimens

The Meker burner was adjusted to produce an average heat flux of 82 ± 2 kW/m^2 over a 10 s exposure, as measured by a copper disk test sensor. The conditioned fabric or shim stock specimens were mounted in the specimen holder and placed on the apparatus. The computer program prompted the operator as to which sensor (ASTM D 4108 or ISO 9151 copper disk, or skin simulant) was being used. Standard bench top tests were run using two procedures.

In manual bench top tests, the operator manually started the test by placing the burner directly under the specimen. A hall effect sensor sent a signal to the computer to start recording data. The sensor temperature and Stoll criterion data were displayed on the computer screen as the test proceeded. Once the Stoll criterion was reached, the operator stopped the test by removing the burner from under the fabric. The Hall effect sensor sent a signal to the computer to stop taking data. The time required to exceed the Stoll criterion was displayed on the screen, and printed to a datafile along with the temperature history for the test sensor.

In bench top tests which used the shutter, the shutter was automatically moved to the closed position to protect the fabric from the flame (Figure 4.6, top photograph). The operator started the test by placing the burner under the specimen. The hall effect sensor then sent a signal to the shutter to pneumatically open. As the test proceeded (Figure 4.6, bottom photograph) the temperature and Stoll criterion were again displayed. However, with this option, the shutter automatically closed once the Stoll criterion was exceeded. The computer also stopped taking data at this point. The time required to exceed the Stoll criterion was displayed on the screen, and printed to a datafile along with the temperature history for the test sensor.

4.4.2 Fixed Duration Bench Top Tests

In a flash fire, a person might be exposed to a high heat flux for a short period of time (e.g. 3 to 5 s). After the exposure ends, there will continue to be an energy transfer between the fabric and the underlying skin which can produce second and/or third degree burns some time after the exposure has ended. Existing bench top tests, such as the first two test procedures, expose a fabric and consider test data until a second degree burn criterion or a given sensor temperature rise is exceeded, rather than for some fixed period of time. In addition, these tests do not provide any information about the deeper burn damage which might occur after the exposure ends.

Behnke [3], in developing the TPP test, which led to the development of ASTM D 4108, stated that a protective clothing test procedure could either measure the true protection offered by the clothing, or rate the materials used in protective garments.

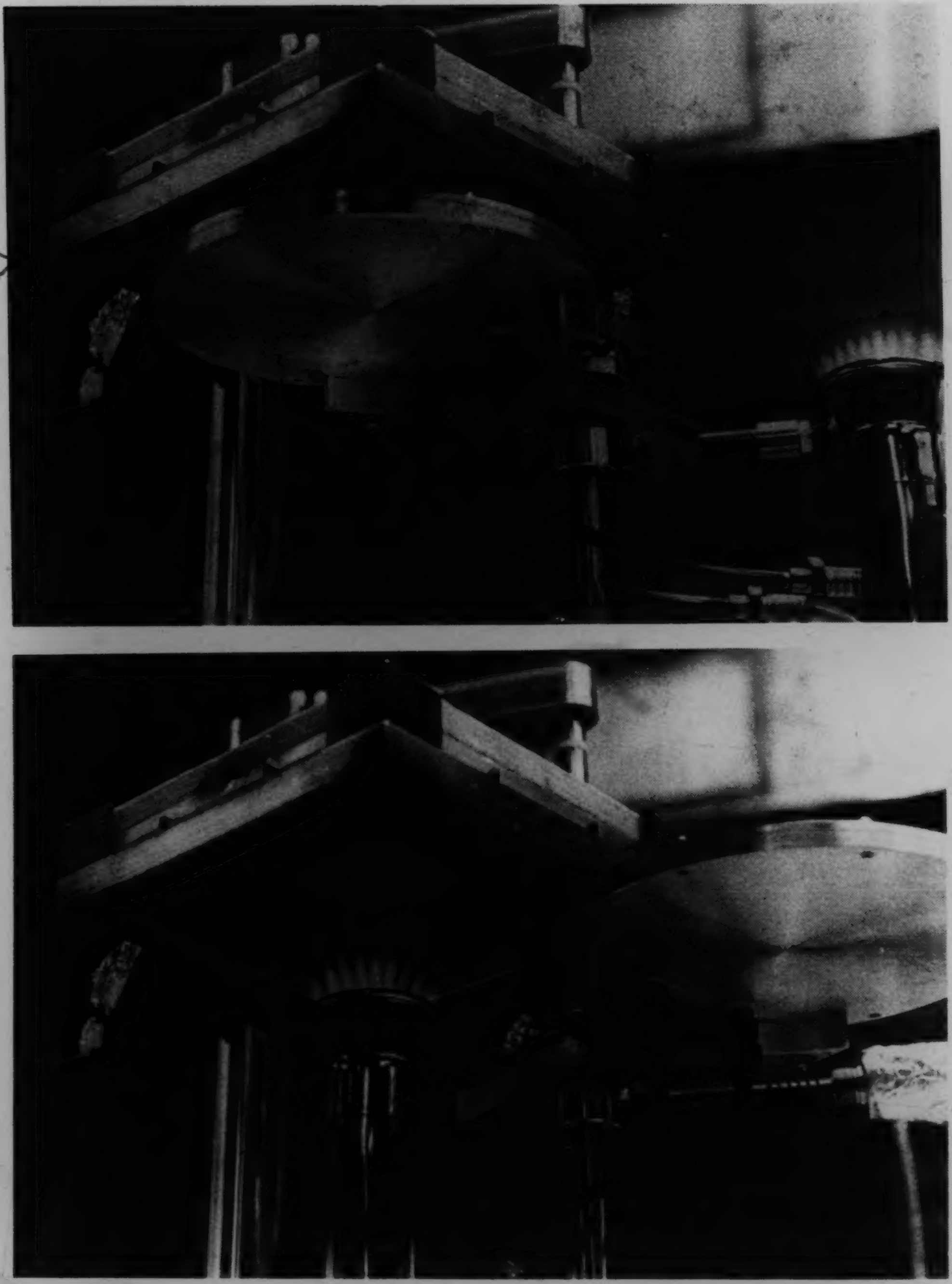

Figure 4.6 Bench Top Test Using a Shutter. Top Photograph - Shutter Closed Prior to Test, Bottom Photograph - Shutter Open, Exposing Fabric to Flame

The first option was difficult because of the task of attempting to duplicate all aspects of a given exposure during the heating and cooling of a garment. The second approach was therefore taken. It also had the advantage of not being tied to a given exposure, and hence was able to provide information which might prove useful about a given fabric under a wide range of exposure conditions. Other investigators [4] have since reminded people that TPP and other bench top test results are not intended to be used as estimates of the protection time provided by a given fabric. A rating method based on times to the Stoll second degree burn criterion was chosen, as the purpose of the test method was to assist in the design of materials which would prevent even second degree burns, let alone third degree burns, under flash fire conditions.

In the time since the development of the TPP test, others (e.g. Holcombe and Hoschke [4], Freeston, et al. [128], and Schoppee, et al. [129]) have studied another alternative for bench top tests, a fixed duration test. This method would still be used to rate fabrics rather than to determine the true protection they offer, but would utilize a different exposure from existing test methods. Here the fabric would be exposed to a simulated flash fire for a fixed duration indicative of the length of exposure in a flash fire (e.g. 3-5 s). Data are taken during this exposure and for some time afterwards. These data can be analyzed to estimate the amount of second and third degree burn damage which might occur to skin behind the particular fabric being tested. For example, Schoppee, et al. [129] exposed fabrics for 3 or 6 s in bench top tests, and measured temperatures at a depth of 500 μm in skin simulant sensors during the exposure and for some time afterwards. However, they did not know of a suitable method to convert these data into surface heat fluxes and hence burn predictions. Therefore they suggested that fabrics be rated on the maximum measured temperature at a given depth in a skin simulant. The use of skin simulants to measure the heat flux history in bench top tests and to use this information in conjunction with Henriques burn integral was also reported by Holcombe and Hoschke [4], but no results were given.

In the development of thermal mannequin testing programs at the University of Alberta and elsewhere (Section 1.4.2), experience has been gained in the use of skin simulants and the analysis of data from these simulants. The very large increases in computing power available to researchers and testing laboratories since the development of the original TPP test have also made it possible to easily, quickly, and economically analyze data from skin simulants. Therefore, it may now be possible to develop fixed duration tests using skin simulants. Alternatively, the present copper disk bench top test sensor might also be suitable for fixed duration tests.

Some investigators have compared results from thermal mannequin tests to bench top tests. These include Behnke [130], Dale, et al. [38], Geshury [72], Crown, et al. [131], and Neal, et al. [132]). However, a thermal mannequin exposure, while nominally the same heat flux as a bench top test, could be considerably different due to factors such as the different burners and orientations used in each test method. To the author's knowledge, no one has published a comparison between the results of fixed duration bench top tests with skin simulants or copper disks, and the results of existing bench top test methods. This will allow for differences in the test sensors and methods for treating test data to be examined.

The following procedure was used here. The operator was prompted for the length of exposure in seconds. Exposures of 10 s duration were used[26]. The test then proceeded in a similar manner to the bench top test using a shutter described above, other than the shutter remained open for the length of time specified by the operator. At the end of this time period, the shutter closed. Data were recorded until 60 s had elapsed from the beginning of the test. This allowed analysis of the energy transfer from the fabric specimen to the sensor after the exposure ended, such as currently is done with the thermal mannequin at the University of Alberta.

---

[26] While a typical flash fire is of the order of 3 to 5 s in duration, it was found that unless the particular fabrics used in this study were placed in contact with the test sensors, third degree burns were not predicted for these materials for 3 to 5 s duration tests. As one of the objectives of this part of the study was to compare different methods of predicting deeper skin burn damage, 10 s duration exposures were used.

4.4.3 Fabric and Shim Stock Temperature Measurements

If fabric or shim temperature measurements were required, the fixed duration test procedure outlined above was used. Fabric or shim temperatures measured by the thermocouples were recorded during and after this fixed duration flame exposure. The fabric temperature was also measured simultaneously using the infrared thermometer. Alternatively, bench top test sensor data was recorded at the same time as the thermocouple fabric or shim temperature measurements.

4.5 Experimental Results

As mentioned in the introduction to this chapter, the objectives of this experimental work were to gather data which could be compared with the results from the numerical model described previously, and to address some of the limitations of current bench top test techniques. In this section the results of experimental work conducted to meet these objectives are discussed in turn.

4.5.1 Effect of Differences in Specimen Preparation on Test Results

Fabric specimens were tested using facilities in the Textiles laboratories of the Department of Human Ecology, and in the Department of Mechanical Engineering at the University of Alberta. Fabric specimens were tested within 30 minutes of being removed from the conditioning room when the facilities in the Department of Human Ecology were used. As the Department of Mechanical Engineering does not have its own conditioning room, and the conditioning room in the Department of Human Ecology is located approximately five minutes away on foot, enough fabric samples for about a half day of testing were place in sealed plastic bags and brought over to the Mechanical Engineering building at a time. Therefore, individual samples were tested at times anywhere from about 30 minutes to 4 hours of being removed from the conditioning room. As the weather conditions in Edmonton varied considerably during the time that tests were performed (e.g. according to ASHRAE [133], the temperature in Edmonton can range from colder than -34°C to warmer than 29°C), it was important to determine the effect of these long delays on test results. As many of the tests were performed during the fall and winter, and hence would be exposed to conditions which were drier than in the conditioning room, it was decided to compare the performance of fabrics which were tested soon after being removed from the conditioning room with those which had been oven dried. Times required to exceed the Stoll criterion and back surface temperature measurements made with type K thermocouples were compared for tests using Kevlar®/PBI and Nomex® IIIA fabrics spaced 1/4 in. (6.4 mm) from the copper disk test sensor. Comparisons between the temperature histories are shown in Figures 4.7 and 4.8. The average times required to exceed the Stoll criterion are shown in Table 4.1.

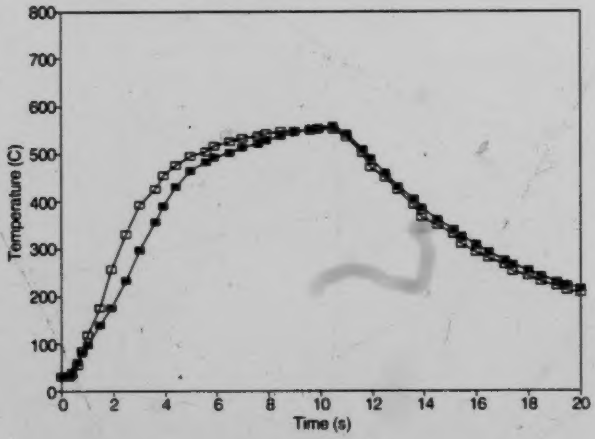

Figure 4.7 Comparison Between Measured Temperatures of Back of Kevlar®/PBI Fabric Specimens - Conditioned (■) and Oven-dried (☐)

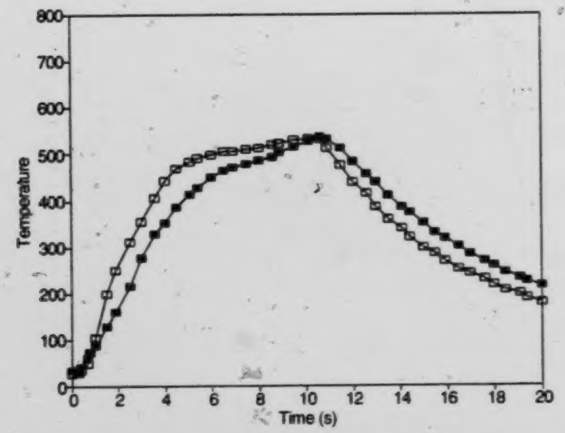

Figure 4.8 Comparison Between Measured Temperatures of Back of Nomex® IIIA Fabric Specimens - Conditioned (■) and Oven-dried (□)

Table 4.1 Average Times Required to Exceed Stoll Criterion for Conditioned and Oven-Dried Fabric Specimens

Preparation of Sample	Time to Exceed Stoll Criterion (s)	
	Kevlar®/PBI	Nomex® IIIA
Conditioned	6.4	7.0
Oven-Dried	6.1	6.6

As shown in Figures 4.7 and 4.8, and Table 4.1, there were minimal differences in the temperature histories and the times to the Stoll criterion for the fabrics in their conditioned and oven-dried states. The backside temperatures were slightly higher in the oven-dried case, as there was no ablative effect of moisture. This in turn caused the slight decreases in the times required to exceed the Stoll criterion. These results are similar to those presented by Lee and Barker [50], who compared temperature histories and TPP results for conditioned, dried, and very wet samples. Therefore it would appear that the relatively long delays between conditioning and testing the fabrics should have minimal effects on test results.

4.5.2 Fabric and Shim Temperatures

The temperatures of fabric and shim specimens were measured during and after a 10 s exposure to a heat flux of 82 ± 2 kW/m^2 using Type K thermocouples and the infrared thermometer. The temperatures of the painted shim stock pieces are shown in Figures 4.9 through 4.11. The temperatures of the front and back of the shim stock measured using 40 A.W.G. thermocouples were very close (Figure 4.9). This was expected given that, as shown in Section 2.9.3, the shim stock pieces could be modelled using the lumped heat capacity method.

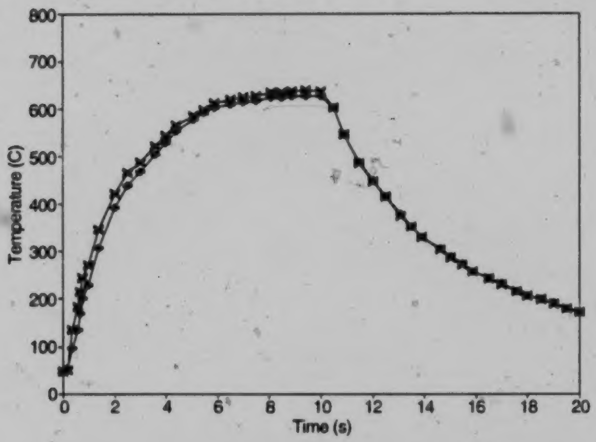

Figure 4.9 Comparison Between Temperatures of Front (X) and Back (+) of Painted Shim Stock Pieces Measured Using 40 AWG Type K Thermocouples

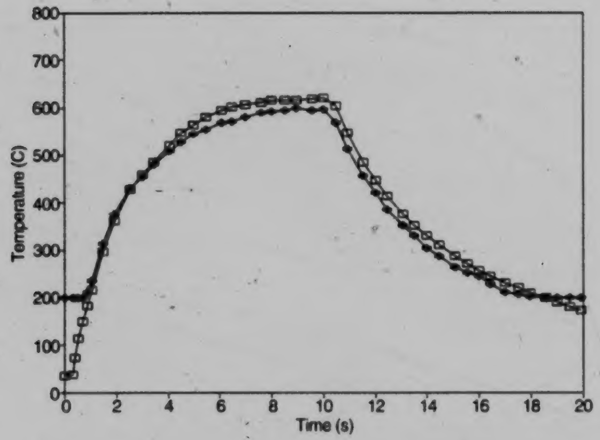

Figure 4.10 Comparison Between Temperatures of Back of Painted Shim Stock Pieces Measured using 36 A.W.G. Type K Thermocouple (□) and Infrared Thermometer (+)

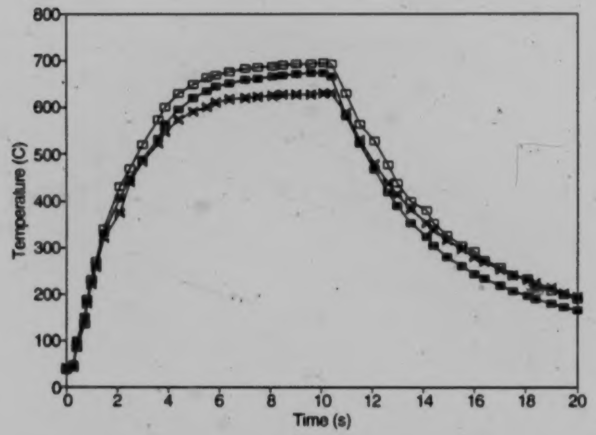

Figure 4.11 Comparison Between Temperatures of Painted Shim Stock Pieces Measured Using Type K Thermocouples in Tests Using Various Air Gap Widths (■ - 3/4 in. (19.1 mm), □ - 1/2 in. (12.7 mm), X - 1/4 in. (6.4 mm))

The temperatures of the back side of the shim stock measured using a 36 A.W.G. thermocouple and the infrared thermometer were also very close (Figure 4.10). The response of the infrared thermometer is extremely rapid, as the manufacturer states that the rise time from 10 to 90% is 50 ms [134]. The response of the thermocouple will be much slower. Sparrow [135] shows that the time constant for 90% response, τ, for a thermocouple measuring the temperature of a flow of gas or fluid is given by

$$\tau = 2.303 \frac{mc_p}{hA_s} \tag{4.4}$$

Assuming the junction to be twice the size of the diameter of each wire, and using the mass and specific heat of this particular thermocouple, it can be shown that the time constant is equal to about 565/h. Therefore, for example, for a flow with a convective heat transfer coefficient, h, of 250 W/m^2·°C, the time constant will be about 2.3 s. For the case here where the thermocouple is measuring the temperature of a solid it is attached to, the calculation of the time constant is much more difficult, according to Sparrow [135]. However, the fact that the thermocouple and infrared temperatures are very similar for the shim stock appears to indicate that time lag effects will be minimal in the measurement of shim stock temperatures with thermocouples. However, it should be noted that the temperatures measured at the beginning of the exposure could not be compared as infrared thermometer readings are only available after the temperatures exceeded 200°C. In addition, it must be remembered that the time response of the thermocouple placed on the shim will be different from that when it is placed on a fabric. This is because the thermal conductivity of the shim stock is much higher than that of the fabric, and the fabric structure is not homogeneous like the shim stock pieces.

Another reason for the small differences between the measurements of the thermocouple and the infrared device is the fact that the thermocouple reads the bare metal temperature (some paint must be scraped off in order to attach the thermocouple with the strain gauge welder), while the infrared thermometer reads the slightly lower painted back surface temperature. In addition, the infrared thermometer reads a weighted average temperature of the circular area (diameter of about 1 cm) inside its viewing area, while the thermocouple measures the temperature at its junction.

One problem with using an infrared thermometer in this application is the absorption of radiation by gases from thermal degradation reactions, or by particles or gases in the atmosphere. In the flame and the atmosphere, the major absorption bands of interest are those of carbon dioxide and water vapour. The infrared thermometer used here has a centre wavelength of 5.5 μm. The closest absorption band to this wavelength is that of water vapour, which is centred at 6.3 μm [67]. To determine if absorption will be a problem in this case, the charts of Wyatt, et al. [136] for the transmittance of water vapour as a function of wave number and amount of water vapour were consulted. These charts indicate that for atmospheric conditions and for the distance of 0.5 m between the infrared thermometer and the fabric used here, the transmittance should be greater than 0.9. This would result in an error of less than 3% in the absolute temperature measured by the infrared thermometer ($0.9^{1/4} = 0.974$). Even if the transmittance was only 0.8, this would still result in an error of less than 5%. (In a similar manner, small errors in the value of the emissivity used for the shim stock (or fabric) will have a very small effect on the temperatures indicated by the infrared thermometer.) To confirm this result, the infrared thermometer was pointed through the flame at the front surface of a shim stock specimen during an exposure. These temperature measurements were then compared with those made by pointing the device at the back surface in a subsequent test (this comparison is not shown here). The very small differences between these measurements indicated that significant portions of radiation were not intercepted by the flame or atmosphere on the way to the infrared thermometer.

It was also found that the variations in shim stock temperatures measured during bench top tests with different air gaps did not follow any regular pattern, such as shim temperatures increasing with increasing air gap (as the larger air gaps should delay the energy transfer from the heated shim to the sensor). This is shown in Figure 4.11. The maximum temperatures measured in the samples after 10 s ranged from about 600 to 700°C. Each of the curves shown represents a single test which was representative of all of the tests conducted using that particular air gap width. There were some differences in the temperatures measured at each air gap width. For example, when no back was placed on the apparatus, there was a difference of 39 K between the lowest and highest value of the maximum temperature the shim stock reached during the exposure. This was about 4% of the average maximum absolute temperature for all of the tests. The range in the infrared thermometer measurements was 24 K (about 3% of the average maximum absolute temperature). As these variations are significant when compared with the data shown in Figure 4.11, it is difficult to make any definite conclusions about the effect of the air gap width on the thermal response of the shim stock pieces.

Unlike the shim stock, fabrics will have an internal temperature gradient. Therefore, thermocouples and the infrared thermometer were used to measure the temperatures of the front and back surfaces of the fabric specimens. It was found that measuring the temperature of the front surface with thermocouples was very difficult. For example, Figures 4.12 and 4.13 show a few examples of how inconsistent these measurements were compared with the measurements of the temperatures of the back surfaces. Some of the problems included insulation on thermocouple wire igniting and burning, thermocouple wires breaking in the flame, and failure of the Nomex® thread which caused the thermocouple to fall into the flame, or at the very least to lose contact with the fabric. Good thermal contact was very difficult to achieve even for the thermocouples mounted on the back surface, due to the nature of the fabrics. In addition, the nonhomogeneous nature of the fabric makes it difficult to say exactly what temperature is being measured on the fabric surface. The infrared thermometer avoids the contact part of this problem, but reads a temperature which is a weighted average of everything it "sees" within its viewing area, including points on the surface and at depth within the fabric [137]. Therefore, the fabric temperatures which the thermocouples and the infrared thermometer measure will be quite different. Figure 4.14 shows an example of the magnitude of this difference. This difference will be discussed further in Section 5.1.1.

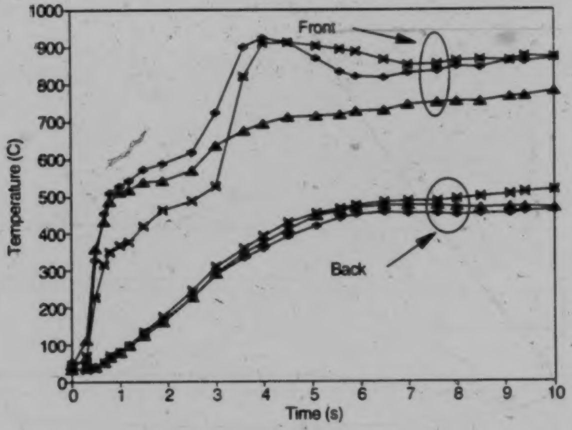

Figure 4.12 Comparison Between Temperatures of Nomex® IIIA Fabric Specimens Measured using Thermocouples in Tests Using Various Air Gap Widths (+ - 1/4 in. (6.4 mm), ▲ - 1/2 in. (12.7 mm), X - 3/4 in. (19.1 mm))

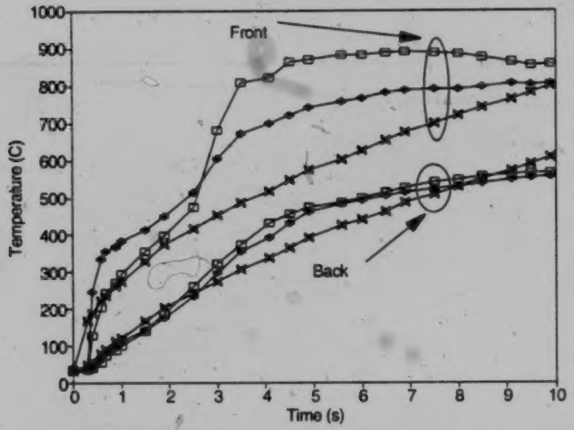

Figure 4.13 Comparison Between Temperatures of Kevlar®/PBI Fabric Specimens Measured using Thermocouples in Tests Using Various Air Gap Widths (+ - 1/4 in. (6.4 mm), X - 3/4 in. (19.1 mm), □ - none)

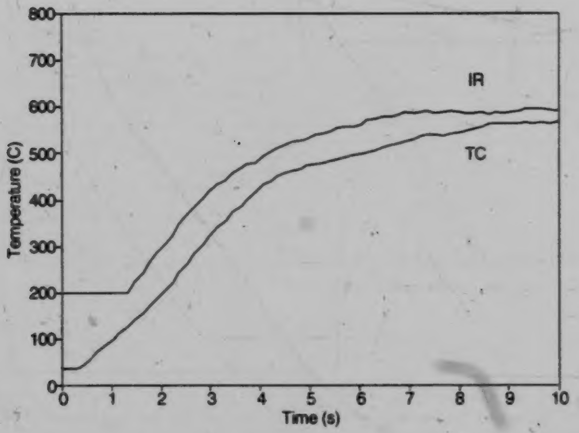

Figure 4.14 Comparison Between the Temperatures of Back of Kevlar®/PBI Fabric Specimens Measured Using Infrared Thermometer (IR) and Type K Thermocouple (TC)

Unlike the temperature measurements of the shim stock pieces at various air gaps, there appeared to be some pattern to the temperature measurements of the fabric specimens using various air gaps. Figures 4.15 and 4.16 show that the temperatures of the fabrics increased with increasing air gap size, as might be expected. The air gap width appeared to have a larger effect on the thermal response of the Nomex® IIIA specimens than the Kevlar®/PBI specimens. Again, caution must be exercised, as the temperatures plotted are simply those from one experiment at each gap. Variations in the data were larger with the fabric specimens than the shim stock pieces. For example, the range in the maximum temperature of the back surface of the Nomex® specimens measured with no insulating block was 70 K, 9% of the average maximum absolute temperature for this series of tests. The range was 48 K for the Kevlar®/PBI specimens, or 6% of the average maximum absolute temperature. The infrared thermometer temperature measurements appeared to be more consistent. For example, the range was 18 K for the Nomex® IIIA samples, 2% of the average maximum absolute temperature.

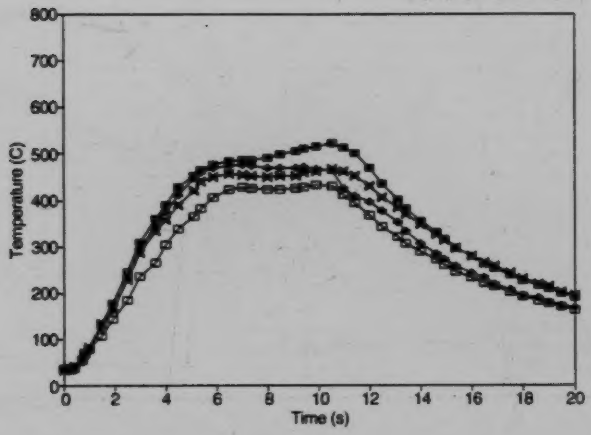

Figure 4.15 Comparison Between Temperatures of Back of Nomex® IIIA Fabric Specimens Measured in Tests Using Various Air Gap Widths (□ - 1/8 in. (3.2 mm), X - 1/4 in. (6.4 mm), + - 1/2 in. (12.7 mm), ■ - 3/4 in. (19.1 mm))

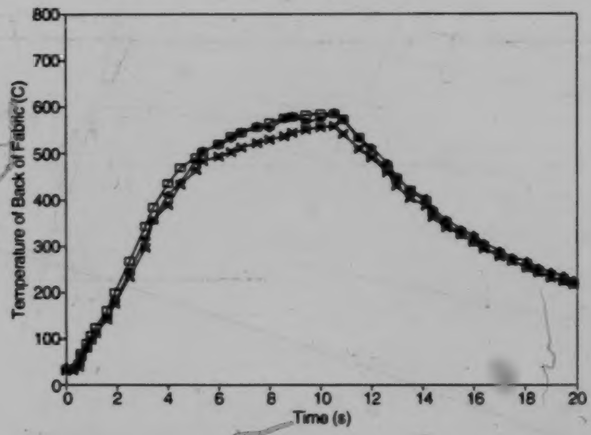

Figure 4.16 Comparison Between Temperatures of Back of Kevlar®/PBI Fabric Specimens Measured Using Type K Thermocouples in Tests Using Various Air Gap Widths (X - 1/4 in. (6.4 mm), + - 1/2 in. (12.7 mm), □ - 3/4 in. (19.1 mm))

A comparison between the temperatures of the front and back "surfaces" of the two fabrics measured by the infrared thermometer is shown in Figure 4.17. The tests were not done simultaneously, as only one infrared thermometer was available. A comparison between the temperatures of the back surface of the fabric specimens measured by the thermocouples is shown in Figure 4.18.

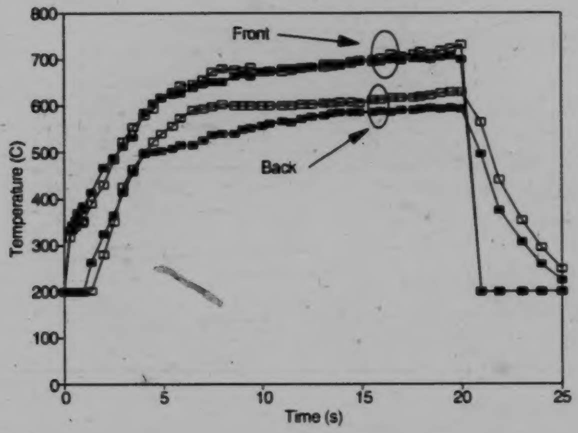

Figure 4.17 Comparison Between Temperatures of Front and Back of Nomex® IIIA (■) and Kevlar®/PBI (□) Fabric Specimens Measured Using Infrared Thermometer During 20 s Exposure

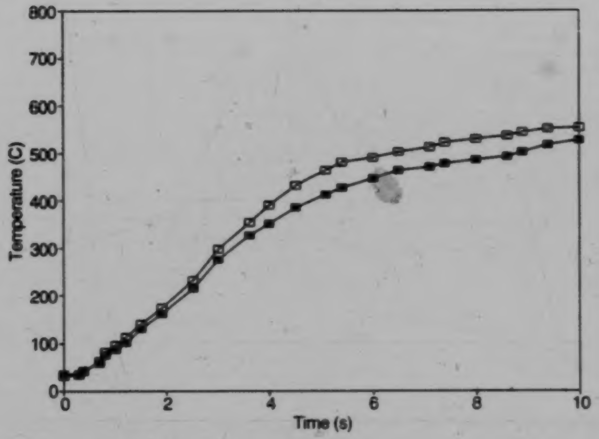

Figure 4.18 Comparison Between Temperatures of Back of Nomex® IIIA (■) and Kevlar®/PBI (□) Fabric Specimens Measured Using Type K Thermocouples During 10 s Exposure

The infrared thermometer measurements show that the "front" temperatures were about the same for each of the fabrics. The "back" temperatures were very close until they reached about 500°C (after about 5 s) where the Nomex® IIIA temperatures began to heat at a slower rate to a lower maximum temperature than the Kevlar®/PBI specimen. Both specimens cooled at about the same rate after the exposure ended (the "front" temperatures immediately dropped below 200°C (the minimum temperature which could be measured by the infrared thermometer) when the exposure ended as the shutter moved in between the fabrics and the infrared thermometer). The temperatures of the back surfaces of the fabrics measured by the thermocouples showed the same general trends, but the fabrics began to heat at different rates after about 2 s rather than 5 s. This could be due to the fact that the thermocouple measured the temperature at a point rather than a weighted average value. Note also that these data were for 10 to 20 s exposures, and that there were no large increases in temperatures after about the first 5 to 7 s. These findings will be discussed in the light of other experimental observations and bench top test results in the next chapter.

4.5.3 Interrupted Mass Loss Test Results

In Section 3.2.5 thermal gravimetric analysis (TGA) results for the fabric samples were presented. It was noted that TGA results can vary depending on the sample heating rate. The fabrics were heated at a rate of 20°C per minute in the TGA tests, whereas the fabric temperature measurements shown in this chapter indicate that the heating rate in bench top tests is of the order of hundreds of degrees Celsius per second during the initial part of the exposure to the flame. In order to gain an appreciation as to how much the higher heating rates in bench top tests affect the mass losses from the specimen, interrupted mass loss tests were conducted using the bench top test apparatus.

The interrupted mass loss tests were based on the work of Shalev [48] who used an "interrupted exposure experiment" to determine the variations in thermal and other properties of fabrics with time of exposure to a 50% convective/50% radiative heat flux. Exposure times ranging from 0.5 to 9 s in 0.5 s increments were used in his work. A similar procedure was used here. The masses of individual fabric samples were determined immediately before and after these fabrics were exposed to the Meker burner for times from 0.5 to 10.0 s, in 0.5 s increments. All of the mass loss was assumed to come from the exposed area of the fabric. The percentages of the original mass remaining after each exposure are plotted in Figures 4.20 and 4.21 against the temperature of the front of the fabric measured by the infrared thermometer. Also plotted in these figures are the corresponding TGA test data for each fabric.

As discussed in Section 3.2.5 and illustrated in Figures 4.19 and 4.20, the temperature at which the thermal degradation of the fabric samples began increased and the entire mass loss curve shifted to the right with an increase in fabric heating rate. It must be cautioned that the masses in the interrupted mass loss tests were obtained a short time after the individual tests ended, rather than continually during the heating process as in the TGA tests. This may cause the measured mass losses of the fabric specimens to be lower than the actual mass losses if moisture from the surrounding is absorbed before the specimen can be placed on the scale. In addition, the temperatures used to plot the bench top test data are weighted average values for the front of the fabric (as discussed in the above Section), while the TGA data are plotted against a temperature

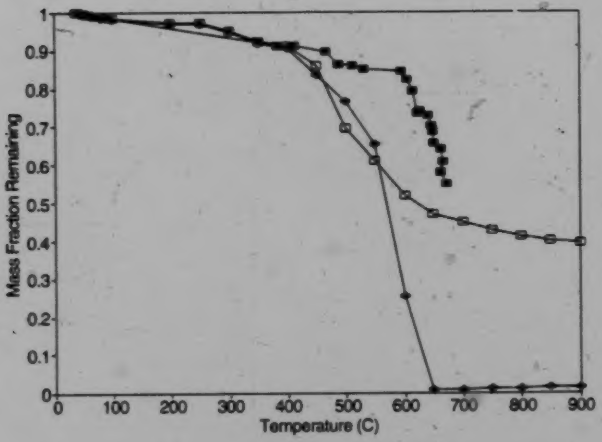

Figure 4.19 Interrupted Mass Loss (■) and TGA (□ Helium, + Oxygen) Test Results for Nomex® IIIA Fabric Specimens

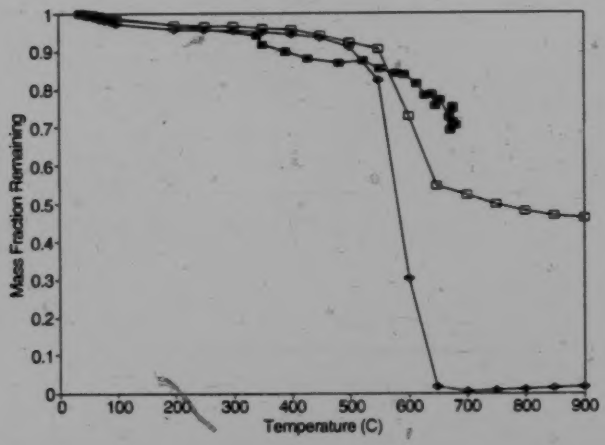

Figure 4.20 Interrupted Mass Loss (■) and TGA (□ Helium, + Oxygen) Test Results for Kevlar®/PBI Fabric Specimens

which is more indicative of the entire fabric specimen. Regardless of these points, the interrupted mass loss data does show that the increase in heating rate does tend to delay the thermal degradation of the fabric specimens.

While the heating of the fabric by a flame is not exactly the same as the heating of a fabric in either an inert or an oxidating environment, it is expected that the flame exposure would be closer to the case of an inert environment [117]. This is also indicated by Figures 4.19 and 4.20, where the mass loss curves obtained from the bench top tests are closer to the TGA curves in the helium environment than those measured in an oxygen environment.

These interrupted mass loss tests were also found to help qualitatively describe the thermal response of the fabrics during bench top tests. Comparisons between the appearances of the fabric specimens at 1.0 s increments are shown in Figure 4.21 for the two fabrics. The fabric specimens were also examined using a microscope for changes in their fibrous structure. Observations at key exposure times which indicate changes to the fibrous structure are shown in Tables 4.2 and 4.3 below.

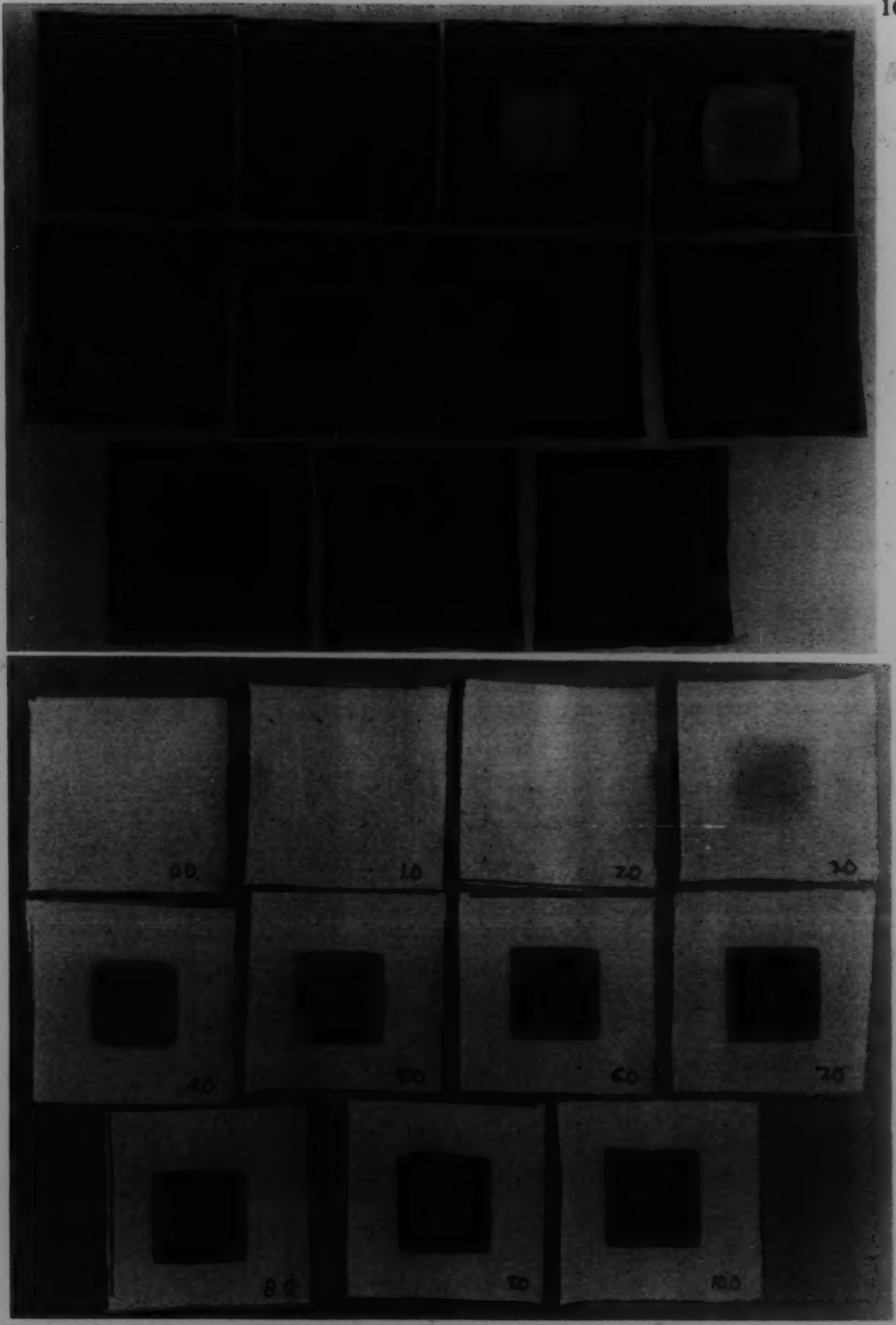
0.0
1.0
2.0
3.0
4.0
5.0
6.0
7.0
8.0
9.0
10.0

Figure 4.21 Nomex® IIIA (top photograph) and Kevlar®/PBI (bottom photograph) Fabric Specimens from Interrupted Mass Loss Tests

Table 4.2 Summary of Macro and Microscopic Changes to Nomex® IIIA Fabrics During Bench Top Test Exposures

Length of Exposure (s)	Macroscopic Observations	Microscopic Observations
0.5-1.0	Front surface of fabric began to discolour	A few damaged fibres were seen; ends of these fibres appeared to have melted
1.5	Blue colour partially gone from exposed area	Dye appears to be gone from surface of some of fibres in exposed area
2.0	Practically none of exposed area remains blue; exposed area began to get brittle	No blue dye seen on surfaces of fibres Fibrous structure remained unchanged; some damage to the edges of individual fibres
3.0	No blue colour left in exposed area	Fibres in front surface yarns began to melt Fibres in back surface yarns reasonably intact, with some surface damage
3.5	Fabric structure appeared more open when held up to light	Fibres damaged, appeared to have melted together Light can penetrate some areas of fibres
5.0	Fabric structure does not appear as open when held up to light as 3.5 s specimen Fabric yarn structure appeared to remain intact	Fibres have turned brown and melted together; very few individual fibres can be identified
10.0	Very similar to fabric specimens for exposures from 5.0 to 9.5 s	Very difficult to identify individual fibres

Table 4.3 Summary of Macro and Microscopic Changes to Kevlar®/PBI Fabrics During Bench Top Test Exposures

Length of Exposure (s)	Macroscopic Observations	Microscopic Observations
1.0	Appeared to be same as unexposed fabric	Slightly larger number of loose fibres on edges of surface yarns than unexposed sample
2.0	No apparent discolouration	Noticeable charring on some loose surface fibres
2.5-3.0	First noticeable discolouration	Some charring and melting of fibres in front surface yarns; apparent mechanical damage to a few of these No apparent changes to fibres in back surface yarns
4.0	More noticeable discolouration	Increased damage to individual fibres in front surface yarns; most still appeared to be mechanically sound Damage to limited number of fibres in back surface yarns
4.5-5.0	More discolouration.	Considerable damage to individual fibres in front surface yarns; Most fibres and yarns themselves appear to be intact and mechanically sound. All fibres in back surface yarns discoloured; some "fraying" on surfaces of these fibres; structure and arrangement of individual fibres in yarns appeared to have changed.
6.0-8.0	Similar to observations at 5.0 s, with increased discolouration	Similar to observations at 5.0 s, with increased damage to individual fibres At 8.0 s, fibres in front surface yarns began to change colour.

Table 4.3 Summary of Macro and Microscopic Changes to Kevlar®/PBI Fabrics During Bench Top Test Exposure (continued)

Exposure Time (s)	Macroscopic Observations	Microscopic Observations
10.0	Similar to observations from 5.0 to 9.5 s, with more discolouration	Fibres in front surface yarns changed colour, were damaged, but most still appeared intact Fibres in back surface yarns had not changed colour

It would appear that the dye was removed from the Nomex® IIIA fabrics (or modified in some other way) within the first few seconds of the exposure, and then thermal decomposition began. From a macroscopic viewpoint, there were no large changes in the appearance of this fabric after about 5.0 s. The yarn structure of the fabric remained intact. However, the microscopic observations indicated that the fibres which make up the individual yarns melted together once thermal decomposition began. These observations agree with the temperature and mass loss measurements shown in Figures 4.12, 4.17 and 4.19. The TGA tests showed an initial mass loss due to the evaporation of moisture, then a mass loss at about 300°C. The observations in Table 4.2 indicate that the blue dye appeared to be removed from the Nomex® IIIA samples after about 1.5 to 2.0 s. The infrared thermometer temperature measurements shown in Figure 4.17 indicate that at 1.5 to 2.0 s, the front surface temperatures of the Nomex® IIIA had climbed beyond 300°C, while the back surface temperatures are well on their way to climbing above 300°C. TGA data indicates that thermal decomposition begins at about 425°C. The observations in Table 4.2 indicate that fibres in the Nomex® IIIA specimens began to melt after 3.0 to 5.0 s. According to the infrared temperature data, the front surface temperature was about 500° at 3.0 s, while the back surface temperature reached 500°C after about 4.0 to 5.0 s. These temperatures are roughly in the range indicated by the TGA results for the beginning of thermal decomposition of the material.

As the Kevlar®/PBI fabric was not dyed, there was no dye removal (or alteration) stage before thermal decomposition. In addition, the fibre and yarn structures of these fabric specimens did not appear to suffer the same damage during the exposures as the Nomex® IIIA samples. They were not noticeable brittle after the exposures and retained much of their initial strength when pulled taut after being removed from the specimen holder. The fabric specimens did not indicate any signs of thermal decomposition of the front of the material until after 3.0 to 4.0 s, and after 4.5 to 6.0 s on the back surface. These observations agree with the temperature and TGA data in Figures 4.13, 4.17 and 4.20. TGA data indicate that thermal decomposition should not begin until about 550°C. The infrared thermometer data indicate that it takes up to 4.0 s for much of the front surface to reach this temperature and up to 6.0 s for the back surface to reach this temperature.

Videotaped observations showing the front and back sides of the fabric during exposures also agreed with experimental data. For example, thermochemical reactions can clearly be seen beginning on the front of the Nomex® IIIA specimens after about 3 s. Materials first glow red when they reach a temperature of about 550°C [90]. Spots within the Nomex® IIIA fabric specimens were clearly seen to glow red from the back view of the fabric after about 5 s. The temperatures measured by the infrared thermometer were greater than 600°C on the front side and greater than 550°C on the back side at this time (Figure 4.17). Similarly a few spots on the front of the Kevlar®/PBI specimens began to glow red after 3 s, and eventually most of the front surface glowed red after about 6 s. These observations are consistent with the temperatures of surface yarns measured using thermocouples (Figure 4.13), and the weighted average temperatures of the front surface measured by the infrared thermometer (Figure 4.17).

This good agreement among the temperature and mass loss measurements, and the micro and macroscopic observations increases the confidence in these temperature and mass loss measurements. All of these observations and measurements will be compared with results from the numerical model in the next chapter.

4.5.4 Bench Top Test Results at Different Air Gap Widths

As mentioned earlier in Section 2.4, there are many questions surrounding the energy transfer in the air space between the fabric and test sensor. In order to attempt to answer at least some of these questions, bench top tests with various air spaces were performed.

In addition to the 1/4 in. (6.4 mm) air gap, other air gaps between 1/8 in. (3.2 mm) and 3/4 in. (19.1 mm) were used when conducting bench top tests of painted shim stock, and Kevlar®/PBI, and Nomex® IIIA fabric samples. Tests in which the specimens were placed in contact with the sensor were also run. The times required to exceed the Stoll criterion for tests using these various air spaces are shown for each of three materials tested in Figures 4.22 through 4.24. It should be noted that results for spacings lower than about 1/4 in. (6.4) may not be entirely meaningful, as the fabrics and shim stock pieces can deform during the exposure. This can increase or decrease the air gap width from its nominal value, which for a given deformation will have a larger effect on the width of the air space, and hence test results, at these smaller air gaps than the larger air spaces (e.g. Figure 4.22). In addition, results for the contact case may also be misleading as the fabric or shim can deform so as to no longer be in contact with the sensor.

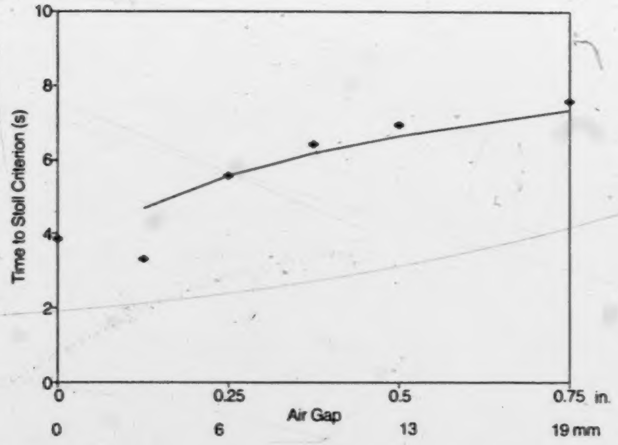

Figure 4.22 Measured Times Required to Exceed Stoll Criterion for Painted Shim Stock Samples Tested using Various Air Gaps (Solid Line - $t_{Stoll} \alpha \Delta x^{1/4}$)

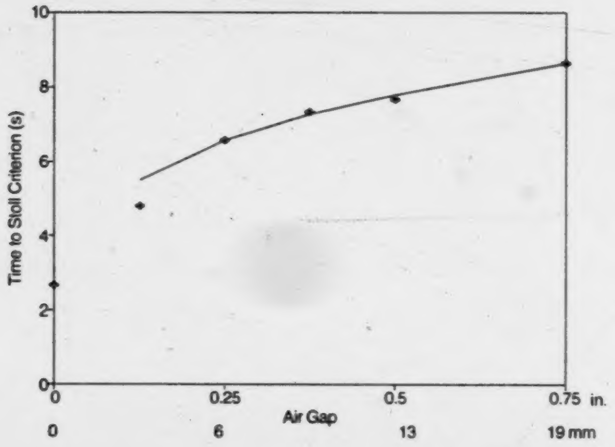

Figure 4.23 Measured Times Required to Exceed Stoll Criterion for Nomex® IIIA Fabric Samples Tested using Various Air Gaps (Solid Line - $t_{Stoll} \alpha \Delta x^{1/4}$)

It should be noted that the data shown in these figures were based on experiments conducted using a bench top test apparatus in the Textiles laboratories in the Department of Human Ecology at the University of Alberta, rather than the apparatus in the

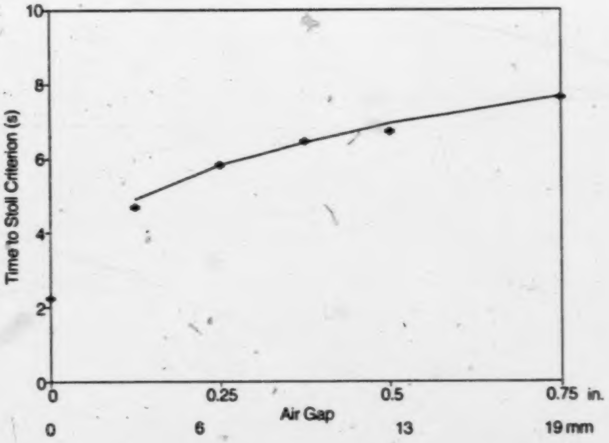

Figure 4.24 Measured Times Required to Exceed Stoll Criterion for Kevlar®/PBI Fabric Specimens Tested using Various Air Gaps (Solid Line - $t_{Stoll} \alpha \Delta x^{1/4}$)

Department of Mechanical Engineering described earlier in this chapter. Therefore, these fabrics were tested fairly soon after being removed from the conditioning room. It should also be noted that the copper disk sensor used in these tests was of the ASTM D 4108 design, and had a mass of about 18.4 g, rather than the 18 g mass of the ISO 9151 sensor (which was used in all of the other experimental work). Therefore, these bench top test results will be different from those presented elsewhere in this thesis. However, they should still illustrate the effect of the air gap width on test results.

It was found that variations in the time to the Stoll criterion with increasing air gap width for air spaces of 1/4 in. (6.4 mm) or greater could be approximately represented by the relation

$$t_{stoll}(x) \ \alpha \ \Delta x^{1/4} \tag{4.5}$$

This relationship is plotted in Figures 4.22 through 4.24 and will be discussed along with the other bench top test results in the next chapter.

4.5.5 Flow Visualization

A flow visualization study was also conducted to help to determine if there is in fact a critical air gap thickness beyond which natural convection would occur. The results of this study should also help to gain an appreciation for the structure of any natural convection cells which would occur beyond such a critical air gap width. The emphasis here was on determining the onset of convection, rather than a detailed description of the convection cells themselves. However, these cells could certainly be studied further using the techniques discussed in this section.

It was first necessary to determine how to mark the flow patterns in the air gaps. It was found that the movement of water vapour, gaseous products of thermal degradation, and/or dyes released from the fabric into the air gap during an exposure served well to mark the flow patterns in the air space. For the painted shim stock samples, it was found that the high temperature manifold paint used to cover the shim samples began to smoke very shortly after the exposure began, and that this smoke could also mark the flow in the air space. Therefore it was not necessary to introduce anything external into the air space to observe the flow. This simplifies the design of the experiments as it is not necessary to determine whether the introduction of an external source of smoke influences the convection patterns which are to be observed.

The bench top test apparatus was then altered as shown in Figure 4.25. In order to observe the flow patterns in the air space, the insulating block and test sensor on top of the specimen holder and spacer were replaced by a clear piece of pyrex glass 1.6 mm thick. A slide projector lamp was mounted above the apparatus and two razor blades were taped over the lamp in order to produce a very thin beam of light across the air space. This allows the photographer to isolate a single cross-section of the flow pattern across the air gap. Still and video cameras were mounted in turn in front of the air gap and at about 20° to the horizontal to record the flow patterns within the air gap. Photographs and videotape of the top views of the patterns in the air gap were also taken, with and without the use of the thin beam of light from the slide projector (transparent plastic sides were used in conjunction with metal corner supports in these cases so as to allow light in through the side of the apparatus). However, the still photographs from this top view were not as useful as the side views in showing the formation and structure of the convection cells, due to the fact that the smoke did not photograph well against the fabric or shim backgrounds. It was also difficult to produce good photographs of the front views of the fabrics. Therefore, only still photographs of the front views of the air gaps with the painted shim stock pieces are reproduced here in Figures 4.26 through 4.29. (The videotape did the best job of capturing the phenomena, but of course cannot be reproduced in this thesis.) Observations for the different air spaces are discussed below, as well as the differences between the patterns shown in the photographs here and those for the fabric specimens.

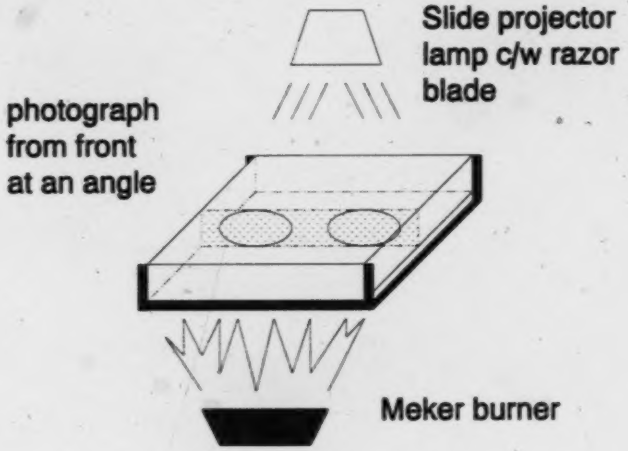

Figure 4.25 Flow Visualization Arrangement

The flow patterns observed in the 3/4 inch (19.1 mm) air gap above the shim stock pieces are shown in Figure 4.26. Immediately after the exposure began, a plume of smoke rose from the heated portion of the middle of the shim stock, moved to the glass plate, and then split into two, forming two convection cells, each about the entire half-width of the air space (Figure 4.26 - top photograph). It took 3 to 4 s for the entire cell to form. After about 5 or 6 s, the plume in the middle disappeared, and the two cells remained. Motion in the cells was fairly rapid and regular (middle photograph). This pattern continued until about 3 to 5 s after the flame was removed, when the cells began

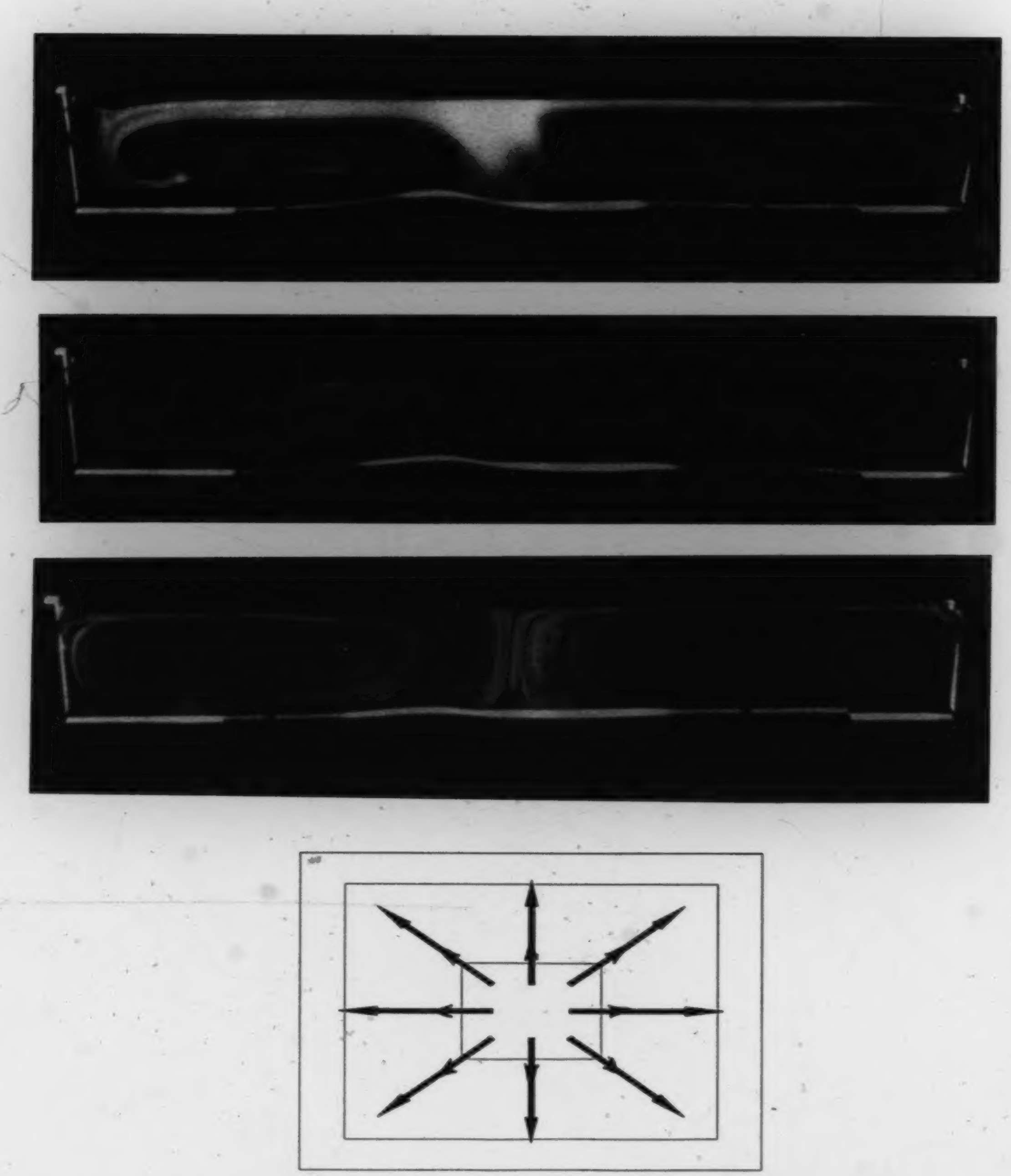

Figure 4.26 Flow Patterns Observed in 3/4 in. (19.1 mm) Air Gap (from top to bottom- immediately after exposure began, after about 5 - 6 s, about 3-5 s after exposure ended, sketch of top view of cells)

to creep back towards the middle (bottom photograph). These cells continued to move in a fairly rapid and regular manner, and did not die out until the top plate was removed and the smoke in the air gap dissipated. The photographs show only a single cross-section of the air gap. The top view of the air gap, also sketched in Figure 4.26, shows an arrangement of similar pairs of cells to those in the photographs, which were arranged like petals on a flower.

It was thought that the movement of the cells out of the middle of the heated portion of the shim stock was due to hot gases forcing the cells to the side. When the flame was taken off, the temperatures above the middle of the heated portion of the shim stock should decrease, which should would cause the cells to return to occupy the entire cross-section of the air space.

The patterns observed with the in the air spaces of 3/4 in. (19.1 mm) above the two fabric specimens were similar to those in the tests with the solid shim pieces.

The flow patterns observed in the 1/2 in. (12.7 mm) air gap above the shim stock pieces are shown in Figure 4.27. The flow patterns at the very beginning of the exposure were similar to those in the 3/4 in. (19.1 mm) air gap (Figure 4.27 - top photograph - taken after about 1 s). As the exposure ended, the larger cells began to break into multiple smaller cells (middle photograph - taken just as exposure ended). This continued in the time immediately after the exposure ended (bottom photograph - taken about 5 s after the exposure ended). The cells did not appear to be as strong as those in the 3/4 in. (19.1 mm) air gap. This is expected as the Rayleigh number, a measure of the relative magnitude of the buoyancy and viscous forces (Section 2.4.2), is proportional to the air gap width cubed. The top view of the cells was similar to that shown in Figure 4.26.

The flow patterns in 1/2 in. (12.7 mm) air spaces above heated Nomex® IIIA specimens were slightly different from those above the shim stock pieces, producing smaller multiple cells almost immediately, rather than just before the exposure ended. Flow patterns did not appear to be as regular as those in the same air gap width above the shim stock pieces. The difference in flow patterns may be caused by larger driving forces for the mass transfer of the smoke from the Nomex® IIIA specimens or hot gases penetrating the fabric structure from the flame. The relative magnitudes of these effects

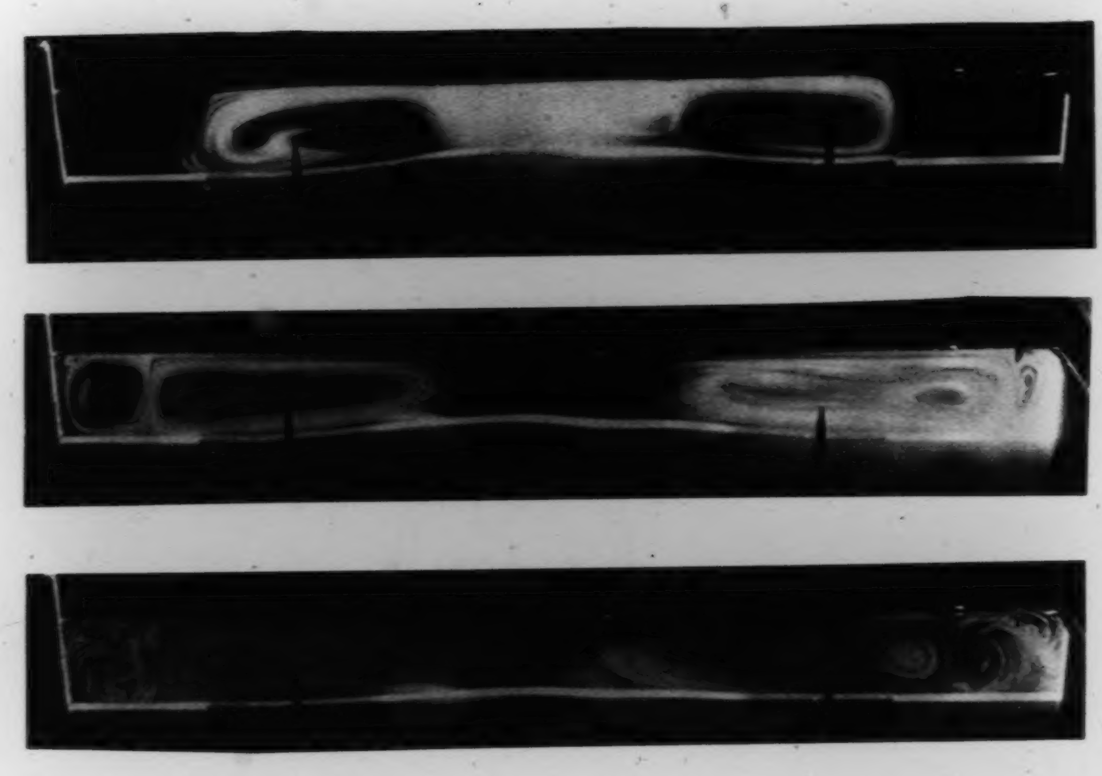

Figure 4.27 Flow Patterns Observed in 1/2 in. (12.7 mm) Air Gap (from top to bottom-about 1 s after exposure begins, after about 5 - 6 s, immediately after exposure ends)

with respect to the driving forces for natural convection may be larger at these smaller air gaps than at the 3/4 in. (19.1 mm) air gap. It should also be noted that the shim stock deforms during these exposures more than the fabric specimens, so that what may be a nominal 1/2 in. (12.7 mm) air gap may in fact be closer to a 3/8 in. (9.5 mm) air gap. This deformation can be seen in the middle part of the shim stock in Figure 4.27. In fact, the flow patterns in the 1/2 in. (12.7 mm) air gap above the Nomex® IIIA specimens were similar to those in the 3/8 in. (9.5 mm) air gap above the shim pieces (which deformed to about 1/2 in. (12.7 mm)), discussed immediately below.

It is more difficult to identify the flow patterns in 1/2 in. (12.7 mm) air spaces above the Kevlar®/PBI specimens as the smoke in the air space is about the same colour as the fabric itself. In this case the patterns appeared to be more like those above the shim stock pieces than those above the Nomex® IIIA specimens for the same air gap width.

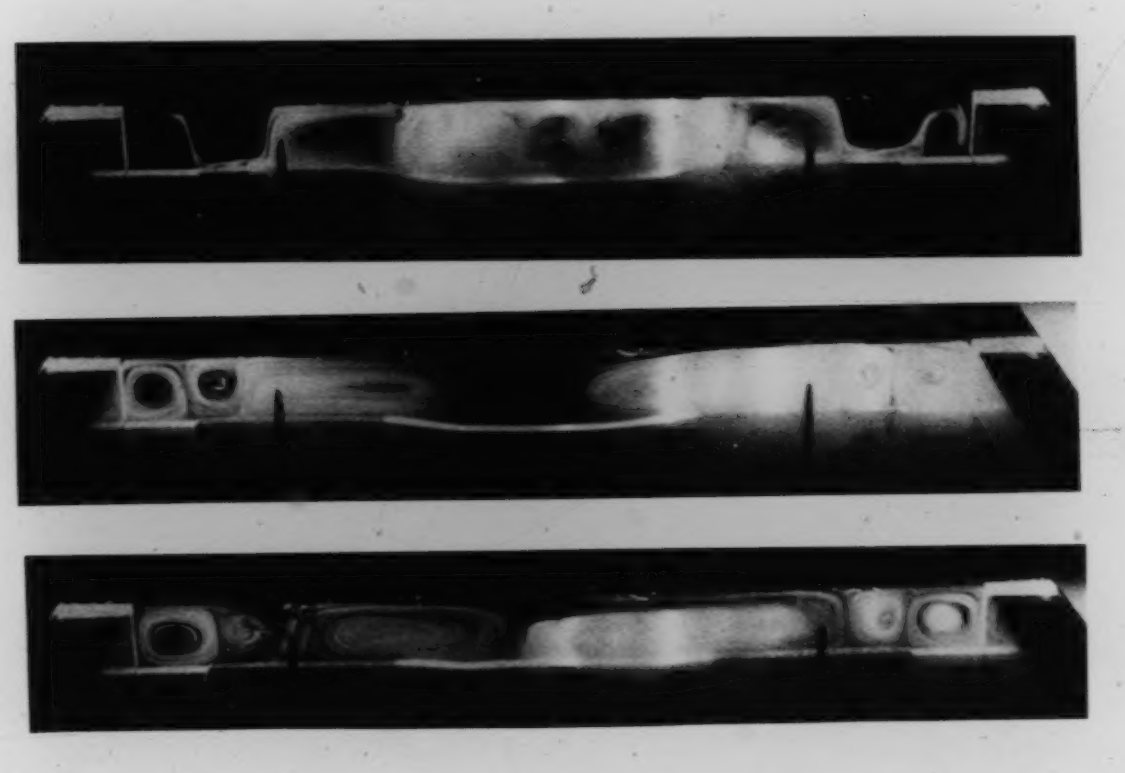

Figure 4.28 Flow Patterns Observed in 3/8 in. (9.5 mm) Air Gap (from top to bottom - about 4 s after exposure begins, just before exposure ends, about 4 s after exposure ends)

The flow patterns observed in the 3/8 in. (9.5 mm) air gap above the shim stock pieces are shown in Figure 4.28. Initially the flow patterns looked similar to those in the 1/2 in. (12.7 mm) air gap. It took about 4 s for the cells to reach the sides of the air space (Figure 4.28 - top photograph). Multiple small cells formed on the sides of the cavity during the exposure (middle photograph - taken just before the end of the exposure). When the exposure ended, these cells began to move very slowly towards the heated portion in the middle of the shim stock (bottom photograph - taken roughly 4 s after the exposure ended).

The flow patterns in the 3/8 in. (9.5 mm) air space above the Nomex® IIIA specimens were different from those above the shim stock pieces, in that there appeared to be smaller multiple cells above the heated portion of the fabric during the exposure. These appeared to begin to die out fairly soon after the exposure ended. Once again, these different flow patterns may have been due to a larger amount of smoke available above the heated portion of the Nomex® IIIA fabric than above the heated portion of the shim stock. The flow patterns in the 3/8 in. (9.5 mm) air space above the Kevlar®/PBI specimens were again difficult to see. However, they did appear to be similar to those above the Nomex® IIIA specimens.

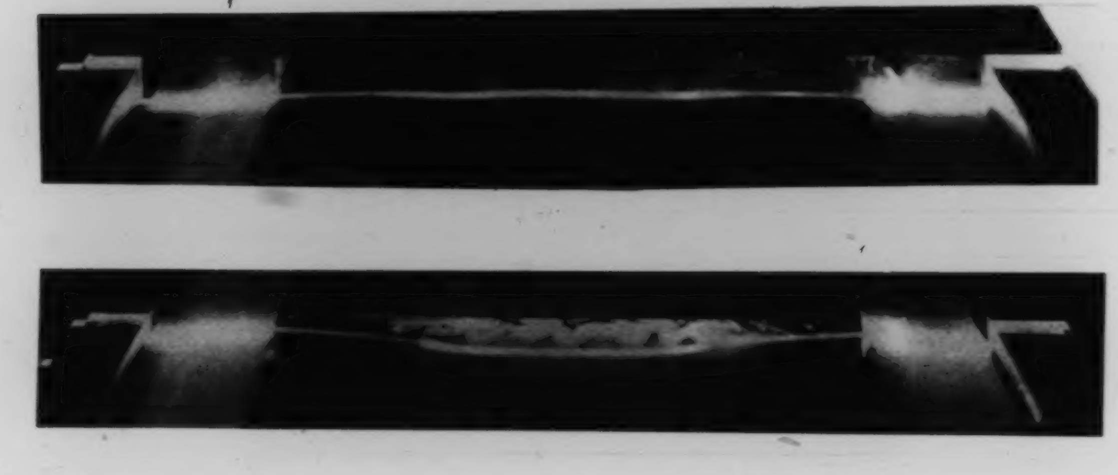

Figure 4.29 Flow Patterns Observed in 1/4 in. (6.4 mm) (top) and 1/8 in. (3.2 mm) (bottom) Air Gaps

The flow patterns observed for the 1/4 in. (6.4 mm) and 1/8 in. (3.2 mm) air gaps above shim stock pieces are shown in Figure 4.29[27]. In both cases relatively weak convection cells appeared above the heated portion of the shim stock during the exposure, and dissipated after the burner was removed. The shim stock piece with the nominal 1/8 in. (3.2 mm) air gap deformed considerably (Figure 4.29 - bottom photograph), so the behaviour shown may not be indicative of what actually happens in a 1/8 in. (3.2 mm) air gap.

In the 1/4 in. (6.4 mm) air gap above the Nomex® IIIA specimens, a large number of tiny cells formed above the heated portion of the fabric about 2 s after the exposure began. These cells looked very similar to the Benard cells shown in heat transfer texts (e.g. Holman [93]). Most of the cells died quickly after the flame was removed, although a few persisted for up to about 8 s afterwards. There appeared to be some sort of convection cells in the 1/4 in. (6.4 mm) air space above the Kevlar®/PBI specimens, but it was difficult to determine if these were similar to Benard cells, because of the colours of the smoke and fabric. In the 1/8 in. (3.2 mm) air gaps above both fabric samples, no regular flow patterns were observed.

The flow visualization study described here clearly demonstrated that natural convection occurs in air gap widths of about 1/4 in. (6.4 mm) or larger in bench top tests. It also illustrates how the strength of the natural convection cells depends strongly on the air gap size, which is expected by looking at the dependence of the Rayleigh number on the cube of the air gap width. It also appeared that the flow patterns above some of the fabrics were different from those above the shim stock pieces at air gaps of less than 1/2 in. (12.7 mm). This may be due to the porous nature of the fabrics or effects of the mass transfer of the smoke from the fabric specimens.

---

[27] it should be noted that the smallest air gap which can be used with a specimen holder with restraining pins is 3/8 in. (9.5 mm). Therefore the shim and fabric samples with 1/4 in. (6.4 mm) and 1/8 in. (3.2 mm) air gaps were held in place with masking tape on a specimen holder without pins. The masking tape is seen on the sides of the air gaps in Figure 4.30.

4.5.6 Existing and Modified Bench Top Test Results

Earlier in this chapter, the differences between copper disk and skin simulant test sensors and the analysis of their data were discussed. In order to compare these sensors and methods of data analysis, bench top tests using the copper disk and skin simulant sensors were performed using Nomex® III (rather than IIIA), and Kevlar®/PBI specimens. As mentioned in Section 4.4.2, 10 s duration exposures were used to test the fabric specimens. Data were also taken for 50 s after the exposure ended in order to provide information to compare the protection times for deeper skin burns predicted by the test sensors for these particular fabrics. The fabric specimens were placed in contact with, and spaced 1/4 in. (6.4 mm) away from the test sensor. The results of these tests are shown in Table 4.4 below. The data shown in the tables are the mean values, while the values for the individual tests can be found in Appendix 7.

Table 4.4 Comparison Between Bench Top Results Using Two Different Test Sensors

a) Second Degree Burn Damage

Fabric	Spacing	Skin Simulant - Time to 2° Burn (s)	Copper Disk - Time to 2° Burn (s)	
		(Henriques)	Stoll	Henriques
Kevlar®/PBI	contact	2.8	2.7	2.5
	1/4 in. (6.4 mm)	5.6	6.4	5.9
Nomex® III	contact	2.8	3.0	2.8
	1/4 in. (6.4 mm)	5.9	6.8	6.3

Table 4.4 Comparison Between Bench Top Results Using Two Different Test Sensors (continued)

b) Third Degree Burn Damage

Fabric	Spacing	Skin Simulant - Time to 3° Burn (s) (Henriques)	Copper Disk - Time to 3° Burn (s) (Henriques)
Kevlar®/PBI	contact	13.1	13.1
	1/4 in. (6.4 mm)	23.6	33.7
Nomex® III	contact	12.5	12.8
	1/4 in. (6.4 mm)	27.3	no burn

The times to second and third degree burn predicted using the two sensors for the contact case were quite close (Table 4.4). However, when the 1/4 in. (6.4 mm) air space was used, the results using the two sensors were considerably different. These differences were due to two major factors: the differences in the heat fluxes indicated by the two types of sensors, and the different methods used to predict second degree burn damage. The former can be seen by comparing the data in the columns marked "Henriques" for the two sensors, while the latter can be seen by comparing the second degree burn predictions in the columns marked "Stoll" and "Henriques" for the copper disk.

The first reason for differences in the results using the two test sensors is the fact that the two heat flux sensors did not indicate the same value of the instantaneous heat flux at each time step. The effect of these differences on burn predictions can be seen by comparing the second or third degree burn predictions made using Henriques burn integral for each of the two sensors. The magnitude of the differences in heat fluxes can also be seen by examining the heat flux histories from a typical test (Figure 4.30). For the sake of clarity, the heat flux history from the copper disk calculated using only data points at 0.5 s increments is shown in Figure 4.30, whereas all the data points were utilized in calculating the heat flux histories and subsequent burn predictions shown in Table 4.4.

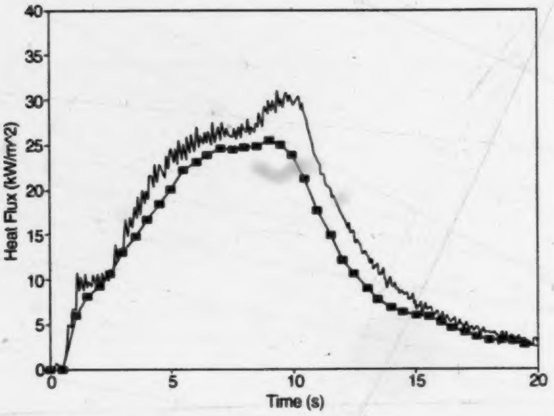

Figure 4.30 Comparison Between the Heat Fluxes Measured Behind a Kevlar®/PBI Fabric Specimen by Copper Disk (■) and Skin Simulant Heat Flux Sensors (solid line) for a 10 s Exposure Using a 1/4 in. (6.4 mm) Air Gap

The differences in the heat fluxes indicated by the two sensors can be due to the following reasons.

Differences in sensor surface temperatures: If the test sensor surface temperatures are different, this can result in a difference in the measured heat fluxes. The temperature histories of the copper disk and skin simulant for a particular test utilizing a 1/4 in. (6.4 mm) air gap are shown in Figure 4.31. Earlier in the exposure, the skin simulant temperature rose more rapidly than the copper disk temperature. After the exposure ends, the skin simulant temperature fell more rapidly than the copper disk temperature.

In order to deal with these differences, Grimes, et al. [125] designed a copper heat flux sensor so that its temperature would remain below that of the skin simulant sensor for the exposure of interest to them. However, the response of the sensor after the exposure ends and the fabric cools was not considered. In addition, no estimate was given as to the effect of the surface temperatures of the various sensors on the heat fluxes which they indicated.

The heat transfer from the test fabrics to the test sensors was by radiation,

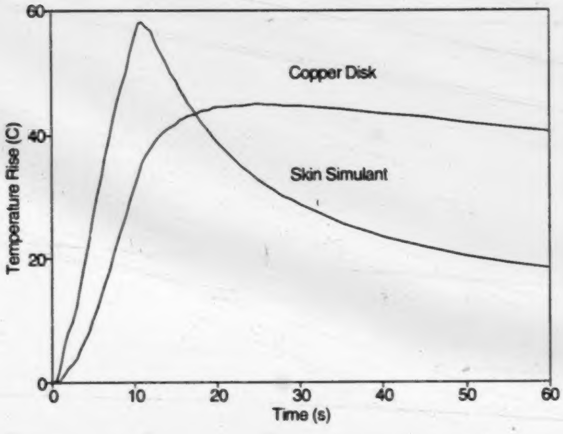

Figure 4.31 Comparison Between Measured Copper Disk and Skin Simulant Temperature Rises Behind a Kevlar®/PBI Fabric Specimen During and After a 10 s Exposure using a 1/4 in. (6.4 mm) Air Gap

conduction/convection, and the transfer of the products of thermal degradation reactions in the fabrics. It was found that the sensor temperature differences seen here had a negligible effect on the heat transfer by radiation. The differences in sensor temperatures may have a small effect on the conduction/convection heat transfer, as these differences can affect the nature of the thermal boundary layer adjacent to the sensor surface. In addition if the surface temperature of a sensor is much different from that of the sensor block it is mounted in, this sharp discontinuity in the surface temperature of the sensor/block combination can also affect the thermal boundary layer [138]. The sensor temperature may also have some effect on the amount of products which can condense on its surface.

These sensor temperatures will also have an effect on the actual calculation of the incident heat flux history. For example, the method used to calculate the instantaneous heat flux incident on the copper disk depends on knowing the slope of the temperature - time curve (Equation (4.2)) at the particular point of interest. While the slope is quite steep during the heating portion of the exposure, it is very small during the cooling portion (Figure 4.31). Therefore, one would expect that it would be quite difficult to determine the slope and hence the heat flux at longer time steps for the copper disk.

Physical Nature of the Sensor Surface: The physical nature of the surface also can affect the heat transfer. Radiation heat transfer can be affected by the surface roughness of the sensor. The copper disk and skin simulant surfaces have different textures. Buildups of residue can also affect heat flux measurements [138]. As copper disks were found to be easier to clean than skin simulants, this may affect the results using the skin simulants more than the copper disks.

Thermal Properties used in Treating the Data: The equations used to determine the heat fluxes for the skin simulant sensors are based on an assumption that the thermal properties are constant throughout the exposure (techniques which take these variations into account are also available (e.g. Cook [139]). In addition, as the heat flux at any time is directly proportional to the thermal absorptivity of the skin simulant ($(k\rho c_p)^{1/2}$) in Equation (4.3), any errors in the calibration of the skin simulants will have a significant effect on the values of the heat flux indicated by these sensors.

Differences in Construction of Individual Sensors: Differences in the construction of individual skin simulant or copper disk heat flux sensors can affect the heat fluxes indicated by these sensors. For example the mass of solder used to attach thermocouple wires to copper disks can affect the heat fluxes measured with the disks [138].

As the heat fluxes measured by the two sensors were not compared to a third heat flux transducer for these exposures, one cannot say that the values measured by either sensor were more correct than those measured by the other. However both sensors do have a certain amount of uncertainty associated with their measurements.

As a final check on how differences in heat fluxes measured with the two sensors can affect bench top test results, a square wave heat flux of various intensities from 20 to 30 kW/m^2 for 10 s was used as an input to the skin temperature and burn prediction model used here. These square wave flux histories were similar to those measured behind the fabrics with a 1/4 in. (6.4 mm) air gap (Figure 4.30). Small changes in the incident heat flux produced deceptively large differences in the times predicted to burns, especially third degree burns (Table 4.5).

Table 4.5 Times to Second and Third Degree Burn Predicted for Various Square Wave Heat Fluxes Between 20 and 30 kW/m^2 Incident on Human Skin for 10 s

Heat Flux (kW/m^2)	Time to 2° Burn (s)	Time to 3° Burn (s)
20	3.72	no burn
22	3.24	no burn
24	2.84	no burn
26	2.54	27.0
28	2.28	21.0
30	2.08	18.0

Because of the exponential nature of Henriques burn integral, small changes in skin temperatures can cause large differences in the values of the burn integral. Third degree burns are said to occur when the value of Henriques burn integral, Ω, calculated from the temperature history at the base of the dermis layer of skin, is unity. For example, for an incident flux of 24 kW/m^2 for 10 s, the value of Ω for this depth in the skin was found to be 0.625 after 60 s. For an incident flux of 26 kW/m^2 for 10 s, the value of Ω was 2.16 after 60 s. Thus, no third degree burns were said to occur for the 24 kW/m^2 exposure, whereas third degree burns were said to occur for the 26 kW/m^2 exposure. As the fluxes under many of the garments of interest in these tests fall into this range of exposures, which by the definition used here may barely produce third degree burns, caution must be exercised in considering the times to third degree burn determined in these tests.

The other reason for the differences in the results of the two sensors is the fact that two different methods were used to predict the times to second degree burn damage. The magnitude of the differences in burn predictions made using the two techniques can be seen by comparing the second degree burn predictions made using the Stoll criterion and Henriques' burn integral for the copper disk in Table 4.4. Differences between results using these two techniques were less than 10%. As mentioned in Section 1.3.2, the Stoll second degree burn criterion is strictly valid only for use with a square wave heat flux [12]. Henriques burn integral, on the other hand, can be used for any heat flux history. As would be expected, the results using the two techniques were closest when the heat flux is closest to a square wave, as in the contact case. The predictions were further apart for the 1/4 in. (6.4 mm) air gap case, where the heat flux is less of an ideal square wave, but the differences were still not very large. Therefore, while the Stoll criterion is strictly only valid for square wave heat fluxes, such as on bare skin, it still can be used with confidence for data obtained under fabrics when the heat fluxes are reasonably close to a square wave. If only second degree burn predictions are of interest, then using the simpler Stoll criterion should be adequate, rather than having to use the more complicated skin heat transfer model and Henriques burn integral.

It should be noted that this portion of the study was exploratory in nature. Therefore the findings in this section are based on a limited number of tests using sensor and data analysis techniques which in some cases are under development. Some of the differences in heat fluxes measured by the two sensors may be due to problems associated with the construction and calibration of the individual sensors used in these tests. These differences may be reduced as construction and calibration techniques for these sensors are improved. Clearly more work is required before definite conclusions can be drawn as to the differences between the bench top test sensors used here.

4.6 Summary

The experimental apparatus and procedure have been described in this chapter. Temperature measurements of fabric and shim stock specimens during and immediately after bench top test exposures using an infrared thermometer and thermocouples were presented. Results from bench top tests of these materials were also shown. Qualitative observations about the thermal response of fabrics were discussed, and shown to agree with quantitative observations such as the aforementioned temperature measurements. Flow visualization techniques were used to show that natural convection can occur in air gaps of about 1/4 in. (6.4 mm) or larger in bench top tests, and to briefly describe the flow patterns which can occur in the air gaps. Bench top test result obtained using copper disk and skin simulant test sensors were also compared.

CHAPTER 5: DISCUSSION OF NUMERICAL AND EXPERIMENTAL RESULTS

In this chapter the numerical and experimental results shown in Chapters 3 and 4 will be compared. Applications of these results to the design of thermal protective fabrics and to the development of modified bench top test methods for these materials will be discussed.

5.1 Comparison of Experimental and Numerical Results

Predictions of the thermal response of the fabric and bench top test results made using the numerical model were compared with corresponding experimental results. These comparisons are discussed in turn below.

5.1.1 Thermal Response of Fabric

In Section 3.3 predicted temperatures of Nomex® IIIA and Kevlar®/PBI fabric specimens were presented. In Section 4.5.2, fabric temperature measurements made using thermocouples and an infrared thermometer were described. It was shown that the shim stock temperatures measured using thermocouples and the infrared thermometer were similar, while fabric temperatures measured using the two methods were quite different from one another. These results were due to the fact that the thermocouples indicated the temperature at a given point, while the infrared thermometer measured a weighted average temperature of the volume within its viewing area.

Temperature measurements made using either of the two methods will be more appropriate in different applications. For example, the temperatures measured by a thermocouple at a particular point on the fabric can provide a better indication of the conditions a yarn or fibre at that location were subjected to than the weighted average temperatures measured by the infrared thermometer. However, in the case of the numerical model, the fabric was treated as a homogeneous slab with thermal properties representative of the complex fabric structure. Only temperatures indicative of the gross behaviour of the fabric and its interaction with the flame and the test sensor can therefore be determined using this model. Hence, it is appropriate to compare the numerical results with the temperatures measured using the infrared thermometer, rather than those measured using thermocouples.

The temperatures predicted by the numerical model are compared with those measured using the infrared thermometer in Figures 5.1 through 5.3 for the shim stock pieces and the two fabrics.

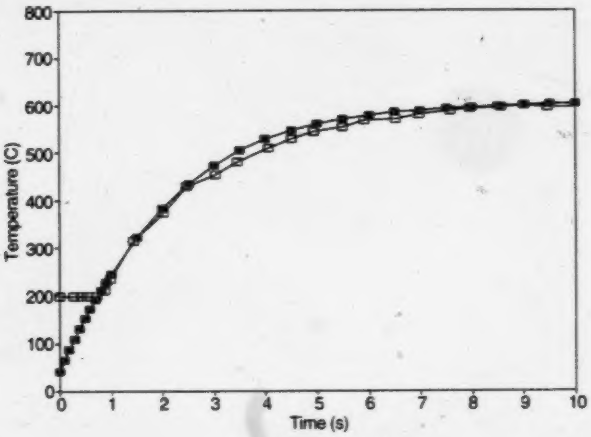

Figure 5.1 Comparison Between Temperatures of Back of Painted Shim Stock Pieces Predicted Using Numerical Model (■) and Measured Using Infrared Thermometer (□)

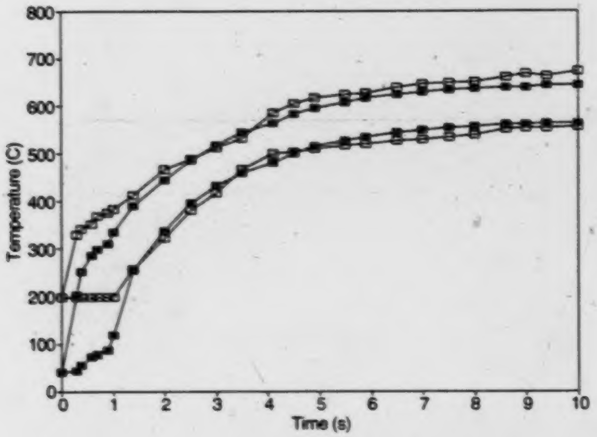

Figure 5.2 Comparison Between Temperatures of Front and Back of Nomex® IIIA Fabric Specimens Predicted Using Numerical Model (■) and Measured Using Infrared Thermometer (□)

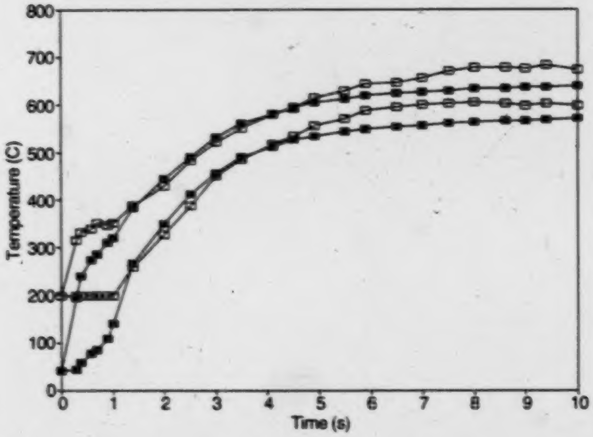

Figure 5.3 Comparison Between Temperatures of Front and Back of Kevlar®/PBI Fabric Specimens Predicted Using Numerical Model (■) and Measured Using Infrared Thermometer (□)

As shown in Figure 5.1 the predicted shim stock temperatures were very close to those measured using the infrared thermometer (about 5% difference in absolute temperatures at 4 s, and 1% at 10 s). As shown in Figures 5.2 and 5.3, the predicted fabric temperatures were also close to those measured using the infrared thermometer, especially after the first few seconds of the exposure. The absolute temperatures predicted by the model were less than 4% different from those measured using the infrared thermometer during the latter parts of the 10 s exposures. In Section 4.5.3, it was shown that these temperature measurements agreed with macro and microscopic observations made during and after interrupted exposure tests of the fabrics. Therefore, as the temperatures predicted by the numerical model are consistent with the experimental results, they are also consistent with these qualitative observations.

All of the materials appeared to eventually reach steady-state conditions during the 10 s exposures. This can be explained by looking at the interactions between the fabric and the flame, ambient, and test sensor. For example, the incident heat flux was calculated based on the temperature and fourth power of temperature of the front of the fabric. Therefore, as the fabric heats up, the magnitude of the incident heat flux will decrease. For example, the nominal heat flux used in bench top tests is 80 kW/m^2. This is determined using a copper calorimeter, which under this particular heat flux would be heated to temperatures of around 200°C during calibration exposures of 10 to 12 s. The fabric on the other hand will be heated to temperatures of about 700°C in 10 s. Assuming the same flame temperature, emissivity, and other parameters used in the numerical model, the net heat flux to the fabric or disk can be determined using the sum of the radiative and convective heat transfers, given previously as Equations (2.21) and (2.22).

$$\begin{aligned} q_{net} = {} & h_{fl}\,(T_g - T_{x=0}) \\ & + \left(\sigma \varepsilon_g T_g^{\,4} - \sigma \varepsilon_{fab} F_{fab\text{-}amb}\,(1 - \varepsilon_g)\,(T_{x=0}^{\,4} - T_{amb}^{\,4}) \right. \\ & \left. - \frac{\sigma (T_{x=0}^{\,4} - T_{bh}^{\,4})}{\left(\dfrac{1 - \varepsilon_{fab}}{\varepsilon_{fab}} + \dfrac{1}{F_{fab\text{-}bh}(1 - \varepsilon_g)} + \dfrac{A_{fab}}{A_{bh}} \dfrac{(1 - \varepsilon_{bh})}{\varepsilon_{bh}} \right)} \right) \end{aligned} \tag{5.1}$$

The net heat fluxes incident on the front surface of a fabric or disk are as follows for front surface temperatures between 100 and 700°C.

Table 5.1 Predicted Net Heat Flux Incident on Front Surface of Fabric or Copper Disk from Meker Burner Flame for Various Front Surface Temperatures

Front Surface Temperature (°C)	Net Heat Flux Incident on Surface (kW/m^2)
100	83
200	77
300	71
400	62
500	50
600	35
700	16

Hence for the copper disk at 200°C, the net heat flux will be 77 kW/m^2, while for the fabric at 700°C, the net heat flux will be 16 kW/m^2. This decrease in net heat flux will eventually lead to steady-state conditions, as the net heat flux to the front face of the fabric will be balanced by the net heat flux from the back of the fabric, which will increase as the temperature of the back surface of the fabric increases. This steady-state behaviour was also shown in Figure 4.17, where a 20 s flame exposure was used rather than the usual 10 s exposure. The temperatures of the front and back of the fabric measured by the infrared thermometer were practically constant after about the first 7 s, with the exception of the temperature of the back of the Nomex® IIIA fabric sample which remained constant after about 13 s.

Some possible reasons for the differences between the predicted temperatures and those measured using the infrared thermometer were discussed previously in Chapter 4, such as time response, absorption of radiation by the atmosphere and the value of emissivity assumed for the fabric or shim stock. These were shown to have very small effects on the temperatures measured using the infrared thermometer. Other reasons for the differences between the numerical and experimental results include the following.

Limitations in the numerical model: As discussed in Chapter 2, there were many simplifying assumptions made in modelling the fabric. For example, the thickness was assumed to be constant during the exposure, while Shalev and Barker [47,48] have shown that the thickness changes during a bench top test exposure. As shown by the parametric study in Section 3.4.1, the time required to exceed the Stoll criterion increased linearly with thickness. Therefore changes in the thickness during the test could easily account for some of the differences between the predicted and measured fabric temperatures. As well, the thicknesses were measured at a pressure of 1 kPa, which may be different from the pressure exerted on the fabric by the hot gases from the flame.

Other assumptions were made. The boundary condition on the front of the fabric was shown to be very important in the parametric study (Section 3.4.7). The numerical model assumed a suddenly applied heat flux at time zero, while the bench top tests used a shutter. This will be discussed further in the next section when the results of the numerical model are compared with bench top test results. In addition, the effects of the flat black paint, such as the energy associated with the paint being vapourized, were not included in the model of the shim stock. Mass transfers of moisture and/or products of thermal decomposition reactions were neglected. While the effect of moisture regain on the apparent heat capacity of the fabric was included, the effects of moisture on other thermal properties such as the thermal conductivity were not included. Regardless of all of these points, the agreement with experimental results was very good, especially considering all of the assumptions made.

Values of Thermal Properties Used: Many of the parameters used in the model were estimated using simple heat transfer theory, or could only be measured crudely. The predicted temperatures were closer to those measured by the infrared thermometer later in the exposure than in the beginning of the exposure. The results of the parametric study indicated that variations in individual values of thermal properties had more effect on the temperatures predicted during the first few seconds of the exposure than the temperatures closer to the end of the exposure, where the behaviour was governed more by the boundary conditions used. All of this would indicate that the boundary conditions on the front and back of the fabric were modelled reasonably well, and that the particular values used for some of the thermal properties in the model may not be completely correct. Therefore, more effort could be put into determining more accurate values of the relevant thermal properties of interest for the model. This point will be discussed again after the results of the numerical model are compared with actual bench top test results.

All thermochemical reactions were assumed to be endothermic: The DSC results (Section 3.3) give information on endothermic reactions involving these fabrics in an inert environment up to 500°C. The flame contact exposure should involve a relatively inert environment [117], and hence exothermic reactions are not expected (especially given that the limiting oxygen index values for Nomex®, and PBI are reported as 0.285 and 0.415, respectively [140]). If somehow there was enough oxygen available from the air gap or the surroundings (if there is not an enclosed air space behind the fabric) some exothermic reactions might occur in the fabric structure. Therefore, these would add energy to the fabric and increase the temperatures from those predicted by the model. While the bench top test modelled here is strictly a flame exposure, other bench top tests use radiant heat sources instead of, or in addition to a laboratory burner. In these tests, exothermic reactions will be more of a possibility. The modelling of these and other tests will be discussed further along with other possible future work in the next chapter.

While the numerical results were compared with the infrared thermometer measurements, some other errors pertinent to the thermocouples should be mentioned in passing. One of these was contact resistance. Nomex® thread was used to attach the thermocouples to the fabric, which itself may lead to some error as the thermocouple may be recording the response of this particular Nomex® thread rather than the response of the fabric. Examining fabric specimens after the exposures, the thermocouples did not appear to be in perfect contact with the surface yarns after the exposure ended. The small amount of air between the thermocouple junction and the fabric surface will then produce some error in thermocouple measurements. This was particularly noticeable with the temperatures on the front of the fabric. In other cases the Nomex® thread used to sew the thermocouple wires to the surface yarns did not survive the entire exposure and the thermocouple fell into the flame. Therefore the temperatures measured using the thermocouples were less consistent on the front of the fabric than those on the rear of the fabric (Figures 4.12 and 4.13). It was also noted that some of the thermocouple wire insulation was slightly discoloured after some of the exposures. If the insulation which is between the two wires melts, then a second junction could be formed at some location away from the centre of the exposed portion of the fabric. The temperature measured by the thermocouple would then be this temperature rather than the temperature at the original junction.

5.2 Bench Top Test Results

Bench top tests measure the energy transferred between heated fabrics and test sensors. These energy transfers are governed primarily by the temperatures of the back surface of the fabric. A comparison of the predicted and measured temperatures of the bench top test sensor mounted 1/4 in. (6.4 mm) behind metal shim stock pieces, and Nomex® IIIA and Kevlar®/PBI fabric specimens are shown in Figures 5.4 through 5.6. Predicted times required to exceed the Stoll criterion are also given on the Figures, along with data measured using the bench top apparatus. Two sets of measured data are given, one for bench top tests where the shutter was used, and another for manual bench top tests (Section 4.4.1).

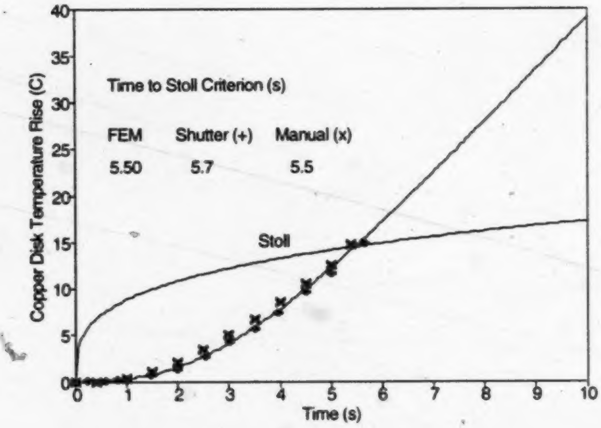

Figure 5.4 Comparison Between Copper Disk Temperatures and Bench Top Test Results Predicted By Numerical Model and Measured During Actual Bench Top Tests of Painted Shim Stock Pieces Using 1/4 in. (6.4 mm) Air Gaps

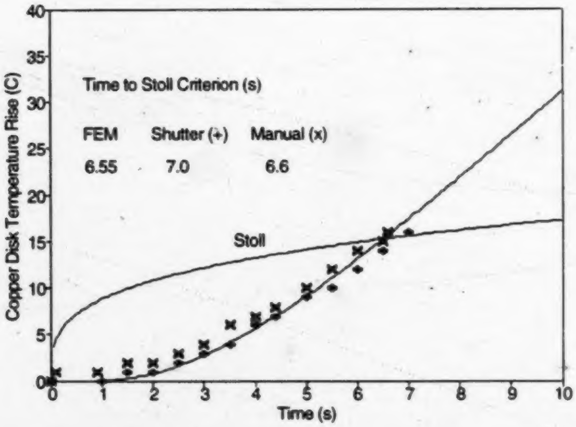

Figure 5.5 Comparison Between Copper Disk Temperatures and Bench Top Results Predicted By Numerical Model and Measured During Actual Bench Top Tests of Nomex® IIIA Fabric Specimens Using 1/4 in. (6.4 mm) Air Gaps

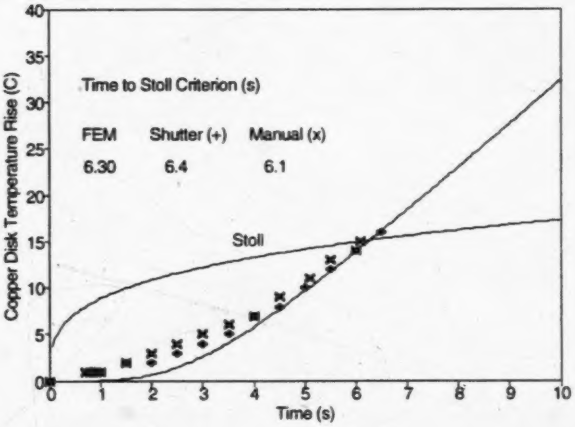

Figure 5.6 Comparison Between Copper Disk Temperatures and Bench Top Test Results Predicted By Numerical Model and Measured During Actual Bench Top Tests of Kevlar®/PBI Fabric Specimens Using 1/4 in. (6.4 mm) Air Gaps

The sensor temperatures and bench top test results predicted using the numerical model were quite close to those measured during actual bench top tests using a 1/4 in. (6.4 mm) air space. Predicted times required to exceed the Stoll criterion were within 6% of those measured during actual bench top tests. In the numerical model the high heat flux was placed on the model exactly at time zero. In the manual tests time zero is when the hall effect sensor determined the burner was in place. Therefore the fabric was preheated for a fraction of a second as the burner was moved manually into place and the hall effect sensor sends a signal to the computer to begin taking data. This is opposite to the case of the bench top tests with the shutter where it may take up to 0.2 s for the shutter to open, and hence the fabric may not be exposed to the full flame for up to 0.2 s after time zero. These differences can be seen in the experimental data presented in Figures 5.4 to 5.6 (e.g. note how quickly the copper disk temperature increases at the beginning of the manual test of the Nomex® IIIA fabric - Figure 5.5). Therefore, it would be expected that the results of the numerical model, where the full flux is placed on the fabric at time zero, should be somewhere in between the two sets of experimental results. This is what is seen in Figures 5.4 through 5.6. The small differences in the numerical and predicted results will be due to many of the same reasons outlined in Section 5.1 above. The differences between the results of bench top tests with and without a shutter also demonstrate the importance of completely reporting the test conditions along with any bench top test results.

While the copper disk test sensor was used in the numerical model and most of the experimental work, the predicted responses of skin simulant sensors placed behind the fabrics were also compared with experimental results in Figures 5.7 and 5.8.

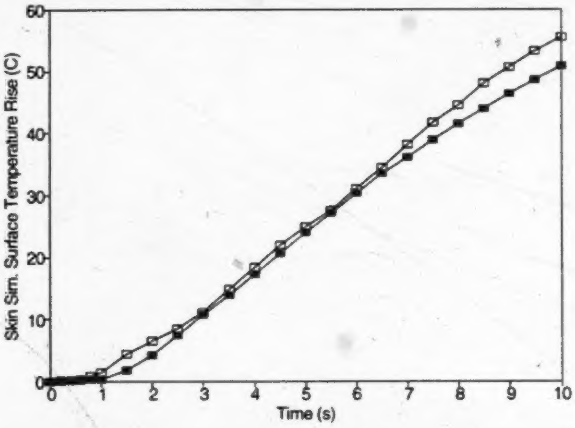

Figure 5.7 Comparison Between Skin Simulant Temperatures Predicted by Numerical Model (■) and Measured (□) During Actual Bench Top Tests of Nomex® III Fabric Specimens using 1/4 in. (6.4 mm) Air Gap

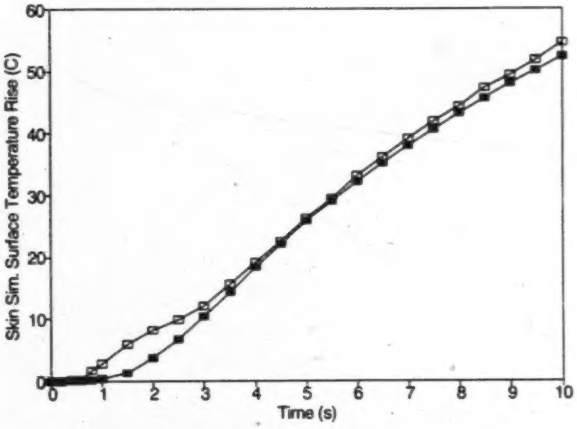

Figure 5.8 Comparison Between Skin Simulant Temperatures Predicted by Numerical Model (■) and Measured (□) During Actual Bench Top Tests of Kevlar®/PBI Fabric Specimens using 1/4 in. (6.4 mm) Air Gap

Once again, the agreement between the numerical and experimental results was very good. It should also be noted that Figure 5.7 compares numerical results for Nomex® IIIA and experimental results for Nomex® III. However, as discussed in Section 3.1, the differences between the performance of Nomex® III and IIIA are expected to be minimal.

The above comparisons indicate that the numerical model did a good job of predicting the energy transfers across 1/4 in. (6.4 mm) air gaps. Other air gaps were also used in the numerical and experimental work. Recalling the discussions in Sections 3.4.8 and 4.5.5, natural convection was predicted to begin at air spaces of about 8 mm using the numerical model, and air spaces of about 6 mm based on the flow visualization study. One possible reason for the numerical model not predicting natural convection to begin at the smaller air gaps was the fact that a critical Rayleigh number of about 1700 was used. This is the critical Rayleigh number for a horizontal enclosure with solid top and bottom boundaries. The bottom boundary in the case of a fabric is porous, while the bottom boundary in the case of the shim stock is solid. There was not a large difference in the flow visualization observations between the shim stock and fabric specimens, hence it would appear that at least qualitatively, the porous bottom boundary does not have a large effect on the onset of natural convection. However, calculating the Rayleigh number based on the entire height of the enclosure may not be appropriate here. In the literature search for studies related to natural convection in enclosures in Chapter 2, the work of Goldstein and Volino [79] was discussed. These investigators examined transient natural convection in thick layers of water, and used a Rayleigh number based on a conduction layer thickness rather than the entire height of the enclosure. Although the enclosures studied in this thesis research do not meet their particular criteria for thick layers, perhaps a Rayleigh number based on a height other than the height of the entire enclosure would be appropriate here as well.

The results from the numerical model are compared with the bench top test results using various air spaces in Figure 5.9. It should again be noted that the predicted values are based on a copper disk test sensor mass of 18 g, while experimental results were for a sensor with a mass of 18.4 g. Regardless of this, it should be still possible to at least compare the general trends in the two sets of data.

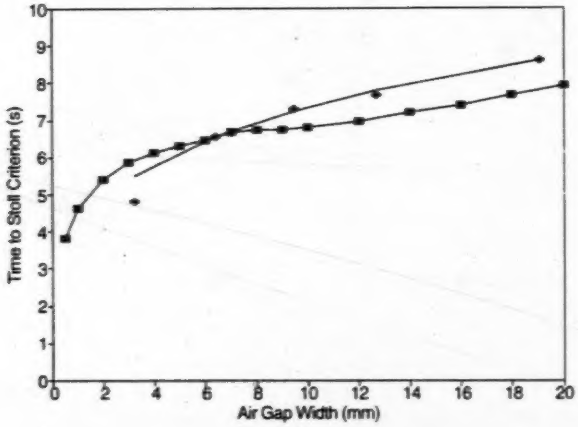

Figure 5.9 Comparison Between Predicted (■) and Measured (+) Times to Exceed Stoll Criterion for Nomex® IIIA Fabric Specimens Tested Using Various Air Gaps

It was shown in Chapter 4 that the times required to exceed the Stoll criterion at larger air gaps were approximately proportional to the air gap width taken to the one-fourth power. The numerical results did not exhibit this behaviour. Hence, the model did not do as good a job of predicting the results of bench top tests at larger air gaps than 1/4 in. (6.4 mm). The first inclination is to assume that the reason for this is that the simple relations used to estimate the natural convection heat transfer in air gaps do not do an adequate job of predicting the energy transfer by this process at the larger air gaps when the convection becomes more vigourous. This may be true to a degree, however comparing the predicted Rayleigh numbers for various air gaps (Figure 3.30) with the flow visualization observations in Chapter 4, the numerical model at the very least does a good job of illustrating the large differences in the nature of the flow patterns at the various air gaps. In addition, in the discussion of Figures 3.29 and 3.31, it was noted that while the natural convection may become more vigourous at larger air gaps, the heat transferred by natural convection is basically constant at all air gaps. Therefore another explanation for the decreased ability of the model to predict bench top test results at these larger air gaps must be found.

Recall that the main mode of energy transfer is by thermal radiation between the heated fabric and the test sensor, and that the view factor decreases with increasing air gap (Figure 3.32). Also remember that the numerical model assumes that the heat flux and temperatures are uniform across the surfaces of the fabric. This will not be true for a real fabric. For example, the Meker burner flame was assumed to be at a uniform temperature. In an actual flame, there will be some temperature distribution, such as those shown in Lewis and von Elbe [68]. The fabric structure is such that the temperature distribution will not be uniform on the back of the fabric. Even when the bottom surfaces of horizontal enclosures are heated evenly, numerical models (e.g. Pallares, et al. [89]) have shown that a Nusselt number distribution is still expected across the boundaries, and the patterns in the flow can be very complicated. In addition, the fabric temperatures predicted and measured on the back of the fabric samples were not the same.

The effective thermal conductivity used to model the energy transfers across the air gap was given earlier as Equation (2.31).

Inspecting Equation (5.2) it is immediately apparent that this effective thermal

$$k_{eff} = \left[\frac{\sigma(T_{fab}^2 + T_{sens}^2)\,(T_{fab} + T_{sens})}{\left(\frac{A_{sens}}{A_{fab}} \left(\frac{1 - \varepsilon_{fab}}{\varepsilon_{fab}} + \frac{1}{F_{fab-sens}} \right) + \frac{(1 - \varepsilon_{sens})}{\varepsilon_{sens}} \right)} + h_{gap} \right] \Delta x \qquad (5.2)$$

conductivity is highly dependent on the absolute temperature of the back of the fabric raised to the third power. The energy transfer itself is dependent on the fourth power of the temperature. Therefore small differences in the temperature of the back of the fabric will have large effects on the energy transfer across the gap. In order to gain an appreciation for the magnitude of the differences in bench top test results due to small differences in temperatures of the back of the fabric, the copper disk was modelled separately as a lumped capacity system with a convective and radiative heat flux on its surface described in a similar manner to Equation (5.2) above. The heat flux incident on the copper disk at each time step was determined in a iterative manner using the above formulation and the temperature of the back of the fabric measured at that particular time step. The process was repeated assuming the back of the fabric temperature to be 0.9 and 0.95 of its absolute measured value. It was found that for air gaps of 1/4 in. (6.4 mm) differences of 5% and 10% in the absolute temperature of the back of the fabric produced differences of 6% and 13% in times to exceed the Stoll criterion, respectively (i.e. using absolute temperatures which were 5% lower caused an increase in 6% in the predicted time to exceed the Stoll criterion). At air gaps of 3/4 in. (19.1 mm) differences of 5% and 10% in the absolute temperature of the back of the fabric produced differences of 9% and 18% in times to exceed the Stoll criterion, respectively. Clearly, the effect of these temperature distributions on bench top test results will be greater at the larger air gaps.

Another source of error is the fact that the transfers of energy by moisture and decomposition products were not included in the numerical model. The role of moisture is an area of some debate. In terms of thermal decomposition products some authors have indicated that these may not transfer a significant amount of energy for certain fabrics (e.g. Shalev [48]), while others indicate that they do for other fabrics (e.g. Davies, et al.

[76] and Backer, et al. [45]). If these products do transfer significant amounts of energy to the test sensor the amount of time required to exceed the Stoll criterion will decrease. Examining Figures 5.4 through 5.8, the measured test sensor temperatures increased quicker than the temperatures predicted by the model immediately after the exposure began and just before it ended. These observations could possibly be due to mass transfer of moisture and thermal decomposition products. It is expected that mass transfers will have more of an effect at larger air gaps, where the flow visualization study indicated that the motion in the air space was more vigorous than in the smaller air gaps.

Despite these errors, the numerical model did a good job of predicting the results of bench top tests at the 1/4 in. (6.4 mm) air gaps used in some standard test methods. As test methods do not use the larger air gaps included in this study, it is of lesser importance that the model did not do as good a job of predicting bench top test results at the larger air gaps. However, the model did do a reasonable job of at least qualitatively predicting the trends in the behaviour of the convection cells at different air gaps. If more accuracy is required at these larger air gaps, the model likely will need to be modified to include aspects such as temperature distributions across the back of the fabric and mass transfer. It may also have to include a more rigorous treatment of the natural convection in the air gap, as well as possibly coupling the radiation and convection heat transfer, and including the effects of transient natural convection and localized heating, as discussed in Section 2.4.

5.2 Implications of Research to Fabric Design

The numerical and experimental results have indicated that varying individual thermal properties have different effects on the thermal response of the fabrics studied here, and the bench top test results of these fabrics. It has also been shown that the temperature history of the back of the fabric in bench top test determines the rate at which the temperature will rise in the copper disk test sensor, and hence the amount of time required to exceed the Stoll criterion. In the parametric study conducted in Chapter 3, it was shown that increasing the thickness, increasing the moisture content, decreasing the thermal conductivity, and increasing the specific heat all will cause the temperature of the back of the fabric to increase at a lower rate, and hence will delay the time until the Stoll criterion is exceeded. It was also shown that increasing the energy required for the thermal decomposition reactions will have a minor effect on increasing time required to exceed the Stoll criterion. If these reactions occur at lower temperatures, this will also delay the onset of the Stoll criterion, as the temperatures of the back of the fabric will begin to rise at a slower rate earlier in the exposure once these reactions begin than if these reactions occurred at higher temperatures.

Much of the above discussion is intuitively obvious from basic heat transfer theory. One of the contributions of this work has been to quantify the magnitudes of these effects on the thermal response of the fabric and bench top test results. As a practical example of how differences in the response of the fabric and bench top test results can be predicted on the basis of variations in some of these properties, recall the predicted and measured fabric and copper disk temperatures of the Nomex® IIIA and Kevlar®/PBI samples shown in Figures 5.2, 5.3, 5.5, and 5.6. For bench top tests using an air gap of 1/4 in. (6.4 mm), the predicted times required to exceed the Stoll criterion were 6.55 and 6.30 s, for the Nomex® IIIA and Kevlar®/PBI specimens, respectively. The measured values were 7.0 and 6.4 s, respectively. The thermal and thermochemical properties used in the numerical model for the two fabrics were given in Table 3.2. Basically the only differences between the two materials, as far as the numerical model was concerned, was that the Nomex® IIIA specimens were slightly thicker (0.7 versus 0.6 mm), contained less moisture (5% versus 8%), and underwent thermal decomposition reactions at a lower temperature range (425 to 625° versus 550° to 650°C). From the parametric study, it is known that the differences in the thicknesses and the initial moisture contents can cause some of the differences in the bench top results of the two materials. However, the differences in the thermal decomposition temperature range can also be responsible for some of the difference in the bench top results of the two fabrics. A comparison between the temperatures of the back side of the two fabrics measured using the infrared thermometer (Figure 4.17) showed that the two fabrics had similar back side temperatures until about 5 s when the back of the Nomex® IIIA specimen began to heat at a much slower rate than the Kevlar®/PBI specimen. As this is in the approximate temperature range where the thermal decomposition of the Nomex® IIIA fabric was said to begin (Sections 3.2.5 and 4.5.3), the reason for the different heating rates may very well be the thermal decomposition reactions occurring at lower temperature in the Nomex® IIIA specimen.

Therefore, these findings would tend to indicate that fabrics will perform better in bench top tests if endothermic thermal decomposition reactions occur at lower temperatures. However, these findings are based on a simple heat transfer model which does not take into account changes to the integrity of the fabric caused by thermal decomposition, or mass transfer and subsequent energy transfers to the copper disk test sensor by products of thermal decomposition reactions. Therefore, depending on the behaviour of a particular fabric, these findings may or may not be valid.

5.3 Implications of Research to Bench Top Test Methods

5.3.1 Use of Air Gaps in Bench Top Tests

The numerical and experimental results indicate that the width of the air gap in bench top tests does play an important role in the thermal response of fabrics and the results of bench top tests. The energy transfer between the heated fabric and test sensor is mostly by thermal radiation for practically all of the exposure. The decrease in the value of the view factor with an increase in spacing between the fabric and the test sensor is responsible for much of the increase in times required to exceed the Stoll criterion as the air gap increases. There was no optimal value of this air gap, as some investigators have speculated (Table 2.1). Therefore, there is no real advantage to conducting bench top tests with air gaps at spacings larger than 1/4 in. (6.4 mm). The advantages and disadvantages of tests which place the fabric in contact with the test sensor were outlined previously in Section 2.4.1.

5.3.2 Modified Bench Top Test Methods

As mentioned earlier, existing bench top tests are relatively simple, economical, and easy to use. The modified test methods discussed in Chapter 4 are more complicated, and require more specialized equipment and software. They do however provide more information than existing bench top tests.

Fixed duration tests which use copper disks as heat flux sensors have several advantages. The disks are rugged, can be cooled and reused quickly, and have relatively well known thermal properties. However, fluctuations in the heat flux histories due to the methods used to treat the data are more severe than with skin simulant sensors, and may affect burn predictions. In order to smooth these fluctuations, routines which only use data at larger time steps than with the skin simulant system can be used, but these will decrease the accuracy to which the times to second and third degree burn can be estimated. In addition, this smoothed flux history may miss aspects of the actual heat flux history (e.g. Fig. 4.30 at about 2.0 s). However, if used in a test where one is only concerned whether second burns occur, rather than the time to second degree burns (such as some thermal mannequin tests), these routines may be acceptable. If methods can be found to reduce the fluctuations and use all of the test data points, this will increase the confidence with which these tests could be used.

Fixed duration tests which utilize skin simulants have fewer problems with fluctuations in the heat flux histories. Therefore all the data can be used in routines, and times to given severity of burns can be estimated more accurately. However, these sensors do have significant cool-down times, and therefore multiple sensors must be used in tests of fabrics, possibly introducing some variability into results. Alternatively, individual sensors can be reused, but a significant length of time is required between tests for the temperature gradients in these sensors to disappear. In addition, these sensors are not as rugged as the copper disks, and more difficult to clean. Disposable skin simulant sensors are one possible solution to some of these problems. Whereas the properties of the copper disk are fairly well known, the properties of the skin simulant sensors must be determined through calibration. The accuracy of any heat flux measurement made with these sensors is then directly related to the accuracy of the measurements of the relevant thermal properties.

It has also been noted that copper disk heat flux sensors are said to act as a heat sink when in contact with fabrics, thus slowing the heating of the fabric, which could possibly help fabrics perform better in tests by delaying the onset of thermal decomposition reactions which affect the integrity of the fabric. Stoll [42] discussed the concept of a critical thickness of a material, above which that material will behave the same way no matter what material is placed underneath it. Therefore, in order to determine if such a critical thickness exists for thermal protective fabrics, the Nomex® IIIA fabric in the numerical model was assumed to be in perfect contact with the copper disk test sensor, and human skin (using the skin heat transfer model discussed in [2]). Fabric thicknesses between 0.3 and 5.0 mm were used for simulated bench top test exposures of 10 s. The predicted temperatures of the front surface of the fabric for thicknesses of 0.3, 1.0, and 2.0 mm are compared for the cases of the fabric in contact with the copper disk and skin in Figure 5.10.

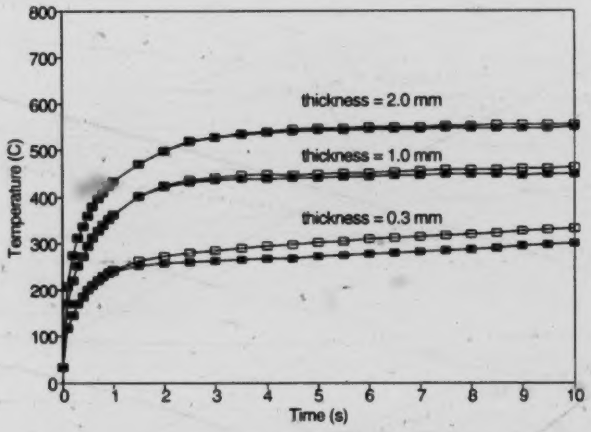

Figure 5.10 Comparison Between Predicted Temperatures of the Front of Fabrics of Various Thicknesses in Perfect Contact with a Copper Disk Test Sensor (■) and Human Skin (□)

Looking at Figure 5.10 it would appear that as the thickness of the fabric increases, the material under the fabric has little or not effect. However the temperatures in Figure 5.10 are just the temperatures of the front surface of the fabric. The temperatures at various depths in a 2.0 mm fabric in perfect contact with a copper disk and human skin are shown in Figure 5.11.

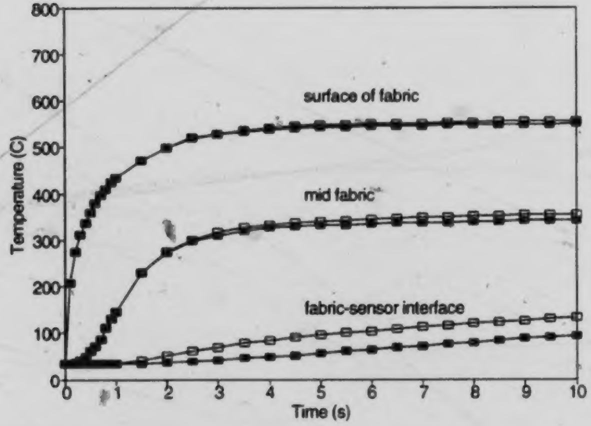

Figure 5.11 Comparison Between Predicted Temperatures at Various Depths in a 2.0 mm Thick Fabric in Perfect Contact with a Copper Disk Test Sensor (■) and Human Skin (□)

Figure 5.11 clearly shows that while the temperatures at the surface are fairly similar, those at depth, especially at the fabric/test sensor (or skin) interface are quite different. This will have an effect on bench top test results, as shown in Table 5.2 below.

Table 5.2 Predicted Times to Second Degree Burn Criteria For Fabrics of Various Thicknesses in Perfect Contact with Copper Disk Test Sensors and Human Skin

Thickness (mm)	Predicted Time to Exceed Stoll Criterion (s) for Copper Disk	Predicted Time to Second Degree Burn (s) for Skin Using Henriques Burn Integral
0.3	1.45	1.40
0.5	1.75	1.65
0.7	2.05	1.90
1.0	2.45	2.25
1.5	3.00	2.75
2.0	3.50	3.15
5.0	6.45	5.80

The predicted times to second degree burn are closer at the smaller thicknesses. The heat fluxes measured by the copper disk and human skin were calculated as outlined in Section 4.3 and are plotted for fabric thicknesses of 0.3 and 2.0 mm in Figure 5.12. Figure 5.12 indicates that the heat fluxes under the thinner fabrics should be closer to a square wave than at the larger thicknesses where it will take longer for the energy from the flame to reach the sensor. Recall that the Stoll criterion is only strictly valid for square wave heat fluxes [12]. In Section 4.5.6, it was shown that the heat flux strays further from the square wave as an air space is introduced between the fabric and test sensor. All of this information may be important when looking at the validity of test results for thick fabrics tested with and without spacers. For example, should copper disk test sensors and the Stoll criterion be used in long duration tests of thick ensembles for fire fighters?

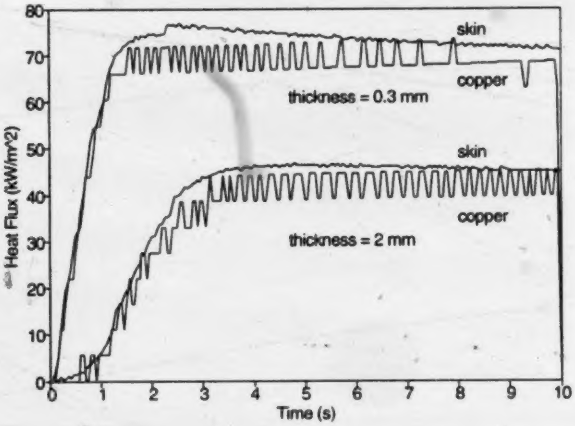

Figure 5.12 Calculated Heat Fluxes Incident on the Surface of Copper Disks and Human Skin in Perfect Contact with Fabrics of Thicknesses of 0.3 and 2.0 mm

5.4 Summary

The fabric temperatures predicted by the numerical model were found to be in good agreement with those determined using the infrared thermometer. Bench top test results predicted by the model were also found to be in good agreement with experimental results when an air gap of 1/4 in. (6.4 mm) was used. The bench top test results at larger spacings were not in quite as good agreement. The results of the parametric study in Chapter 3 indicated that if fabrics can maintain their mechanical integrity during thermochemical reactions, it may be advantageous in terms of bench top test results to have these reactions occur at lower temperature ranges. Implications of the numerical and experimental results to fabric design and bench top test methods were also discussed.

CHAPTER 6: CONCLUSIONS AND RECOMMENDATIONS

In this thesis a numerical model of the heat transfer in fibrous materials under high heat flux conditions has been developed. The results of this model were compared with measurements and observations made during bench top tests of two common inherently flame resistant fabrics. Conclusions and recommendations from this work are described below.

6.1 Conclusions

In terms of the thermal response of the fabric, and the energy transfer from the heated portion of the fabric to the test sensor, the following conclusions can be made.

- It is possible to develop relatively simple models of the heat transfer in inherently flame resistant fabrics during common bench top tests. These models give estimates of the gross thermal response of these materials in the form of effective temperatures, which are weighted average values of the temperatures of small volumes adjacent to the front and back surfaces of the fabric (such as the temperatures measured by an infrared thermometer), rather than the temperatures at specific locations (such as measured by a thermocouple). The absolute temperatures predicted by this model were found to be within 4% of those measured by an infrared thermometer during the latter parts of 10 s exposures to a nominal heat flux of about 82 kW/m^2 from a Meker burner.

- Required times to exceed the Stoll second degree burn criterion predicted by the numerical model were within 6% of those measured during actual bench top tests using air spaces of 1/4 in. (6.4 mm). For tests with larger air spaces, the model was less successful in predicting the results of bench top tests. It was thought that this was due to the limitations of the one-dimensional model in predicting increasingly three dimensional behaviour at these larger air gaps. In addition mass transfer, which might account for significant amounts of energy, was not included in the model.

- No critical value for the width of the air space between the fabric and test sensor was found either numerically or experimentally. The numerical model did predict that natural convection would begin in these air spaces at about 8 mm, while a flow visualization study indicated that natural convection begins at about 6 mm. However, the amount of energy transferred due to natural convection will remain approximately constant as the air gap width increases, because while the convection cells will become more vigorous, the distance the cells must travel to transfer energy to the test sensor also increases. Results from the numerical model also clearly indicated that radiation heat transfer is the dominant form of energy transfer between the heated fabric and test sensor for the particular fabrics studied here. The net heat transfer to the sensor by thermal radiation will decrease with increasing air gap width due to a decrease in the view factor between the heated portion of the fabric and the test sensor. Hence, the overall net heat transfer between the fabric and test sensor will decrease with increasing air gap width.

- A parametric study conducted using the numerical model indicated that the most important parameters in the model were the boundary conditions. The numerical and experimental results demonstrated that during these short exposures to intense heat fluxes the fabric temperatures increased until steady state conditions were reached. At this point there will be a balance between the net heat transfer from the flame to the front surface of the fabric and from the fabric to the test sensor. The parametric study also indicated that increasing the thickness, increasing the moisture regain, decreasing the thermal conductivity, and increasing the specific heat of the fabric will slow the rate at which the temperature of the back surface of the fabric increases, and hence increase the time required to exceed the Stoll criterion. Increasing the amount of energy associated with thermal decomposition reactions had a minor effect on predicted fabric temperatures and bench top results. However, if thermal decomposition reactions take place at lower temperatures, these can slow the heating of the back surface of the fabric, and thus increase the time required to exceed the Stoll criterion (assuming these reactions do not have detrimental effects on the mechanical integrity or other important properties of the fabric). These results were used to explain the differences in bench top test results of two common inherently flame resistant fabrics.

Applying the results of the numerical and experimental work to the evaluation of existing and modified bench top test methods, several other conclusions can be made.

- From the heat transfer perspective the planar geometry used in existing bench top tests is an adequate representation of the more complex geometry of the human body. Similarly, one-dimensional models of the heat transfer in human skin are adequate for analyzing data from thermal mannequin tests.

- Fixed duration exposure tests of protective fabrics show some promise. These can provide more information about fabrics under conditions which may be more indicative of a flash fire or some other exposure. They could be used after fabrics have been tested using existing bench top test methods and prior to testing full garments with thermal mannequins.

- Copper disk and skin simulant heat flux sensors each have several advantages and disadvantages. Skin simulant heat flux sensors can be used to provide more information from bench top tests, but the required data analysis routines are somewhat complicated, and the sensors themselves are less practical to use than copper disks. Copper disk heat flux sensors are more practical to use than skin simulants, but data from these sensors are more difficult to analyze if information about predicted times to deeper skin burns are required.

- Second degree burn predictions made using the Stoll criterion and Henriques burn integral are similar when the incident heat flux is close to a square wave. As the heat flux becomes less like a square wave, the differences between predictions made using the two methods increase. For bench top tests involving single layer fabrics placed in contact with the test sensor or spaced about 6 mm from the sensor, the Stoll criterion can be used with some confidence, even though the heat flux incident on the sensor is not exactly a square wave. If multiple layers of fabrics or very thick fabrics are tested, it is expected that the heat flux will become progressively less like a square wave, and the differences between results using the two methods to predict skin burns will increase.

6.2 Recommendations

The following recommendations for future research are made as a result of this study.

- Heat flux data from explosions has shown that peak heat fluxes during some industrial accidents may be twice as large as those used in existing bench top tests. Measurements of heat fluxes in actual flash fires and other industrial accidents should be made to determine whether larger heat fluxes should be used in standardized tests of protective fabrics and garments.

- It was shown that from the heat transfer point of view, the curvature of the human body does not have an effect on skin modelling and the design of bench top test apparatus. The effects of the geometry of the body on thermal shrinkage of fabrics, and energy transfers between the fabric and skin or test sensor should be investigated. If deemed necessary, a small scale test that better represents the curvature of the human body could be developed.

- The air space in the bench top test studied here is a horizontal enclosure locally heated from below. Air spaces in thermal mannequin tests and in some actual flash fires involve vertical enclosures. Differences between the two orientations of enclosures and their effects on test results should be examined.

- Apparent heat capacity values for the two fabrics were based on estimates made from incomplete information from the differential scanning calorimeter (DSC). This was due to the fact that the particular DSC used here could only heat the sample up to about 500°C, whereas the thermal decomposition reactions in these materials did not finish until temperatures higher than 500°C. Data from other DSC's or other instruments with higher maximum temperatures could be used to more accurately determine the energies involved in the thermal decomposition reactions.

- Numerical and experimental results in this thesis are for bench top tests which use a laboratory burner as a heat source. It was shown that the heat flux from the burner was approximately 75% convective and 25% radiative. Other bench top tests use heat sources with different percentage of convective and radiative incident energy. If a radiative heat source is used, oxygen may be available to support oxidative thermochemical reactions on the front surface of the fabric, which would be exothermic, rather than endothermic like the reactions modelled in this work. The thermal response of these fabrics during a radiative exposure should therefore also be modelled.

- The use of copper disk and skin simulant heat flux sensors for bench top tests of materials for longer duration exposures to moderate heat fluxes should be investigated. For example, a comparison between the second degree burn predictions made using the Stoll criterion and Henriques burn integral should be made using heat flux histories from under multiple layer fabric samples subjected to heat fluxes and durations indicative of structural fire fighting. In addition, the feasibility of using disposable skin simulant sensors for bench top tests should be examined.

6.3 Caution

In applying the results of the work in this thesis, it must be remembered that these results are applicable only to common bench top tests of two particular protective fabrics. The numerical model only considered heat transfer in these materials, and from the heated fabrics to the test sensor. Other modes of energy transfer, such as mass transfer, may also be important. The mechanical integrity of the fabrics during and after bench top tests was not considered. An exposure to a laboratory Meker burner was used, which is different than an actual flash fire or other industrial accidents. The fabrics were placed in a horizontal position and heated from below, while a flash fire may result in fabrics being heated in different orientations. The parametric study described in this thesis independently varied individual parameters, while there will actually be some interdependence of the individual parameters. Fabrics were simply washed and conditioned before being tested, while garments in the field may have been used for some time before being exposed to a flash fire. Human response during an accidental exposure was not considered. Hence, for these and other reasons, the results and discussion in this thesis may not be applicable to the performance of actual protective fabrics or garments during actual flash fires or other industrial accidents. The model described here should not be used to make estimates of the protection which these or other materials can provide in a flash fire or other accident. The model is only intended to be used to gain an appreciation for the physics involved in bench top tests of these fabrics, and to try to explain differences in bench top tests between different materials.

In addition, the intention of this work was not to recommend either of the two fabrics used in this study, or any other particular fabric, for use in thermal protective clothing. The test results presented here are based on tests of specimens from limited quantities of two fabrics supplied to the author, and hence may not be representative of other specimens of the same fabrics or other bench top test results of these fabrics.

REFERENCES

---

1. Neal, T.E., "Thermal Performance and Comfort: Industrial Protective Apparel", presented at the DuPont Nomex® Protective Apparel Seminar, Edmonton, May, 1996

2. Torvi, D.A., "A Finite Element Model of Heat Transfer in Skin Subjected to a Flash Fire", M.Sc. Thesis, University of Alberta, Edmonton, Alberta, 1992

3. Behnke, W.P., "Predicting Flash Fire Protection of Clothing From Laboratory Tests Using Second-Degree Burn to Rate Performance", Fire and Materials, Vol. 8, 1984, pp. 57-63

4. Holcombe, B.V., and Hoschke, B.N., "Do Test Methods Yield Meaningful Performance Specifications?", Performance of Protective Clothing: First Volume ASTM STP 900, R.L. Barker and G.C. Coletta, eds., American Society for Testing and Materials, West Conshohocken, PA, 1986, pp. 327-339

5. Krasny, J., Rockett, J.A., and Huang, D., "Protecting Fire Fighters Exposed in Room Fires: Comparison of Results of Bench Scale Test for Thermal Protection and Conditions During Room Flashover", Fire Technology, Vol. 24, 1988, pp. 5-19

6. Dale, J.D., Weckman, B., and Ackerman, M., "HFOG (House Full of Gas) III Part B: The Explosion and Aftermath", Proceedings, 1995 Spring Technical Meeting, The Combustion Institute, Canadian Section, 1995, paper #43

7. Soroka, A.J., "Thermal Protective Clothing", presented at the DuPont Nomex Protective Apparel Seminar, Edmonton, Alberta, May, 1992

8. Canadian General Standards Board, CAN/CGSB-4.175-M87 Part 1: Burning Behaviour of Textiles and Textile Products - Vocabulary, Ottawa, 1987

9. Crown, E.M., and Kerr, N., Textile Science II: Learning Systems in Home Economics Modules 14 to 26, University of Alberta, Edmonton, Alberta, 1992

10. Joseph, M.L., Essentials of Textiles, Holt, Rinehart and Winston, Inc., New York, 1988

11. Diller, K., "Analysis of Skin Burns", in Heat Transfer in Medicine and Biology", A. Shitzer and R.C. Eberhart, Eds., Plenum Press, New York, 1985, pp. 85-134

12. Stoll, A.M., and Chianta, M.A., "Method and Rating System for Evaluation of Thermal Protection", Aerospace Medicine, Vol. 40, 1969, pp. 1232-1238

13. Stoll, A.M., and Greene, L.C., "Relationship Between Pain and Tissue Damage Due to Thermal Radiation", Journal of Applied Physiology, Vol. 14, 1959, pp. 373-382

14. Henriques, F.C., Jr., "Studies of Thermal Injuries V. The Predictability and the Significance of Thermally Induced Rate Processes Leading to Irreversible Epidermal Injury", Archives of Pathology, Vol. 43, 1947, pp. 489-502

15. Diller, K.R., Hayes, L.J, and Blake, G.K., "Analysis of Alternate Models for Simulating Thermal Burns", Journal of Burn Care and Rehabilitation, Vol. 12, 1991, pp. 177-189

16. Takata, A.N., Rouse, J., and Stanley, T., "Thermal Analysis Program", I.I.T. Research Institute Report IITRI-J6286, Chicago, 1973

17. Diller, K.R., Klutke, G.A., "Accuracy Analysis of the Henriques Model for Predicting Thermal Burn Injury", Advances in Bioheat and Mass Transfer: Microscale Analysis of Thermal Injury Processes, Instrumentation, Modeling, and Clincial Applications, HTD-Vol. 268, American Society of Mechanical Engineers, New York, 1993, pp. 117-123

18. Crown, E.M., and Rigakis, K.B., Making Protective Clothing Decisions, Textile Analysis Service, Department of Human Ecology, University of Alberta, 1989

19. Stull, J.O., Connor, M., and Heath, C.A., "Development of a Combination Thermal and Chemical Protective Ensemble for U.S. Navy Fire Fighting Applications", Performance of Protective Clothing: Fifth Volume, ASTM STP 1237, James S. Johnson and S. Z. Mansdorf, eds., American Society for Testing and Materials, West Conshohocken, PA, 1996, pp. 408-427

20. Conn, J.J., and Grant, G.A., "Review of Test Methods for Material Flammability", Department of National Defence Research Establishment Ottawa Contractor Report DREO/PSD/CRS-02/91, March 1991

21. Canadian General Standards Board, CAN/CGSB-4.2 No. 27.5-M87: Flame Resistance - 45° Angle Test - One Second Flame Impingement, Ottawa, 1987

22. American Society for Testing and Materials, ASTM D 1230 - 94: Standard Test Method for Flammability of Apparel Textiles, West Conshohocken, PA, 1994

23. Canadian General Standards Board, CAN/CGSB-4.2 No. 27.10-M91: Flame Resistance - Vertically Oriented Textile Fabric or Fabric Assembley Test, Ottawa, 1991

24. Canadian General Standards Board, CAN/CGSB-4.2 No. 27.4-94/ISO 6940:1984: Textile Fabrics - Burning Behaviour - Determination of Ease of Ignition of Vertically Oriented Specimens, Ottawa, 1994

25. General Services Administration, Federal Standard for Textile Materials (U.S.A.) 191A 5903, Flame Resistance of Cloth; Vertical, Washington, 1989

26. American Society for Testing and Materials, ASTM D 3659-80 Standard Test Method for Flammability of Apparel Fabrics by Semi-Restraint Method, West Conshohocken, PA, 1993

27. American Society for Testing and Materials, ASTM D 2863 Measuring the Minimum Oxygen Concentration to Support Candle-like Combustion of Plastics (Oxygen Index), West Conshohocken, PA, 1995

28. Brewster, E.P., and Barker, R.L., "A Summary of Research on Heat Resistant Fabrics for Protective Clothing", American Industrial Hygiene Association Journal, Vol. 44, 1983, pp. 123-130

29. American Society for Testing and Materials, ASTM D 4108-87 Standard Test Method for Thermal Protective Performance of Materials for Clothing By Open-Flame Method, West Conshohocken, PA, 1987

30. Day, M., "A Comparative Evaluation of Test Methods and Materials for Thermal Protective Performance", Performance of Protective Clothing: Second Symposium, ASTM STP 989, S.Z. Mansdorf, R. Sager, A.P. Nielsen, eds., American Society for Testing and Materials, West Conshohocken, PA, 1988, pp. 108-120

31. International Organization for Standardization, ISO 9151 Protective Clothing Against Heat and Flame - Determination of Heat Transmission on Exposure to Flame, Geneva, Switzerland, 1995

32. Canadian General Standards Board, CAN/CGSB-155.1 - M88 Fire Fighters' Protective Clothing for Protection Against Heat and Flame, Ottawa, 1988

33. National Fire Protection Association, NFPA 1971, Standard on Protective Clothing for Structural Fire Fighting, Quincy, Massachusetts, 1991

34. Norton, M.J.T., Kadolph, S.J., Johnson, R.F., and Jordan, K.A., "Design, Construction, and Use of Minnesota Woman, A Thermally Instrumented Mannequin", Textile Research Journal, Vol. 55, 1985, pp. 5-12

35. Stoll, A.M., and Chianta, M.A., "Heat Transfer Through Fabrics as Related to Thermal Injury", Transactions of the New York Academy of Sciences, Vol. 33, 1971, pp. 649-669

36. Elkins, W. and Thompson, J.G., "Instrumented Thermal Mannikin", Acurex Corporation, Aerotherm Division Report AD-781 176, 1973

37. Behnke, W.P., Geshury, A.J., and Barker, R.L., "Thermo-Man® and Thermo-Leg: Large Scale Test Methods for Evaluation Thermal Protective Performance", Performance of Protective Clothing: Fourth Volume, ASTM STP 1133, James P. McBriarty and Norman W. Henry, eds., American Society for Testing and Materials, West Conshohocken, PA, 1992, pp. 266-280

38. Dale, J.D., Crown, E.M., Ackerman, M.Y., Leung, E., and Rigakis, K.B., "Instrumented Mannequin Evaluation of Thermal Protective Clothing", Performance of Protective Clothing: Fourth Volume, ASTM STP 1133, James P. McBriarty and Norman W. Henry, eds., American Society for Testing and Materials, West Conshohocken, PA, 1992, pp. 717-733

39. Ukponmwan, J.O, "The Thermal-insulation Properties of Fabrics", Textile Progress, Vol. 24, Number 4, 1993

40. "Bioengineering Heat Transfer", Advances in Heat Transfer, Vol. 22, Academic Press, Inc., Boston, 1992

41. Chen, N.Y., "Transient Heat and Moisture Transfer Through Thermally Irradiated Cloth", PhD Thesis, Massachusetts Institute of Technology, Cambridge, Massachusetts, 1959

42. Stoll, A.M., Chianta, M.A., and Munroe, L.R., "Flame Contact Studies", Transactions of the ASME, Journal of Heat Transfer, Vol 86, 1964, pp. 449-456

43. Griffith, M.V., and Horton, G.K., "The Transient Flow of Heat Through a Two-Layer Wall", Proceedings of the Physical Society (London), Vol. 58, 1946, pp. 481-487

44. Stoll, A.M., and Chianta, M.A., "Burn Production and Prevention in Convective and Radiant Heat Transfer", Aerospace Medicine, Vol. 39, 1968, pp. 1097-1100

45. Backer, S., et al., Textile Fabric Flammability, The MIT Press, Cambridge, Massachusetts, 1976

46. Morse, H.L., Thompson, J.G., and Clark, K.J., "Analysis of the Thermal Response of Protective Fabrics", Acurex Corporation, Aerotherm Division Report AFML-TR-73-17, 1973

47. Shalev, I., and Barker, R.L., "Predicting the Thermal Protective Performance of Heat Protective Fabrics From Basic Properties", Performance of Protective Clothing: First Volume ASTM STP 900, R.L. Barker and G.C. Coletta, eds., American Society for Testing and Materials, West Conshohocken, PA, 1986, pp. 358-375

48. Shalev, I. "Transient Thermophysical Properties of Thermally Degrading Fabrics and Their Effect on Thermal Protection", Ph.D. thesis, North Carolina State University, Raleigh, North Carolina, 1984

49. Lee, Y.M., and Barker, R.L, "Thermal Protective Performance of Heat-Resistant Fabrics in Various High Intensity Heat Exposures", Textile Research Journal, Vol. 57, 1987, pp. 123-132

50. Lee, Y.M., and Barker, R.L., "Effect of Moisture on the Thermal Protective Performance of Heat-Resistant Fabrics Heat-Resistant Fabrics", Journal of Fire Sciences, Vol. 4, 1986, pp. 315-331

51. Ko, W.L., Quinn, R.D., and Gong, L., "Finite-Element Reentry Heat-Transfer Analysis of Space Shuttle Orbiter", NASA Technical Paper 2657, NASA Ames Research Center, Dryden Flight Research Facility, Edwards, California, 1986

52. Milke, J.A., and Vizzini, A.J., "Modeling and Evaluation of the Thermal Response of Fire Exposed Composites", Heat and Mass Transfer in Fires, HTD Vol. 141, American Society of Mechanical Engineers, 1990, pp. 15-21

53. Kushida, G., et al., "Heat and Mass Transport from Thermally Degrading Thin Cellulosic Materials in a Microgravity Environment", Transactions of the ASME, Journal of Heat Transfer, Vol. 114, 1992, pp. 494-502

54. Chaboki, A., et al., "Experimental and Numerical Results for Thermophysical Properties and Thermal Response of a Fire-Retardant Polymer", Experimental/Numerical Heat Transfer in Combustion and Phase Change, HTD Vol. 170, American Society of Mechanical Engineers, New York, 1991, pp. 1-9

55. Huang, H.C., and Usmani, A.S., Finite Element Analysis for Heat Transfer: Theory and Software, Springer-Verlag, New York, 1994

56. Yao, M., and Chait, A., "A Conservative Formulation of the Apparent Heat Capacity Method for Heat Transfer Problems with Phase Change", Current Developments in Numerical Simulation of Flow and Heat Transfer, ASME HTD-Vol. 275, American Society of Mechanical Engineers, New York, 1994, pp. 35-42

57. Fanucci, J.P., "Thermal Response of Radiantly Heated Kevlar and Graphite/Epoxy Composites", Journal of Composite Materials, Vol. 21, 1987, pp. 129-139

58. Farnworth, B., "Mechanisms of Heat Flow Through Clothing Insulations", Textile Research Journal, Vol. 53, 1983, pp. 717-725

59. Stuart, I.M., and Holcombe, B.V., "Heat Transfer Through Fiber Beds by Radiation with Shading and Conduction", Textile Research Journal, Vol. 54, 1984, pp. 149-157

60. Woo, S.S., Shalev, I., and Barker, R.L., "Heat and Moisture Transfer Through Nonwoven Fabrics Part I: Heat Transfer", Textile Research Journal, Vol. 64, 1994, pp. 149-162

61. Futschik, M.W., and Witte, L.C., "Effective Thermal Conductivity of Fibrous Materials", General Papers in Heat and Mass Transfer, Insulation, and Turbomachinery, HTD-Vol. 271, American Society of Mechanical Engineers, New York, 1994, pp. 123-134

62. Gaydon, A.G., The Spectroscopy of Flames, Second Edition, Chapman and Hall, London, 1974

63. Hottel, H.C., and Sarofim, A.F., Radiative Transfer, McGraw-Hill Book Company, New York, 1967

64. van de Hulst, H.C., Light Scattering by Small Particles, Dover Publications, Inc., New York, 1981

65. Davis, S.M., "Relationship of Fiber Type, Mass and Cover to the Sun Protection Factor of Fabrics, M.Sc. thesis, University of Alberta, Edmonton, Alberta, 1995

66. Jakob, M., Heat Transfer, Volume II, John Wiley & Sons, New York, 1957

67. Siegel, R., and Howell, J.R., Thermal Radiation Heat Transfer, Second Edition, Hemisphere Publishing Corporation, Washington, 1981

68. Lewis, B., and von Elbe, G., Combustion, Flames, and Explosions of Gases, Third Edition, Academic Press, Inc., Orlando, 1987

69. Martin, H., "Heat and Mass Transfer between Impinging Gas Jets and Solid Surfaces", Advances in Heat Transfer, Vol. 13, 1977, pp. 1-60

70. Geshury, A.J., "Effect of the Simultaneous Application of Heat and Dynamic Mechanical Forces on the Thermal Protection Performance of Aramid Fabrics", Ph.D. thesis, North Carolina State University, Raleigh, North Carolina, 1990

71. Rees, W.H., "The Transmission of Heat Through Textile Fabrics", The Journal of the Textile Institute, Vol. 32, 1941, pp. T149-T166

72. Cain, B., and Farnworth, B., "Two New Techniques for Determining the Thermal Radiative Properties of Thin Fabrics", Journal of Thermal Insulation, Vol. 9, 1986, pp. 301-323

73. Veghte, J. H., Fire Fighters' Protective Clothing: Design Criteria, Second Edition, Janesville Division of Lion Apparel, Dayton, Ohio, 1988

74. Danielsson, U., Convection Coefficients in Clothing Air Layers, Doctoral thesis, Department of Energy Technology, Division of Heating and Ventilation, The Royal Institute of Technology, Stockholm, Sweden, 1993

75. MacAdams, W.H., Heat Transmission, Third Edition, McGraw-Hill Book Company, New York, 1954

76. Davies, J.M., McQue, B., and Hoover, T.B., "Heat Transferred by Decomposition Products from Cotton Fabrics Exposed to Intense Thermal Radiation", Textile Research Journal, Vol. 35, 1965, pp. 757-769

77. Hoschke, B.N., Holcombe, B.V., and Plante, A.M., "A Critical Appraisal of Test Methods for Thermal Protective Clothing Fabrics", Performance of Protective Clothing, ASTM STP 900, R.L. Barker and G.C. Coletta, Eds., American Society for Testing and Materials, West Conshohocken, PA, 1986, pp. 311-326.

78. Benisek, L., and Phillips, W.A., "Protective Clothing Fabrics. Part II. Against Convective Heat (Open-Flame) Hazards", Textile Research Journal, Vol. 51, 1981, pp. 191-196

79. Goldstein, R.J., and Volino, R.J., "Onset and Development of Natural Convection Above a Suddenly Heated Horizontal Surface", Journal of Heat Transfer, Vol. 117, 1995, pp. 808-821

80. Catton, I., "Natural Convection in Enclosures", Proceedings, 6th International Heat Transfer Conference, 1978, Vol. 6, pp. 13-31

81. Hollands, K.G.T., Raithby, G.D., and Konicek, L., "Correlation Equation for Free Convection Heat Transfer in Horizontal Layers of Air and Water", International Journal of Heat and Mass Transfer, Vol. 18, 1975, pp. 879-884

82. Mantle-Miller, W.J., Kazmierczak, M., and Hiawy, B., "Natural Convection in a Horizontal Enclosure with Periodically Changing Bottom Wall Temperature", Natural Convection in Enclosures, HTD - Vol. 198, American Society of Mechanical Engineers, 1992, pp. 49-56

83. Torrance, K.E., Orloff, L., and Rockett, J.A., "Experiments on Natural Convection in Enclosures with Localized Heating From Below", Journal of Fluid Mechanics, Vol. 36, Part 1, 1969, pp. 21-31

84. Torrance, K.E., and Rockett, J.A., "Numerical Study of Natural Convection in an Enclosure with Localized Heating from Below--Creeping Flow to the Onset of Laminar Instability", Journal of Fluid Mechanics, Vol. 36, Part 1, 1969, pp. 33-54

85. MacGregor, R.K., "Free Convection Through Vertical Plane Layers - Moderate and High Prandtl Number Fluids", Transactions of the ASTM, Journal of Heat Transfer, Vol. 91, 1969, pp. 391-403

86. Gray, D.D., and Giorgini, A., "The Validity of the Boussinesq Approximation for Liquids and Gases", International Journal of Heat and Mass Transfer, Vol. 19, 1976, pp. 545-551

87. Kuo, D.C., and Ball, K.S., "Essential Differences Between Boussinesq and Variable Density Simulations of Bifurcations in Rayleigh-Benard Convection", Bifurcation Phenomena and Chaos in Thermal Convection, HTD-Vol. 214/AMD-Vol. 138, American Society of Mechanical Engineers, 1992, pp. 25-32

88. Sparrow, E.M., and Gregg, J.L., "The Variable Fluid-Property Problem in Free Convection", Transactions of the ASME, Vol. 80, 1958, pp. 879-886

89. Pallares, J., Cuesta, I., Grau, F.X., and Giralt, F., "Natural Convection in a Cubical Cavity Heated from Below at Low Rayleigh Numbers", International Journal of Heat and Mass Transfer, in press

90. Drysdale, D., An Introduction to Fire Dynamics, John Wiley and Sons, Chichester, 1985

91. Willeke, K., and Baron, P.A., eds., Aerosol Measurement: Principles, Techniques, and Applications, Van Nostrand Reinhold, New York, 1993

92. Stelzer, J.F., and Welzel, R., "Experiences in Non-Linear Analysis of Temperature Fields with Finite Elements", International Journal for Numerical Methods in Engineering, Vol. 24, 1987, pp. 59-73

93. Holman, J.P., Heat Transfer, Sixth Edition, McGraw-Hill Book Company, New York, 1986

94. Diller, K.R., and Hayes, L.J., "A Finite Element Model of Burn Injury in Blood-Perfused Skin", Transactions of the ASME, Journal of Biomechanical Engineering, Vol. 105, 1983, pp. 300-307

95. Osman, M.M., and Afify, E.M., "Thermal Modelling of the Normal Woman's Breast", Transactions of the ASME, Journal of Biomechanical Engineering, Vol. 106, 1984, pp. 123-130

96. Chen, D.S.D., Singh, R.K., Haghighi, K., and Nelson, P.E., "Finite Element Analysis of Temperature Distribution in Microwaved Cylindrical Potato Tissue", Journal of Food Engineering, Vol. 18, 1993, pp. 351-368

97. Craggs, A., University of Alberta, private communication, 1990

98. Wu, Ray-Shing, Cheng, K.C., Craggs, A., "Convective Instability in Porous Media with Maximum Density and Throughflow Effects by Finite-Difference and Finite-Element Methods", Numerical Heat Transfer, Vol. 2, 1979, pp. 303-318

99. Kakaç, S., and Yener, Y., Heat Conduction, Second Edition, Hemisphere Publishing Corporation, Washington, 1985, pp. 349

100. Carslaw, H.S., and Jaeger, J.C., Conduction of Heat in Solids, 2nd ed., Oxford University Press, London, 1959

101. For Flame Resistance In an Anti-Static Garment...Put Protective Apparel Of DuPont Nomex® IIIA To Work For You, DuPont Advance Fiber Systems Technical Literature, E.I. du Pont de Nemours & Company, Wilmington, DE, 1992

102. Canadian General Standards Board, CAN/CGSB-4.2 No. 37-M87: Textile Test Methods: Fabric Thickness, Ottawa, 1987

103. Williams, S.D., and Curry, D.M., Thermal Protection Materials: Thermophysical Property Data, NASA Reference Publication 1289, National Aeronautics and Space Administration, Scientific and Technical Information Program, Washington, 1992

104. Bomberg, M., "Application of Three ASTM Test Methods to Measure Thermal Resistance of Clothing", Performance of Protective Clothing: Fourth Volume, ASTM STP 1133, J.P. McBriarty and N.W. Henry, eds., American Society for Testing and Materials, West Conshohocken, PA, 1992, pp. 399-417

105. Baker, D.L., Wool, M.R., and Schaefer, J.W., "A Dynamic Technique for Determining the Thermal Conductivity of Charring Materials", Thermal Conductivity-Proceedings of the Eighth Conference-1968, C.Y. Ho, and R.E. Taylor, eds., Plenum Press, New York, 1969, pp. 823-836

106. Properties of Polybenzimidazole High-Performance Fiber, PBI Products Division Technical Literature, Hoechst Celanese, Charlotte, 1989

107. Chatfield, D.A., Einhorn, I.N., Mickelson, R.W., and J.H. Futrell, "Analysis of the Products of Thermal Decomposition of an Aromatic Polyamide Fabric", Journal of Polymer Science, Vol. 17, 1979, pp. 1367-1381

108. Jackson, R.H., "PBI Fiber and Fabric - Properties and Performance", Textile Research Journal, Vol. 48, 1978, pp. 314-319

109. Brown, J.R., and Ennis, B.C., "Thermal Analysis of Nomex® and Kevlar® Fibers", Textile Research Journal, Vol. 47, 1977, pp. 62-66

110. Jaffe, M., "Fibers", Chapter 7 in Thermal Characterization of Polymeric Materials, E.A. Turi, ed., Academic Press, New York, 1981

111. Wendlandt, W.W., and Gallagher, P.K., "Instrumentation", Chapter 1 in Thermal Characterization of Polymeric Materials, E.A. Turi, ed., Academic Press, New York, 1981

112. Henderson, J.B., and O'Brien, E.F., "Measurement of the Decomposition Kinetics of a Polymer Composite using a High-Temperature, High-Heating-Rate Simultaneous Thermal Analyzer", High Temperatures-High Pressures, Vol. 19, 1987, pp. 103-109

113. Bingham, M.A., and Hill, B.J., "Comparison of Thermal Characteristics of Materials Examined by Thermogravimetry and Flammability Tests", Journal of Thermal Analysis, Vol. 9, 1976, pp. 71-81

114. Shlensky, O.F., Aksenov, L.N., and Shashkov, A.G., Thermal Decomposition of Materials: Effect of Highly Intensive Heating, Elsevier Science Publishers, Amsterdam, 1991

115. Mraw, S.C., "Differential Scanning Calorimetry", Chapter 11 in Specific Heat of Solids, CINDAS Data Series on Material Properties Vol. I-2, C.Y. Ho, ed., Hemisphere Publishing Corporation, New York, 1988

116. In Protective Coveralls, PBI Makes the Difference (HPF-P6), Hoechst Celanese Corporation, Charlotte, NC, 1993

117. Schoppee, M.M., Welsford, J.M., and Abbott, N.J., "Resistance of Navy Outerwear Garments and Fire-Resistant Fabrics to Extreme Heat", Technical Report No. 153, Navy Clothing and Textile Research Facility, Natick, Massachusetts, 1983

118. Chouinard, M.P., Knodel, D.C., and Arnold, H.W., "Heat Transfer from Flammable Fabrics", Textile Research Journal, Vol. 43, 1973, pp. 166-175

119. Baitinger, W.F., and Konopasek, L., "Thermal Insulative Performance of Single-Layer and Multiple-Layer Fabric Assemblies", Performance of Protective Clothing, ASTM STP 900, R.L. Barker and G.C. Coletta, eds., American Society for Testing and Materials, West Conshohocken, PA, 1986, pp. 421-437

120. Lee, Y.M., "Analysis of Thermal Protective Performance of Heat Resistant Polymeric Fabrics", Ph.D. thesis, North Carolina State University, Raleigh, N.C., 1986

121. Schoppee, M.M., Skelton, J., and Abbott, N.J., "The Transient Thermomechanical Response of Protective Materials to Radiant Heat", AFML-TR-77-72, Air Force Materials Laboratory, Dayton, Ohio, 1977

122. Powell, R.L., et al., Thermocouple Reference Tables Based on the IPTS-68, National Bureau of Standards Monograph 125, Omega Press, Stamford Connecticut, 1975

123. Doebelin, E.O, Measurement Systems: Application and Design, McGraw-Hill Book Company, New York, 1983, pp. 664.

124. Beck, J.V., Blackwell, B., and St. Clair, C.R., Jr., Inverse Heat Conduction: Ill-posed Problems, John Wiley & Sons, Inc., 1985.

125. Grimes, R., Mulligan, J.C., Hamouda, H., and Barker, R., "The Design of a Surface Heat Flux Transducer For Use In Fabric Thermal Protection Testing", Performance of Protective Clothing: Fifth Volume, ASTM STP 1237, James S. Johnson and S.Z. Mansdorf, eds., American Society for Testing and Materials, West Conshohocken, PA, 1996, pp. 607-624.

126. Diller, T.E., "Advances in Heat Flux Measurements", Advances in Heat Transfer, Vol. 23, 1993, pp. 279-283.

127. Cook, W.J., and Felderman, E.J., "Reduction of Data from Thin-Film Heat-Transfer Gauges: A Concise Numerical Technique", American Institute of Aeronautics and Astronautics (A.I.A.A.) Journal, Vol. 4, 1966, pp. 561-562.

128. Freeston, W.D., et al., "Flammability and Heat Transfer Characteristics of PBI Fabric", Air Force Materials Laboratory Report AFML-TR-70-267, Air Force Materials Laboratory, Wright Patterson Air Force Base, Dayton, Ohio, 1971

129. Schoppee, M., Welsford, J.M., Abbott, N.J., "Protection Offered by Lightweight Clothing Materials to the Heat of a Fire", Performance of Protective Clothing, ASTM STP 900, R.L. Barker and G.C. Coletta, Eds., American Soceity for Testing and Materials, West Conshohocken, PA, 1986, pp. 340-357.

130. Behnke, W.P., "Predicting Flash Fire Protection of Clothing from Laborartory Tests Using Second-degree Burn to Rate Performance", Fire and Materials, Vol. 8, 1984, pp. 57-63.

131. Crown, E.M., Ackerman, M.Y., Dale, J.D., and Rigakis, K., "Thermal Protective Performance and Instrumented Mannequin Evaluation of a Multi-Layer Garment System", Proceedings of the AGARD 75th Aerospace Medical Panel Symposium on the Support of Air Operations Under Extreme Hot and Cold Weather Conditions (AGARD Conference Proceedings 540), 1993, pp. 14-1 - 14-8.

132. Neal, T.E., Rappaport, J.B., and Swain, R.A., "Correlation of Bench-Scale Thermal Testing with Manikin Testing", presented at the Eighth Annual Conference on Protective Clothing, Clemson University, May, 1994

133. "Weather Data", Chapter 24 in ASHRAE Handbook of Fundamentals, American Society of Heating, Refrigerating, and Air Conditioning Engineers, Inc., Atlanta, 1989

134. Barnes Engineering Company, Instruction Manual Optitherm Series 12-8700 Infrared Thermometers, Stamford Connecticut, no date

135. Sparrow, E.M., "Error Estimates in Temperature Measurement", Chapter 1 in Measurements in Heat Transfer, Second Edition, E.R.G. Eckert and R.J. Goldstein, eds., Hemisphere Publishing Corporation, Washington, 1976, pp. 1-23

136. Wyatt, P.J., Stull, V.R., and Plass, G.N., "The Infrared Transmittance of Water Vapour", Applied Optics, Vol. 3, 1964, pp. 229-241

137 Edwards, D.K., "Thermal Radiation Measurements", Chapter 10 in Measurements in Heat Transfer, Second Edition, E.R.G. Eckert and R.J. Goldstein, eds., Hemisphere Publishing Corporation, Washington, 1976, pp. 425-473

138 Benisek, L., Edmondson, G.K., Mehta, P., and Phillips, W.A., "The Contribution of Wool to Improving the Safety or Workers Against Flames and Molten Metal Hazards", Performance of Protective Clothing, ASTM STP 900, R.L. Barker and G.C. Coletta, Eds., American Soceity for Testing and Materials, West Conshohocken, PA, 1986, pp. 405-420.

139 Cook, W.J., "Determination of Heat-Transfer Rates from Transient Surface Temperature Measurements", American Institute of Aeronautics and Astronautics (A.I.A.A.) Journal, Vol. 8, 1970, pp. 1366-1368.

140. van Krevelen, D.W., "Some Basic Aspects of Flame Resistance of Polymeric Materials", Polymer, Vol. 16, 1975, pp. 615-620

141. Pennes, H.H., "Analysis of Tissue and Arterial Blood Temperatures in Resting Human Forearm", Journal of Applied Physiology, Vol. 1, 1948, pp. 93-122

142. Marsh, M.C., "The Thermal Insulating Properties of Fabrics", Proceedings of the Physical Society (London), Vol. 42, 1930, pp. 577-588

143. Lamb, G.E.R., "Heat and Water Vapor Transport in Fabrics Under Ventilated Conditions", Textile Research Journal, Vol. 62, 1992, pp. 387-392

144. Shitzer, A., and Chato, J.C., "Analytical Solutions to the Problem of Transient Heat Transfer in Living Tissue", Transactions of the ASME Journal of Biomechanical Engineering, Vol. 100, 1978, pp. 202-210

145. Shitzer, A., "A Study of the Thermal Behavior of Living Biological Tissue With Application to Thermal Control of Protective Suits", Ph.D. Thesis, University of Illinois at Urbana-Champaign, 1971

146. Bailey, R.W., Human Performance Engineering - A Guide for Systems Designers, Prentice-Hall, Inc., Englewoods Cliffs, N.J., 1982

APPENDICES

APPENDIX 1: EFFECTS OF CYLINDRICAL GEOMETRY ON HEAT TRANSFER IN HUMAN SKIN UNDER FLASH FIRE CONDITIONS

The shape of the human body exhibits complex three-dimensional geometry. Despite this three-dimensional geometry, bench top fabric tests involve only planar geometry. In addition, heat transfer models used to analyze data from thermal mannequin tests (discussed in Chapter 4) are also one-dimensional. By studying the effects of the geometry of the body on the heat transfer within the skin under conditions similar to flash fires, it can be determined whether or not one-dimensional heat transfer models of the skin are adequate.

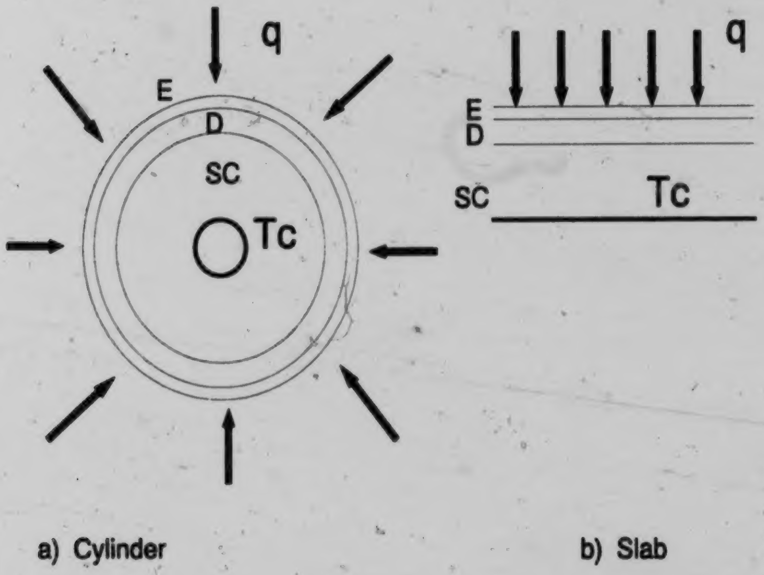

Figure A1.1 Idealized Models Which Treat Skin as a Cylinder or a Slab (e - epidermis, d - dermis, s - subcutaneous, T_c core temperature of body)

A model of the conduction heat transfer within the skin under flash fire conditions was developed. The skin was treated as a series of hollow cylinders and as a semi-infinite slab, as shown in Figure A1.1. The epidermis (e), dermis (d), and subcutaneous layers of the skin are shown, as well as the base of the subcutaneous region, the temperature of which was assumed to remain at the body's core temperature, T_c. The heat flux, q, was assumed to be constant over the surface area considered. In actual mannequin tests, while investigators try to keep the flux as constant as possible over the mannequin, it does vary from location to location due to factors such as the position of the mannequin and burners relative to one another, the nature of the flames, and the fluid flow surrounding the mannequin. This of course would also be the case in an actual flash fire. In addition, the inhomogeneous nature of protective fabrics may cause the heat flux at different points on the surface of the skin under a particular fabric to be different during garment tests. However, in mannequin tests, the heat flux histories recorded by individual sensors are analyzed independently. Therefore this approach is satisfactory. If a model of the entire three-dimensional mannequin shape and its surroundings was attempted, then the flux should not be treated as constant over the surface.

In the cylindrical model, a series of hollow cylinders were used as a first approximation to the body's complex geometry. This practice has been used by many other investigators. Pennes [141] used this approach when deriving his bioheat transfer equation. Others have also used fabric-covered cylinders in experimental work (e.g. Marsh [142], and Lamb [143]).

The Fourier field equation in cylindrical coordinates is:

$$\frac{\partial^2 T}{\partial r^2} + \frac{1}{r}\frac{\partial T}{\partial r} + \frac{1}{r^2}\frac{\partial^2 T}{\partial \theta^2} + \frac{\partial^2 T}{\partial z^2} = \frac{1}{\alpha}\frac{\partial T}{\partial t} \qquad \text{(A1.1)}$$

where θ is the angular position, and

z is the distance in the direction in the plane pointing into the paper

As the heat flux is assumed to be constant over the surface of the body, the third term on the left hand side of (A1.1) can be neglected. It can also be shown that if the ratio of the squares of the outside radius and half-length of the cylinder is small (say less than

0.10, which is the case with human skin), then the last term on the left hand side can also be neglected. This leaves the following equation.

$$\frac{\partial^2 T}{\partial r^2} + \frac{1}{r}\frac{\partial T}{\partial r} = \frac{1}{\alpha}\frac{\partial T}{\partial t} \tag{A1.2}$$

The skin was also idealized as a semi-infinite slab. The Fourier field equation for a slab, in rectangular cartesian coordinates is

$$\frac{\partial^2 T}{\partial x^2} = \frac{1}{\alpha}\frac{\partial T}{\partial t} \tag{A1.3}$$

Comparing (A1.2) and (A1.3), the two equations, and hence their solutions for a given set of boundary conditions, will be equal when

$$\frac{\partial^2 T}{\partial r^2} + \frac{1}{r}\frac{\partial T}{\partial r} = \frac{\partial^2 T}{\partial x^2}$$

i.e. when

$$\frac{1}{r}\frac{\partial T}{\partial r}$$

can be neglected.

This will occur when the thickness of the hollow cylinder is relatively small compared with its outside radius. In some cases, it is intuitively obvious that this condition will be met. For example, heat transfer in the earth close to the surface is often treated by ignoring the curvature of the earth. On the other hand, the curvature of the body changes considerably from location to location. Therefore, when looking at heat transfer in the skin under flash fire conditions, it is not obvious for which, if any, body locations this condition will be met.

A search of the bio heat transfer literature found only one attempt at quantifying when this assumption was valid. Shitzer [144], while modelling transient and steady state heat transfer in skin when cooled by tubes placed in contact with the skin, found that analytical solutions for rectangular and cylindrical geometries gave similar results.

Transient solutions were similar for cylindrical and rectangular geometries, with slightly longer times for the cylindrical case to reach steady state conditions, due to the effect of the radii on time dependent terms in the solution.

Steady state solutions for rectangular and cylindrical cases were not significantly different [145], especially as the values of the inner and outer radii increased. When the inner radius was greater than or equal to about 60 mm, the rectangular results were adequate for practical purposes. He partially explained this by examining the approximate series expansions which can be used to represent Bessel functions, and comparing their values to the series in the rectangular solution.

However, it should be noted that this work was for the case of very small fluxes on the surface of the skin, where temperature changes occur over long periods of time. Shitzer's models also contained terms representing blood perfusion and metabolic heat generation, effects which are often negligible in flash fire situations. In addition, Shitzer was not interested in the effects of geometry on burn predictions, which are highly temperature sensitive, and which are of main concern here.

In order to decide if the curvature of the body must be taken into account in predicting burns under flash fire conditions, the solutions of (A1.2) and (A1.3) were compared for typical geometries of the human body, under boundary conditions indicative of a flash fire. To simplify matters, the temperature throughout the skin was assumed to be constant prior to the exposure. The initial and boundary conditions are then as follows:

$$T\ (r,t=0)\ =\ T_i \qquad \text{(A1.4)}$$

$$T\ (r=r_i,t)\ =\ T_i \qquad \text{(A1.5)}$$

$$k\ \frac{\partial T}{\partial r}\ =\ q(t) \qquad (r\ =\ r_o\ ,\ t > 0) \qquad \text{(A1.6)}$$

where r_i and r_o are the inner and outer radius of the hollow cylinder, respectively, and the heat flux, q(t), is given by

$$\begin{aligned} q(t) &= q_o \quad 0 < t \le t_{ex} \\ &= 0 \quad t > t_{ex} \end{aligned} \tag{A1.7}$$

where t_{ex} is the time of exposure to the high intensity heat flux, q_0.
The initial and boundary conditions for the semi-infinite slab are the same as those given in Equations (A1.4) to (A1.7), only expressed in cartesian coordinates.

The closed form solution for the slab is given in Carslaw and Jaeger [100] as

$$\begin{aligned} T(x,t) = T_i + \frac{2q_o}{\sqrt{k\rho c}} \Bigg(& \sqrt{t}\ ierfc\left(\frac{x}{2\sqrt{\alpha t}}\right) \\ & - \sqrt{t - t_{ex}}\ ierfc\left(\frac{x}{2\sqrt{\alpha(t - t_{ex})}}\right) S(t) \Bigg) \end{aligned} \tag{A1.8}$$

where ierfc is the integral of the complimentary error function and S(t) is the step function which is equal to 1 when $t > t_{ex}$.

The closed form solution for the hollow cylinder is given in Carslaw and Jaeger [100] as

$$\begin{aligned} T = T_i + \frac{q_o}{k} \Bigg[& r_o \ln\left(\frac{r}{r_i}\right) \\ & - \pi \sum_{n=1}^{\infty} \exp(-\alpha\lambda_n^2 t)\, \frac{J_1(r_o\lambda_n)J_o(r_i\lambda_n)\left(Y_o(r\lambda_n)J_o(r_i\lambda_n) - J_o(r\lambda_n)Y_o(r_i\lambda_n)\right)}{\lambda_n\left(J_o^2(r_i\lambda_n) - J_1^2(r_o\lambda_n)\right)} \Bigg] \end{aligned} \tag{A1.9}$$

where J_o, J_1, Y_o, Y_1 are Bessel Functions, and λ_n are the roots of

$$J_o(\lambda r_i)Y_1(\lambda r_o) - Y_o(\lambda r_i)J_1(\lambda r_o) = 0 \tag{A1.10}$$

The original intent was to compare the results of the two closed form solutions. While it is quite simple to evaluate the closed form solution for the slab geometry, the presence of the Bessel functions in the solution for the cylindrical geometry make it very difficult to evaluate. Therefore, it was decided to evaluate both of these equations using the finite element method.

While the finite element model of the skin previously developed by the author [2] was used for the slab geometry, a new model had to be developed for the cylindrical geometry. The previous model consisted of 5 cubic Hermitian elements (1 in the epidermis, and 2 in each of the dermis and subcutaneous), while the new model consisted of 18 linear elements (8 in the epidermis, and 5 in each of the dermis and subcutaneous). These lower order elements were used in this preliminary work, because the finite element matrix equations associated with them were considerably easier to derive for the cylindrical case than those for the Hermitian elements. It was thought that if a cylindrical model was deemed necessary for the major body of work in this study, that higher order elements could then be used.

Three body locations were chosen to compare the results. These were the arm, leg, and trunk. Using data from an ergonomic handbook [146], the outside radius of the cylinder could be determined by assuming a cylinder with a circumference, C, equal to the measured perimeter of the body parts, and remembering that

$$C = 2\pi r$$

This gave the following outer radii for the cylinders.

arm	5 cm
leg	9 cm
trunk	15 cm

As in the author's previous work [2], the following values of the thickness of the different layers of skin, consistent with other investigators, were used here.

epidermis	80 μm
dermis	2 mm
subcutaneous	1 cm

The inner radii were then simply determined by subtracting the total thickness of the three layers of skin (12.08 mm) from the outer radius. Two other outer radii, 50 and 100 cm, were also used. These served as a test of the cylindrical model as it was assumed that its results would tend to those of the rectangular model as the radius increased.

Heat fluxes between 10 and 63 kW/m^2 for 10 s were used as test cases. These heat fluxes include the range of heat fluxes which might be expected to be incident on the skin under a fabric during small scale or thermal mannequin tests, based on the measurements described in Chapter 4. In both models, the surface of the skin is insulated after the exposure ends. The models continued to predict skin temperatures and estimate the extent of thermal damage to the skin up to 50 s after the exposure ended. The temperature time histories for the two models were analyzed using a routine which calculates the value of Henriques burn integral in time, and determines when second and third degree burns occur.

The temperatures predicted using the models were fairly close. The burn predictions made using the two models are compared in Table A1.1, below, for the arm where the differences between the two models should be largest.

Table A1.1 Comparison Between Times to Second and Third Degree Burn Determined Using the Cylindrical (r_o = 5 cm - arm) and Slab Models

Heat Flux (kW/m^2)	Time to 2° Burn (s)		Time to 3° Burn (s)	
	Cylindrical model	Slab model	Cylindrical model	Slab model
10	no burn	no burn	no burn	no burn
21	3.82	3.86	no burn	no burn
30	2.30	2.24	no burn	no burn
42	1.38	1.36	12.20	12.0
63	0.78	0.76	9.34	9.1

The burn predictions made using the two models were within 3% of each other. These results indicate that the cylindrical geometry has practically no effect on the prediction of second and third degree burns under flash fire conditions. Therefore the one dimensional heat transfer models used to analyze thermal mannequin test data appear to be adequate. From the heat transfer perspective, planar bench top tests should also be adequate.

APPENDIX 2: COMPARISON OF RADIATION HEAT TRANSFER ESTIMATES IN THE AIR GAP WITH AND WITHOUT ABSORPTION

Two infinite parallel plates with emissivities of ε_1 and ε_2 and at temperatures T_1 and T_2 are shown in Figure A2.1. A gas of emissivity ε_g at an average temperature of T_g is in the space in between the plates.

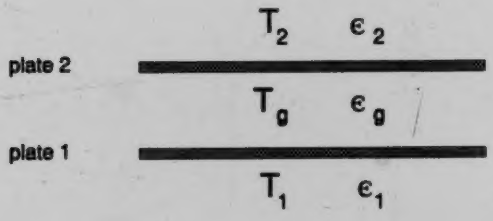

Figure A2.1 Two Infinite Parallel Plates with a Gas in Between Them

The net heat flux from plate 1 to plate 2 is given by (assuming that $T_1 > T_2$)

$$q_{rad} = \frac{\sigma\,(T_1^{\,4} - T_2^{\,4})}{\left(\dfrac{1-\varepsilon_1}{\varepsilon_1} + 1 + \dfrac{1-\varepsilon_2}{\varepsilon_2}\right)} \tag{A2.1}$$

If absorption of the radiation from plate 1 by a gas in the space between the two plates and the subsequent emission of thermal radiation by this gas to plate 2 is included, the grey gas method described by Hottel and Sarofim [63] can be used to estimate the heat flux incident on plate 2

$$q_{net} = \left(1 - \frac{\alpha_{g1}\sigma\varepsilon_1 T_1^{\,4} - \alpha_{g2}\sigma\varepsilon_2 T_2^{\,4}}{\dfrac{\sigma(T_1^{\,4} - T_2^{\,4})}{\left(\dfrac{1-\varepsilon_1}{\varepsilon_1} + \dfrac{1-\varepsilon_2}{\varepsilon_2} + 1\right)}} \right) \left(\frac{\sigma\,(T_1^{\,4} - T_2^{\,4})}{\left(\dfrac{1-\varepsilon_1}{\varepsilon_1} - \dfrac{1-\varepsilon_2}{\varepsilon_2} + 1\right)} \right) + \left(\frac{\varepsilon_1 + 1}{2}\right)\left(\varepsilon_g \sigma T_g^{\,4} - \alpha_{g2}\sigma\varepsilon_2 T_2^{\,4} \right) \qquad \text{(A2.2)}$$

The wall temperatures of the enclosure were estimated as 900 K and 350 K, respectively. These were approximately the maximum temperatures measured on the back face of the shim stock pieces or fabric specimens and in the copper disk test sensors when an air space was used (see Chapter 4).

Next the partial pressures of carbon dioxide and water vapour inside the air space were estimated. Complete combustion and stoichiometric air was assumed. The chemical structures of Nomex®, Kevlar®, and PBI are shown in Figure 1.2. The number of carbon, hydrogen, oxygen, and nitrogen atoms are as follows:

Molecule	C	H	N	O
Nomex®	14	10	2	2
Kevlar®	14	10	2	2
PBI	20	12	4	0

Writing the chemical formula for the complete combustion of Nomex® or Kevlar®

$$C_{14}H_{10}N_2O_2 + \frac{31}{2}\,O_2 + \frac{31}{2}\,(3.76)\,N_2 \rightarrow 14\,CO_2 + 5\,H_2O + 16.03\,(3.76)\,N_2 \qquad \text{(A2.3)}$$

Using this formula the volume fractions of CO_2 and H_2O in the products were 0.18 and 0.06, respectively (on a wet basis). Using the same method the volume fractions of CO_2 and H_2O in the products of the combustion of PBI were found to be 0.17 and 0.05, respectively. In order to be conservative, it was assumed for this calculation that the volume fractions of CO_2 and H_2O in the products were 0.3 and 0.1. It was further assumed that the total pressure of the combustion products was 1 atm. Therefore, the partial pressures of CO_2 and H_2O were 0.3 and 0.1 atm.

To determine the emissivity and transmissivity of the gas, the charts of Hottel [63] will be used. The mean beam length for infinite parallel plates is 1.8 times the space between the plates, or 2.0 times this space for optically thin layers of gas. In this case it is expected that the gas layer will be optically thin, and thus the 2.0 factor is chosen. The air gap will be taken as 3/4 in. (19.1 mm) wide, the largest air gap examined in this study. If absorption is found to be unimportant at this air gap, it will also be assumed unimportant at the smaller air gaps. The mean beam length is therefore 2.0 x .019 m = 0.038 m.

The emissivities and then the absorptivities of the individual gases were first calculated by taking into account each surface.

$$\alpha_{H_2O,i} = \left(\frac{T_g}{T_i}\right)^{0.45} \varepsilon_g(T_i\ ,\ p_{H_2O}\ L\ \frac{T_i}{T_g}\ ) \tag{A2.4}$$

$$\alpha_{CO_2,i} = \left(\frac{T_g}{T_i}\right)^{0.65} \varepsilon_g(T_i\ ,\ p_{CO_2}\ L\ \frac{T_i}{T_g}\ ) \tag{A2.5}$$

For the carbon dioxide and water vapour in the air gap being considered the following values were obtained.

Gas	Emissivities, $\varepsilon'_{g,i}$		Absorptivities, $\alpha'_{g,i}$	
	i = 1	i = 2	i = 1	i = 2
H_2O	0.016	0.016	0.015	0.023
CO_2	0.06	0.042	0.053	0.069

The emissivities of each of the gases were also calculated using the temperature of the gas and the products of their partial pressures and the mean beam length.

$$\varepsilon_{H_2O}(T_g\ ,\ p_{H_2O}L)\ =\ 0.016 \qquad \text{(A2.6)}$$

$$\varepsilon_{CO_2}(T_g\ ,\ p_{CO_2}L)\ =\ 0.0055 \qquad \text{(A2.7)}$$

The above two emissivities were added to get the total emissivity of the gas mixture, 0.07 (no spectral overlap correction was required because of the short mean beam length here).

The absorptivities of the gas mixtures relative to each surface were calculated by simply adding the values for each gas/surface combination shown above. Again, because of the short mean beam length, no corrections were required.

$$\alpha_{g,i}\ =\ \alpha_{H_2O,i}\ +\ \alpha_{CO_2,i} \qquad \text{(A2.8)}$$

$$\alpha_{g,1}\ =\ 0.068$$

$$\alpha_{g,2}\ =\ 0.092$$

The original estimate of the gas temperature was now checked using an energy balance on the gas.

$$\varepsilon_g T_g^{\ 4}\ =\ \frac{\alpha_{g,1}T_1^{\ 4}\ +\ \alpha_{g,2}T_2^{\ 4}}{2} \qquad \text{(A2.9)}$$

This gave a gas temperature of 753 K, thus confirming the original estimate.

The calculated values of ε_g, $\alpha_{g,1}$, and $\alpha_{g,2}$ were now used in Equation (A2.2) to estimate the net heat transfer to plate 2 from plate 1 and the gas in the space between the plates. The shim stock temperatures measured during a bench top test were used as the transient temperatures of plate 1. The radiative heat fluxes were now equated to the rate of energy storage in plate 2, which is assumed to be copper and the same thickness, Δx, as the disks used in bench top fabric tests, assuming a lumped capacity system

$$q_{rad} = \rho c \Delta x \frac{\partial T}{\partial t} \tag{A2.10}$$

This non-linear equation was solved for the temperature of the plate 2 at each moment in time using the Newton-Raphson false position method. The temperatures calculated for the plate using the radiative heat fluxes calculated from Equations (A2.1) and (A2.2) are compared below, as are the estimated times to exceed the Stoll criterion.

Table A2.1 Effect of Absorption on Predicted Times Required to Exceed Stoll Criterion and Copper Disk Temperatures Rise

Equation Used to Calculate Radiative Flux	Time to Stoll Criterion (s)	Copper Disk Temperature Rise at 5.8 s	Copper Disk Temperature Rise at 20 s
(A2.1) (absorption not included)	5.77	15.0	54.9
(A2.2) (absorption included)	5.99	14.5	53.1
Percentage Difference	4	3	3

It should be noted that the difference in times to the Stoll criterion is actually deceptively large as 5.99 s was only one time step larger than 5.77 s. As can be seen by the above comparison, including absorption in the model of the heat transfer by radiation in the space between the heated fabric or shim and the test sensor or skin had a very small effect for a 3/4 in. (19.1 mm) air space. As it will have even less of an effect at the smaller air spaces (as the mean beam length will be even smaller), it can safely be neglected in this model.

APPENDIX 3: DERIVATION OF FINITE ELEMENT MATRIX EQUATION

As discussed in Chapter 2, the differential equation for heat transfer in the fabric-air gap-test sensor system under flash fire conditions is

$$C^{\wedge}(T)\,\frac{\partial T}{\partial t} = k(T)\frac{\partial^2 T}{\partial x^2} + \gamma\, q_{rad}\exp(-\gamma x) \tag{A3.1}$$

where

$$q_{rad} = \sigma\varepsilon_g T_g^{\,4} - \sigma\varepsilon_{fab}F_{fab\text{-}amb}\,(1-\varepsilon_g)\,(T_{x=0}^{\,4} - T_{amb}^{\,4}) - \frac{\sigma(T_{x=0}^{\,4} - T_{bh}^{\,4})}{\left(\dfrac{1-\varepsilon_{fab}}{\varepsilon_{fab}} + \dfrac{1}{F_{fab\text{-}bh}(1-\varepsilon_g)} + \dfrac{A_{fab}}{A_{bh}}\dfrac{(1-\varepsilon_{bh})}{\varepsilon_{bh}}\right)} \tag{A3.2}$$

The equation was solved subject to the following initial and boundary conditions:

$$T(x, t=0) = T_i(x) \tag{A3.3}$$

where $T_i(x)$ is some initial temperature gradient in the fabric-air gap-skin system.

$$-k(T)\,\frac{\partial T}{\partial x}\bigg]_{x=0} = q_{conv} = h_{fl}\,(T_g - T_{x=0}) \tag{A3.4}$$

$$T(x=L_b, t) = T_c \quad (t>0) \tag{A3.5}$$

The Hermitian temperature element was used here. All the terms in Equation (A3.1) are brought to the left hand side, and the Hermitian temperature interpolation polynomials are substituted for the temperature and its derivatives. Noting that

$$T = <f>^T <T_e> \tag{A3.6}$$

$$\frac{\partial T}{\partial x} = <f'>^T <T_e> \tag{A3.7}$$

$$\frac{\partial^2 T}{\partial x^2} = <f''>^T <T_e> \tag{A3.8}$$

$$\frac{\partial T}{\partial t} = <f>^T <\dot{T}_e> \tag{A3.9}$$

where $<f'>^T$ and $<f''>^T$ are the row vectors of the first and second derivatives of the interpolation polynomials with respect to x, Equation (A3.1) now becomes

$$C^{\wedge}(T\ )<f>^T <\dot{T}_e> - k <f''>^T <T_e> - \gamma\ q_{rad} \exp(-\gamma x) = R(x) \tag{A3.10}$$

where the right hand side of Equation (A3.10) is equal to a residual, R(x), which is a function of x.

Galerkin's equation is

$$\int_0^l <f>R(x)dx = 0 \tag{A3.11}$$

Substituting Equation (A3.10) into Equation (A3.11) for R(x) gives

$$\int_0^l \Big[C^{\wedge} <f> <f>^T <\dot{T}_e> - k <f> <f''>^T <T_e> \\ - <f>\ \gamma\ q_{rad} \exp(-\gamma x) \Big] dx = 0 \tag{A3.12}$$

Rearranging terms, Equation (A3.12) becomes

$$\left(\int_0^l C^{A} \langle f \rangle \langle f \rangle^T \, dx \right) \langle \dot{T}_e \rangle - \left(\int_0^l k \langle f \rangle \langle f'' \rangle^T \, dx \right) \langle T_e \rangle - \left(\int_0^l \langle f \rangle \, \gamma \, q_{rad} \exp(-\gamma x) \, dx \right) = 0 \tag{A3.13}$$

Integrating the second term on the left hand side by parts gives

$$-\int_0^l k \langle f \rangle \langle f'' \rangle^T \langle T_e \rangle \, dx = -k \langle f \rangle \langle f' \rangle^T \langle T_e \rangle \Big]_0^l + \int_0^l k \langle f' \rangle \langle f' \rangle^T \langle T_e \rangle \, dx \tag{A3.14}$$

As temperatures and fluxes must be continuous across element boundaries, and remembering that

$$T = \langle f \rangle^T \langle T_e \rangle$$

$$k \frac{\partial T}{\partial x} = k \langle f' \rangle^T \langle T_e \rangle$$

the first term on the right hand side of Equation (A3.14) will cancel out at all of the interior element interfaces. Therefore only values of this term at the exterior nodes (i.e. x = 0 (surface of the fabric), and x = L_b (base of the air gap behind the test sensor)) will be of concern.

At x = 0, the first term on the right hand side of Equation (A3.14) becomes:

$$-k \langle f \rangle \langle f' \rangle^T \langle T_e \rangle \Big]_{x=0} = -k \langle f \rangle \left(\frac{\partial T}{\partial x} (x=0) \right)$$

Applying the boundary condition [illegible]ven by Equation (A3.4), this term becomes

$$<f>\, h_{fl}\, (T_g - T_{x=0}) \tag{A3.15}$$

At x = L, the first term on the right hand side of Equation (A3.14) cannot be simplified further using the boundary condition given by Equation (A3.5). Therefore this term remains as

$$-k <f> <f'>^T <T_e> \Big]_{x=L} \tag{A3.16}$$

Equations (A3.15) and (A3.16) are substituted into Equation (A3.14), and the resulting equation is substituted into Equation (A3.13). Sorting like terms gives

$$\begin{aligned} &\left(\int_0^l k <f'> <f'>^T dx - k <f> <f'>^T \Big]_{x=L} \right) <T_e> + \left(\int_0^l C^A <f> <f>^T dx \right) <\dot{T}_e> \\ &- \left(\int_0^l <f> \gamma\, q_{rad} \exp(-\gamma x)\, dx \right) - <f> \Big]_{x=0} \left(h_{fl} \left(T_g - T \Big]_{x=0} \right) \right) = 0 \end{aligned} \tag{A3.17}$$

or

$$\Big([A] - [k] \Big) <T_e> + [B] <\dot{T}_e> - <BC> = 0 \tag{A3.18}$$

where

$$[A] = \frac{1}{30\, l} \begin{vmatrix} 36k & 3l & -36k & 3l \\ 3l & 4l^2/k & -3l & -l^2/k \\ -36k & -3l & 36k & -3l \\ 3l & -l^2/k & -3l & 4l^2/k \end{vmatrix} \tag{A3.19}$$

(Note that the values of this and the other integrals are tabulated in Wu, et al. [98].)

$$[k] = \begin{vmatrix} \cdot & \cdot & \cdot & \cdot & \cdot & \cdot \\ \cdot & \cdot & \cdot & \cdot & \cdot & \cdot \\ \cdot & \cdot & 0 & 0 & 0 & 0 \\ \cdot & \cdot & 0 & 0 & 0 & 0 \\ \cdot & \cdot & 0 & 0 & 0 & 1 \\ \cdot & \cdot & 0 & 0 & 0 & 0 \end{vmatrix} \qquad \text{(A3.20)}$$

$$[B] = \frac{C^{\wedge}\, l}{420\, k} \begin{vmatrix} 156k & 22l & 54k & -13l \\ 22l & 4l^2/k & 13l & -3l^2/k \\ -54k & 13l & 156k & -22l \\ -13l & -3l^2/k & -22l & 4l^2/k \end{vmatrix} \qquad \text{(A3.21)}$$

$$\langle BC\rangle = \langle f\rangle \Big]_{x=0} q_{conv}(t) + \int_0^l \langle f\rangle\, \gamma\, q_{rad}(t) \exp(-\gamma x)\, dx$$

$$\langle BC\rangle = \begin{vmatrix} q_{conv}(t) + \gamma\, q_{rad}(t) \exp(-\gamma\, X) \left(\frac{2W_1}{l^3} - \frac{3W_2}{l^2} + W_4\right) \\ \gamma\, q_{rad}(t) \exp(-\gamma X) \left(\frac{1}{k}\left(\frac{W_1}{l^2} - \frac{2W_2}{l} + W_3\right)\right) \\ \gamma\, q_{rad}(t) \exp(-\gamma X) \left(\frac{-2W_1}{l^3} + \frac{3W_2}{l^2}\right) \\ \gamma\, q_{rad}(t) \exp(-\gamma X) \left(\frac{1}{k}\left(\frac{W_1}{l^2} - \frac{W_2}{l}\right)\right) \\ \cdots \\ \cdots \\ \cdots \end{vmatrix} \qquad \text{(A3.22)}$$

where X is the value of the global x coordinate at the local origin or the particular element being considered, and

$$W_1 = -\frac{1}{\gamma}\left(l^3 \exp(-\gamma l\ ) \right) + \frac{3}{\gamma}\left[-\frac{1}{\gamma} l^2 \exp(-\gamma l\ ) + \frac{2}{\gamma^3}\left[(-\gamma l\ -1\ ) \exp(-\gamma l) + 1 \right] \right] \tag{A3.23}$$

$$W_2 = -\frac{1}{\gamma}\, l^2 \exp(-\gamma l\ ) + \frac{2}{\gamma^3}\left[(-\gamma l\ -\ 1\ ) \exp(-\gamma l\ ) + 1 \right] \tag{A3.24}$$

$$W_3 = \frac{1}{\gamma^2}\left[(-\gamma l\ -\ 1\ ) \exp(-\gamma l\ ) + 1 \right] \tag{A3.25}$$

$$W_4 = \frac{1}{\gamma}\left[1 - \exp(-\gamma l\ ) \right] \tag{A3.26}$$

It should be noted that the above matrices are based on the following temperature response vector.

$$\left\langle \begin{matrix} T_1 \\ k_1(\frac{\partial T}{\partial x})_1 \\ T_2 \\ k_2(\frac{\partial T}{\partial x})_2 \end{matrix} \right\rangle \tag{A3.27}$$

This temperature response vector must be used in order to ensure compatibility of the fluxes at the element boundaries, as the thermal conductivity and other properties are not uniform throughout all the elements.

The Crank-Nicholson technique is used to solve the resulting equations in time.

The Crank-Nicholson equation is

$$<T^{(j+1)}> = <T^{(j)}> + \frac{\Delta t}{2}\left(<\dot{T}^{(j)}> + <\dot{T}^{(j+1)}> \right) \qquad \text{(A3.28)}$$

where (j) and (j+1) represent time steps (j) and (j+1), respectively. Premultiplying Equation (A3.28) by [B], substituting Equation (A3.18) into the resulting equation, and rearranging terms gives

$$\begin{aligned} \left([B] + \frac{\Delta t}{2}\left([A] - [k] \right) \right) <T^{(j+1)}> \\ = \left([B] + \frac{\Delta t}{2}\left(-[A] + [k] \right) \right) <T^{(j)}> \\ + \frac{\Delta t}{2}\left(<BC^{(j)}> + <BC^{(j+1)}> \right) \end{aligned} \qquad \text{(A3.29)}$$

or

$$[LHS] <T^{(j+1)}> = <RHS> \qquad \text{(A3.30)}$$

As noted in Chapter 2, these equations have been linearized by making several assumptions, including assuming that the incident heat flux and thermal properties can be calculated by using temperatures at the previous time step. Therefore in this particular case the <BC> vectors at time steps j and j+1 in Equation (A3.29) will be identical.

Details of the computer program which uses this approximate finite element matrix equation are found in Section 2.8.

APPENDIX 4: SAMPLE DATAFILE

The following is a sample datafile generated by the finite element program. Data for all time steps are printed to this file, and it may then be edited by the user. Here, the file has been edited to conserve space.

```
09-13-1996
15:09:01
FINITE ELEMENT SOLUTION
USING HERMITIAN TEMPERATURE INTERPOLATION FUNCTION
NUMBER OF ELEMENTS =          9
CONVECTIVE HEAT TRANSFER COEFFICIENT (W/M^2 C) = 40.0
EXPOSURE TIME (S) = 10
TOTAL TIME OBSERVED (S) = 10
AIR GAP (MM) = 6.35
VIEW FACTOR = .4586348831653595

TEMPERATURE-TIME HISTORY AT VARIOUS DEPTHS

                  TEMPERATURE (C)
TIME (S)     FABRIC SURF   MID FABRIC    FABRIC BASE   COPPER DISK
  0.00            40.0        40.0            40.0          30.0
  0.05           157.7        40.1            39.9          30.0
  0.10           148.0        40.4            39.9          30.0
  0.15           160.9        42.3            39.9          30.0
  0.20           187.2        46.7            40.2          30.0
  0.25           201.4        52.6            40.9          30.0
  0.30           210.7        58.6            42.5          30.0
  0.35           218.6        65.2            45.1          30.0
  0.40           225.8        69.4            48.4          30.0
  0.45           234.0        74.1            52.2          30.0
  0.50           242.7        80.3            56.4          30.0
  1.00           299.6       150.6            93.7          30.0
  2.00           398.8       309.5           282.2          30.5
  3.00           484.2       420.9           397.4          32.0
  4.00           545.7       484.5           460.3          34.5
  5.00           594.2       534.4           507.4          37.8
  6.00           632.8       573.8           544.3          41.7
  7.00           664.3       605.3           573.4          46.4
  8.00           688.5       630.1           596.3          51.5
  9.00           706.8       648.9           613.6          57.2
 10.00           720.3       662.5           626.2          63.1

TIME TO REACH STOLL CRITERION (S) = 6.85
```

APPENDIX 5: SKIN SIMULANT TEMPERATURE GRADIENTS

Thermocouples were placed inside a skin simulant heat flux sensor. Temperatures at the surface and at depths of 5, 10, 15, and 20 mm were recorded. The sensor was exposed to heat fluxes of about 13, 17, and 90 kW/m^2 from a 380 W movie projector lamp powered by a variable voltage power supply. Exposures of 1, 3, 5, and 10 s were used. Originally the values of the heat fluxes incident on the sensors were determined using a Gardon gauge. However, as the diameter of the Gardon gauge is much smaller than the skin simulant sensor, the heat flux indicated by the Gardon gauge was larger than that incident on the entire surface of the skin simulant. Therefore, the heat flux incident on the skin simulant was determined using the closed form solution for the temperature at the surface of a semi-infinite solid with constant thermal properties subjected to a suddenly applied heat flux, q_o [100]

$$q_o = \frac{\sqrt{k\rho c\pi}\ \Delta T}{2\sqrt{t}} \qquad \text{(A5.1)}$$

The temperature histories at various depths in the sensor during and after a 10 s exposure to a heat flux of about 17 kW/m^2 are shown in Figure A5.1. The heat flux used in this particular test is similar to the heat fluxes measured behind single layer fabrics during some bench top tests (e.g. Figure 4.30). While data up to a time of 200 s is shown here, data was actually taken for up to 30 minutes. At the beginning of this exposure, the temperature difference within the sensor was less than 1°C. It took over 10 minutes after the exposure ended for the sensor to cool enough so that the temperature difference was again less than 1°C. For the larger heat fluxes, such as those which would be incident on a bare sensor during a calibration run for a bench top or mannequin test, it should take longer for the sensor to cool. For example, when the sensor was exposed to a flux of about 90 kW/m^2 for 10 s, it took over 30 minutes for the surface temperature to cool to within 1°C of its value prior to the beginning of the exposure.

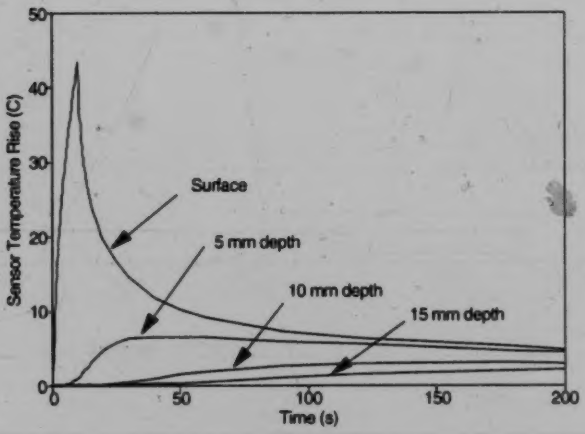

Figure A5.1 Temperature Histories at Various Depths in Skin Simulant Sensor Subjected to Heat Flux of about 17 kW/m^2 for 10 s

A finite element heat transfer model of the sensor was developed. This was similar to the skin heat transfer model previously developed by the author [2]. The results from this model were compared with the temperature measurements at various depths in the skin simulants. For example, Figure A5.2 shows a comparison between the predicted and measured temperatures at the surface for a 10 s exposure to a heat flux of about 17 kW/m^2. The temperatures predicted by the numerical model were similar to those measured in the skin simulant. The differences between the two results are due to the limitations of the numerical model. Specifically, the model assumed a uniform initial temperature within the sensor, while in practice there was a small temperature gradient. In addition, there is some uncertainty in determining the value of the heat flux. Installation of the thermocouples in the sensor will also change the heat transfer within it.

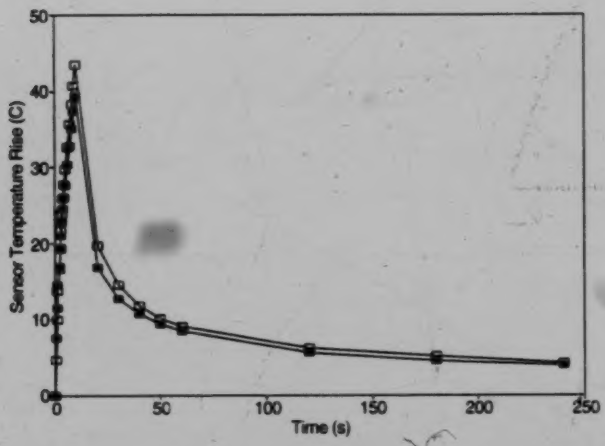

Figure A5.2 Comparison Between Predicted (■) and Measured (□) Surface Temperatures of a Skin Simulant During and After a 10 s Exposure to a Heat Flux of About 17 kW/m^2

The numerical model was then used to determine the magnitude of gradients which would remain in the sensor after given exposures, and the effect of these gradients on burn predictions made using the sensor. First, the model was used to determine the gradients remaining in the sensor under the following conditions.

- Square wave heat flux of 84 kW/m^2 for 5 s, with a natural convection boundary condition. This might represent a calibration run for a bench top or mannequin test. It was found that under these conditions that it took over 15 minutes to get the gradients in the sensors below 3°C.
- Heat flux histories measured under single layer fabrics during bench top tests, with free convection occuring immediately after the test ends and the fabric is removed. Here it took about 10 minutes after the test ended for the gradients to decay to less than 2°C.

In both of these cases, increasing the natural heat transfer coefficient increased the rate of cooling. For example, increasing the natural convection heat transfer coefficient on the front of the sensor from 5 to 20 W/m^2·°C decreased the time for the gradient to decay to less than 3°C for a sensor exposed to a heat flux of 84 kW/m^2 for 5 s by about

5 minutes.

In order to determine the effect of residual temperature gradients within skin simulant sensors on burn predictions, the numerical model was used to determine the thermal response of the simulants to heat flux histories from bench top or mannequin tests for various initial sensor temperature gradients. These temperature histories were then used to determine heat flux histories using the method described in Appendix 6. The heat flux histories were then used to predict times to second and third degree burn. Some examples of the comparisons between the times predicted for second degree burns for several heat flux histories are shown in Table A5.1 below.

Table A5.1 Comparison Between Second Degree Burn Predictions Made Using Skin Simulant Sensors with Various Initial Temperature Gradients

Description of Simulated Test	Predicted Time to Second Degree Burn (s) for Various Initial Sensor Temperature Gradients			
	ΔT = 0°C	ΔT = 1°C	ΔT = 2°C	ΔT = 5°C
bench top test with 1/4 in. (6.4 mm) air gap	5.00	5.00	5.00	5.05
bench top test with 1/2 in. (12.7 mm) air gap	6.21	6.26	6.26	6.37
thermal mannequin test #1	19.00	20.05	23.01	no burn
thermal mannequin test #2	8.02	8.02	8.02	8.02

In a similar manner, data from thermal mannequin test #1, above, was also used to compare the times predicted to third degree burns. It was found that the predicted time to third degree burn increased from 42 s with no initial temperature gradient, to 44 s and 48 s for initial gradients of 1°C and 2°C, respectively. With an initial gradient of 5°C, no third degree burns were predicted.

Clearly, the initial gradient will have an effect on the prediction of slower developing second and third degree burns. Therefore, for fixed duration and mannequin tests it is important to allow enough time for the sensor to cool to the point where the internal temperature gradients are as small as possible before beginning the next test. This may take up to 30 minutes depending on the exposure. For bench top tests, a number of sensors could be used, so as to allow the sensors enough time to cool sufficiently before they are used again.

APPENDIX 6: DETAILS OF CALCULATION OF HEAT FLUXES FROM SURFACE TEMPERATURES OF SKIN SIMULANT SENSOR

Data from skin simulant heat flux sensors can be analyzed to determine the temperature-time history in skin for the exposure of interest, and skin burns can then be predicted using Henriques burn integral [14]. A computer program written to analyze data is this manner is described below.

The surface temperature readings from the skin simulant heat flux sensor can be used to calculate the values of the heat flux incident on the surface at any time using Duhamel's theorem [100]. This theorem states that if $u_1(x,t)$ is the response of a linear homogeneous system (initially at zero) to a single unit step input, the response, $u_f(x,t)$, of the system to a time varying, continuous input, F(t), is given by

$$u_f(x,t) = \int_0^t F(\tau) \frac{\partial u_1(x,t-\tau)}{\partial \tau} d\tau \qquad \text{(A6.1)}$$

Therefore, to calculate the incident heat fluxes from the surface temperature history, the surface heat flux response to a single unit step input must be known.

The closed form solution for a semi-infinite solid at an initial temperature of T_i subjected to a step surface temperature change to T_s is

$$\frac{T - T_i}{T_s - T_i} = 1 - \frac{2}{\sqrt{\pi}} \int_0^{\frac{x}{2\sqrt{\alpha t}}} \exp(-y^2) dy \qquad \text{(A6.2)}$$

The surface heat flux response to this step surface temperature change is

$$
\begin{aligned}
q(t) = -k \left.\frac{\partial T}{\partial x}\right]_{=0} &= \frac{2k}{\sqrt{\pi}} (T_s - T_i) \frac{\partial}{\partial x} \int_0^{\frac{x}{2\sqrt{\alpha t}}} \exp(-y^2)\, dy \\
&= \frac{2k}{\sqrt{\pi}} (T_s - T_i) \left[\frac{\partial}{\partial \left(\frac{x}{2\sqrt{\alpha t}} \right)} \int_0^{\frac{x}{2\sqrt{\alpha t}}} \exp(-y^2)\, dy \right] \frac{\partial \left(\frac{x}{2\sqrt{\alpha t}} \right)}{\partial x} \qquad \text{(A6.3)} \\
&= \frac{2k}{\sqrt{\pi}} (T_s - T_i) \left[\left(\exp\left(\frac{-x^2}{4\alpha t} \right) \right) \frac{1}{2\sqrt{\alpha t}} \right]_{=0} \\
&= \frac{k}{\sqrt{\pi \alpha t}} (T_s - T_i)
\end{aligned}
$$

For a single, unit step in surface temperature, $T_s - T_i = 1$. Therefore the heat flux response is

$$
q(t) = \frac{k}{\sqrt{\pi \alpha t}} \qquad \text{(A6.4)}
$$

Substituting Equations (A6.3) and (A6.4) into Equation (A6.1), the heat flux response for a variable surface temperature is

$$
\begin{aligned}
Q(t) = \int_0^t (T_s(\tau) - T_i) \frac{\partial q(t-\tau)}{\partial t}\, d\tau &= \frac{k}{2\sqrt{\pi\alpha}} \int_0^t \frac{T_i - T_s(\tau)}{(t - \tau)^{3/2}}\, d\tau \\
&= \frac{k}{2\sqrt{\alpha\pi}} \left[\int_0^t \frac{T_s(t) - T_s(\tau)}{(t - \tau)^{3/2}}\, d\tau + \int_0^t \frac{T_i - T_s(t)}{(t - \tau)^{3/2}}\, d\tau \right] \qquad \text{(A6.5)} \\
&= \sqrt{\frac{k\rho c}{\pi}} \left[\frac{1}{2} \int_0^t \frac{T_s(t) - T_s(\tau)}{(t - \tau)^{3/2}}\, d\tau + \frac{T_s(t) - T_i}{t^{1/2}} \right]
\end{aligned}
$$

The integral in (A6.5) can be evaluated using standard numerical techniques, such as the Trapezoidal rule

One problem immediately presents itself when one attempts to integrate Equation (6.5) numerically. At the upper limit of integration, t = τ, and the term to be integrated will become 0/0. Cook and Felderman [127] have developed an alternative approach to solving this equation numerically, which avoids this problem. Values of $T_s(\tau)$ are determined at $\tau = t_i = i \cdot \Delta t$, $i = 0,1,2,\ldots n$ ($\Delta t = t/n$). $T_s(\tau)$ is then approximated by a piecewise linear function of the form

$$T_s(\tau) = T_s(t_{i-1}) + \frac{T_s(t_i) - T_s(t_{i-1})}{\Delta t}(\tau - t_{i-1}) \tag{A6.6}$$

where

$$t_{i-1} \leq \tau \leq t_i \quad i = 1,2,\ldots,n \tag{A6.7}$$

$T_s(\tau)$ from equation (A6.6) is substituted into equation (A6.5), and the resulting expression is integrated, producing

$$Q_n(t) = \sqrt{\frac{k\rho c}{\pi}} \left[\frac{T_s(t_n)}{t_n^{1/2}} + \sum_{i=1}^{n-1} \left(\frac{T_s(t_n) - T_s(t_i)}{(t_n - t_i)^{1/2}} - \frac{T_s(t_n) - T_s(t_{i-1})}{(t_n - t_{i-1})^{1/2}} + 2\frac{T_s(t_i) - T_s(t_{i-1})}{(t_n - t_i)^{1/2} + (t_n - t_{i-1})^{1/2}} \right) + \frac{T_s(t_n) - T_s(t_{n-1})}{(\Delta t)^{1/2}} \right] \tag{A6.8}$$

No integration approximations are involved in the above expression, and the accuracy of the result is limited only by the ability of the piecewise linear expression to represent the actual surface temperature history.

Once the heat flux incident on the sensor has been determined for each time step, this information can be placed into a model of the heat transfer in the skin. The author's multiple layer finite element model of the skin was used [2]. The temperature-time history at the basal layer in the skin is then used in conjunction with Henriques burn integral to determine the time to second degree burn, while the temperature-time history at the dermal base is used along with the burn integral to determine the time to third degree burn.

This program is slightly different from the previous skin model in that rather than using a constant or square wave heat flux as the surface boundary condition, a variable heat flux boundary condition was used. Therefore, before using this program, it was tested against several closed form solutions. It can be shown that for a variable flux, q(t), the temperature in a semi-infinite solid, initially at constant temperature is [100]

$$T(x,t) - T(x,0) = \frac{\alpha^{1/2}}{k\pi^{1/2}} \int_0^t q(t-\tau)\, \exp(-\frac{x^2}{4\alpha t})\, \frac{d\tau}{\tau^{1/2}} \qquad \text{(A6.9)}$$

The model successfully predicted the temperatures due to the several simple transient heat flux boundary conditions, q(t). In addition, the model was checked by "reconstructing" temperature-time histories taken from test data using skin simulant sensors. The model first calculated the surface heat flux history from this known temperature history measured in a test, then used this flux history to successfully predict the original temperatures.

APPENDIX 7: DATA FROM INDIVIDUAL FIXED DURATION TESTS

In Table 4.4, mean times to predicted second and third degree burns are given for tests using copper disk sensors and skin simulants. Data from individual tests used to determine these mean values are given below.

Second Degree Burn Damage - Skin Simulant - Henriques Burn Integral

Fabric	Spacing	Mean Time to 2° Burn (s)	Test Data
Kevlar®/PBI	contact	2.8	2.63
			2.91
			2.70
			2.91
Kevlar®/PBI	1/4 in. (6.4 mm)	5.7	5.66
			5.65
			5.66
			5.44
			5.71
			5.38
			5.82
			5.66
			5.55
			5.82
Nomex® III	contact	2.8	2.91
			2.80
			2.80
Nomex® III	1/4 in. (6.4 mm)	5.9	5.99
			5.82
			5.99

Second Degree Burn Damage - Copper Disk - Henriques Burn Integral

Fabric	Spacing	Mean Time to 2° Burn (s)	Test Data
Kevlar®/PBI	contact	2.5	2.48
			2.52
			2.64
Kevlar®/PBI	1/4 in. (6.4 mm)	5.9	5.88
			5.82
			5.82
			6.04
			6.05
			5.88
			6.04
Nomex® III	contact	2.8	2.75
			2.75
			2.85
Nomex® III	1/4 in. (6.4 mm)	6.3	6.37
			6.32
			6.21

Second Degree Burn Damage - Copper Disk - Stoll Criterion

Fabric	Spacing	Mean Time to 2° Burn (s)	Test Data
Kevlar®/PBI	contact	2.7	2.59
			2.69
			2.80
Kevlar®/PBI	1/4 in. (6.4 mm)	6.4	6.38
			6.20
			6.32
			6.42
			6.43
			6.38
			6.42
Nomex® III	contact	3.0	2.97
			2.97
			3.07
Nomex® III	1/4 in. (6.4 mm)	6.8	6.86
			6.80
			6.71

Third Degree Burn Damage - Skin Simulant - Henriques Burn Integral

Fabric	Spacing	Mean Time to 2° Burn (s)	Test Data
Kevlar®/PBI	contact	13.1	13.02
			12.97
			13.18
Kevlar®/PBI	1/4 in. (6.4 mm)	23.6	23.73
			22.46
			23.84
			22.58
			21.14
			23.95
			26.03
			24.17
			22.41
			25.43
Nomex® III	contact	12.5	12.46
			12.47
			12.47
Nomex® III	1/4 in. (6.4 mm)	27.3	29.83
			24.88
			27.24

Third Degree Burn Damage - Copper Disk - Henriques Burn Integral

Fabric	Spacing	Mean Time to 2° Burn (s)	Test Data
Kevlar®/PBI	contact	13.1	12.96
			13.12
			13.24
Kevlar®/PBI	1/4 in. (6.4 mm)	33.7	33.56
			31.14
			30.20
			36.85
			37.68
			32.63
			34.06
Nomex® III	contact	12.8	12.81
			12.70
			12.85
Nomex® III	1/4 in. (6.4 mm)	no burn	no burn
			no burn
			no burn

CURRICULUM VITAE

Previous Education:

- Master of Science in Mechanical Engineering, University of Alberta, 1992
    - thesis title: A Finite Element Model of Heat Transfer in Skin Subjected to a Flash Fire
- Bachelor of Science in Mechanical Engineering, The University of Calgary, 1987

Industrial Experience:

- Design Engineer, Engineered Air, Calgary (July, 1987 to August, 1990)

Professional Associations:

- Association of Professional Engineers, Geologists, and Geophysicists of Alberta (APEGGA)
    - Professional Engineer
- American Society for Engineering Education (ASEE)
    - Student Member
- American Society of Heating, Refrigerating, and Air-Conditioning Engineers (ASHRAE)
    - Student Member

Personal:

- Married (one child)
- Canadian citizen; born June 10, 1965 at St. Lambert (Montreal), P.Q.